Ground heat storage : thermal analyses of duct storage systems

Hellström, Göran

1991

GROUND HEAT STORAGE

Thermal Analyses of Duct Storage Systems

I. Theory

Göran Hellström

April 1991

Department of Mathematical Physics
University of Lund
Sweden

"Nature, to be commanded, must be obeyed".
– Novum Organum, Francis Bacon, (1564-1626).

To Lena, Sandra, and Magnus

Preface

My involvement in this field began in 1977, when Johan Claesson asked me to participate in a research group with focus on the thermal analyses of ground heat storage systems. I am indebted to Johan Claesson, who has taught me the mysteries of mathematical modeling.

I should like to express my thanks to Pia Bruhn, who typed the manuscript. I am grateful to Ewa Westberg and Lilian Johansson for correcting my old drawings and for drawing the new ones.

I also want to thank Jesper Arvidson and Thomas Blomberg for their unselfish help with completing the final manuscript.

The support by the Swedish Council for Building Research (BFR) and the Swedish National Energy Administration (STEV) is gratefully acknowledged.

Table of Contents

Chapter 1

Ground Heat Storage

1.1 Introduction

The heating demand in energy supply systems normally exhibits large seasonal variations. In many of these systems there are periods when base load production units, which provide energy at a low marginal cost, are not fully utilized. At other times, expensive peak power resources must be used (Margen 1985). For some energy sources, such as solar energy and surplus waste heat, the lowest availability coincides with periods of large heating demands.

A device where heat can be stored for some period of time may improve the economy of the energy supply system. The basic idea is to charge the store when cheap energy (e.g. heat from base load production units, cogeneration plants, and incineration plants; industrial waste heat; summer solar energy, air, and surface water) is available and to discharge when the stored heat can replace more expensive sources (e.g. heat from peak power units; winter solar energy). This substitution of energy will decrease the operational costs of the energy supply system. The reduction of the dimensioning peak power capacity may cut capital investments (Margen 1985).

House heating by solar energy often requires a heat storage device in order to operate efficiently. This is especially true at northern latitudes where the winter season is characterized by low insolation and, consequently, cold climate and large heating demands. Seasonal heat storage allows for conventional flat plate and unglazed collectors, which are relatively inexpensive, to make efficient use of the intense solar radiation during the summer. The energy supply system may then receive major contributions from solar energy throughout the year (Dalenbäck 1990).

Heat storage on a short term basis can compensate for the influence of brief spells of cold weather, shutdowns of energy production units due to maintenance or operational problems, and diurnal variations in the heat load

curve. Short term storage allows for more frequent use of the store, thereby permitting a higher capital cost per unit of installed storage capacity. A heat store that is mainly intended for seasonal storage may become economically more competitive if it allows also for short-term storage.

Due to the large amounts of energy involved, the seasonal storage capacity must be very large. A full-scale application may require a storage capacity equivalent to more than 100,000 m^3 of water. Considering this size of storage unit, it is perhaps not surprising that the most favorable conditions for long-term storage of heat are to be found in the ground, where large storage volumes can be obtained at a relatively low cost.

There are three basic types of heat stores in the ground. The first type uses the ground directly as storage medium. The heat transfer between the heat carrier fluid and the storage region takes place via a duct system. Examples of such ground heat exchangers are boreholes in bedrock and plastic tubes in clay deposits. The second type uses water as storage medium. The water is contained in a rock cavern, a pit or pond, or in a buried tank. In the third type, the storage medium consists of the ground water and the solid matrix in an aquifer. The ground water is via a well system used as a heat carrier medium.

This report deals with the first of the three basic types, namely, ground heat stores with a duct system. The principal use of ground heat stores is seasonal heat storage. This type of storage is not particularly well suited for short-term variations in the rate of heat injection and extraction from the store. The systems were heat is stored in a water volume (rock caverns, pits, ponds) are often the more flexible in this respect, and it is also easier to maintain and utilize a stratification of the storage temperature. A combination of ground heat stores for seasonal storage and a water-based buffer storage for short-term storage has been proposed, thus combining the low cost of the ground heat store with the higher capacity of the water-based storage for short-term variations in the heat load (Margen 1983; Lund and Östman 1985).

Duffie and Beckman (1975) summarize the desirable characteristics that an energy storage unit should posses. The characteristics applicable to storage of sensible heat are as follows:

1. The unit should be capable of receiving and discharging heat at the maximum rate without excessive temperature differences

2. The unit should have small losses, which includes heat losses out of the unit as well as degradation of thermal stratification within the unit

3. The unit must be inexpensive

The major advantage of the ground heat store is the low construction cost. The heat losses from the store depend on the size and shape of the store,

the average storage temperature during a cycle, and the thermal properties of the ground. The fraction of the stored heat that is lost during a cycle increases with higher temperatures and decreases with larger volumes. High-temperature storage cannot be used in small systems without heat losses being prohibitively large. Low-temperature storage, with heat pumps connecting the store to the heat load, are less demanding on size or heat sources. An important problem is the temperature differences required to transfer heat between the heat carrier fluid in the ducts and the store. This temperature difference is proportional to the heat transfer rate. The heat transfer capacity of the ducts depends on the arrangements of the heat transfer ducts in the ground and within boreholes in rock, and on the thermal properties of the materials involved in the heat flow process.

In order to optimize the energy system with a ground heat store, it is necessary to have analytical tools by which the thermal behavior of the store can be assessed. An understanding of the fundamental thermal processes is also necessary for a proper dimensioning of the store and an intelligent use of simulation models.

1.2 Aim of this study

The *aim of this study* is to present a theory of thermal analyses of ground heat storage. The general goal of the thermal analyses is to master the response of the ground heat exchanger, i.e. the relation between heat transfer rate and temperature of the heat carrier fluid, under various conditions. This study particularly addresses the problems of heat transfer from the heat carrier fluid to the store and the heat losses from the store.

1.3 Applications and further studies

The theory presented in this study has been applied in many further studies. This will be reported in a forthcoming Part II (Applications and further studies). A brief description of the contents of Part II is given below.

Over the years, our research group in Lund has developed several computer programs for the thermal analyses of duct ground heat storage systems. The programs deal with all aspects of the thermal processes, from the fundamental cases treated in this study to detailed three-dimensional simulation models with arbitrary time-dependent loading conditions. The concept of a local and a global thermal process has been exploited to develop a fast and detailed simulation model — the duct ground heat storage model (DST). It has been widely used. This and all other models will be presented in detail.

The computer programs are used for extensive parameter studies concerning the heat transfer capacity of the ground heat exchanger and the annual heat balance for some common types of heat stores. The simulations of four field experiments are also presented. The agreements between measured and simulated heat balances are good.

A laboratory experiment has been performed to investigate the effect of free convection on the heat transfer from U-pipes in a water-filled borehole. The results from this experiment are given.

Finally, a method for proper thermal dimensioning of a ground heat store is developed based on the theory and the further studies.

Chapter 2

System Description

A *duct ground heat storage* system is defined as a system where heat is stored directly in the ground. A duct or channel system is used for heat exchange between a heat carrier fluid, which circulates through the ducts, and the storage region. The heat transport in the ground is mainly by ordinary heat conduction. Thus there are two basic constituents of a duct ground heat store: the geological medium that provides the storage capacity and the ground heat exchanger.

Figure 2.1 shows a heat store where the heat exchanger consists of a large number of boreholes drilled in the rock. A heat store in clay, figure 2.2, may use U-shaped loops of plastic tubes.

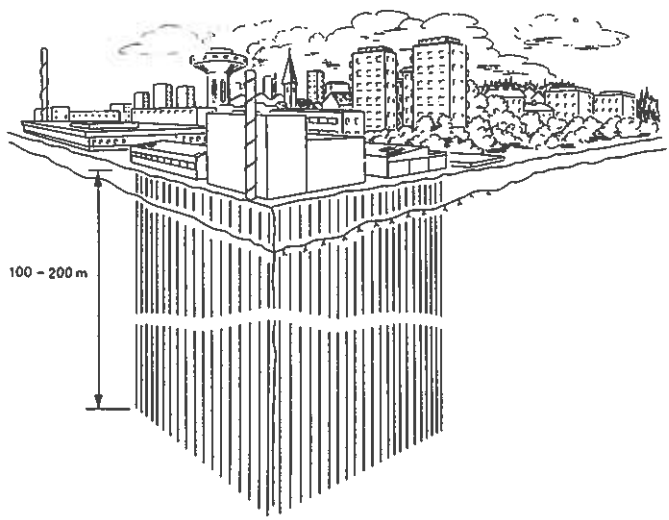

Figure 2.1. Ground heat store using boreholes in rock.

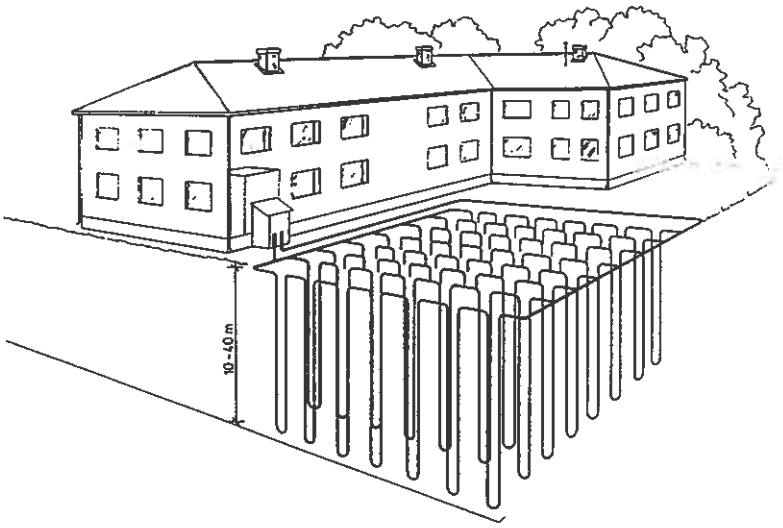

Figure 2.2. Ground heat store using U-shaped loops of plastic pipes in clay.

2.1 Storage volume

The storage volume is the ground region perforated by the ducts. The main heat transfer mechanism in the water-saturated ground is ordinary heat conduction, which depends on the thermal properties, the thermal conductivity and the heat capacity, of the ground material.

The fraction of the stored heat that is lost to the surrounding ground decreases as the size of the store is made larger. Thus, the store must have a certain size in order to avoid excessive heat losses. A compact shape of the storage volume is desirable, since heat losses are roughly proportional to the area exposed to the surroundings. Typically, the ground region has the shape of a parallelepiped or a cylinder with vertical symmetry axis.

The storage volume is usually at a shallow depth. This leads to large temperature gradients between ground surface and the upper parts of the store. It may then be economic to arrange for some sort of thermal insulation at the ground surface. One possibility is to cover the land area above the store with a shallow layer of soil with low thermal conductivity.

2.2 Ground heat exchangers

We will use the term *ground heat exchanger* for each duct or channel that is used for heat exchange in the ground. The specific arrangement of these

ground heat exchangers depends mainly on the geological medium. The properties of rock set it apart from softer media like clay, sand soil, and peat. There are significant differences in the design of the ground heat exchanger for these two types of ground.

2.2.1 Borehole with concentric inner tube

In solid rock the duct system typically consists of a large number of boreholes, which are uniformly placed in the storage region. Vertical boreholes with diameter of 4-6″ and a spacing of about 4 meters have been used in most of the systems built in Sweden. Those sites where the ground surface area available for the system is limited require another arrangement. The boreholes are then drilled to form a diverging bundle with increasing duct spacing toward depth.

Each borehole has one or more flow channels in the upward and downward directions for circulation of the heat carrier fluid. The most simple arrangement of the flow channels is to insert a single plastic tube through which the heat carrier fluid is transported down to the bottom of the borehole. The region between the plastic tube and the borehole wall constitutes the channel for upward flow. The fluid is extracted from the top of this channel to the main distribution system. The main advantage of this arrangement, which will be called an *open system*, is that the heat carrier fluid is in direct contact with the surrounding rock in the flow channel outside the plastic tube. This provides for good heat transfer between the heat carrier fluid and the surrounding rock.

2.2.2 Borehole with closed U-shaped loop

Unfortunately, the geohydrological and the geochemical conditions at a specific site are often unfavorable for an open system. A common alternative is to provide a *closed system* by inserting one or more U-shaped loops of plastic tubing into the borehole. The base of the loops reaches the bottom of the borehole. The heat transfer from the heat carrier fluid to the surrounding rock takes place via the plastic material and the ground water or the material that fills the borehole. The heat transfer is, consequently, not as good as for the open system.

2.2.3 Closed U-shaped loops in clay

In clay, sandy soil, or peat deposits, the duct system can be obtained by driving down vertical U-shaped loops of thin plastic tubes. For the existing seasonal stores in clay and sandy soil, the spacing between each such ground heat exchanger is typically about 2 meters. This spacing is shorter than that used for boreholes in rock mainly due to the lower thermal conductivity of

clay. Ground heat exchangers with two U-shaped loops driven down together may also be used. In shallow deposits, the duct system may be arranged by installing horizontal pipes.

2.3 Introductory example

A large-scale heat store in bedrock was built in Luleå, Sweden, in 1982-83. The store consists of 115,000 m^3 of crystalline rock with 120 vertical boreholes drilled to a depth of 65 m, of which the upper 3.5 m penetrate the overburden. The boreholes are placed in a quadratic pattern with a spacing of 4 m. The borehole diameter is 0.152 m (6"). See figure 2.3.

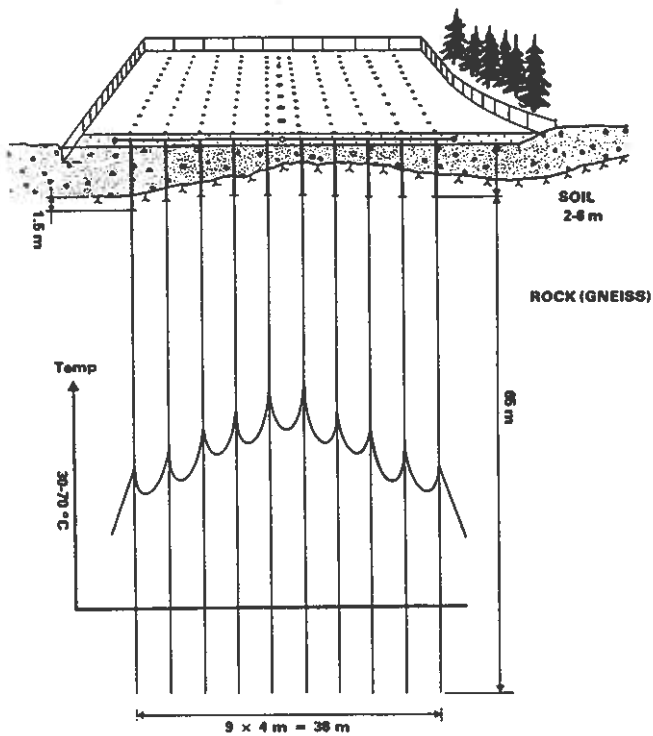

Figure 2.3. The ground heat store at Luleå University of Technology.

The boreholes are fitted with a plastic tube through which the heat carrier fluid is transported to the bottom of the borehole. The region between the plastic tube and the borehole constitutes the channel for upward flow. The details of the ground heat exchanger are shown in figure 2.4.

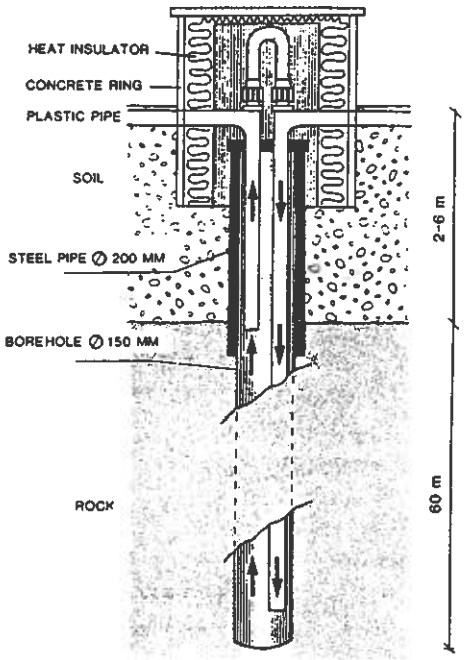

Figure 2.4. The ground heat exchanger at Luleå University of Technology.

The bedrock heat store in Luleå is an experimental and demonstration installation. It supplies part of the space heating load of one university block. The annual heat requirement of the building is about 2.7 GWh, which is equivalent to the heat demand of about 100 single-family houses in northern Sweden. The store has not been designed to supply the tap water production of the building. It is charged with 2 GWh produced by surplus gas combustion from the Swedish Steel Company's (SSAB) steelworks. The store is connected to the municipal district heating system, through which heat is transported to the store. During the winter season about 1 GWh is recovered, of which 20 % is extracted via heat pumps. Additional heat is supplied by the district heating system. The storage temperature varies between 30 °C and 60 °C during the year. The Division of Water Resources Engineering (WREL) of the University of Luleå is responsible for the research work (Nordell 1987, 1990).

The circulation path of the heat carrier fluid through the heat store is shown in figure 2.5. The central pipe supplies water at a temperature of about 70 °C during heat injection. The water is then divided into 24 lines

coupled in parallel. Each line has 5 boreholes coupled in series. After passage through the boreholes the cooled water returns via two collecting pipes at the borders of the store. During heat extraction the flow direction is reversed. The pump flow rate varies between 0.002 and 0.020 m^3/s.

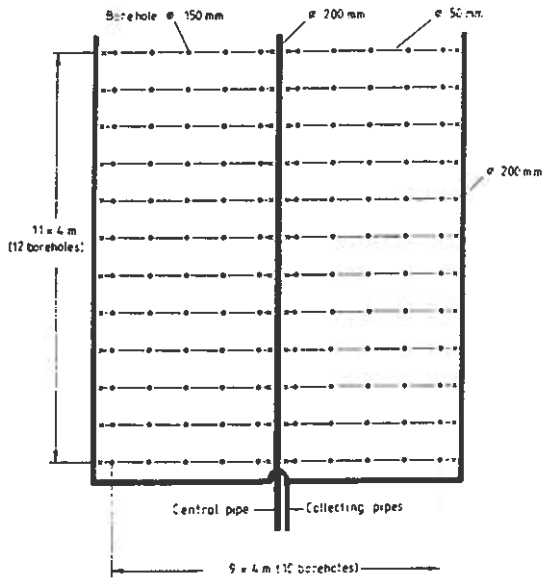

Figure 2.5. The circulation path of the heat carrier fluid through heat store at Luleå University of Technology.

The thermal behavior of the store during the initial three years was simulated before the operation started in 1983. The numerical simulation models that will be described in Part II were used. The simulations are based on the borehole configuration, the flow path through the store, measured thermal properties of the ground, and preliminary loading conditions. The simulations concern the initial three annual cycles. Figure 2.6 shows the calculated mean storage temperature (solid line) and the temperature in the center of the store at a point between the central boreholes (dashed line). The mean storage temperature varies between 30 °C and 60 °C. After three annual cycles the bedrock around the store has been heated so that the annual heat loss from the store is almost constant. The heat loss for the given loading conditions was about 40 %.

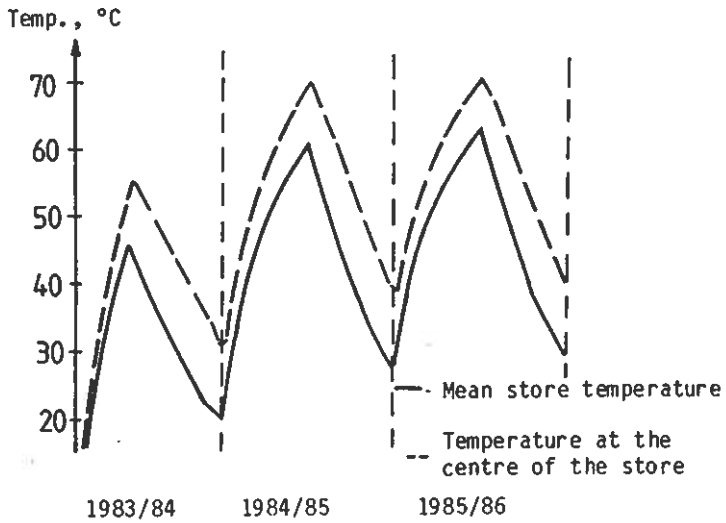

Figure 2.6. Simulated mean storage temperature and temperature at the center of the store during the three initial cycles. Heat store at Luleå University of Technology.

The simulated temperature field in a horizontal cut through the store at a depth of 35 meters is shown in Figure 2.7. The full temperature field is also shown by the figure on the cover. The thermal process exhibits symmetry in relation to the x-axis and y-axis in the figure. The conditions concern the end of the injection period during the third annual cycle.

Large temperature gradients can be observed close to boreholes. This is especially obvious in the colder parts of the store. The heat transport near each borehole is mainly in the radial direction. Outside the store, the temperature field has a smoother character where the thermal influence from the individual boreholes, the "local" variations, cannot be discerned. The temperature field outside the store depends on the "global" temperature level of the store.

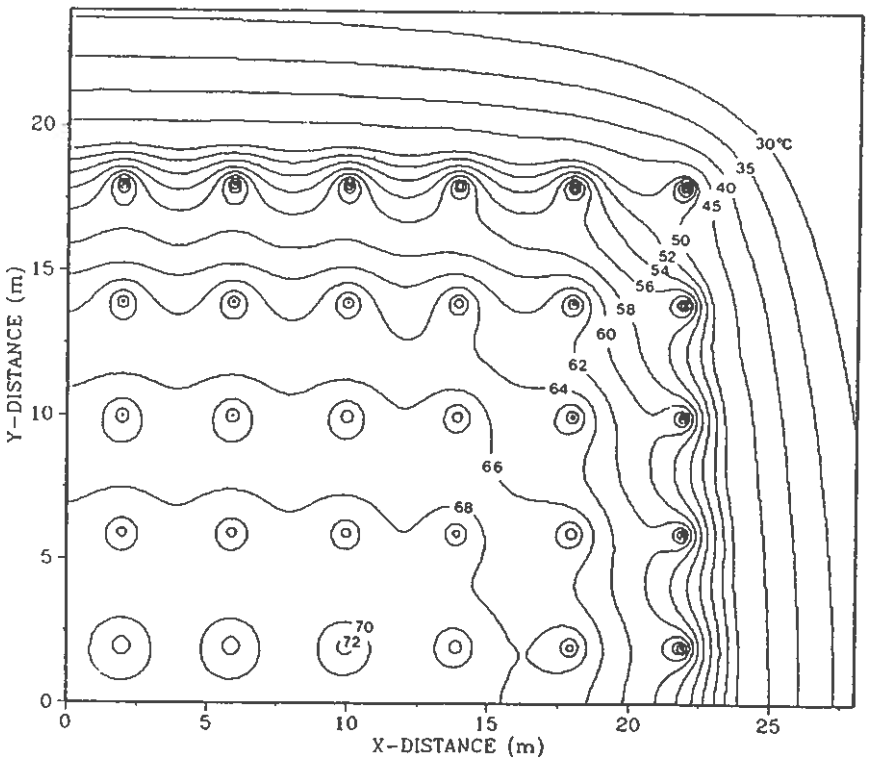

Figure 2.7. Simulated temperature field in a horizontal cut through the store at a depth of 35 m at the end of the third cycle. One-fourth of the store is shown. Heat store at Luleå University of Technology.

2.4 Description of thermal processes

The thermal process in a ground heat store can be divided into a *local process* around each ground heat exchanger (duct, borehole, plastic tube, etc.) and a macroscale or *global process* in the storage volume and the surrounding ground. Figure 2.7 shows both processes. The complete temperature field may be regarded as a superposition of a global, smooth temperature field and local temperature fields with steep gradients near the heat exchangers. A basic problem in the analysis is the interaction between the local thermal process and global thermal process.

The local process around each duct is very important. It depends to a large extent on the specific arrangements of the flow channels in the ground heat exchanger. A precise description is necessary in order to obtain the right amount of injected and extracted heat. The heat flow from the duct to the ground is determined by the fluid temperature, the heat transfer properties, and the temperature in the ground surrounding the pipe. These temperatures, and by that the heat flow, will vary also along the ducts. The amounts of injected and extracted heat will govern the global thermal process. The local values of the global temperature field are on the other hand necessary for the local problem.

The large-scale heat flow in the storage region determines the heat losses from the store. It has a genuinely three-dimensional character that must be accounted for. Typically, the ground consists of horizontal strata of different geological material. The thermal properties may vary accordingly. Thermally insulating material is often placed on the ground surface above the store to reduce heat losses. These factors and other large-scale heterogeneities of the thermal properties will influence the global thermal process.

2.5 Heat extraction boreholes

A ground heat store with deep boreholes in rock appears to be very similar to a system with multiple heat extraction boreholes (Eskilson 1987), yet there are fundamental differences in purpose and design of these systems.

Ground heat extraction systems strive after a maximum thermal interaction with the surrounding ground, while the thermal influence between adjacent boreholes is undesirable. Ideally, the boreholes should be placed as far apart as possible.

A heat storage system, on the other hand, favors minimum interaction with the ground surrounding the storage volume. A store with perfect thermal insulation would be preferable. Thermal interaction between adjacent boreholes is required in order to keep the temperature difference between the heat carrier fluid and the store at an acceptable level, and also, to raise the annual mean storage temperature above the natural undisturbed ground temperature. The mean temperature in the store will vary during the season in accordance with heat transfer rates and heat losses.

Chapter 3

Literature Survey

3.1 Conceptual development

The oil crisis in the early 70's gave incentive for development of alternative energy sources. The need for long-term energy storage became evident. The most favorable conditions for long-term storage of heat appeared to be in the ground where large storage volumes can be obtained at a low cost. Theoretical studies and field experiments involving heat storage in the ground were initiated around 1975 (Shelton 1975; Givoni 1977; de Marsily 1978).

The concept of *storing* heat in bedrock was first described by the French scientist Brun (1965, 1967) in 1965. His design shows an admirable grasp of the basic principles of ground heat storage. The first field experiments were initiated around 1976 in France (Guimbal 1976) and in Sweden (Platell and Wikström 1981). Since then, the conceptual and technical aspects of heat storage in bedrock have been further developed primarily in Sweden (Hydén et al. 1983; Andersson et al. 1983; Lundin 1985; Nordell 1987, 1990). There has also been some recent activity in Finland (Lahtinen 1983; Puntilla and Saastamoinen 1983). The basic design involves drilling a matrix of boreholes to create a heat exchanger within the rock. Conventional well-drilling technology has been used, but further development is required due to the usually big number of boreholes in the store (Schunnesson 1983).

Theoretical studies of large-scale heat storage in clay deposits were first reported by Modin (1977) in 1977. Field experiments (Ausseur and Vachaud 1978; Rosenblad 1983) as well as large-scale applications (Hultmark 1981) of this storage technique followed shortly afterwards. During the 80's a few more heat stores have been built in clay (Olsson 1983; Chuard et al. 1983; Lehtmets 1990) and in sandy soil (Wijsman 1983). Seasonal storage in clay for greenhouses has also been investigated (Areskoug and Wigström 1980; Nir 1983). The construction methods for heat storage in soft geological media,

such as clay and sandy soil, seem to be fairly well established, although the design of the ground heat exchanger may be further improved (Hellström et al. 1985; Wilén et al. 1985). Heat storage in clay deposits has in the past been restricted to the low-temperature range due to the possible detrimental effects on the geotechnical properties of clay at high temperatures (Adolfsson et al. 1983). There is, however, a current interest to use heat storage in clay at high temperatures (Sundberg 1990; Landtechnik Weihenstephan 1990).

In order to optimize the energy system with a ground heat store, it is necessary to have analytical tools by which the thermal behavior of the store can be assessed. The local thermal processes around a duct have been studied in detail (Claesson et al. 1985; Claesson and Hellström 1988). Numerical studies of the natural convection induced by heating a store in sandy soil and the influence of regional flow have been done (van Meurs 1985). Simple methods for estimation of the thermal performance are available (Claesson et al. 1985). Detailed simulation models for the store (Hadorn 1981; Hellström 1982; Hadorn and Chuard 1983; Wijsman and van Meurs 1985; Eskilson and Claesson 1988; Baudoin 1988) or an energy system with a ground heat store (Mazzarella 1989; Lund and Östman 1985) have been developed.

The first conference devoted to ground heat storage was held in 1978 (Lawrence Berkeley Laboratory 1978). Since then, the know-how of long-term heat storage in the ground has grown considerably (Swedish Council for Building Research 1983; Public Works of Canada 1985; Agence Francaise pour la Maîtrise de l'Énergie 1988). The Seasonal Thermal Energy Storage (STES) Newsletter, which is published by the International Council for Thermal Energy Storage, provides a quarterly review of current research activities.

3.2 Solar energy and seasonal storage

In 1979, the International Energy Agency initiated an investigation to establish the feasibility and cost-effectiveness of central solar heating plants with seasonal storage (CSHPSS). During the investigation a large amount of technical and economical data has been compiled and analytical tools have been developed. The status report published in 1990 (Dalenbäck) is an important source of information on this subject. Let us quote the most important conclusions regarding ground heat storage:

- The key issue for further development of CSHPSS, in order to be cost-effective in all countries, is further development of the storage technology. Specifically there is a need for internationally coordinated R&D on high temperature storage.

- Development of simple and general design tools, to be used by designers and consultants in feasibility studies, is also an important issue.

- For many preliminary studies, however, sufficiently accurate results can probably be obtained by simpler methods based on analytical solutions of simplified models.

- One of the distinguishing characteristics of a CSHPSS as compared to other solar and non-solar heating plants is that, because of their large size and coupling with the ground, they respond very slowly to changes in operation. It usually takes a very long time to evaluate their performance and to determine experimentally the most effective control strategies.

  In most plants it will be impractical to attempt to develop the best operational strategy, based on observations of the plant operation, because of the very slow rates of change and the susceptibility to stochastic variables such as the weather. It is, therefore, cost effective to study the response of CSHPSS to control strategies by the use of accurate dynamic system models.

- Seasonal storage offers a way to integrate solar energy with other renewable and waste heat energy sources. CSHPSS are technically feasible and economically competitive with fossil fuels, for large load applications of more than 50 GWh per year, or about 2000 residential units.

An international state-of-art review on this topic has also been published by Bankston (1988).

3.3 Field experiments

A fair number of field experiments and full-scale projects have been completed. These applications include storage in clay, peat, sandy-soil, moraine, and rock. They are summarized in Table 1. The largest stores are located at Kungsbacka, where a clay volume of 80,000 m^3 is used, and at Finspång, with a rock volume of 220,000 m^3.

TABLE 2.1. Characteristics of field experiments on ground heat storage. Site of store, start of operation, size (m^3), storage temperature range (°C), type of ground heat exchanger (GHE), load type, and type of energy source. Abbreviations: HB=horizontal bundle of pipes, VU=vertical single U-pipe, VU2=vertical double U-pipe, VP=vertical single bisected pipe, VS=vertical annular steel pipe, VA=vertical annular pipe, CA=closed annular duct, OA=open annular duct, CU=closed single U-pipe, RU=residential unit, F=France, I=Italy, NL=Netherlands, SUI=Switzerland, S=Sweden.

Location	Year	Size	Temp	GHE	Load	Source
CLAY						
Alnarp[1], S	1979	1,500	10–45	HB	Greenhouse	Solar
Kullavik[2], S	1983	8,100	10–55	VU	40 RU	Solar
Kungsbacka[3], S	1981	80,000	10–16	VU	School	Solar
Söderköping[4], S	1987	36,000	5–30	VU2	School, Sport	Air
Utby[5], S	1979	1,000	4–12	VP	1 RU	Air
Varese[6], I	1981	3,000		VS		Solar
Vaulruz[7], SUI	1983	3,500	4–45	HB	Garage, office	Solar
MORAINE						
Meyrin[8], SUI	1988	20,000	5–30	VU2	Office	Solar
PEAT						
Härryda[9], S	1981	18,000	6–16	HB	School	Solar
SANDY SOIL						
Gronningen[10], NL	1983	23,000	30–60	VU	96 RU	Solar
Neuchâtel[11], SUI	1981	4,500	5–25	VP	12 RU	Solar
ROCK						
Cormontreuil[12], F	1986	15,000	20–60	CA	Function hall	Solar
Finspång[13], S	1985	220,000	10–35	CU	750 RU, sport	Waste
Finspång[14], S	1984	42,000	15–30	CU	Super market	Waste
Luleå I[15], S	1981	7,000	5–45	OA		
Luleå II[16], S	1983	115,000	30–65	OA	District heat	Waste
Märsta, S[17]	1985	32,000	4–14	CU	42 RU	Air
Sigtuna, S[18]	1978	10,000	10–40	CA	1 RU	Solar
Vallentuna[19], S	1984	10,000	0–15	CU		

References: 1. Areskoug and Wikström (1980), 2. Olsson (1983), 3. Hultmark (1981), 4. Lehtmets (1990), 5. Rosenblad (1983), 6. Aranovitch et al. (1985), 7. Hadorn et al. (1985), 8. Guisan et al. (1990), 9. Lundin (1985), 10. Wijsman (1983), 11. Mathey and Pilonel (1985), 12. Baudoin (1988), 13-14. Magnusson and Sundberg (1990), 15. Andersson et al. (1983), 16. Nordell (1990), 17. Lundin (1985), 18. Platell and Wigström (1981), 19. Lundin (1985).

Chapter 4

Outline of Contents

This chapter gives an outline of the contents and the conceptual structure of this study. Basic ideas and concepts are presented. The presentation starts from the heat carrier fluid and the heat exchanger and proceeds 'outwards' with increasing characteristic time-scales to end with the global thermal process.

There is a thermal process between the heat carrier fluid and the ground immediately outside the heat exchanger, which is represented by a *fluid-to-ground thermal resistance*. The heat exchangers interact with the surrounding ground in a *local thermal process* around each heat exchanger. Finally, there is a macroscale or *global process* in the storage volume and the surrounding ground.

The fluid-to-ground resistance and the local process determine the heat transfer capacity of the ground heat exchanger. These two parts depend on the thermal properties and the specific arrangements of the flow channels in the ground heat exchanger, the thermal properties of the surrounding ground, and the distances between adjacent heat exchangers. The global process determines the heat losses from the store. It has a genuinely, three-dimensional character that must be accounted for. A basic problem in the analysis is the interaction between the local thermal process and global thermal process.

4.1 Fluid-to-ground thermal resistance

The heat transfer between the fluid and the ground involves many processes. There is convective heat transfer at the duct wall, and heat conduction in the pipe walls, filling materials, etc. There are also contact resistances at the interfaces between different materials. It is assumed that the heat capacity of the material between the fluid and the ground is small, so that the capacitive effects of these parts can be neglected.

The thermal resistances associated with these different parts may be assembled to form a single fluid-to-ground thermal resistance R_b (K/(W/m)). The basic relation between the heat injection/extraction rate, q (W/m), and the difference between the fluid temperature T_f and the temperature T_b in the ground immediately outside the ground heat exchanger is then:

$$T_f - T_b = q \cdot R_b \tag{4.1}$$

4.1.1 Convective heat transfer in ducts

There are the two basic flow channel geometries to consider, namely, circular tubes and circular-tube annuli. See figure 4.1.

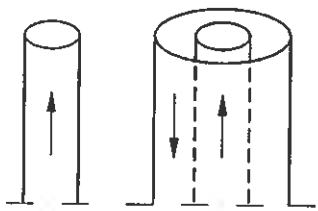

Figure 4.1. Convective heat transfer in a circular tube and a circular-tube annulus.

The convective heat transfer during laminar flow may give rise to thermal resistances between the heat carrier fluid and the duct wall that are comparable to the thermal resistance between the duct wall and the store. Thus, the convective heat transfer is important.

An extensive literature survey on the convective heat transfer is presented in Chapter 7.

4.1.2 Ducts in a composite region

The procedure to calculate the fluid-to-ground thermal resistance is straightforward, except for the case of ducts in a composite region such as boreholes with U-shaped inner pipes and similar arrangements. The borehole outside the pipes is assumed to be filled with a solid material. The two-dimensional problem is illustrated schematically in figure 4.2. The heat flow between the flow channels and the borehole wall will be represented by a thermal Δ-circuit. An advanced analytical method, the multipole method, has been developed to obtain the resistances for this case.

Formulas for R_b for many types of ground heat exchangers are given in Chapter 8.

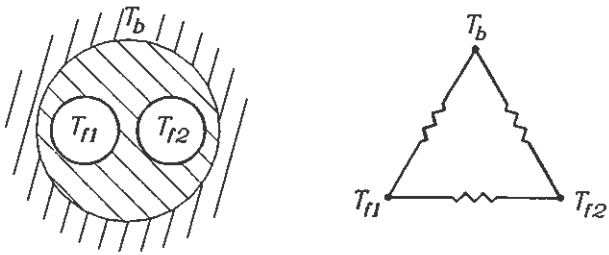

Figure 4.2. Ducts in a composite region and the corresponding Δ-circuit.

4.1.3 Effective fluid-to-ground thermal resistance

The temperature varies *along* the flow channels with an ensuing internal heat exchange between the pipes. This problem is studied in sections 8.5-6. Relatively simple formulas for an effective fluid-to-ground thermal resistance are derived for simplified boundary conditions along the ground heat exchanger. This effective thermal resistance R_b^* is defined by:

$$\bar{T}_f - \bar{T}_b = \bar{q} \cdot R_b^* \tag{4.2}$$

Here, $\bar{T}_f$, $\bar{T}_b$, and $\bar{q}$ are the average values along the ground heat exchanger.

4.2 Local thermal process

The local thermal process concerns the ground volume around a heat exchanger. The ground heat exchangers are assumed to be uniformly placed in the storage region. In this study we will consider in particular rectangular and hexagonal duct patterns according figure 4.3.

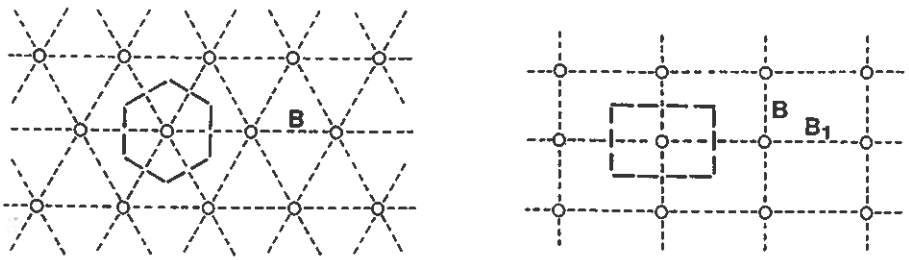

Figure 4.3. Hexagonal (left) and rectangular (right) duct pattern.

A certain ground region may be assigned to each ground heat exchanger due to symmetry. See figure 4.3. The cross-sectional area of this local ground region is denoted A_p. For the rectangular duct pattern with a duct spacing B and B_1, the cross-sectional area is $A_p = B \cdot B_1$.

The average temperature in the ground region that is assigned to a ground heat exchanger is called the *local average temperature* T_m. We are interested in the relation between heat injection rate q and the difference $T_f - T_m$. This gives the important heat transfer capacity of the heat exchanger system.

The heat injection rate $q(t)$ may by superposition be divided into simpler components. An analysis based on step-pulses is presented in chapter 10, while periodic components are dealt with in chapter 11. A useful concept is the so-called steady-flux regime, which is dealt with in considerable detail in Chapter 9.

4.2.1 Step-pulse analysis

The heat injection rate $q(t)$ may be approximated by step-wise constant values. See figure 4.4, left. Any such $q(t)$ may by superposition be regarded as a series of simple heat injection steps. The problem is reduced to the basic heat injection step $q(t) = +1, t > 0$, which is shown in figure 4.4, right.

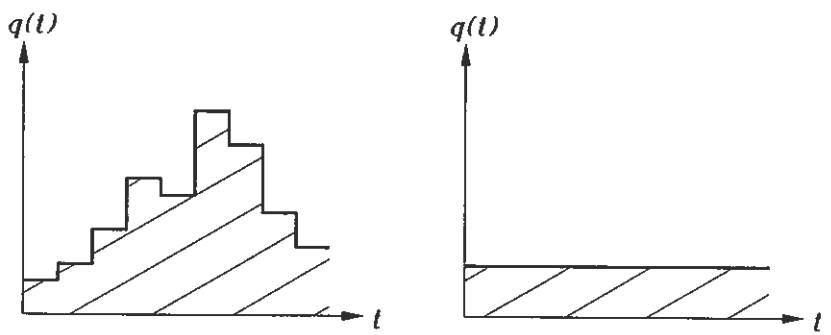

Figure 4.4. Step-wise constant heat injection (left) and the basic heat injection step (right).

Let $T_f^q(t)$ denote the fluid temperature for a heat injection step q_1. We may define a time-dependent step-pulse resistance $R_q(t)$:

$$T_f^q(t) - T_m = q_1 \cdot R_q(t) \tag{4.3}$$

The step-pulse analysis is presented in chapter 10.

4.2.2 Steady-flux regime

Consider the basic heat injection step. During a first period there is no interaction between the different heat exchangers, but after a certain time there will be a full interaction between adjacent heat exchangers. The heat flux through the boundaries (dashed lines in figure 4.3) of the local region around a ground heat exchanger is zero due to symmetry. The temperature in the local region will then increase linearly with time. There is a time-independent temperature profile through the local region. This case of constant heat injection or extraction of long duration is characterized by the fact that the heat flow field in the local ground region do not change with time. We have the important *steady-flux* regime.

The difference between $T_f(t)$ and $T_m(t)$, which both increase linearly with time, becomes constant. This defines the steady-flux thermal resistance R_{sf}:

$$T_f - T_m = q \cdot R_{sf} \tag{4.4}$$

Analytical solutions and in particular formulas for R_{sf} for many pertinent cases are reported in Chapter 9.

4.2.3 Periodic processes

Periodic solutions are studied in Chapter 11. The relation between the heat injection rate and the fluid temperature during a regular periodic (sinusoidal) variation shows the characteristics of the thermal behavior. The ratio between the complex-valued amplitudes of the fluid temperature and the heat injection rate defines the complex-valued periodic resistance $\hat{R}_g$ of the local ground region.

$$\hat{T}_f = \hat{q} \cdot (\hat{R}_g + R_b) \tag{4.5}$$

4.2.4 Thermal resistances

The heat transfer capacity between heat carrier fluid and surrounding local region is obtained from formulas of the types (4.1-5). They involve the thermal resistances R_b, R_b^*, $R_g(t)$, R_{sf} and $\hat{R}_g$, which all have the dimension K/(W/m). This representation with resistances makes it possible to compare quite simply and directly different parts of the total heat transfer capacity of the ground heat exchangers. Many such studies will be presented in the forthcoming part II.

4.3 Global process

The local average temperature T_m in the region around a heat exchanger will vary along and between the heat exchangers. It represents a global temperature field in the storage region, upon which the local temperature fields are superimposed. This global temperature field and the temperature field in the surrounding ground will be referred to as the *global thermal process.* This global process is then coupled to the injection/extraction rates of the heat exchangers, but it is not in any other way dependent on the local thermal processes.

The global heat flows through the storage boundaries give the heat losses from the store. During the initial years there is a transient *thermal build-up* of the temperature field around the store. The annual heat losses will gradually approach a *steady-state* value. During the storage cycle there is a superimposed *periodic variation.* These three fundamental components of the global process are dealt with in Chapter 12.

4.3.1 Steady-state heat loss

The steady-state component, which is dealt with in section 12.2, concerns the steady-state heat flow process in the surrounding ground between the surface of the store and the ground surface. There is a suitable constant temperature T_m on the storage surface and the mean annual temperature T_0 at the ground surface. The heat loss Q_s (W) may by dimensional analysis be written in the following way:

$$Q_s = \lambda(T_m - T_o)L \cdot h \tag{4.6}$$

Here L is a scaling length and h a dimensionless heat loss factor. The quantity $1/(\lambda Lh)$ is the thermal resistance between T_m and T_o.

The heat loss is obtained by calculating the three-dimensional steady-state temperature field. Storage volumes with a rectangular or cylindrical shape have been studied.

4.3.2 Thermal build-up

The thermal build-up refers to the extra heat needed during the intial years in order to attain the steady-state temperature levels in the ground around the store.

Let $Q_t(t)$ denote the transient heat loss through the storage surface, when it is kept at an average level T_m from the start $t = 0$. The initial temperature in the ground is T_o. From a dimensional analysis we get:

$$Q_t = \lambda(T_m - T_o)L \cdot h_t \tag{4.7}$$

The dimensionless transient heat loss factor h_t is time-dependent. It tends to the steady-state value h for large times. Values for different storage geometries are given in section 12.3. The quantity $1/(\lambda L h_t)$ corresponds to R_q in the pulse analysis.

4.3.3 Periodic heat loss

The periodic variation of the storage surface during the storage cycle induces a periodic heat flux through the surface against the ground. This process is discussed in section 12.4. We obtain in complex-valued notation expressions of the type:

$$\hat{Q}_1 = \hat{T}_1 / \hat{R}_{\text{ground}} \tag{4.8}$$

Very handy expressions for the periodic thermal resistance of the ground around the store are given in section 12.4.

Chapter 5

Basic Assumptions and Thermal Properties

The thermal analyses of the ground heat store are based on a few assumptions about the thermal process in the ground. These assumptions are stated in section 5.1. The validity of these assumptions is discussed in section 5.2.

5.1 Basic assumptions

The basic assumptions for the thermal analyses are:

1. The heat transport in the ground takes place solely by heat conduction.
2. The thermal properties in the ground, or in a subregion of the ground, can be represented by constant values.

5.2 Discussion of heat transport mechanisms

The heat transport in the ground may take place by conduction, convection, evaporation/condensation, and radiation.

Heat conduction apart, the most important mode is convective heat transfer caused by ground water movement through the storage region. There may be both regional flow, caused by hydraulic gradients at the site of the store, and natural convection induced by the increased temperatures in the storage region. The regional groundwater flow may increase the heat losses from a store located in a permeable ground layer. A numerical study by van Meurs (1985) concerning a porous medium with homogeneous hydraulic properties indicates that the heat store requires a protecting hydraulic screen if the ground water flow exceeds 50 mm/day. Ground water flow in crystalline rock takes place through fissures and fractured zones within the rock mass. The

magnitude of the ground water flow through the storage region depends on the number of fissures, the width of the fissures, the extension of the fractured zones, and the local hydraulic gradients. These factors are very site-specific and a general statement about the influence on the thermal behavior of the heat store is difficult to make. The experience from the field projects realized to date shows that large storage volumes can be obtained in bedrock where ground water flow presents minor problems. However, it is obvious that under certain conditions the influence of ground water flow in crystalline rock can cause considerable heat losses.

The heating of a water-saturated ground material will induce natural convection due to the temperature-dependent density of water. Buoyancy flow will cause warmer water with lower density to flow upwards. For a ground heat store in a porous medium the natural convection currents will be most pronounced at the vertical boundaries of the store. These currents will cause warm water to flow out from the upper part of the store and cold water to flow into the lower part. The magnitude of the buoyancy flow depends primarily on the temperature levels of the store and the surrounding ground, the horizontal and vertical permeability of the ground material, and the vertical extension of the store (Hellström et al. 1988). Numerical studies (van Meurs 1985; Lund 1985) show that, under normal applications, the thermal performance of the store will be affected if the permeability of the ground exceeds 10^{-12} m^2. However, the presence of interspersed horizontal layers of clay, which are practically impermeable, will reduce the natural convection.

In the unsaturated zone, where the degree of water-saturation varies considerably, temperature gradients will cause moisture migration. High porosity, low degree of water-saturation, and temperatures above 25°C are conditions at which moisture migration becomes an important mode of heat transfer (Sundberg 1988). Although this moisture migration is unimportant as a heat transfer mechanism for other conditions, it may still have an effect on the thermal properties of the soil. As an example, large heat injection rates may cause the soil around a duct to dry up. Since dry soil has a much lower thermal conductivity than wet soil, this will create an undesirable insulating effect between the heat carrier fluid and the storage capacity. Thereby the heat transfer capacity of the ground heat exchanger will be reduced.

In a longer perspective, it is possible that moisture migration will reduce the water content at the upper surface of a store, which will lower heat capacity in this region. A similar problem occurs when the ground water level fluctuates within the storage volume. This leads to large variations in thermal properties.

Radiative heat transport can usually be neglected, unless there are large fractions of air in regions with large temperature gradients.

As a conclusion, heat conduction is the main heat transport mechanism in water-saturated low-permeability soils and rocks, while high permeabil-

ity materials are likely to be influenced by convection. Heat transport by evaporation/condensation may occur in high-porosity materials with low or intermediate degree of water-saturation and high temperatures.

5.3 Thermal properties

The thermal properties of the ground are mainly determined by the mineral content, the porosity, and the degree of water-saturation. The thermal properties of these constituents are roughly those given in Table 5.1.

TABLE 5.1. Thermal conductivity λ (W/mK) and volumetric heat capacity C (MJ/m^3K) of minerals, water, and air. Approximate values.

	λ	C
Minerals	2-7	~2
Water	0.6	4.2
Air	0.024	0.0013

The thermal conductivity tends to decrease with increasing porosity, since both water and air are less conductive than minerals. The heat capacity, on the other hand, increases with higher water content.

When ground heat exchangers are inserted in soils, the installation procedure may disturb the soil structure near the heat transfer ducts. Such small-scale inhomogeneities are not significant for the large-scale heat flow in the store, but may have to be accounted for in the local thermal process around the ducts.

Thermal properties of soils and rocks in Sweden are given in Appendix A. Crystalline rocks have a low porosity on the order of a few percent. The thermal conductivity is then determined mainly by its mineral contents. The values for Swedish rocks range from 2 to 5 W/mK, with a typical value of 3-4 W/mK. The thermal conductivity of granite decreases with about 10% for a temperature change from 0°C to 100°C (Brehm 1989).

The porosity of sedimentary rocks in Sweden is on the order of 10-20%. Mineral content, porosity, and degree of water-saturation level will decide the thermal properties.

The porosity of soils varies in a wider range. Some kinds of moraine have a porosity of 15%, while peat may contain almost 100% water. The thermal properties are strongly dependent on the degree of water-saturation.

To sum up, the important factor for variations in thermal properties during a storage cycle is the degree of water-saturation. Changes in water-saturation level occur in the unsaturated zone, especially near the ground water level. In permeable materials there may also be significant fluctuations in the ground-water level.

Chapter 6

Mathematical Equations and Methods

An overview of the basic equations and conditions that govern the thermal process in the ground will be presented in this section.

6.1 Partial differential equations

The heat transport in the ground is assumed to take place solely by heat conduction. Fourier's law states that the heat flow $\vec{q}$ at a given point in a solid is proportional to the gradient of the temperature $T(x, y, z, t)$, namely:

$$\vec{q} = -\lambda \nabla T \tag{6.1}$$

The components of the heat flow vector are:

$$q_x = -\lambda \frac{\partial T}{\partial x} \quad q_y = -\lambda \frac{\partial T}{\partial y} \quad q_z = -\lambda \frac{\partial T}{\partial z} \tag{6.2}$$

The proportionality constant λ is the thermal conductivity of the solid. The thermal conductivity may depend on the spatial coordinates, temperature, etc. We will assume that the ground is either homogeneous, or composed of several subregions with homogeneous, but different, thermal properties. The thermal conductivity has a constant value for each such subregion.

A heat balance for an element of volume gives:

$$C \frac{\partial T}{\partial t} + \nabla \cdot \vec{q} = 0 \tag{6.3}$$

where C is the volumetric heat capacity ($\mathrm{J/m^3K}$) of the ground. Inserting the heat flow vector (6.1) yields the general heat equation:

$$\nabla \cdot (\lambda \nabla T) = C \frac{\partial T}{\partial t} \tag{6.4}$$

In the case of constant thermal properties this simplifies to:

$$\nabla^2 T = \frac{1}{a}\frac{\partial T}{\partial t} \tag{6.5}$$

Here, $a = \lambda/C = \lambda/(\rho c)$ with the dimension m^2/s is the thermal diffusivity. Expressed in cartesian coordinates, (x, y, z), eq. (6.5) becomes:

$$\frac{\partial^2 T}{\partial x^2} + \frac{\partial^2 T}{\partial y^2} + \frac{\partial^2 T}{\partial z^2} = \frac{1}{a}\frac{\partial T}{\partial t} \tag{6.6}$$

This is the three-dimensional formulation of the time-dependent heat equation. The two- and one-dimensional cases are obtained by omitting one or two terms on the left side of (6.6).

For cylindrical heat stores and ducts with a circular cross-section, the heat equation (6.5) is preferably expressed with use of cylindrical coordinates (r, z):

$$\frac{\partial^2 T}{\partial r^2} + \frac{1}{r}\frac{\partial T}{\partial r} + \frac{\partial^2 T}{\partial z^2} = \frac{1}{a}\frac{\partial T}{\partial t} \tag{6.7}$$

In the analysis of ducts, the heat conduction in the axial direction is often neglected. We will then have a thermal process in the radial direction:

$$\frac{\partial^2 T}{\partial r^2} + \frac{1}{r}\frac{\partial T}{\partial r} = \frac{1}{a}\frac{\partial T}{\partial t} \tag{6.8}$$

6.1.1 Steady-state equation

At steady-state conditions, the temperature field does not change with time. It becomes a function only of the spatial coordinates. From (6.5) we have that $\nabla^2 T = 0$, which in cartesian coordinates is expressed by:

$$\frac{\partial^2 T}{\partial x^2} + \frac{\partial^2 T}{\partial y^2} + \frac{\partial^2 T}{\partial z^2} = 0 \tag{6.9}$$

6.1.2 Steady-flux equations

The steady-flux regime is characterized by a uniform, constant temperature increase at each point in the ground. The temperature consists of two parts: one part that only depends on the spatial coordinates, and one part that gives the linear increase with time:

$$T(x, y, z, t) = T_{sf}(x, y, z) + \frac{Qt}{C_T} \tag{6.10}$$

Here, Q is the total heat injection rate to the considered bounded region. The heat capacity (J/K) of the bounded region V is denoted C_T. It is given by:

$$C_T = \int_V C(x, y, z)\, dxdydz \tag{6.11}$$

Insertion of (6.10) in (6.5) shows that the steady-flux temperature profile T_{sf} satisfies the equation:

$$\nabla^2 T_{sf} = \frac{Q}{\lambda C_T / C} \tag{6.12}$$

For constant C the right-hand side becomes $Q/(\lambda V)$. The boundary conditions are given constant heat fluxes on different parts of the boundary.

The heat content of the steady-flux temperature profile is set to zero:

$$\int_V C(x,y,z)\, T_{sf}(x,y,z)\, dxdydz = 0 \tag{6.13}$$

In the case of constant heat capacity, this requirement simplifies to:

$$\int_V T_{sf}(x,y,z)\, dxdydz = 0 \tag{6.14}$$

which means that the average value of the steady-flux temperature is zero.

6.1.3 Equations for periodic solutions

The conditions of a periodic thermal process are such that temperatures and heat flows are repeated with a certain time interval. The duration of this interval, the period time, will be denoted t_p. Any periodic process can by Fourier series expansions be represented by a linear combination of sine- and cosine functions (Carslaw and Jaeger 1959; p. 180).

A complex-valued representation of the temperature is used:

$$T(x,y,z,t) = \hat{T}(x,y,z)\, e^{i2\pi t/t_p} \tag{6.15}$$

The function $\hat{T}(x,y,z)$ contains the spatial dependence. The symbol $\hat{}$ indicates that the temperature is complex-valued. The time-dependence is given by the factor:

$$e^{i2\pi t/t_p} = \cos(2\pi t/t_p) + i \cdot \sin(2\pi t/t_p) \tag{6.16}$$

Real-valued solutions are obtained by taking the real or imaginary part of (6.15). Let $u(x,y,z)$ and $v(x,y,z)$ denote the real and imaginary part of $\hat{T}(x,y,z)$, so that

$$\hat{T}(x,y,z) = u(x,y,z) + i \cdot v(x,y,z) \tag{6.17}$$

The *absolute value* and the *argument* of $\hat{T}$ become:

$$|\hat{T}| = \sqrt{u^2 + v^2} \qquad \arg(\hat{T}) = \arctan\left(\frac{v}{u}\right) \qquad \text{for } u > 0 \tag{6.18}$$

The complex-valued temperature can then be expressed in polar form:

$$\hat{T} = |\hat{T}| \cdot e^{i \cdot \arg(\hat{T})} \tag{6.19}$$

The real-valued expressions for $T(x,y,z,t)$ are now by (6.15) and (6.19):

$$T(x,y,z,t) = |\hat{T}| \cdot \cos\left\{2\pi t/t_p + \arg[\hat{T}(x,y,z)]\right\} \tag{6.20}$$

$$T(x,y,z,t) = |\hat{T}| \cdot \sin\left\{2\pi t/t_p + \arg[\hat{T}(x,y,z)]\right\} \tag{6.21}$$

The temperature $T(x,y,z,t)$ satisfies the heat equation. By (6.15) and (6.5) the partial differential equation for the complex-valued temperature $\hat{T}$ becomes:

$$\nabla^2\hat{T} = \frac{2\pi i}{at_p}\hat{T} = \left(\frac{1+i}{d_p}\right)^2\hat{T} \tag{6.22}$$

Here, d_p is a characteristic length for the periodic thermal process defined by:

$$d_p = \sqrt{\frac{at_p}{\pi}} \tag{6.23}$$

It will be called the *penetration depth*. It will be further discussed in section 12.4.1.

6.1.4 Heat sources

The details of the heat exchange between the ducts and the ground are not important for the large-scale heat flow process in the store and the surrounding region. The heat injection from the ducts may in the large-scale problem be treated as a heat source. The heat equation (6.4) takes the following form when a heat source q_v (W/m^3) is added:

$$\nabla \cdot (\lambda \nabla T) + q_v = C\frac{\partial T}{\partial t} \tag{6.24}$$

6.2 Boundary conditions

Three types of boundary conditions will be used in the analyses: prescribed surface temperature, prescribed heat flux, and heat flow proportional to the temperature difference over a surface thermal resistance.

When the ground region is composed of several subregions with different thermal properties, there are internal boundaries between these subregions. The conditions at these internal boundaries must also be considered.

6.2.1 Prescribed surface temperature

The boundary condition with prescribed surface temperature does not need many comments. The boundary temperature is simply a prescribed function of time. The simplest case being a constant value. An example is the ground surface temperature, which often will be represented by a constant average value.

6.2.2 Prescribed heat flux

The heat flux q (W/m^2) in the normal direction of the boundary may also be a prescribed function of time. From (6.1) we have:

$$-\lambda \frac{\partial T}{\partial n} = q(t) \qquad (\mathrm{W/m^2}) \tag{6.25}$$

where $\partial T/\partial n$ denotes the derivative in the direction of the inward normal of the boundary.

The heat injection rate from the ducts will usually be given per unit axial length of the ground heat exchanger. The boundary condition (6.25) for a duct with a radius r_b is then:

$$-2\pi r_b \lambda \left.\frac{\partial T}{\partial r}\right|_{r=r_b} = q(t) \qquad (\mathrm{W/m}) \tag{6.26}$$

6.2.3 Surface thermal resistance

The heat transfer from the fluid in the ducts to the surrounding ground takes place via the material of the duct wall. The heat equation is, however, not solved for the thermal process in the duct wall, since the time scale of this process is comparatively short. The effect of the duct wall is included as a surface thermal resistance between the fluid and the ground. The heat flow is proportional to the temperature difference over this resistance. The boundary condition for a circular duct with the radius r_b becomes:

$$q(t) = -2\pi r_b \lambda \left.\frac{\partial T}{\partial r}\right|_{r=r_b} = [T_f - T(r = r_b)] \cdot \frac{1}{R_b} \qquad (\mathrm{W/m}) \tag{6.27}$$

where the fluid-to-ground thermal resistance (K/(W/m)) is denoted R_b, the fluid temperature is T_f, and the temperature in the ground immediately outside the duct wall is $T(r = r_b)$.

It is common to express this type of boundary condition with use of a heat transfer coefficient α (W/m^{2}K). The heat flux q' (W/m^2) is then:

$$q'(t) = -\lambda \left.\frac{\partial T}{\partial r}\right|_{r=r_b} = \alpha [T_f - T(r = r_b)] \qquad (\mathrm{W/m^2}) \tag{6.28}$$

From (6.27) and (6.28) we obtain a relation between the thermal resistance R_b and the heat transfer coefficient α for a circular pipe, namely:

$$R_b = \frac{1}{2\pi r_p \alpha} \tag{6.29}$$

Thermal insulation sheets are also treated as surface thermal resistances. Consider a thermal insulation at the ground surface. The ground surface

temperature is T_0, and the temperature in the ground below the insulation is $T(z = 0)$. The coordinate z gives the depth below the ground surface. The boundary condition becomes:

$$-\lambda \frac{\partial T}{\partial z}\bigg|_{z=0} = [T_0 - T(z = 0)] \cdot \frac{1}{R} \qquad (\mathrm{W/m^2}) \qquad (6.30)$$

where R is the thermal resistance of the insulation.

6.2.4 Internal boundaries

When the ground consists of several subregions with different thermal properties, there are further conditions that must be fulfilled: The heat flow in the normal direction and the temperature must be continuous at the interfaces between the subregions.

6.3 Initial conditions

Transient problems require that the temperature field is known at the start of the calculation. For processes that involve the storage region and the surrounding ground, we will use the natural, undisturbed temperature. Thermal processes with a limited range of thermal influence around the ducts will usually by analyzed with temperatures taken relative to the large-scale average temperature in the ground.

6.4 Heat balance for heat carrier fluid

In ground heat exchangers, there is a convective heat flow along the flow channels and a transverse heat exchange between the fluid and the ground. The temperature gradients in the axial direction are small, so that axial heat conduction can be neglected. A heat balance for the fluid at a certain point of a circular flow channel with the radius r_b gives:

$$C_f \pi r_b^2 \frac{\partial T_f}{\partial t} = 2\pi r_b \lambda \frac{\partial T}{\partial r}\bigg|_{r=r_b} - C_f V_f \frac{\partial T_f}{\partial z} \qquad (6.31)$$

The temperatures in the fluid and in the ground are T_f and T, respectively. The volumetric heat capacity of the fluid is C_f, the fluid flow rate is V_f ($\mathrm{m^3/s}$), and z is a coordinate along the flow channel. The term on the left gives the rate of energy increase. The first term on the right is the rate of heat transfer from the ground to the duct, while the last term gives the contribution from the convective heat flow in the pipe.

A special case of (6.31) is so-called local steady-state conditions, when the transient effects of the fluid can be neglected. The heat flow from the ground then balances the convective heat flow in the ducts:

$$C_f V_f \frac{\partial T_f}{\partial z} = 2\pi r_b \lambda \left.\frac{\partial T}{\partial r}\right|_{r=r_b} \tag{6.32}$$

The analysis of the temperature variations along the flow channels (see sections 8.6, 9.4, and 11.5) yields especially simple formulas if we use an average fluid temperature $\bar{T}_f$ defined by:

$$\bar{T}_f = \frac{1}{2}(T_{fin} + T_{fout}) \tag{6.33}$$

where T_{fin} and T_{fout} are the inlet and outlet temperature, respectively. A heat balance for the fluid gives a relation between the heat injection rate Q and the inlet and outlet fluid temperatures for a ground heat exchanger.

$$T_{fin} - T_{fout} = \frac{Q}{C_f V_f} \tag{6.34}$$

If $\bar{T}_f$ and Q are known, the inlet and outlet temperatures can, by (6.33) and (6.34), be calculated from:

$$\begin{aligned} T_{fin} &= \bar{T}_f + \frac{Q}{2C_f V_f} \\ T_{fout} &= \bar{T}_f - \frac{Q}{2C_f V_f} \end{aligned} \tag{6.35}$$

6.5 Superposition technique

A complicated thermal process can often be treated as a superposition of several components, where each component has a rather simple structure. These components can then be analyzed separately. An advantage of this procedure is that the understanding of the thermal process is enhanced.

The superposition technique can be applied if the governing equations are linear, which requires that the thermal properties are independent of temperature. In this study we will use constant thermal properties. Thereby, the superposition technique can be used without restrictions.

As an illustration of the superposition technique, let us consider a one-dimensional thermal process in the region $0 < x < L$. The linearity of the heat equation implies that if u_n is a solution of

$$\frac{\partial^2 u_n}{\partial x^2} = \frac{1}{a}\frac{\partial u_n}{\partial t} \tag{6.36}$$

,then any linear combination of such solutions is also a solution, namely

$$u(x,t) = \sum_{n=1}^{N} a_n u_n(x,t) \tag{6.37}$$

The coefficients a_n are determined by the initial condition:

$$u(x,0) = \sum_{n=1}^{N} a_n u_n(x,0)$$

and the boundary conditions, for instance prescribed surface temperatures:

$$\begin{aligned} u(0,t) &= \sum_{n=1}^{N} a_n u_n(0,t) \\ u(L,t) &= \sum_{n=1}^{N} a_n u_n(L,t) \end{aligned} \tag{6.38}$$

Superposition can be performed in both space and time. As an example, let us take analyses of ground heat exchangers with multiple heat transfer channels. The temperature field from a single channel is used as the fundamental solution. Superimposing one such solution for each heat transfer channel gives the total temperature field. This type of superposition is described in sections 8.4.1, 9.3.1 and 10.3.

The variation of the heat injection rate can often be approximated by a sequence of step-pulses. A step-pulse during the time $t_1 \leq t \leq t_2$ is obtained by superimposing two step-changes in heat injection rate. See figure 6.1.

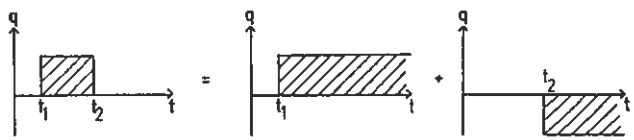

Figur 6.1. Step-pulse obtained by superimposing two step-changes in heat injection rate.

The total heat injection rate is a sequence of such step-pulses. An example is shown in figure 6.2. This means that the basic solution is the unit step change. Any piece-wise constant heat injection is obtained from a suitable superposition of unit steps.

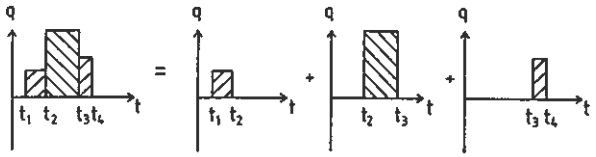

Figur 6.2. Sequence of step-pulses.

6.6 Similarities

It is interesting to note the similarities of the above special cases of the heat equations. We have for steady-state, steady-flux, periodical, and general transient conditions:

$$\begin{array}{lcll} \nabla^2 T & = & 0 & \text{(steady-state)} \\ \nabla^2 T & = & \text{constant} & \text{(steady-flux)} \\ \nabla^2 \hat{T} & = & \text{constant} \cdot i \cdot \hat{T} & \text{(periodic)} \\ \nabla^2 T & = & \frac{1}{a}\frac{\partial T}{\partial t} & \text{(general transient)} \end{array} \tag{6.39}$$

This will be reflected in certain similarities of the solutions. In chapter 10, we will use the Laplace transform of the general transient heat equation (6.42), which is:

$$\nabla^2 \tilde{T} = \frac{p}{a} \cdot \tilde{T} - T\,|_{t=0} \tag{6.40}$$

which is complex-valued and of the same type as the heat equation (6.41) for periodic variations.

An equation of this type is also obtained in chapter 12. The heat injection from the ducts is here treated as a heat source in a steady-state solution for the large-scale process:

$$\nabla^2 T = \frac{T - T_f}{\ell^2} \tag{6.41}$$

Chapter 7

Convective Heat Transfer in Ducts

This chapter presents a literature survey of convective heat transfer in circular tubes and circular-tube annuli, which are the two basic flow channel geometries that will be considered. Ground heat exchangers in softer media typically use circular tubes. Circular tubes are also inserted in boreholes to form closed U-shaped loops. The case of the circular-tube annulus is found in the outer flow channel in boreholes with a concentric inner tube.

A common trait of these flow channels is that they are vertical and extremely long. The length-to-diameter ratio is on the order of 1000. The heat carrier fluid is often plain water.

The convective heat transfer during laminar flow may give rise to thermal resistances between the heat carrier fluid and the duct wall that are comparable to the thermal resistance between the duct wall and the store, especially during short-time variations of heat transfer rates. Thus, the convective heat transfer is important.

The aim of this chapter is to present formulas and tables that are suitable for calculation of convective heat transfer in ground heat exchangers. The first section gives a brief review of the fundamentals of convective heat transfer, and introduces the dimensionless numbers commonly used in the analysis. Formulas for the heat transfer during laminar and turbulent flow are given for circular tubes and circular-tube annuli in section 7.2 and 7.3, respectively.

The main references for the information presented in this chapter are the Handbook of Heat Transfer Fundamentals (Rohsenow et al. 1985) and the VDI-Wärmeatlas (1988). Recommended textbooks on this subject are Principles of Heat Transfer by Kreith and Bohn (1986), and Konvektive Wärmeübertragung by Merker (1987).

7.1 Introduction

The temperature difference and the thermal resistance determine the heat flow between two surfaces. The thermal resistance in a solid depends on the geometry and the thermal properties of the solid. The term "thermal resistance" will also be employed to mean the heat transfer resistance between the bulk temperature T_B of the fluid and the temperature T_w at the wall of the flow channel (or duct).

The following nomenclature will be used:

R_{fc} Heat transfer resistance between the heat carrier fluid in a circular flow channel and the wall of the flow channel.

R_{fai} Heat transfer resistance between the heat carrier fluid in a annular flow channel and the inner wall of the flow channel.

R_{fao} Heat transfer resistance between the heat carrier fluid in a annular flow channel and the outer wall of the flow channel.

The bulk, mixing-cup, or flow-average temperature T_B is the temperature that would be obtained if the fluid at a given cross-section of a pipe were collected and mixed. It is the enthalpy-average temperature of the bulk fluid:

$$T_B \int_0^{r_p} \rho_f c_f v(r)\, 2\pi r\, dr = \int_0^{r_p} \rho_f c_f v(r) T(r)\, 2\pi r\, dr \tag{7.1}$$

Here, ρ_f is the density, c_f the heat capacitivity, $v(r)$ the velocity profile, and r_p the radius of a circular pipe. For an incompressible fluid with constant density and heat capacitivity, this reduces to

$$T_B = \frac{\int_0^{r_p} v(r)\, T(r)\, r\, dr}{\int_0^{r_p} v(r)\, r\, dr} \tag{7.2}$$

In engineering practice, a simple approximate average value,

$$T_B = \frac{T_{inlet} + T_{outlet}}{2} \tag{7.3}$$

is used in the calculation of *average* heat-transfer coefficients (Pitts and Sissom 1977; VDI-Wärmeatlas 1988).

The heat transfer between the moving fluid and the wall of the flow channel is a complicated process. It depends on the flow conditions, i.e. the velocity distribution and temperature distribution, in the fluid. The flow conditions are, on the other hand, influenced by the magnitude of the heat transfer and its variation on the surface. The convective heat transfer is usually calculated

with use of the dimensionless Nusselt's number, which is defined as the ratio between actual heat transfer and conductive heat transfer:

$$\mathrm{Nu} = \frac{\text{Actual heat transfer}}{\text{Conductive heat transfer}} \tag{7.4}$$

The Nusselt's number at a given length x from the entrance of a pipe is often denoted Nu_x, whereas the mean value for the whole pipe is Nu.

The definition of the Nusselt's number is easy to conceive when applied to heat transfer through a fluid bounded by to parallel surfaces. The distance between the surfaces is L and the temperature difference is ΔT. The conductive heat flux q'_{cond} becomes:

$$q'_{cond} = \frac{\lambda_f \Delta T}{L} \tag{7.5}$$

Here, λ_f is the thermal conductivity of the fluid. The actual, or convective, heat flux q'_{actual} is given by the heat transfer coefficient α defined by:

$$q'_{actual} = \alpha \Delta T \qquad (\mathrm{W/m^2}) \tag{7.6}$$

According to the definition we get:

$$\mathrm{Nu} = \frac{q'_{actual}}{q'_{cond}} = \frac{\alpha L}{\lambda_f} \tag{7.7}$$

It is standard practice to use a relation of this type for heat transfer in other geometries as well. A characteristic length L must then be chosen. For heat transfer in pipes it quite natural to choose the pipe diameter D.

The Nusselt's number depends on the flow conditions in the duct. Convection induced by a pump is called forced convection. If it is due to buoyancy forces caused by density differences in the fluid it is called natural or free convection. Dimensional analyses of the basic momentum and energy balance equations show that the Nusselt's number becomes a function of two dimensionless parameters: Reynold's number Re and Prandtl's number Pr for forced convection, and Rayleigh's number Ra and Pr for free convection. The functional dependence on these parameters does not follow from the dimensional analysis, but it is common to assume a power dependence of the type $\mathrm{Nu} = C\mathrm{Re}^m\mathrm{Pr}^n$. The constant C and the exponents m and n are determined by fitting to experimental data.

The Reynold's number Re gives the ratio between inertial and viscous forces in the fluid. Let v_f denote the average flow velocity in the duct and μ_f the dynamic viscosity. The inertial forces are proportional to the kinetic energy $\rho_f v_f^2$; the viscous forces are proportional to the shear stress $\mu_f v_f / L$. Hence,

$$\mathrm{Re} = \frac{\rho_f v_f L}{\mu_f} \tag{7.8}$$

The Prandtl's number (7.14) gives the ratio between two transport coefficients: kinematic viscosity ν_f for the momentum transport, and the thermal diffusivity a_f for the energy transport.

Two other dimensionless numbers sometimes used in convective heat transfer are the Peclet number:

$$\mathrm{Pe} = \mathrm{Re}\ \mathrm{Pr} \tag{7.9}$$

,and the Graetz number:

$$\mathrm{Gz} = \frac{c_f V_f}{\lambda_f L} = \frac{\pi}{4}\mathrm{Re}\ \mathrm{Pr}\frac{D}{L} \tag{7.10}$$

Here, the fluid flow rate (m^3/s) is denoted V_f, the fluid thermal conductivity λ_f, the pipe diameter D, and the pipe length L.

For free convection there is the Grashof's number that gives the ratio between buoyancy forces and viscous forces. It depends on the temperature difference ΔT, the thermal expansion coefficient β ($\Delta\rho/\rho = -\beta\Delta T$), the gravity constant g ($\approx$9.81 m/s^2), the kinematic viscosity ν_f, and a characteristic length L:

$$\mathrm{Gr} = \frac{gL^3}{\nu_f^2}\beta\Delta T \tag{7.11}$$

This number is closely related to the Rayleigh number:

$$\mathrm{Ra} = \mathrm{Gr}\ \mathrm{Pr} = \frac{gL^3}{a_f\nu_f}\beta\Delta T \tag{7.12}$$

The following relation may be used to estimate the relative influence of forced versus free convection:

$$\frac{\mathrm{Gr}}{\mathrm{Re}^2} = \frac{\rho_f g\beta\Delta T}{\rho_f v_f^2/L} \sim \frac{\text{Buoyancy force per unit volume}}{\text{Inertial forces per unit volume}} \tag{7.13}$$

If $\mathrm{Gr}/\mathrm{Re}^2 \ll 1$ then there is primarily forced convection, whereas free convection dominates if $\mathrm{Gr}/\mathrm{Re}^2 \gg 1$.

7.1.1 Heat-Carrier Fluid

The heat carrier fluid is often plain water. Sometimes small quantities of water treatment chemicals are added to prevent bacterial growth etc.

The properties of heat carrier fluids are functions of temperature and pressure. The pressure dependence, however, can for these applications be neglected. The relevant properties of the heat carrier fluid are thermal conductivity λ_f, density ρ_f, heat capacitivity c_f (J/kgK), the dynamic viscosity

μ_f (kg/ms), and the thermal expansion coefficient β (1/K). The thermal diffusivity a_f, the kinematic viscosity ν_f, and Prandtl's number Pr become:

$$a_f = \frac{\lambda_f}{\rho_f c_f} \qquad \nu_f = \frac{\mu_f}{\rho_f} \qquad \mathrm{Pr} = \frac{\nu_f}{a_f} = \frac{\mu_f c_f}{\lambda_f} \tag{7.14}$$

The thermophysical properties of water are given in Table 7.1 (VDI-Wärmeatlas 1988).

TABLE 7.1 Thermophysical properties of water

T	ρ	c_p	λ	μ	Pr	β
°C	kg/m^3	kJ/kgK	W/mK	10^{-6} kg/ms	-	10^{-3}/K
0	999.8	4.217	0.562	1791.8	13.44	-0.0852
5	1000.0	4.202	0.572	1519.6	11.16	0.0055
10	999.8	4.192	0.582	1307.6	9.42	0.0823
15	999.2	4.186	0.591	1139.0	8.07	0.1486
20	998.3	4.182	0.600	1002.6	6.99	0.2067
25	997.2	4.180	0.608	890.8	6.13	0.2586
30	995.8	4.178	0.615	797.7	5.42	0.3056
35	994.1	4.178	0.622	719.5	4.83	0.3488
40	992.3	4.179	0.629	653.1	4.34	0.3890
45	990.3	4.180	0.635	596.3	3.93	0.4267
50	988.1	4.181	0.640	547.1	3.57	0.4624
55	985.7	4.183	0.646	504.3	3.27	0.4963
60	983.2	4.185	0.651	465.8	3.00	0.5288
65	980.5	4.187	0.655	433.8	2.77	0.5590
70	977.7	4.190	0.660	404.5	2.57	0.5900
75	974.7	4.193	0.663	378.3	2.39	0.6190
80	971.4	4.196	0.667	355.0	2.23	0.6473
85	968.5	4.200	0.670	333.9	2.09	0.6748
90	965.1	4.205	0.673	315.0	1.97	0.7018
95	961.7	4.210	0.675	297.8	1.86	0.7284

In low-temperature applications, where the temperature of the heat carrier fluid may fall below 0 °C, substantial amounts of glycol must be added to prevent freezing. It must be observed that common types of glycol, such as ethylene and propylene glycol, have thermophysical properties that differ much from those of water (Perry and Chilton 1973). For a given flow rate, a mixture of water and glycol will have a lower heat transfer coefficient than pure water. Because of the higher viscosity of glycols, the flow rate required to avoid laminar flow will be larger than for pure water.

7.1.2 Laminar flow

In laminar flow there is no mixing of the fluid by eddy motion. The fluid particles will follow given paths, streamlines, and the heat transfer between

the bulk fluid and the duct wall takes place by conduction. Fluids have a low thermal conductivity and the heat transfer coefficients are relatively small. In industrial heat exchanger equipment, laminar flow conditions are therefore avoided (Coulson and Richardson 1960). It should be noted, however, that the relative influence of the heat transfer coefficient is smaller for a ground heat exchanger due to the large thermal resistance between the duct wall and the storage capacity.

Fully developed laminar flow is an idealization, which is difficult to obtain in practice except in very small passages. Natural convection currents are usually present. Then the heat conduction is not the only mode of heat transfer to be considered (Knudsen and Katz 1958).

7.1.3 Turbulent flow

During turbulent flow, the fluid is constantly mixed due to eddy currents and the fluid temperature becomes fairly uniform in the flow channel. Most of the temperature drop between the fluid and the wall of the flow channel takes place in a thin laminar layer at the wall (Kreith 1965). The heat transfer rate is controlled by the thermal conductivity and the thickness of this boundary layer. The thickness of the boundary layer decreases with higher flow velocities, and hence the heat transfer is enhanced.

In industrial heat exchangers, the heat exchanger area required decreases with higher flow velocities. In practice, however, it has been found that increases in pumping costs and operating expenses often outweigh the savings in initial cost under continuous operating conditions. As a result, commercial heat-exchange equipment uses flow velocities corresponding to a Reynold's number of about 50,000 (Kreith 1965). In ground heat exchangers, where the heat transfer coefficient in the pipe is less important, the optimum flow velocity for the heat exchange is probably lower when economical aspects are taken into account.

7.1.4 Transition zone

At flow velocities with a Reynold's number below 2300 the flow is usually considered to be laminar. As the velocity increases there will be gradual change to turbulent flow, which is considered to be fully developed at Re=10,000. Between these two values the flow condition is in the so-called *transition zone*. When the transition from laminar to turbulent flow starts there is certain amount of mixing due to eddy currents. This results in a marked increase in the heat transfer about Re=2300. The flow conditions are unstable and not completely determined by the Reynold's number, but influenced by the shape of the entrance, roughness of tube wall, pipe geometry, free-convection

effects, change in viscosity when large heating rates occur, etc (Hausen 1976; Rohsenow et al. 1985). Kreith (1965) remarks that fluctuations in pressure drop and heat transfer have been observed. The evaluation of the heat transfer is more uncertain in this region, particularly at the lower end of the range, due to the many parameters involved. Because of this, there is a recurring recommendation in the literature to avoid the transition zone in heat exchanger design. On the other hand, Ede (1967) states that fairly stable conditions may be obtained by use of an abrupt entrance that forces the flow to be turbulent.

7.1.5 Boundary conditions

The boundary conditions, i.e. temperature and heat flux at the wall, along the flow channel have a significant effect on the heat transfer coefficient. The two extreme cases ordinarily considered in analytical studies and experimental investigations are that of constant wall temperature or constant heat flux along the length of the duct. In the case of constant wall temperature T_w, the fluid temperature T_f satisfies:

$$C_f V_f \frac{dT_f}{dx} = -\frac{1}{R_f}(T_f - T_w) \tag{7.15}$$

Here, x is the length along the flow channel, C_f ($= \rho_f c_f$) is the volumetric heat capacity (J/m^{3}K), V_f is the flow rate (m^3/s), and R_f (K/(W/m)) is the thermal resistance between the bulk fluid and the wall. With constant inlet fluid temperature T_{inlet} and thermal resistance R_f, the fluid temperature along the flow channel becomes:

$$T_f(x) = T_w + (T_{inlet} - T_w)\,\mathrm{e}^{-x/(R_f C_f V_f)} \tag{7.16}$$

The corresponding heat flow decreases exponentially along the axis:

$$q(x) = \frac{1}{R_f}(T_{inlet} - T_w)\,\mathrm{e}^{-x/(R_f C_f V_f)} \qquad \text{(W/m)} \tag{7.17}$$

In the case of constant heat flux along the flow channel, the right side of (7.15) is replaced by the heat flow q. Integration gives a linear variation of fluid temperature along the flow channel:

$$T_f(x) = T_{inlet} - \frac{q\,x}{C_f V_f} \tag{7.18}$$

There is a constant temperature difference between the fluid and the wall:

$$T_w(x) = T_f(x) - q\,R_f \tag{7.19}$$

The Nusselt's number obtained at constant heat flux is always greater than that for constant wall temperature. The difference is much smaller for turbulent flow than for laminar flow, and it becomes quite negligible for Pr>1 (Rohsenow et al. 1985).

7.1.6 Hydrodynamic entry length

The fluid enters a pipe with almost uniform velocity. At the entrance, the fluid immediately adjacent to the wall is brought to rest. A laminar layer develops, and as the fluid flows along the duct, it increases in thickness until a stable laminar velocity profile has been established. If the flow velocity is high enough to give turbulent conditions, the laminar boundary layer quickly breaks down and a turbulent boundary layer will be developed (Kreith 1965). The length from the entrance at which the velocity profile becomes fully developed is called the *hydrodynamic entry length.* According to Merker (1987) the accepted definition of fully developed flow is when the velocity in the center of the pipe has attained 99 % of its asymptotic value.

The hydrodynamic entry length during laminar flow for the idealized case of fully developed temperature profile at the entrance may be written (Merker 1987):

$$L_{hyd} = \left[0.056 + \frac{0.60}{\mathrm{Re}(1 + 0.035\mathrm{Re})}\right] \mathrm{Re}D \tag{7.20}$$

Beyond this distance the *local* Nusselt's number is less than 1.05 times the asymptotic Nu.

For turbulent flow, the entrance effects disappear about 10-15 pipe diameters from the entrance (Rohsenow et al. 1985; Merker 1987).

7.1.7 Thermal entry length

The development of the temperature profile, or the thermal boundary layer, in a fluid is similar to that of the hydrodynamic boundary layer. At the entrance the temperature is generally uniform, but as the fluid flows along the duct, the heated or cooled layer increases in thickness until heat is transferred to or from the fluid in the center of the pipe (Kreith 1965). In the case of fully developed velocity profile, the thermal entry length is that distance from the beginning of heat transfer at which the Nusselt's number becomes independent of length (Knudsen and Katz 1958).

The thermal entry length for laminar flow with fully developed velocity profile at the entrance becomes:

$$\begin{array}{ll} \text{Constant wall temperature:} & L_{th} = 0.0335\,\mathrm{RePr}D \\ \text{Constant heat flux:} & L_{th} = 0.0431\,\mathrm{RePr}D \end{array} \tag{7.21}$$

Beyond this distance the *local* Nusselt's number is less 1.05 times the limiting Nu (Merker 1987).

Merker (1987) gives the following relations for the ratio between the thermal entry length L_{th} and the hydrodynamic entry length L_{hyd} during laminar flow:

Constant wall temperature:	$L_{th}/L_{hyd} = 0.6\,\mathrm{Pr}$	$\mathrm{Re} > 1000$
Constant heat flux:	$L_{th}/L_{hyd} = 0.77\,\mathrm{Pr}$	$\mathrm{Re} > 1000$

(7.22)

For water, where the Prandtl's number varies from 11.2 at 5 °C to 1.9 at 95 °C, the thermal entry length will be slightly larger, but of the same magnitude as the hydrodynamic entry length. This means that the velocity profile and the temperature profile will develop simultaneously, which is a more complex situation. The local Nusselt's number will vary along the duct until both the velocity profile and the temperature profile is fully developed. The heat transfer is somewhat higher during such combined entry.

For turbulent flow, the thermal and hydrodynamic entry lengths are characteristically much shorter than for laminar flow. The turbulent flow becomes fully developed after just 10-15 pipe diameters (Merker 1987; Rohsenow et al. 1985). Thus, the entrance effects are frequently neglected in heat transfer design (Bennet and Myers 1962; Rohsenow et al. 1985). One may note that the Nusselt's number is higher at the entrance, so it is slightly conservative to neglect this effect. For laminar flow in water, the effects of combined entry may have a large influence (>5 %) for a length of about 100 pipe diameters (Merker 1987).

7.1.8 Semi-empirical formulas

The heat transfer coefficients for a given situation can be obtained by either an experiment or a theoretical study. The results from careful laboratory experiments differ appreciably (Ede 1967). It is known that the Nusselt's numbers during turbulent flow are strongly affected by variations in fluid properties over the flow cross-section induced by large temperature differences. Some of the uncertainty in the experiments is due to temperature effects large enough to influence the results (Rohsenow et al. 1985).

The theoretical methods involve solving a set of coupled partial differential equations either by analytical or numerical methods. The classical approach was to employ a number of simplifying assumptions to make the problem tractable by analytical methods. The analytical solutions, with their explicit parameter dependence, formed the basis for correlations with experimental results. Corrections were then tailored to handle the influence of processes not covered by the solutions. For instance, the analytical solutions take no account of superimposed free convection, which in practice occurs during laminar and transitional flow (Ede 1967). If free convection is excluded, then the

heat transfer does not depend on the inclination of the pipes. Most experimental data available concern horizontal pipes. Furthermore, the thermophysical properties are assumed to be constant. For water, especially the viscosity shows a strong temperature dependence, see Table 7.1. There is usually some amount of viscosity effects present. Analytical solutions are reviewed by Kays and Crawford (1980).

Numerical solutions started to appear in the early sixties and it is the field of current activity. The versatility of the numerical algorithms and the rapid increase in the availability of computing power have made theoretical investigations the primary source for many engineering applications. The results from the numerical calculation are often presented in form of large tables.

The boundary conditions involve two idealized situations, constant wall temperature and constant heat flux. These conditions are assumed to prevail along the whole flow channel. The boundary conditions of a pipe in a ground heat exchanger may not be as simple. Due to more irregular boundary conditions and ensuing viscosity effects the flow conditions will rarely be fully developed.

It should be emphasized that the material presented here is not a discussion on the methods but a presentation of results obtained by these methods. Due to the particularities of the application to ground heat exchangers: vertical, extremely long, low temperatures in some application, the formulas will be compared in order to make a recommendation. The influence of different processes will be estimated.

7.2 Circular tube

In this section we will treat the heat transfer resistance R_{fc} between the heat carrier fluid and the wall of a circular flow channel with the radius r_p. The average velocity of the heat carrier fluid is denoted v_f (m/s). The fluid flow rate V_f (m^3/s) is then:

$$V_f = v_f \pi r_p^2 \tag{7.23}$$

Sometimes the Reynold's number is written Re_D to emphasize that the pipe diameter $D{=}2r_p$ is chosen as a characteristic length. This convention will not employed here. The Reynold's number for the circular pipe is defined by:

$$\mathrm{Re} = \frac{v_f D}{\nu_f} = \frac{2 r_p v_f \rho_f}{\mu_f} \tag{7.24}$$

Alternatively, the Reynold's number may be expressed with use of the fluid flow rate (7.23):

$$\mathrm{Re} = \frac{4\rho_f}{\pi\mu_f}\frac{V_f}{2r_p} \tag{7.25}$$

The heat transfer depends to a large extent on whether the flow in the channel is laminar or turbulent. The flow is unconditionally laminar for Re< 2300, and it is unconditionally turbulent for Re> 10,000. In the *transition zone* with 2,300<Re<10,000 the flow conditions are not completely determined by the Reynold's number. See sections 7.1.2-4.

The Nusselt's number for the circular pipe is defined by:

$$\mathrm{Nu} = \frac{\alpha D}{\lambda_f} = \frac{\alpha 2r_p}{\lambda_f} \tag{7.26}$$

Here α is the heat transfer coefficient ($\mathrm{W/m^2K}$). It is given per unit area and may vary along the pipe. See section 6.2.3. The Nusselt's number usually concerns the average value of α along the whole channel. The heat flow per unit area between the fluid and the wall then becomes $\alpha\Delta T$, where ΔT is the difference between the bulk fluid temperature (7.3) and the wall temperature. The heat flow from the pipe per unit length is q (W/m). We get the following relation:

$$\alpha\,\Delta T = \frac{q}{2\pi r_p} \qquad (\mathrm{W/m^2}) \tag{7.27}$$

The thermal resistance R_{fc} between the fluid and the pipe wall becomes:

$$R_{fc} = \frac{1}{2\pi r_p\,\alpha} \qquad \Delta T = q\,R_{fc} \tag{7.28}$$

From (7.26) and (7.28) we finally get:

$$R_{fc} = \frac{1}{\pi\lambda_f \mathrm{Nu}} \tag{7.29}$$

The Nusselt's number Nu depends primarily on the dimensionless parameters Re, Pr, and D/L. In this chapter, D denotes the pipe diameter and L the pipe length in order to conform with the standard nomenclature on heat transfer. The magnitude of the ratio D/L for a ground heat exchanger is:

$$\frac{20}{0.1} = 200 < \frac{L}{D} < \frac{200}{0.1} = 2000 \tag{7.30}$$

The influence of entrance effects can usually be neglected during turbulent flow, whereas it is still necessary to take the axial variation of the Nusselt's number into account during laminar flow (Ede 1967). See also sections 7.1.6-7.

Other processes that may influence the heat transfer are discussed in sections 7.2.3-6.

7.2.1 Laminar Flow

Numerous formulas exist for laminar flow in a circular tube. Some of them are valid for rather short pipes. Our interest is formulas that are valid for long pipes (L/D>200).

A characteristic length for the thermal entry is RePrD. A dimensionless tube length may then formed by:

$$L^* = \frac{L}{\mathrm{RePr}D} \tag{7.31}$$

Older references report rather low accuracy ±25 % of correlations between formulas and experimental values (Coulson and Richardson 1960). This is probably caused by presence of free convection currents in the experiments; an effect that is not accounted for by the formulas. See section 7.2.4 for further discussion of free convection.

Constant wall temperature

The asymptotic value for the Nusselt's number during fully developed velocity and temperature profile with constant wall temperature is:

$$\mathrm{Nu} = 3.657 \qquad (\textit{Asymptotic value}) \tag{7.32}$$

Hausen (1976) has developed a formula for the case of a fully developed velocity profile at the entrance:

HAUSEN:

$$\mathrm{Nu} = 3.66 + \frac{0.0668/L^*}{1 + 0.04\,(L^*)^{-2/3}} \tag{7.33}$$

Rohsenow et al. (1985) and Merker (1987) give the following algebraic equation proposed by Shah and London (1978):

SHAH-LONDON:

$$\mathrm{Nu} = \begin{cases} 1.615(L^*)^{-1/3} - 0.2 & \text{for } 0.006 < L^* < 0.03 \\ 3.657 + 0.0499/L^* & \text{for } L^* \geq 0.03 \end{cases} \tag{7.34}$$

When both the velocity and temperature in the fluid are uniform at the entrance, the velocity and temperature profile will develop simultaneously. The heat transfer will be higher than if either the velocity or the temperature

profile is fully developed at the entrance. The effect of *combined* entry is only significant if Pr<10 (Rohsenow et al. 1985). Merker (1987) states that the currently most precise solution for combined thermal and hydrodynamic entry is the numerical solution given by Hornbeck (1965). If the calculated values are used to fit the coefficients of an analytical solution obtained by Stephan (1959), then we get:

MERKER:

$$\mathrm{Nu} = 3.657 + \frac{0.05565\,(L^*)^{-1.3335}}{1 + 0.08386\,\mathrm{Pr}^{0.2}(L^*)^{-0.8559}} \qquad \text{for } L^* > 10^{-4} \qquad (7.35)$$

The deviation from the values calculated by Hornbeck is less than 2 % for Pr=0.7 and less than 5 % for Pr=5.

The Nusselt's number is a function of Reynold's number, Prandtl's number, and the length-to-diameter ratio. The Prandtl's number depends only on the fluid temperature. The formulas by Hausen, Shah-London, and Merker are compared in Table 7.2 for different values of Reynold's number, temperature, and length-to-diameter ratio. The thermophysical properties of water, Table 7.1, are assumed.

TABLE 7.2. Circular tube, laminar flow, constant wall temperature, Comparison of formulas by Hausen (H), Shah-London (S-L), and Merker (M).

T=50 °C L/D=1000				Re=2000 L/D=1000				Re=2000 T=50 °C			
Re	H	S-L	M	T	H	S-L	M	L/D	H	S-L	M
100	3.68	3.67	3.67	10	4.64	4.60	4.72	200	5.32	5.11	5.63
300	3.73	3.71	3.71	20	4.42	4.36	4.52	400	4.59	4.54	4.80
500	3.77	3.75	3.76	30	4.26	4.19	4.35	600	4.32	4.25	4.45
700	3.81	3.78	3.81	40	4.15	4.08	4.23	800	4.17	4.10	4.26
900	3.86	3.82	3.86	50	4.07	4.01	4.14	1000	4.07	4.01	4.14
1100	3.90	3.85	3.91	60	4.02	3.96	4.07	1200	4.01	3.95	4.06
1300	3.94	3.89	3.96	70	3.97	3.91	4.01	1400	3.96	3.91	4.00
1500	3.98	3.92	4.01	80	3.92	3.88	3.95	1600	3.93	3.88	3.95
1700	4.02	3.96	4.06	90	3.89	3.85	3.91	1800	3.90	3.85	3.91
1900	4.05	3.99	4.11					2000	3.88	3.83	3.89
2100	4.09	4.03	4.16								
2300	4.13	4.07	4.21								

The Nusselt's number obtained by the three formulas agree rather well, except when the dimensionless tube length L^* becomes small. The maximum difference in Table 7.2 is 10 % for short pipes (L/D=200).

Constant heat flux

The asymptotic Nusselt's number for fully developed velocity and temperature profile at constant heat flux is:

$$\mathrm{Nu} = 4.364 \qquad (\textit{Asymptotic value}) \tag{7.36}$$

Hausen has given the Nusselt's number for the case of fully developed velocity profile at the entrance (Pitts and Sissom 1977):

HAUSEN:

$$\mathrm{Nu} = 4.36 + \frac{0.023/L^*}{1 + 0.0012/L^*} \tag{7.37}$$

Merker (1987) gives the following algebraic equation proposed by Shah and London (1978):

SHAH-LONDON:

$$\mathrm{Nu} = \begin{cases} 1.953(L^*)^{-1/3} & \text{for } L^* < 0.03 \\ 4.364 + 0.0722/L^* & \text{for } L^* \geq 0.03 \end{cases} \tag{7.38}$$

The accuracy of formula (7.38) compared to the precise numerical calculations performed by Shah and London (1978) is about 3 %.

There are no formulas given for the average Nusselt's number in the case of combined thermal and hydrodynamic entry. However, both Merker (1987) and Rohsenow et al. (1985) present formulas for the local Nusselt's number. These formulas show that the heat transfer is larger during combined entry than for the case with fully developed velocity profile at the entrance (7.38).

The formulas by Hausen and Shah-London are compared in Table 7.3 for different values of Reynold's number, temperature, and length-to-diameter ratio. The thermophysical properties of water, Table 7.1, are assumed.

The formula given by Shah and London is more sensitive to the length-to-diameter ratio L/D. The deviation between the two formulas grows when the characteristic entry length $\mathrm{RePr}D$ increases. The Prandtl's number becomes larger with decreasing temperature. The influence is, of course, larger for short pipes, that is lower L/D values. The Shah-London formula (7.38) is always higher than Hausen's (7.37), but still, according to Merker, a conservative estimate.

TABLE 7.3. Circular tube, laminar flow, constant heat flux. Comparison of formulas by Hausen (H) and Shah-London (S-L).

T=50 °C L/D=1000			Re=2000 L/D=1000			Re=2000 T=50 °C		
Re	H	S-L	T	H	S-L	L/D	H	S-L
100	4.37	4.39	10	4.78	5.72	200	5.14	6.93
300	4.38	4.44	20	4.68	5.37	400	4.76	5.65
500	4.40	4.49	30	4.60	5.14	600	4.63	5.22
700	4.42	4.54	40	4.55	4.98	800	4.56	5.01
900	4.43	4.60	50	4.52	4.88	1000	4.52	4.88
1100	4.45	4.65	60	4.50	4.80	1200	4.50	4.79
1300	4.47	4.70	70	4.48	4.74	1400	4.48	4.73
1500	4.48	4.75	80	4.46	4.68	1600	4.46	4.68
1700	4.50	4.80	90	4.45	4.64	1800	4.45	4.65
1900	4.51	4.85				2000	4.44	4.62
2100	4.53	4.90						
2300	4.55	4.95						

7.2.2 Turbulent Flow

One of the first formulas for turbulent flow was derived by Dittus and Boelter (1930). It is simple to use and for this reason referenced in most text books on heat transfer. The formula takes different forms depending on whether the fluid is being heated or cooled:

DITTUS-BOELTER

$$\mathrm{Nu} = 0.023\,\mathrm{Re}^{0.8}\,\mathrm{Pr}^{0.4} \qquad \text{heating} \tag{7.39}$$

$$\mathrm{Nu} = 0.023\,\mathrm{Re}^{0.8}\,\mathrm{Pr}^{0.3} \qquad \text{cooling} \tag{7.40}$$

The physical properties are evaluated at the mean bulk temperature T_B of the fluid. The accuracy of the formula is reported by Kay and Nedderman (1974) to be ±10 %, while Holman (1968) gives ±25 %. Rohsenow et al. (1985) claims that it is still a very good approximation to the available experimental data in the range 10,000<Re<120,000, 0.7<Pr<120, and L/D >60. Ede (1967)

states that it is probably as accurate as the experimental evidence warrants, and adds that it overestimates the Nusselt's numbers if Re<10,000 and Pr>20.

A similar correlation was presented by Kraussold (1933). It is most accurate when $T_B - T_w \simeq 30$ °C (Hausen 1976). The Nusselt's number for longer pipes, 100<L/D<400, is:

KRAUSSOLD

$$\mathrm{Nu} = 0.024\,\mathrm{Re}^{0.8}\,\mathrm{Pr}^{0.37} \qquad \text{heating} \tag{7.41}$$

$$\mathrm{Nu} = 0.024\,\mathrm{Re}^{0.8}\,\mathrm{Pr}^{0.31} \qquad \text{cooling} \tag{7.42}$$

The different formulas during heating and cooling reflect the influence of temperature dependent properties, particularly the viscosity. Sieder and Tate (1936) modified the formulas given by Kraussold to account for these effects in a more general way:

SIEDER-TATE

$$\mathrm{Nu} = 0.023\,\mathrm{Re}^{0.8}\,\mathrm{Pr}^{1/3}(\mu_B/\mu_w)^{0.14} \tag{7.43}$$

The so-called Sieder-Tate correction term for temperature dependent effects includes the viscosities μ_B and μ_w, which are taken at the bulk temperature T_B and the duct wall temperature T_w, respectively. All other properties are evaluated at the bulk temperature. The Sieder-Tate equation agrees well with experimental data for 0.5<Pr<120, 10,000<Re<10,000,000, and L/D>60. McAdams (1954) gives an accuracy of ±20 % for water and ethylene glycol.

Petuhkov (1970) has developed a correlation that is valid for the constant heat flux case:

PETUHKOV

$$\mathrm{Nu} = \frac{(f/2)\,\mathrm{Re}\,\mathrm{Pr}}{1.07 + 12.7(f/2)^{1/2}(\mathrm{Pr}^{2/3} - 1)} \tag{7.44}$$

where the Fanning friction factor f for smooth pipes is given by

$$f = [1.58\,\ln(\mathrm{Re}) - 3.28]^{-2} \tag{7.45}$$

The Nusselt's number for the constant heat flux case is always greater than for the constant wall temperature case, but the difference is generally much smaller than for the laminar flow. Note, however, that there is little or no effect of wall boundary condition except for the very low Prandtl number range, and it becomes negligible for Pr>1. Kays and Crawford (1980) reports

an accuracy of ±10 % for 10,000<Re<5,000,000, and 0.5<Pr<2,000. Merker (1987) gives an accuracy of 6 % compared with a numerical solution where the velocity distribution has the commonly assumed 1/7-power dependence. A rather complicated formula with an accuracy of 2% can be found in this reference.

Kays and Crawford (1980) states that a simpler formula by Sleicher and Rose (1975) gives results that are very close to that of Petuhkov. Merker (1987) cites, probably correctly, this formula as a work by Notter and Sleicher (1972). The formula is valid for both the constant wall temperature and the constant heat flux case when 10,000<Re<1,000,000 and $0.1<\mathrm{Pr}<10^4$:

NOTTER-SLEICHER

$$\mathrm{Nu} = 5 + 0.015\mathrm{Re}^a\mathrm{Pr}^b \tag{7.46}$$

$$a = 0.88 - 0.24/(4 + \mathrm{Pr}) \tag{7.47}$$

$$b = 0.333 + 0.5e^{-0.6\mathrm{Pr}} \tag{7.48}$$

A modification of the formula by Pethukov has been proposed by Gnielinski (1975), who by this extends the range of validity down to Re=2300. This formula, which includes the transition zone, is recommended in the Handbook of Heat Transfer Fundamentals (Rohsenow et al. 1985) and the VDI-Wärmeatlas (1988):

GNIELINSKI

$$\mathrm{Nu} = \frac{(f/2)(\mathrm{Re} - 1000)\,\mathrm{Pr}}{1 + 12.7(f/2)^{1/2}(\mathrm{Pr}^{2/3} - 1)} \qquad (\mathrm{Re} > 2{,}300) \tag{7.49}$$

where the friction factor f is given by (7.45).

Hausen (1976) refers to the formula (7.49) by Gnielinski and offers the following correlation:

HAUSEN

$$\mathrm{Nu} = 0.0235(\mathrm{Re}^{0.8} - 230)(1.8\mathrm{Pr}^{0.3} - 0.8)\left[(1 + \frac{D}{L})^{2/3}\right](\mu_b/\mu_w)^{0.14} \tag{7.50}$$

According to Hausen this formula gives a more accurate description of the Prandtl's number dependency, which may be important in low temperature applications.

It is known that the Nusselt's numbers during turbulent flow are strongly affected by variations in fluid properties over the flow cross-section induced by large temperature differences. Most formulas presented here assume that the fluid properties are constant. The results are then, strictly speaking, only

applicable for negligibly small temperature differences. Of the formulas in this section, only the Sieder-Tate (7.43) and the Hausen (7.50) correlation explicitly include a correction factor for the temperature dependence. The Dittus-Boelter (7.39-40) and the Kraussold formulas (7.41-42) acknowledge the effect by having different forms for heating and cooling. According to section 7.2.4, a correction term, such as the Sieder-Tate, may be multiplied on the right side on the other equations as well.

In order to show the difference between the results obtained by these formulas, the Table 7.4 gives the Nusselt's number for different fluid temperatures and Reynold's numbers. The thermophysical properties of water, Table 7.1, are used in the calculation of the Prandtl's number. The Sieder-Tate correction term is set equal to 1, i.e. temperature dependent effects are neglected. The Dittus-Boelter and the Kraussold formulas are evaluated for the case of a heating fluid. The term involving the length-to-diameter ratio L/D in the formula by Hausen is set equal to 1.

The formulas by Gnielinski and Hausen give substantially lower Nusselt's number than the other formulas at Re=2300. For other Reynold's numbers the results agree fairly well, except at high Reynold's numbers and low temperatures ($Pr \simeq 4$).

7.2.3 Mixed free and forced convection

The determination of the heat transfer coefficient is further complicated if the buoyancy forces are of the same order of magnitude as the external forces due to forced convection. The free convection in vertical tubes becomes important at low flow rates, Re<10,000, and large temperature differences in the fluid (McAdams 1954; Hausen 1976; Metais and Eckert 1964). The relatively poor agreement of experimental data with theoretical results may be due to the presence of the free convection (Knudsen and Katz 1958). The transition from laminar to turbulent flow may also be affected, so that the laminar flow pattern breaks up at Reynold's number lower than 2300. The formulas for mixed free and forced convection are given for rather small ranges of Reynold's numbers and Rayleigh's or Grashof's number.

In horizontal tubes the additional mixing induced by superimposed free convection results in an increased heat transfer. In vertical tubes, the influence depends on the direction of the buoyancy forces and the external forces. When, for instance, a fluid is being heated, the warmer layers near the duct wall will be less dense than the rest of the fluid and will tend to rise. If the fluid is flowing upwards, see figure 7.1, the velocity profile will be distorted by the superimposed free convection so that the velocity is increased near the duct wall.

TABLE 7.4 Circular pipe, turbulent flow. Comparison of formulas by Dittus-Boelter (D-B), Kraussold (K), Sieder-Tate (S-T), Petuhkov (P), Notter-Sleicher (N-S), Gnielinski (G), and Hausen (H).

Re = 2,300								
T	Pr	D-B	K	S-T	P	N-S	G	H
5	11.16	29.6	28.7	25.2	31.6	32.0	18.1	17.8
20	6.99	24.5	24.1	21.5	26.9	27.3	15.5	14.8
40	4.34	20.1	20.1	18.3	22.7	23.7	13.1	12.1
60	3.00	17.5	17.7	16.3	20.1	21.6	11.7	10.4
80	2.23	15.4	15.7	14.6	17.9	19.6	10.5	9.0
100	1.74	14.1	14.4	13.5	16.5	18.1	9.8	8.1
Re = 5,000								
T	Pr	D-B	K	S-T	P	N-S	G	H
5	11.16	55.0	53.4	46.8	46.8	57.8	58.7	46.6
20	6.99	45.6	44.9	40.1	49.5	48.5	40.4	38.8
40	4.34	37.4	37.4	34.0	41.1	41.2	33.8	31.7
60	3.00	32.6	32.9	30.3	35.9	36.9	29.8	27.3
80	2.23	28.7	29.2	27.2	31.6	33.0	26.4	23.6
100	1.74	26.2	26.8	25.2	28.7	30.1	24.1	21.2
Re = 10,000								
T	Pr	D-B	K	S-T	P	N-S	G	H
5	11.16	95.8	93.0	81.6	103.4	101.2	94.6	92.8
20	6.99	79.4	78.1	69.7	86.4	83.8	79.5	77.3
40	4.34	63.2	65.1	59.2	70.9	70.2	65.8	63.2
60	3.00	56.8	57.3	52.7	61.4	62.4	57.3	54.4
80	2.23	49.9	50.9	47.4	53.4	55.2	50.2	47.1
100	1.74	45.5	46.7	43.9	48.1	49.9	45.5	42.3
Re = 50,000								
T	Pr	D-B	K	S-T	P	N-S	G	H
5	11.16	347	337	296	399	391	399	378
20	6.99	288	283	253	328	319	329	314
40	4.34	236	236	214	263	262	266	257
60	3.00	206	208	191	223	229	227	221
80	2.23	181	184	172	189	199	195	192
100	1.74	165	169	159	168	178	173	172
Re = 100,000								
T	Pr	D-B	K	S-T	P	N-S	G	H
5	11.16	604	587	515	723	708	731	669
20	6.99	501	493	440	589	574	599	557
40	4.34	411	411	373	468	468	480	456
60	3.00	358	362	333	394	407	406	392
80	2.23	315	321	299	332	353	345	340
100	1.74	287	295	277	293	314	306	305

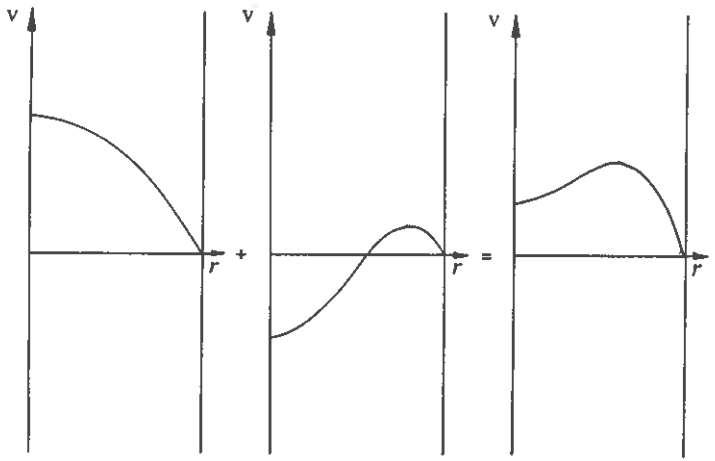

Figure 7.1 Superimposed forced and free convection during aiding flow. The velocity fields for the forced and free convection parts are shown on the left, while the resulting combined velocity field is shown on the right.

This situation, when buoyancy forces and external forces are in the same direction, so-called *aiding flow*, gives an increased heat transfer. Aiding flow also occurs when a cooling fluid is flowing downwards. When the buoyancy forces and external forces are in opposite directions, so-called *opposing flow*, the heat transfer is reduced. An example is given in figure 7.2, with a cooling fluid flowing upwards. The fluid density near the wall is higher than in the center and the fluid tends to sink. A heating fluid flowing downwards also gives opposing flow.

Metais and Eckert (1964) have summarized the flow regimes for vertical tubes. From figure 7.3 the influence of free convection may be estimated qualitatively. The influence of free convection is about 10 % at the interface between the forced convection regime and the mixed free and forced convection regime. The Grashopf's number is to be calculated using the tube diameter D as the characteristic length.

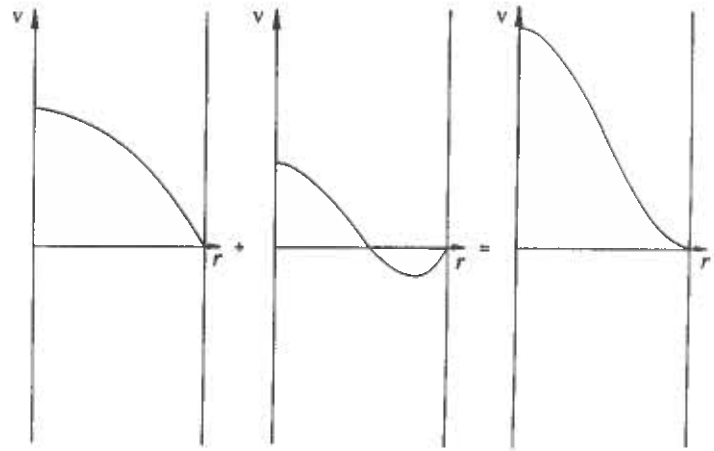

Figure 7.2 Superimposed forced and free convection during opposing flow. The velocity fields for the forced and free convection parts are shown on the left, while the resulting combined velocity field is shown on the right.

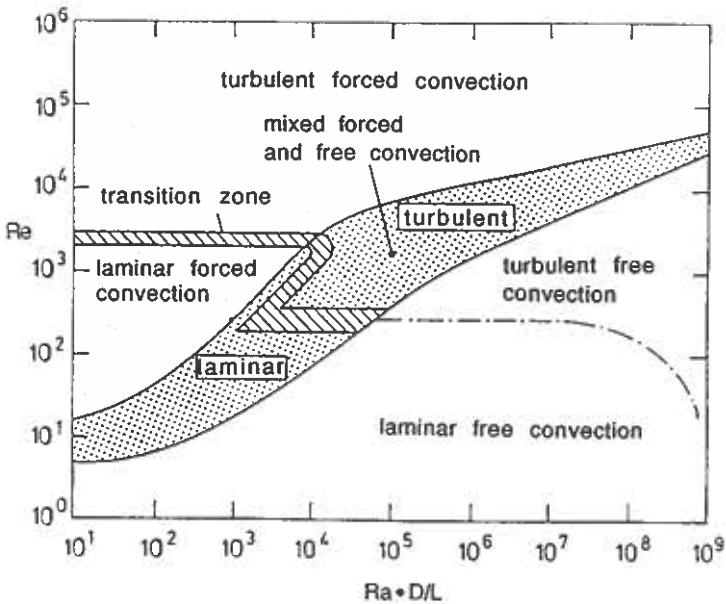

Figure 7.3 Flow regimes for vertical tubes according to Metais and Eckert (1964).

Kreith (1965) gives a similar, but simplified, figure where the curves have been replaced by straight lines. The forced convection regime has the following characteristics: it is bounded at Re=100, below which there is laminar free convection, and there is always turbulent forced convection for Re>10,000. In the range 100<Re<10,000, the forced convection regime is bounded by the following limit:

$$\mathrm{Re} = \left(\frac{\mathrm{Gr}}{36.3}\right)^{0.658} \tag{7.51}$$

For Reynold's numbers lower than this value the influence of free convection is larger than 10 %.

Martinelli and Boelter (1942) studied laminar flow of oil and water in vertical pipes with constant wall temperature. The density is assumed vary linearly with local temperature and other properties are constant. For the case of aiding flow the Nusselt's number becomes:

MARTINELLI-BOELTER

$$\mathrm{Nu} = 1.75 F_1 \left[\mathrm{Gz} + 0.0722(\mathrm{GrPr}D/L)_w^{0.75} F_2\right]^{1/3} \tag{7.52}$$

The factor F_1 corrects for the error due to the use of the arithmetic mean temperature difference. If this correction factor is not included, the Nusselt's number Nu becomes larger than the asymptotic value of $2\mathrm{Gz}/\pi$ for low values of Graetz number Gz. The correction factors F_1 and F_2, which are shown in figure 7.4, depend on the parameter Z:

$$Z = \frac{\pi \mathrm{Nu}}{\mathrm{Gz}} \tag{7.53}$$

Eq. (7.52) has to be solved by an iterative procedure, since the Nusselt's number appears in the parameter Z.

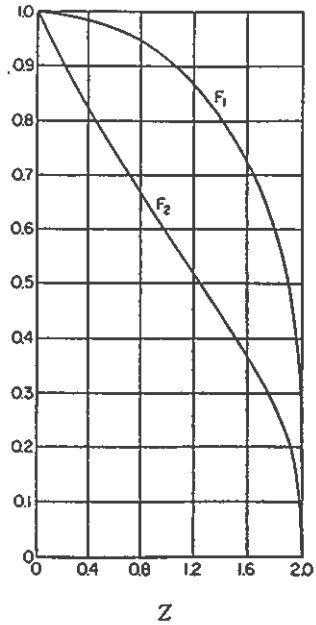

Figure 7.4 The factors $F_1(Z)$ and $F_2(Z)$ used in eq. (7.52). The parameter Z is defined by (7.54).

The Graetz's number Gz should be evaluated at the bulk temperature; Gr and Pr at the wall temperature. The initial temperature difference $T_w - T_{inlet}$ should be used for the temperature difference in Gr. The Grashof's number Gr is based on tube diameter. For the case of opposing flow the factor +0.0722 should be replaced by -0.0722 (Rohsenow et al. 1985). Mullin and Gerhard (1977) have verified the formula, but they remark that the version for opposing flow may underpredict the Nusselt's number. McAdams (1954) reports an accuracy of 25 %.

Although no range of validity except laminar flow is given, there seems to be a problem of applying this formula to very long pipes. The reason for this may be explained as follows. If the term that gives the influence of free convection is neglected (Gr=0), then we have:

$$\mathrm{Nu} = 1.75F_1\mathrm{Gz}^{1/3} = 1.61F_1(\mathrm{RePr}D/L)^{1/3} \qquad (7.54)$$

This is almost identical to the analytical solution for fully developed laminar flow assuming constant viscosity and parabolic velocity distribution. Holman (1968) quotes a comparison made by Knudsen and Katz where the validity of (7.55) is found to be $\mathrm{RePr}D/L > 10$. For $\mathrm{RePr}D/L < 10$ the asymptotic value of the Nusselt's number for constant wall temperature, 3.66, should be used instead. Eq. (7.52) could of course be modified to include this fact, but it is uncertain whether it, as validated by Martinelli and Boelter for mixed free and forced convection, can be extended to this range.

Mixed free and forced convection in vertical tubes has also been studied analytically by Pigford (1955). He included the effect of temperature dependent viscosity. The results are given for viscosity ratios of 0.1, 1, and 10. For viscosity ratios near unity the results are essentially the same as those obtained by Martinelli and Boelter.

7.2.4 Temperature-dependent properties

The fluid properties, especially the viscosity, depend on the fluid temperature. Heating and cooling of a fluid in a duct may result in a large difference in fluid temperature between the center of the pipe and the layer near the pipe wall.

Laminar flow

During heating of the fluid, the temperature near the wall is higher and, consequently, the viscosity is lower. The fluid particles in this region will experience less flow resistance, resulting in higher flow velocities than for the case of constant properties. If this peripheral mass flow increases, there will be a corresponding reduction in the central region of the pipe. In the case of cooling the fluid, the situation is reversed; the peripheral mass flow is reduced due to higher viscosity, and the flow velocities near the center is higher. See figure 7.5.

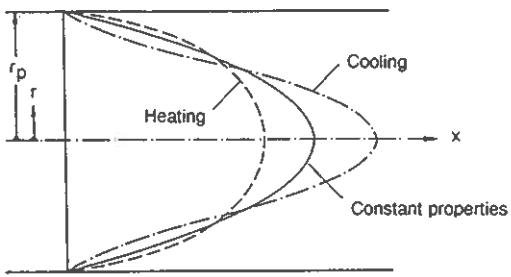

Figure 7.5 The effect of temperature-dependent fluid properties on the velocity field in a tube during laminar flow.

Herwig (1985) gives a correction factor involving several fluid properties for the of constant heat flux:

$$\frac{\mathrm{Nu}}{\mathrm{Nu}_0} = \left(\frac{\rho_w}{\rho_B}\right)^{-0.340-0.128/\mathrm{Pr}_B} \left(\frac{\mu_w}{\mu_B}\right)^{-0.107} \left(\frac{\lambda_w}{\lambda_B}\right)^{0.245} \left(\frac{c_{pw}}{c_{pB}}\right)^{0.255} \qquad (7.55)$$

The Nusselt's number for constant properties is denoted Nu_0. The properties are to be evaluated at wall temperature (index w) and bulk temperature (index B). For water, only the temperature dependence of the viscosity is usually considered. The above formula then reduces to:

$$\frac{Nu}{Nu_0} = \left(\frac{\mu_w}{\mu_B}\right)^{-0.107} \tag{7.56}$$

Yang (1962) studied the effect of temperature dependent viscosity for both a constant wall temperature and a constant heat flux. The results are well approximated by the relation:

$$\frac{Nu}{Nu_0} = \left(\frac{\mu_w}{\mu_B}\right)^{-0.11} \tag{7.57}$$

This correction factor is recommended by the VDI-Wärmeatlas (1988). Joshi and Bergles (1980; 1981) found an exponent of -0.14 for the constant heat flux case and -0.11 for the constant wall temperature case.

Turbulent flow

Many standard formulas for Nusselt's numbers assume constant fluid properties. For liquids only the temperature dependence of the viscosity is of major importance (Kreith 1965; Merker 1987). Since Nusselt's numbers for turbulent flow are strongly affected by variations in fluid viscosity over the flow cross-section, these results are applicable for negligibly small temperature differences.

During turbulent-flow heat transfer the temperature profile is fairly uniform except in the laminar boundary layer near the pipe wall, where there is a sharp temperature gradient. The heat transfer rate is controlled by the thickness of this laminar boundary layer, which is proportional to the fluid viscosity. Consequently, the boundary layer will be thinner and the heat transfer coefficient higher for a fluid being heated than for a fluid being cooled (Bennet and Myers 1962).

It has been found convenient to use constant property analytical solutions, or experimental data with small temperature differences, and then include the viscosity dependence with some kind of a correction factor. The following, fairly simple correction factor has been found to be a good approximation (Kreith 1965; Kays and Crawford 1980; Rohsenow et al. 1985):

$$\frac{Nu}{Nu_0} = (\mu_w/\mu_B)^n \tag{7.58}$$

Here, the Nusselt's number Nu_0 for constant properties and the viscosity μ_B is evaluated at the bulk temperature T_B. The viscosity μ_w is taken at the wall temperature T_w.

Rohsenow et al. (1985) and Merker (1987) recommends the following values of exponent n obtained by Petuhkov (1970):

$$\frac{\mu_w}{\mu_B} > 1 \qquad n = -0.25 \qquad \text{cooling} \tag{7.59}$$

$$\frac{\mu_w}{\mu_B} < 1 \qquad n = -0.11 \qquad \text{heating} \tag{7.60}$$

These values of the exponent give a good fit with experimental data in the range $0.08 < \mu_B/\mu_w < 40$, 10,000<Re<125,000, 2<Pr<140.

There is obviously a stronger influence during cooling of the fluid, when the boundary layer becomes more viscous. For $1< \mu_w/\mu_B <1000$ Hausen (1976) has proposed:

$$\frac{\mathrm{Nu}}{\mathrm{Nu}_0} = 0.645(\mu_w/\mu_B)^{-0.3} + 0.355 \tag{7.61}$$

The fluid temperature, and thus the thermophysical properties, often vary along the direction of the flow. For practical purposes it has been found sufficiently accurate to evaluate the thermophysical properties at the bulk fluid temperature T_B (Kreith 1965).

Axial heat conduction, that is heat conduction in the direction of the flow, is discussed by Merker (1987). He shows that the influence of axial heat conduction in the fluid is less 1 % for $\mathrm{RePr}L/D >100$, which means that the effect is negligible for ground heat exchangers.

The formulas given here have been derived assuming either constant heat flux or constant temperature at the pipe wall. Kays and Crawford (1980) have studied axial variations of heat flux and wall temperature. It is possible to construct a solution for an arbitrary variation of wall temperature or heat flux by superposing of a number fundamental thermal-entry-length solutions. This technique, which is fairly straightforward but rather lengthy, will not be exploited here. We will only quote some general conclusions from these studies: an increasing heat flux, or an increasing temperature difference in the flow direction, leads to higher conductances, whereas the converse leads to lower conductances. These effects may be fairly important during laminar flow. The same tendency apply for turbulent flow, although it is much less pronounced. During turbulent flow, the relative importance of the axial variations are usually negligible at Prandtl number around 1 or higher. As an example, Kays and Crawford take the design of a nuclear reactor cooling system where the heat flux is known function of the length along the tube. If the coolant is a gas or pressurized water, the varying heat flux has very little influence, and it is perfectly adequate to use a Nusselt's number based on constant heat flux theory.

7.2.5 Surface roughness

The formulas presented here assumes that the pipe surface is technically smooth. A rough surface will increase the heat transfer.

The major thermal resistance during turbulent flow is the thin laminar boundary layer adjacent to the wall. The resistance of this layer is proportional to its thickness. Any reduction of the thickness will result in a comparable increase in the heat transfer rate (Knudsen and Katz 1958). The thermal resistance for a rough surface is lower than for a smooth surface because the roughness tends to break up the laminar layer. The effect increases with the Prandtl's number, since the sublayer becomes more important at high Prandtl's number. Many authors refer to studies on this subject made by Dipprey and Sabersky (1963). However, for practical use Kays and Crawford (1980) and Merker (1987) recommend a simple empirical correlation suggested by Norris (1971):

$$\frac{\mathrm{Nu}}{\mathrm{Nu}_{smooth}} = \left(\frac{f}{f_{smooth}}\right)^n \tag{7.62}$$

$$n = 0.68 Pr^{0.215} \tag{7.63}$$

For $f/f_{smooth} > 4.0$ Norris finds that the Nusselt number no longer increases.

The correlation contains the friction factor f, which is a function of the relative roughness and the Reynolds number. A figure showing this relation can be found in most textbooks on convective heat and mass transfer. The relative roughness is the ratio between the absolute roughness e and the hydraulic diameter d_h. When the roughness effects on friction become very large, no further increase in heat transfer is observed because the heat-transfer resistance has become primarily a conduction resistance at the surface.

Cope (1941) reported that smooth pipes are more efficient than rough pipes when compared on the basis of the amount of heat transferred per unit power used to pump the fluid through the pipe.

Artificial roughness is frequently employed to increase the heat transfer. A common and efficient method is to insert a very thin wire along the surface transverse to the flow direction. This so-called internal repeated rib roughness and similar arrangements, such as wire coil or spiral spring inserts, will trip and break up the laminar boundary layers (Rohsenow et al. 1985b; Uttarwar and Raja Rao 1985; Chiou 1987). The friction coefficient is also increased; but if the protrusion is small enough to be primarily within the boundary layer, the increase in pumping power is not disproportionate to the increase in heat transfer (Kays and Crawford 1980). A review of techniques to augment heat transfer is given in Rohsenow et al. (1985b).

During laminar flow the influence of the surface roughness is negligible, since the roughness disturbs only a small part of the viscous layer that extends to the center of the pipe (Merker 1987).

7.2.6 Fouling

The heat transfer formulas given for laminar and turbulent flow concern pipes with clean surfaces. It is a well-known fact that dirt often accumulates on the surfaces of industrial heat-transfer equipment. The layer of dirt represents an additional thermal resistance, *fouling resistance* or *fouling factor*, between the heat carrier fluid and the pipe wall. This fouling resistance will usually increase with time until cleaning is necessary. There are instances where the thickness of the dirt layer ceases to grow after some time. The accumulation rate and the asymptotic value depend on the flow velocity. The thermal conductivities of the dirt deposits may be high, but the thermal conductivity of the fluid contained in pores within the dirt is often much lower. Therefore, the effective thermal conductivity may be almost as low as that of the fluid (Bennet and Myers 1962)

There is a number of mechanisms that may cause fouling of the heat transfer surface: precipitation of dissolved substances, deposits formed by chemical reactions, accumulation of small particles, corrosion, and growth of biological material. The fouling often stems from several of these factors, which may result in synergistic effects.

The fouling factor, which depends on the characteristics of the heat carrier fluid, is usually included when calculating the overall heat transfer coefficient of industrial heat exchangers. It is desirable that the value of the fouling factor to be used is based on previous operating experience of a similar heat exchanger (Kay and Nedderman 1974). Tables with fouling factors can be found in most books on applied heat transfer. Some typical values of the fouling factor R'_{foul} are given in Table 7.5.

TABLE 7.5 Fouling factors (m^2K/W)

Sea water below 50 °C (125 °F)	0.00009
Sea water above 50 °C (125 °F)	0.0002
Treated boiler feed water above 50 °C (125 °F)	0.0002

The additional thermal resistance R_{foul} (mK/W), cf. (6.27), to be added to the heat transfer resistance between the fluid and the wall of a circular pipe becomes:

$$R_{foul} = \frac{R'_{foul}}{2\pi r_p} \tag{7.64}$$

7.3 Circular-Tube Annulus

This section deals with the thermal resistance between the heat carrier fluid and the confining walls of an annulus, i.e. a flow channel between two concentric cylindrical surfaces. The inner cylinder has the radius r_i and the outer cylinder has the radius r_o. The ratio between these radii is denoted:

$$r^* = \frac{r_i}{r_o} \tag{7.65}$$

The mean fluid velocity in the annulus is v_f. The fluid flow rate V_f (m^3/s) is then:

$$V_f = v_f \pi (r_o^2 - r_i^2) \tag{7.66}$$

In this case, the characteristic length used in the calculation of the Reynold's number is chosen to be the hydraulic diameter d_h, which is defined by:

$$d_h = 2(r_o - r_i) \tag{7.67}$$

The Reynold's number for the annulus may then be written as:

$$\mathrm{Re} = \frac{d_h v_f}{\nu_f} = \frac{2(r_o - r_i) v_f \rho_f}{\mu_f} \tag{7.68}$$

Alternatively, the Reynold's number may be expressed with use of the fluid flow rate (7.67):

$$\mathrm{Re} = \frac{4\rho_f}{\pi \mu_f} \frac{V_f}{2(r_o + r_i)} \tag{7.69}$$

The upper limit for unconditional laminar flow lies at Re=1000 for flow channels that are very thin in relation to r_i. The situation then resembles flow in the plane geometry between two flat plates. For wider flow channels the critical value of the Reynold's number increases. For Re>10,000 we have, as for the circular pipe, a flow that is almost certainly turbulent. In the region between the critical value for unconditional laminar flow and Re=10,000 the flow conditions are not completely determined by the Reynold's number alone. See section 7.1.4.

The Nusselt's number for the annulus is defined by:

$$\mathrm{Nu} = \frac{\alpha\, d_h}{\lambda_f} = \frac{\alpha\, 2(r_o - r_i)}{\lambda_f} \tag{7.70}$$

The heat transfer coefficient α (W/m^2K) is given per unit area and may vary along the pipe. See section 6.2.3. The Nusselt's number usually concerns

the average value of α along the whole channel. The heat flow per unit area between the fluid and the wall then becomes $\alpha\Delta T$. Here ΔT is the difference between the bulk fluid temperature T_B and the wall temperature T_w. The heat transfer coefficient differs for the inner and the outer wall, except when the flow channel is very thin. The subscripts i and o refer to conditions on the inner and outer surface, respectively, under any condition of simultaneous heating at both surfaces. The heat flow per unit length from the inner wall to the fluid is q_i (W/m). Then we get:

$$\alpha_i \, \Delta T_i = \frac{q_i}{2\pi r_i} \qquad (\mathrm{W/m^2}) \tag{7.71}$$

The thermal resistance R_{fai} between the fluid and the inner wall becomes:

$$R_{fai} = \frac{1}{2\pi r_i \, \alpha_i} \qquad \Delta T_i = q_i \, R_{fai} \tag{7.72}$$

A relation containing the Nusselt's number Nu_i is obtained with use of (7.71):

$$R_{fai} = \frac{1}{\pi \lambda_f \mathrm{Nu}_i} \left(\frac{1}{r^*} - 1 \right) \tag{7.73}$$

The heat flow per unit length from the outer wall to the fluid is q_o (W/m). The corresponding heat flux is then:

$$\alpha_o \, \Delta T_o = \frac{q_o}{2\pi r_o} \qquad (\mathrm{W/m^2}) \tag{7.74}$$

The heat transfer coefficient between the outer wall and the fluid is denoted α_o. The thermal resistance R_{fao} between the fluid and the outer wall becomes:

$$R_{fao} = \frac{1}{2\pi r_o \, \alpha_o} \qquad \Delta T_o = q_o \, R_{fao} \tag{7.75}$$

From equations 7.71 and 7.76 we finally get:

$$R_{fao} = \frac{1}{\pi \lambda_f \mathrm{Nu}_o} (1 - r^*) \tag{7.76}$$

The Nusselt's numbers Nu_i and Nu_o for the case of a concentric inner pipe can be calculated with use of formulas presented in the VDI-Wärmeatlas (1988) and the Handbook of Heat Transfer Fundamentals (Rohsenow et al. 1985). The results presented here are valid for smooth pipes. The roughness of a borehole wall may increase the Nusselt's number (See section 7.2.5).

The two surfaces of an annular duct can be heated (or cooled) independently. This affects the values of the two Nusselt's numbers. The subscript ii designates conditions on the inner surface when the inner surface alone is

heated or cooled (the opposite surface being insulated), and *oo* designates corresponding conditions on the outer surface.

For the case of *constant heat rate* per unit borehole length, it is possible to express Nu_i and Nu_o for any flux ratio on the two surfaces, in terms of Nu_{ii} and Nu_{oo} and a pair *influence coefficients* θ_i^* and θ_o^*. The following equations are used:

$$\mathrm{Nu}_i = \frac{\mathrm{Nu}_{ii}}{1 - (q_o/q_i)\theta_i^*} \tag{7.77}$$

$$\mathrm{Nu}_o = \frac{\mathrm{Nu}_{oo}}{1 - (q_i/q_o)\theta_o^*} \tag{7.78}$$

Here q_i and q_o are the heat flux at the inner and outer surface, respectively, defined by:

$$q_i = \alpha_i(T_{w,i} - T_B) \tag{7.79}$$

$$q_o = \alpha_o(T_{w,o} - T_B) \tag{7.80}$$

Note that the heat flux is positive when heating the fluid.

During heating of the store the heat flows will have the following signs:

Injection through annulus	$q_i < 0$	$q_o < 0$
Injection through core	$q_i > 0$	$q_o < 0$

During heat extraction from the store the signs will be reversed:

Injection through annulus	$q_i > 0$	$q_o > 0$
Injection through core	$q_i < 0$	$q_o > 0$

Typically, the heat flow q_i between the inner and outer flow channel is much smaller than heat flow q_o between the outer flow channel and the ground.

7.3.1 Laminar flow

The Nusselt's numbers Nu_{ii}, Nu_{oo}, and the influence coefficients θ_i^*, θ_o^* for constant heat flux are given as functions of the tube radius ratio r^* in Table 7.6 (Lundberg et al. 1963).

TABLE 7.6. Circular-tube annulus, constant heat flux, fully developed velocity and temperature profiles.

r^*	Nu_{ii}	Nu_{oo}	θ_i^*	θ_o^*
0.0	∞	4.364	∞	0.0
0.05	17.81	4.792	2.180	0.0294
0.10	11.91	4.834	1.383	0.0562
0.20	8.499	4.883	0.905	0.1041
0.40	6.583	4.979	0.603	0.1823
0.60	5.912	5.099	0.473	0.2455
0.80	5.580	5.240	0.401	0.299
1.00	5.385	5.385	0.346	0.346

The values of Nu_{ii} and Nu_{oo} can also be calculated with use of the following approximations (VDI-Wärmeatlas 1988):

$$Nu_{ii} = 3.66 + 1.2\,(r^*)^{-0.8} \tag{7.81}$$

$$Nu_{oo} = 3.66 + 1.2\,(r^*)^{0.5} \tag{7.82}$$

These formulas are valid for Re<2300 and $0.1 \leq Pr \leq 1000$. They yield slightly lower values than table 7.6.

Lundberg et al. (1963) have shown that it is possible to reduce the problem with fully developed velocity profile to just four fundamental solutions, which can then be combined using superposition techniques to yield a solution for any desired boundary conditions. This technique will not be presented or used in this book, since it involves rather large tables of data for the different fundamental solutions. To be of practical use, this superposition technique requires a computer. The reader is referred to Rohsenow et al. (1985) for further details. It should also be noted that these fundamental solutions do not include free convection effects, which may be important during laminar flow.

The Nusselt's number Nu_i and Nu_o for constant temperature on one wall and the other insulated are given as functions of the tube radius ratio r^* in Table 7.7 (Lundberg et al. 1963).

TABLE 7.7. Circular-tube annulus, constant wall temperature, fully developed velocity and temperature profiles.

r^*	Nu_i	Nu_o
0.0	∞	3.66
0.05	17.46	4.06
0.10	11.56	4.11
0.25	7.37	4.23
0.50	5.74	4.43
1.00	4.86	4.86

VDI Wärmeatlas (1988) gives the following formula for the mean Nusselt's number, Nu_i or Nu_o, with constant temperature on one wall and the other one insulated. (Re<2300, 0.1<Pr<1000, $0 < r^* < 1$). The formula includes entrance effects and a correction term for temperature-dependent properties (see section 7.2.4).

$$Nu = \left[Nu_\infty + f(r^*) \frac{0.19\,Gz^{0.8}}{1 + 0.117\,Gz^{0.467}} \right] \left(\frac{Pr}{Pr_w} \right)^{0.11} \tag{7.83}$$

where

$$Gz = Re\ Pr \frac{d_h}{L} \tag{7.84}$$

The asymptotic Nusselt's number Nu_∞ is obtained from table 7.6 or eqs. (7.82-83). The Prandtl's number Pr_w is taken at the wall temperature T_w. All other fluid properties are evaluated at the bulk fluid temperature T_B.

The shape factor $f(r^*)$ differs for the inner and the outer surface:

$$f_i(r^*) = 1 + 0.14\,(r^*)^{1/2} \tag{7.85}$$

$$f_o(r^*) = 1 + 0.14\,(r^*)^{1/3} \tag{7.86}$$

7.3.2 Turbulent flow

Kays and Leung (1963) have presented tables that are in excellent agreement with experimental data for air (Pr~0.7). There is no reason why they should not be equally valid for high Prandtl's number (Kays and Crawford 1980). The tables, which concern the case of constant heat rate and fully developed flow, are also given in (Rohsenow et al. 1985; Kays and Crawford 1980).

TABLE 7.8. Circular-tube annulus, fully developed turbulent flow, constant heat flux

Reynold's number = 10,000						
	Pr=1		Pr=3		Pr=10	
r^*	Nu_{oo}	θ_o^*	Nu_{oo}	θ_o^*	Nu_{oo}	θ_o^*
0.1	36.5	0.026	61.5	0.013	99.2	0.006
0.2	35.5	0.051	60.0	0.026	98.0	0.013
0.5	34.8	0.111	60.5	0.059	100	0.028
0.8	34.8	0.159	61.3	0.083	100	0.039
1.0	35.0	0.182	60.8	0.095	101	0.045
Reynold's number = 30,000						
	Pr=1		Pr=3		Pr=10	
r^*	Nu_{oo}	θ_o^*	Nu_{oo}	θ_o^*	Nu_{oo}	θ_o^*
0.1	81.8	0.023	147	0.013	246	0.006
0.2	80.0	0.046	145	0.026	243	0.013
0.5	78.0	0.101	144	0.058	246	0.028
0.8	76.5	0.141	142	0.079	243	0.039
1.0	76.8	0.162	142	0.092	241	0.045
Reynold's number = 100,000						
	Pr=1		Pr=3		Pr=10	
r^*	Nu_{oo}	θ_o^*	Nu_{oo}	θ_o^*	Nu_{oo}	θ_o^*
0.1	212	0.021	395	0.012	685	0.006
0.2	206	0.042	390	0.024	680	0.012
0.5	200	0.092	384	0.055	680	0.028
0.8	197	0.129	382	0.078	670	0.039
1.0	197	0.148	380	0.089	680	0.045

TABLE 7.9. Circular-tube annulus, fully developed turbulent flow, constant heat flux

Reynold's number = 10,000						
	Pr=1		Pr=3		Pr=10	
r^*	Nu_{ii}	θ_i^*	Nu_{ii}	θ_i^*	Nu_{ii}	θ_i^*
0.1	58.5	0.412	93.5	0.202	140	0.089
0.2	46.8	0.339	77.4	0.172	120	0.120
0.5	38.2	0.247	66.8	0.129	106	0.059
0.8	35.5	0.200	63.0	0.108	102	0.051
1.0	35.0	0.182	60.8	0.095	101	0.045
Reynold's number = 30,000						
	Pr=1		Pr=3		Pr=10	
r^*	Nu_{ii}	θ_i^*	Nu_{ii}	θ_i^*	Nu_{ii}	θ_i^*
0.1	120	0.338	206	0.175	328	0.081
0.2	99.0	0.284	175	0.151	290	0.074
0.5	83.5	0.218	152	0.121	260	0.059
0.8	78.3	0.181	145	0.102	248	0.051
1.0	76.8	0.162	142	0.092	241	0.045
Reynold's number = 100,000						
	Pr=1		Pr=3		Pr=10	
r^*	Nu_{ii}	θ_i^*	Nu_{ii}	θ_i^*	Nu_{ii}	θ_i^*
0.1	292	0.286	535	0.162	890	0.078
0.2	247	0.248	465	0.143	800	0.072
0.5	212	0.208	402	0.115	715	0.059
0.8	202	0.166	386	0.097	693	0.052
1.0	197	0.148	380	0.089	680	0.045

Based on their experimental data, Petuhkov and Roizen (1965) derived a correlation with formulas for circular pipes. They claim that the formulas are in very good agreement with the tabulated values above given by Kays and Leung (1963). For all investigated pipes the Nusselt's number is given with an accuracy of ±5 %. The heat transfer for turbulent flow in a concentric annulus may then be calculated from modified formulas for turbulent flow in circular pipes:

$$\begin{aligned} Nu_{ii} &= \zeta\, Nu_{pipe}\, 0.86\,(r^*)^{-0.16} && 0.07 \le r^* \le 1 \\ Nu_{oo} &= Nu_{pipe}\,[1 - 0.14\,(r^*)^{0.6}] && 0 \le r^* \le 1 \end{aligned} \tag{7.87}$$

where

$$\zeta = \begin{cases} 1 + 7.5\left(\frac{1/r^* - 5}{Re}\right)^{0.6} & r^* < 0.2 \\ 1 & r^* \ge 0.2 \end{cases} \tag{7.88}$$

Both equations are valid in the range $10^4 \leq Re \leq 3 \cdot 10^5$ at Pr~0.7. VDI-Wärmeatlas (1988) extends the range of validity and gives a range of $0 < r^* < 1$ for (7.88) with the correction factor $\zeta=1$ in the whole interval. The Nusselt's number Nu_{pipe} for turbulent flow in a circular pipe may be obtained from the formulas given by Gnielinski (7.49) or Hausen (7.50). The hydraulic diameter d_h (7.68) should then replace the pipe diameter when the Reynold's number is calculated. According to VDI-Wärmeatlas, the formula is valid for $2300<Re<10^6$, $0.6<Pr<1000$.

7.3.3 Eccentric annular duct

It may be difficult to avoid some degree of eccentric placement of the inner pipe in a real application. The eccentricity will reduce the heat transfer. In the case where the inner pipe is not fixed in a concentric position, but hangs loosely so that it may touch the outer wall, the reduction in heat transfer may be considerable. It is therefore of interest to be able to estimate the effects of eccentricity.

In an eccentric annulus, the Nusselt's number will vary along the periphery of the inner and outer pipe. The average value on the periphery, the effective Nusselt's number, is given as a function of the eccentricity ratio $e^* = e/(r_o - r_i)$. Here, r_i and r_o are the radius of the inner and the outer pipe, respectively. The eccentricity parameter e is the distance between the center of the inner pipe and the center of the outer pipe.

Laminar flow

Shah and London (1978) give the effective Nusselt's number as a function of the eccentricity ratio e^* and radius ratio r^* (7.66) for fully developed laminar flow with constant axial and peripheral heat flux on one surface and the other surface insulated. See Table 7.10.

The effective Nusselt's number decreases with the eccentricity ratio e^*. The Nusselt's number may become substantially lower than for the concentric case, especially at large values of the radius ratio r^*.

Turbulent flow

Judd and Wade (1963) have presented experimental data for turbulent flow of water in an eccentric annulus for the case of heating from the inner surface and the outer surface insulated. They found a small tendency for the effective Nusselt number to decrease with increasing eccentricity.

Leung et al. (1962) give experimental data for the flow of air with fully developed constant heat flux. Measurements were made for heating from both

the inner and the outer surfaces independently with the other surface insulated. They found a decrease in the average Nusselt's number with eccentricity that was considerably larger than that reported by Judd and Wade (1963).

The effect of eccentricity on turbulent-flow heat transfer in circular-tube annuli (experimental data for air) for $30,000 < \mathrm{Re} < 80,000$ is presented by Kays and Crawford (1980). See Table 7.11. It is based on the experimental results of Leung et al. (1962).

TABLE 7.10. Eccentric annular ducts. Laminar flow.
Effective Nusselt's numbers.

	Nu_{ii}						
	e^*						
r^*	0.00	0.20	0.40	0.60	0.80	0.90	0.95
0.05	17.81	16.61	14.09	11.63	9.447	8.458	8.035
0.10	11.91	10.75	8.627	6.840	5.427	4.766	4.511
0.20	8.499	7.136	5.140	3.836	2.971	2.578	2.382
0.40	6.583	4.290	2.391	1.612	1.214	1.050	0.9584
0.60	5.912	2.200	0.9223	0.5790	0.4320	0.3756	0.3439
0.80	5.58	0.5670	0.1927	0.1173	0.0881	0.0774	0.0713
0.90	-	0.1344	0.0435	0.0264	0.0200	0.0177	0.0164
0.95	-	0.0322	0.0103	0.0063	0.0048	0.0042	0.0039
	Nu_{oo}						
	e^*						
r^*	0.00	0.20	0.40	0.60	0.80	0.90	0.95
0.05	4.792	4.584	4.223	4.017	4.000	4.015	4.029
0.10	4.834	4.497	3.962	3.677	3.639	3.653	3.677
0.20	4.883	4.221	3.347	2.932	2.831	2.829	2.828
0.40	4.979	3.299	1.977	1.513	1.356	1.312	1.281
0.60	5.099	1.903	0.835	0.567	0.472	0.440	0.419
0.80	5.240	0.531	0.184	0.116	0.092	0.083	0.078
0.90	-	0.130	0.043	0.026	0.020	0.018	0.017
0.95	-	0.032	0.010	0.006	0.005	0.004	0.004

TABLE 7.11. Eccentric annular ducts. Effective Nusselt's numbers at turbulent flow.

r^*	e^*	$Nu_{ii}^{max}/Nu_{ii}^{conc}$	$Nu_{ii}^{min}/Nu_{ii}^{conc}$	$Nu_{oo}^{max}/Nu_{oo}^{conc}$	$Nu_{oo}^{min}/Nu_{oo}^{conc}$
0.255	0.27	0.99	0.97	1.02	0.93
	0.50	0.94	0.92	0.98	0.86
	0.77	0.92	0.88	0.93	0.77
0.500	0.54	0.96	0.87	1.01	0.78
	0.77	0.87	0.67	0.88	0.62

Chapter 8

Fluid-to-Ground Thermal Resistance

The heat transfer between the heat carrier fluid and the surrounding ground depends on the arrangement of the flow channels, the convective heat transfer in the ducts, and the thermal properties of the materials affected by the thermal process. The thermal resistances associated with these different parts may be assembled to form a single fluid-to-ground thermal resistance. An example is the thermal resistance between the heat carrier fluid and the borehole wall, which has been called the borehole thermal resistance. The fluid-to-ground thermal resistance will be denoted R_b (borehole) to comply with existing nomenclature.

Procedures to calculate R_b can be derived for different types of ground heat exchangers. The configurations considered here are the single duct, the annular duct, and ducts in a composite region. They are treated in sections 8.1, 8.3, and 8.4, respectively. The procedures are straightforward, except for ducts in composite regions, i.e. boreholes with U-shaped inner pipes and similar arrangements. There is then a steady-state, two-dimensional heat conduction problem in the composite region of borehole filling and adjacent ground. See figure 8.1. We are in particular interested in the relations between heat fluxes q_n (W/m) from the pipes and differences between the fluid temperatures (T_{fn}) of the pipes and the borehole wall temperature (T_b). The general relations between temperatures and heat flows are discussed in section 8.2. One simple approach to solve this problem is to represent the flow channels by line sources. A general method for a number of line sources is presented. The case of two pipes placed in a symmetrical position is solved. An advanced analytical method, the multipole method, has been developed to obtain a more accurate solution for this case (Bennet et al 1987). An accurate formula for two symmetric pipes are derived with multipoles of the first order.

If the space between the pipes and borehole wall is filled with a liquid, the influence of natural convection should be accounted for. We have conducted a laboratory experiment to investigate this problem. It will be described in the forthcoming Part II. We assume in this study that the effect of natural convection is negligible.

The procedures to calculate the fluid-to-ground thermal resistances may be implemented in detailed numerical simulation models. It is important that the models use an accurate method to calculate the heat transfer between the different flow channels and the surrounding ground for varying temperatures or heat fluxes *along* the ground heat exchanger. The heat balance equations for the case of two counterflow flow channels, or multiple flow channel arrangements that may be reduced to a similar set of equations due to symmetry properties, are given in section 8.5.

The effectiveness of the borehole heat exchanger, considering the influence of variable temperature along the flow channels and the ensuing heat exchange between these channels, is of interest from an engineering point-of-view. It is possible to derive formulas for an effective fluid-to-ground thermal resistance if the boundary conditions along the ground heat exchanger are simplified. In section 8.6, the cases of uniform ground temperature or heat flux will be considered.

8.1 Single duct

The thermal resistance between the heat carrier fluid and the material immediately outside of a single duct consists of three parts:

- Convective heat transfer resistance R_{fc} between the bulk fluid and the inner surface of the duct. See section 7.2 for the case of a circular pipe.
- Thermal resistance R'_p of the duct wall. See section 8.1.1.
- Contact resistance R_c at the interface between the duct and the surrounding material. See section 8.1.2.

The total thermal resistance between the fluid and the material surrounding the duct then becomes:

$$R_p = R_{fc} + R'_p + R_c \tag{8.1}$$

When the duct is in contact with the surrounding ground, this formula gives the fluid-to-ground thermal resistance. The thermal resistance will then be denoted R_b.

8.1.1 Thermal resistance of pipe wall

The thermal resistance of a circular pipe wall is given by the well-known formula for steady-state heat conduction through an annular region:

$$R'_p = \frac{1}{2\pi\lambda_p}\ln(r_{po}/r_{pi}) \tag{8.2}$$

Here, λ_p is the thermal conductivity of the pipe material. The inner and outer radius of the pipe are r_{pi} and r_{po}, respectively.

8.1.2 Contact resistance

The heat transfer at the interface between heat exchanging duct and the surrounding ground often takes place via a contact thermal resistance. This contact resistance results when the outer surface of the duct is not in perfect thermal contact with the surrounding ground.

In a lined borehole in rock there will usually be a thin gap between the liner and the borehole wall. The thermal resistance of this gap depends on the thermal conductivity λ_s of the material that fills the gap. This contact resistance can be estimated by the formula:

$$R_c = \frac{1}{2\pi\lambda_s}\ln\left(\frac{r_{po}+\delta r}{r_{po}}\right) \tag{8.3}$$

The outer radius of the duct is denoted r_{po} and a characteristic width of the gap is δr. It is assumed the contribution from convective and radiative heat transfer can be neglected in the gap. If δr is small compared to r_{po}, eq. (8.3) can be approximated by:

$$R_c = \frac{1}{2\pi\lambda_s}\frac{\delta r}{r_{po}} \tag{8.4}$$

8.2 General relations between temperatures and heat flows

We are in this chapter studying the local, steady-state heat conduction problem between the heat carrier fluid in the ducts and the adjacent surrounding ground. The process is by definition two-dimensional in a cross-section perpendicular to the ducts. The general case with N channels is illustrated in figure 8.1. The ducts lie in a circular borehole with the thermal conductivity λ_b and the borehole radius r_b. The composite region is bounded by the pipe circles with the inner radii $r_{pi,n}$ at which there are the given fluid temperatures T_{fn}. There is a total thermal resistance R_{pn} between the fluid and the borehole filling as described in section 8.1. The temperature in the ground

close to the borehole will vary somewhat around the borehole. Therefore, we consider an outer boundary with the radius r_c ($> r_b$) where the temperature is T_c.

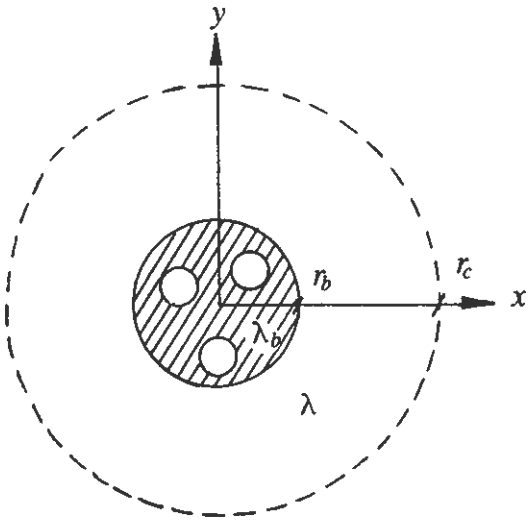

Figure 8.1. Steady-state heat conduction problem for ducts in a composite region of borehole filling material and adjacent ground region. The heat flow from pipe n with the fluid temperature T_{fn} is q_n (W/m). The temperature at the outer radius $r = r_c$ is T_c.

8.2.1 Equation systems

There are N independent temperature differences $T_{fn} - T_c$ and N heat flows q_n. The flow through the outer circle $r = r_c$ is equal to the sum q of all duct heat flows $q_1, \ldots, q_N$. We are interested in the relation between temperatures and heat flows. In the simplest case of a single duct ($N = 1$) we have in accordance with the previous section:

$$T_f - T_b = R_b \cdot q \tag{8.5}$$

Here T_b denotes the temperature in the ground outside the duct.

The heat conduction problem is linear. We have in general:

$$T_{fm} - T_c = \sum_{n=1}^{N} R^c_{mn} \cdot q_n \qquad \text{for } m = 1, \ldots, N \tag{8.6}$$

The coefficients R^c_{mn} are obtained from solutions of the two-dimensional, steady-state problem. The dimension of the coefficients is that of a thermal resistance (K/(W/m)). We have a thermal resistance matrix $[R^c_{mn}]$ to describe

the relation between boundary temperatures and heat flows. It may be noted that the matrix is symmetric according to Maxwell's reciprocity theorem:

$$R^c_{mn} = R^c_{nm} \tag{8.7}$$

The presence of the outer boundary at an arbitrary position $r = r_c$ is somewhat awkward. But we will find in the particular solutions in section 8.4 that the resistances R^c_{mn} depend on r_c in a simple way. In the limit when r_c/r_b is large we get:

$$R^c_{mn} = R^o_{mn} + \frac{1}{2\pi\lambda} \ln\left(\frac{r_c}{r_b}\right) \tag{8.8}$$

Here, the thermal resistances R^o_{mn} are *independent* of the position r_c of the outer boundary.

We now define the temperature T_b by:

$$T_b - T_c = q \cdot \frac{1}{2\pi\lambda} \ln\left(\frac{r_c}{r_b}\right) \qquad q = \sum_{n=1}^{N} q_n \tag{8.9}$$

The borehole temperature T_b is the temperature at $r = r_b$ that gives the correct heat flow q through the annulus $r_b < r < r_c$. It is therefore the *average* temperature around the borehole periphery. Combining (8.6), (8.8), and (8.9) we obtain:

$$T_{fm} - T_b = \sum_{n=1}^{N} R^o_{mn} \cdot q_n \qquad \text{for } m = 1, \ldots, N \tag{8.10}$$

This relation does not depend on the arbitrary outer circle $r = r_c$. It should be noted that the effect of the ground region $r > r_b$ is accounted for in the expressions for R^o_{mn}.

8.2.2 Thermal Δ-circuit for two pipes

A thermal Δ-circuit will be used in the case $N = 2$ to describe the local heat flow between the flow channels and the borehole wall. See figure 8.2. We have for the case of two ducts:

$$\begin{aligned} T_{f1} - T_b &= R^o_{11} q_1 + R^o_{12} q_2 \\ T_{f2} - T_b &= R^o_{12} q_1 + R^o_{22} q_2 \end{aligned} \tag{8.11}$$

The inversion of (8.11) gives the heat flows as functions of the temperatures:

$$\begin{aligned} q_1 &= \frac{R^\circ_{22} - R^\circ_{12}}{R^\circ_{11}R^\circ_{22} - (R^\circ_{12})^2}(T_{f1} - T_b) + \frac{R^\circ_{12}}{R^\circ_{11}R^\circ_{22} - (R^\circ_{12})^2}(T_{f1} - T_{f2}) \\ q_2 &= \frac{R^\circ_{11} - R^\circ_{12}}{R^\circ_{11}R^\circ_{22} - (R^\circ_{12})^2}(T_{f2} - T_b) + \frac{R^\circ_{12}}{R^\circ_{11}R^\circ_{22} - (R^\circ_{12})^2}(T_{f2} - T_{f1}) \end{aligned} \tag{8.12}$$

Introducing thermal resistances R^Δ_1, R^Δ_2, and R^Δ_{12} we get:

$$\begin{aligned} q_1 &= \frac{T_{f1} - T_b}{R^\Delta_1} + \frac{T_{f1} - T_{f2}}{R^\Delta_{12}} \\ q_2 &= \frac{T_{f2} - T_b}{R^\Delta_2} + \frac{T_{f2} - T_{f1}}{R^\Delta_{12}} \end{aligned} \tag{8.13}$$

This pair of equations may be represented schematically by a thermal circuit of Δ-type, which is shown on the right in figure 8.2.

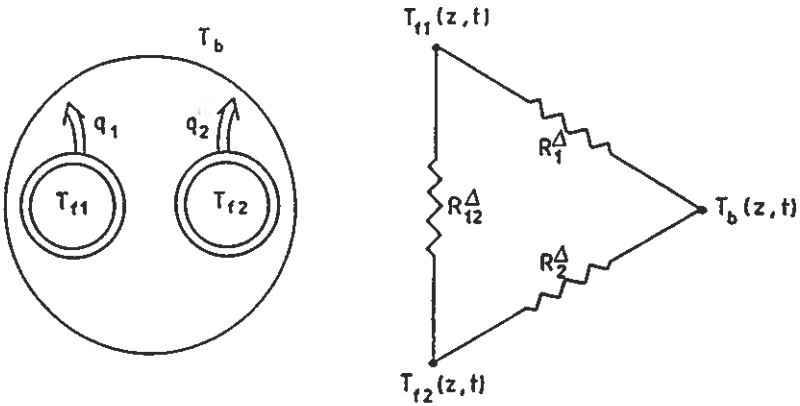

Figure 8.2. Cross-section of the borehole and the corresponding thermal Δ-circuit.

The thermal resistances of the Δ-circuit become from (8.12) and (8.13):

$$R^\Delta_1 = \frac{R^\circ_{11}R^\circ_{22} - (R^\circ_{12})^2}{R^\circ_{22} - R^\circ_{12}} \qquad R^\Delta_2 = \frac{R^\circ_{11}R^\circ_{22} - (R^\circ_{12})^2}{R^\circ_{11} - R^\circ_{12}}$$

$$R^\Delta_{12} = \frac{R^\circ_{11}R^\circ_{22} - (R^\circ_{12})^2}{R^\circ_{12}} \tag{8.14}$$

The fluid-to-ground thermal resistance R_b, defined by (4.1), is obtained by setting $T_{f1} = T_{f2} = T_f$. The resistance between the fluid temperature T_f

and the borehole wall temperature T_b then consists of the two parallel-coupled resistances R_1^Δ and R_2^Δ:

$$R_b = \frac{R_1^\Delta R_2^\Delta}{R_1^\Delta + R_2^\Delta} \tag{8.15}$$

We will also use the total thermal resistance R_a between the two pipes. This resistance R_a is by figure 8.2 a parallel-coupling of two parts; the resistance R_{12}^Δ and the two resistances R_1^Δ and R_2^Δ coupled in series:

$$\frac{1}{R_a} = \frac{1}{R_1^\Delta + R_2^\Delta} + \frac{1}{R_{12}^\Delta} \tag{8.16}$$

The resistance R_a may be obtained by considering the case $q_a = q_1 = -q_2$, which is obtained by a certain choice of T_b and for given T_{f1} and T_{f2}. We have with the use of the difference between the two equations (8.11):

$$q_a \cdot R_a = T_{f1} - T_{f2} = q_a \cdot [R_{11}^o - R_{12}^o - (R_{12}^o - R_{22}^o)] \tag{8.17}$$

So we have:

$$R_a = \frac{R_{12}^\Delta (R_1^\Delta + R_2^\Delta)}{R_1^\Delta + R_2^\Delta + R_{12}^\Delta} = R_{11}^o + R_{22}^o - 2R_{12}^o \tag{8.18}$$

The two expressions for R_a are of course consistent with (8.14).

In the symmetrical case with $R_{11}^o = R_{22}^o$, eqs. (8.14), (8.15), and (8.18) reduce to:

$$R_1^\Delta = R_2^\Delta = R_{11}^o + R_{12}^o \qquad R_{12}^\Delta = \frac{(R_{11}^o)^2 - (R_{12}^o)^2}{R_{12}^o} \tag{8.19}$$

$$R_b = \frac{R_1^\Delta}{2} = \frac{1}{2}(R_{11}^o + R_{12}^o) \tag{8.20}$$

$$R_a = \frac{2R_{12}^\Delta R_1^\Delta}{2R_1^\Delta + R_{12}^\Delta} = 2(R_{11}^o - R_{12}^o) \tag{8.21}$$

8.3 Annular ducts

In the annular duct, which is shown in figures 2.4 and 8.3, there are two thermal resistances to be calculated: the one between the inner circular flow channel and the outer annular flow channel, and the one between the outer flow channel and the borehole wall.

The thermal resistance between the inner and the outer flow channel consists of three parts:

- Convective heat transfer resistance R_{fc} between the bulk fluid in the inner flow channel and the inner surface of the pipe. See Chapter 7.2.

- Thermal resistance R'_p of the pipe wall. See section 8.1.1.
- Convective heat transfer resistance R_{fai} between the outer surface of the pipe and the bulk fluid in the outer flow channel. See Chapter 7.3.

Using the notation of the Δ-circuit in figure 8.2, let the outer annular flow channel and the inner circular flow channel be number 1 and 2 respectively. The total thermal resistance between the two channels is then:

$$R_{12}^{\Delta} = R_{fc} + R'_p + R_{fai} \tag{8.22}$$

The thermal resistance between the outer flow channel and borehole wall is also composed of three parts:

- Convective heat transfer resistance R_{fao} between the bulk fluid in the annular flow channel and the outer surface of the this channel. See Chapter 7.3.
- Thermal resistance R'_p of the liner. See section 8.1.1.
- Contact resistance R_c at the interface between the liner and the borehole wall. See Chapter 8.1.2.

We then have:

$$R_1^{\Delta} = R_{fao} + R'_p + R_c \tag{8.23}$$

There is no direct connection between the inner flow channel and the borehole wall, which implies:

$$R_2^{\Delta} = \infty \tag{8.24}$$

The thermal circuit is shown in figure 8.3.

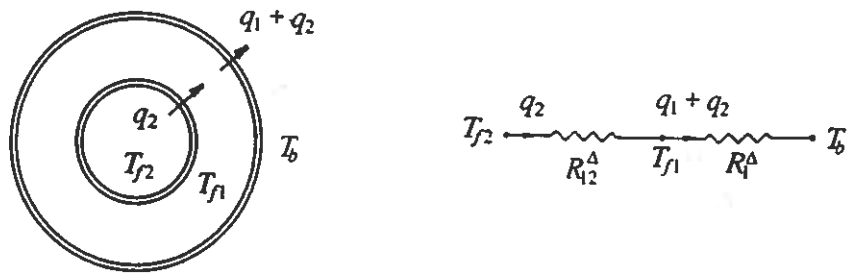

Figure 8.3. Annular ducts and the corresponding thermal circuit.

8.4 Ducts in a composite region

The ground heat exchanger consists of a number of parallel flow channels or ducts in a composite region. The heat flow is two-dimensional in a plane perpendicular to the pipes. The pipes lie in a circular region, which is surrounded by a region of different thermal conductivity. See figure 8.1.

8.4.1 Line-source approximation

The thermal resistances R^o_{mn} can be calculated approximately by representing each pipe with a line source. The steady-state heat flow problem is then solved by use of the superposition technique.

Figure 8.4 shows an example with four pipes in a borehole. The radius of the borehole is r_b. The temperature T_b, which is defined by (8.9), will be an average value around the borehole wall.

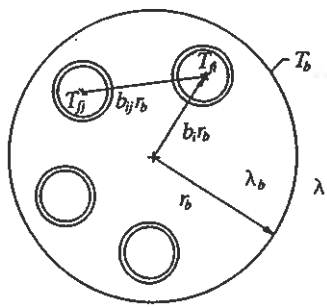

Figure 8.4. Cross-section of a borehole with four flow channels.

Consider the general case with N flow channels in the borehole. The heat injection rate from pipe n is q_n (W/m). The total heat injection rate is given by the sum:

$$q = \sum_{n=1}^{N} q_n \tag{8.25}$$

The center of the pipe n is located at the coordinates (x_n, y_n). The distance from the center of the borehole is given by $b_n r_b$, while the distance between two pipes n and m is $b_{mn} r_b$. Expressed in the coordinates of the pipes, we have:

$$\begin{aligned} b_n &= \frac{\sqrt{x_n^2 + y_n^2}}{r_b} \\ b_{mn} &= \frac{\sqrt{(x_n - x_m)^2 + (y_n - y_m)^2}}{r_b} \qquad \text{for } m, n = 1, \ldots, N \end{aligned} \tag{8.26}$$

The thermal resistance between the fluid and the material immediately outside pipe n is denoted R_{pn}. This resistance is calculated according to section 8.1. There are the following linear relationships for the difference between the fluid temperature T_{fm} and the borehole temperature T_b and the heat flows q_n:

$$T_{fm} - T_b = \sum_{n=1}^{N} R^o_{mn}\, q_n \qquad m = 1, \ldots, N \tag{8.27}$$

The expressions for the line-source thermal resistances R^o_{mm} and R^o_{mn} are derived in Appendix B. They become:

$$\begin{aligned} R^o_{mm} &= \frac{1}{2\pi\lambda_b}\left[\ln\left(\frac{r_b}{r_{pm}}\right) - \sigma\ln(1-b_m^2)\right] + R_{pm} \\ R^o_{mn} &= -\frac{1}{2\pi\lambda_b}\left[\ln(b_{mn}) + \sigma\ln(b'_{mn})\right] \qquad \text{for } m \neq n \end{aligned} \tag{8.28}$$

where

$$b'_{mn} = \sqrt{(1-b_m^2)(1-b_n^2) + b_{mn}^2} \tag{8.29}$$

and

$$\sigma = \frac{\lambda_b - \lambda}{\lambda_b + \lambda} \tag{8.30}$$

The thermal resistance matrix becomes symmetric in accordance with (8.7), since the elements R^o_{mn} and R^o_{nm} are equal.

The heat flows q_n are given by the inverse of the equation system (8.27):

$$q_n = \sum_{n=1}^{N} (R^o_{mn})^{-1}\,(T_{fm} - T_b) \qquad n = 1, \ldots, N \tag{8.31}$$

where $(R^o_{mn})^{-1}$ are the matrix elements of the inverse to the matrix R^o_{mn}.

The sum of q_n, $n = 1, \ldots, N$, gives the total heat flow q. If the fluid temperatures T_{fm} are all set equal to T_f, then we get:

$$q = \frac{T_f - T_b}{R^o_{tot}} \tag{8.32}$$

$$R^o_{tot} = \frac{1}{\sum_{n=1}^{N}\sum_{m=1}^{N}(R^o_{mn})^{-1}} \tag{8.33}$$

8.4.2 Line-source formula for two pipes

The ground heat exchanger with a single U-pipe is a common arrangement. The two shanks of the U-pipe correspond to two pipes in the formalism used here. Explicit formulas for the Δ-circuit resistances will be derived for two

identical pipes placed in a symmetric position. The radii and thermal resistances of the two pipes are equal, so that $r_1 = r_2 = r_p$ and $R_{p1} = R_{p2} = R_p$. The pipes are diametrically opposed with respect to the center of the borehole. The coordinates of the center of the pipes can be chosen as:

$$(x_1, y_1) = (-D, 0) \qquad (x_2, y_2) = (D, 0) \tag{8.34}$$

The line-source resistances R^o_{11} and R^o_{12} are from (8.28):

$$\begin{aligned} R^o_{11} &= \frac{1}{2\pi\lambda_b}\left[\ln\left(\frac{r_b}{r_p}\right) + \sigma \ln\left(\frac{r_b^2}{r_b^2 - D^2}\right)\right] + R_p \\ R^o_{12} &= \frac{1}{2\pi\lambda_b}\left[\ln\left(\frac{r_b}{2D}\right) + \sigma \ln\left(\frac{r_b^2}{r_b^2 + D^2}\right)\right] \end{aligned} \tag{8.35}$$

The Δ-circuit resistance R^Δ_1 is given by (8.19):

$$R^\Delta_1 = \frac{1}{2\pi\lambda_b}\left[\ln\left(\frac{r_b}{r_p}\right) + \ln\left(\frac{r_b}{2D}\right) + \sigma \ln\left(\frac{r_b^4}{r_b^4 - D^4}\right)\right] + R_p \tag{8.36}$$

Eq. (8.21) gives the thermal resistance R_a between the two pipes:

$$R_a = \frac{1}{\pi\lambda_b}\left[\ln\left(\frac{2D}{r_p}\right) + \sigma \ln\left(\frac{r_b^2 + D^2}{r_b^2 - D^2}\right)\right] + 2R_p \tag{8.37}$$

The thermal resistance R^Δ_{12} can now be calculated from (8.19) or (8.21).

8.4.3 Multipole method

A so-called multipole method to compute the steady-state conductive heat flows to and between pipes in a composite cylinder has been presented by Bennet, Claesson, and Hellström (1987). The heat flow is two-dimensional in a circular region perpendicular to the pipes. The pipes lie in an inner circular region, which is surrounded by an annular region of different thermal conductivity.

The multipole method is described briefly in this section. A complete description of this rather complicated method is given by Claesson and Bennet (1987) and by Bennet, Claesson, and Hellström (1987). The final set of equations, which has to be solved in order to get the strength of the multipoles, are given in Appendix C. A computer program that solves the equation system is available (Bennet et al. 1987). It provides a very rapid and accurate way to calculate the temperature field in the composite region and the thermal resistances between the pipes.

Thermal problem

Figure 8.1 shows the considered thermal problem. There are N pipes ($N \geq 1$), that lie within the inner circular region with the radius r_b. The inner circle is surrounded by an annular region with different thermal conductivity. The outer circle has the radius r_c.

The outer radius of pipe n is r_{pn}, and its center lies at (x_n, y_n). There is a constant temperature T_{fn} in pipe n, while the temperature outside the outer circle is T_c.

The annular region, $r_b < r < r_c$, is homogeneous with the thermal conductivity λ. The inner circular region outside the pipes has the thermal conductivity λ_b. The steady-state temperature $T(x, y)$ satisfies the heat conduction equation in the annular region and in the inner circle:

$$\frac{\partial^2 T}{\partial x^2} + \frac{\partial^2 T}{\partial y^2} = 0 \tag{8.38}$$

Cartesian, complex, and polar coordinates will be used:

$$z = x + iy = re^{i\phi} \tag{8.39}$$

The center of pipe n is in complex coordinates:

$$z_n = x_n + iy_n \tag{8.40}$$

We will use the local polar coordinates ρ_n, ψ_n from the center of any pipe n.

$$z - z_n = \rho_n e^{i\psi_n} \tag{8.41}$$

The temperature and the radial heat flux are continuous at the inner boundary $r = r_b$:

$$T|_{r_b-0} = T|_{r_b+0} \tag{8.42}$$

$$\lambda_b \left.\frac{\partial T}{\partial r}\right|_{r_b-0} = \lambda \left.\frac{\partial T}{\partial r}\right|_{r_b+0} \tag{8.43}$$

The boundary condition at pipe n is:

$$T - \beta_n r_{pn} \frac{\partial T}{\partial \rho_n} = T_{fn} \qquad \text{for} \begin{cases} \rho_n = r_{pn} \\ 0 \leq \psi_n \leq 2\pi \end{cases} \tag{8.44}$$

The boundary condition at the outer circle is:

$$T + \beta_c r_c \frac{\partial T}{\partial r} = T_c \qquad \text{for} \begin{cases} r = r_c \\ 0 \leq \phi \leq 2\pi \end{cases} \tag{8.45}$$

The dimensionless coefficient β_n represents the thermal resistance R_{pn} between the fluid in pipe n and the material just outside the pipe:

$$\beta_n = 2\pi\lambda_b R_{pn} \tag{8.46}$$

The resistance R_{pn} can be calculated according to section 8.1.1. There may also be a thermal resistance R_{pc} (K/(W/m)) at the outer circle, which determines the coefficient β_c:

$$\beta_c = 2\pi\lambda R_{pc} \tag{8.47}$$

The thermal resistance coefficients β_n and β_c may take any non-negative value: $0 \leq \beta_n \leq \infty, 0 \leq \beta_c \leq \infty$. The value $\beta_n = +\infty$ means zero heat flux, $\partial T/\partial \rho_n = 0$. The value of T_{fn} is then redundant.

Line sources and multipoles

The thermal problem will be solved with the use of line sources and suitable derivatives of these (so-called multipoles). It is demonstrated by Claesson and Bennet (1987) that this method can represent any temperature variation around the pipe.

The temperature from a single line source q_n (W/m) at z_n becomes with complex notation:

$$T(x,y) = \frac{q_n}{2\pi\lambda} \Re\left[\ln\left(\frac{r_c}{z - z_n}\right)\right] \tag{8.48}$$

where the radius r_c has been introduced for dimensional reasons. The symbol $\Re$ denotes the 'the real part of'.

The complex-valued derivative of the j:th order with respect to z gives $(z - z_n)^{-j}$, which represents the multipole of order j. The multipoles are placed at the centers z_n of the pipes. The temperature from the multipole of order j at pipe n is:

$$T(x,y) = \Re\left[P_{nj}\left(\frac{r_{pn}}{z - z_n}\right)^j\right] \qquad \text{for} \begin{cases} n = 1,\ldots,N \\ j = 1,2,\ldots \end{cases} \tag{8.49}$$

where the pipe radius r_{pn} is introduced for dimensional reasons. The complex numbers P_{nj} give the strength of the multipole:

$$P_{nj} = N_{nj} + i\, M_{nj} \tag{8.50}$$

The temperature satisfies $\nabla^2 T = 0$, since it is the real part of an analytic function.

The multipole (8.49) expressed in local polar coordinates around $z = z_n$ becomes:

$$\Re\left[P_{nj}\left(\frac{r_{pn}}{\rho_n} e^{-i\psi_n}\right)^j\right] = \left(\frac{r_{pn}}{\rho_n}\right)^j \left[N_{nj}\cos(j\psi_n) - M_{nj}\sin(j\psi_n)\right] \tag{8.51}$$

and can thereby represent any variation $\cos(j\psi_n)$ and $\sin(j\psi_n)$ around the pipe at $\rho_n = r_{pn}$. The influences from other pipes can be compensated for in this way.

The variation around the outer circle $r = r_c$ is accounted for by multipoles of the type $P_{cj} \cdot (z/r_c)^j$, where P_{cj} are complex-valued numbers. The boundary conditions (8.42) and (8.43) are satisfied by the introduction of suitable mirror sources and multipoles.

The total temperature field is a sum of terms of the above types. It remains to satisfy the boundary conditions (8.44) and (8.45) at the pipes and the outer circle. This gives an equation for each circular boundary and each order $e^{i\psi_n j}$. The final set of equations is given in Appendix C.

8.4.4 Multipole approximation for two pipes

We will in this section use the multipole method to derive an approximate formula of higher accuracy than the line-source approximation for the case of two pipes in a composite region. Figure 8.5 shows the situation.

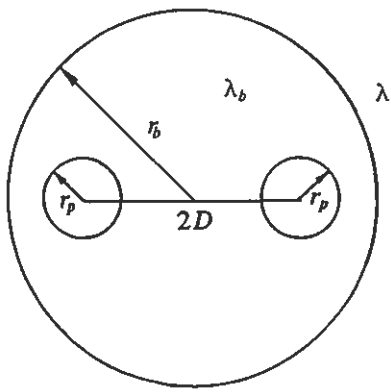

Figure 8.5. Two pipes in a composite region.

The radii of the two pipes are equal, so that $r_{p1} = r_{p2} = r_p$. The positions of the two pipes are:

$$z_1 = -D \qquad z_2 = D \tag{8.52}$$

The thermal resistances at the pipes are equal and there is no thermal resistance at the outer boundary. From (8.46-47) we have:

$$\beta_1 = \beta_2 = \beta \qquad \beta_c = 0 \tag{8.53}$$

We will only use the multipoles of the first order (J=1).

Symmetric problem

We begin with the derivation of the thermal resistance for the heat flow between the two pipes and the inner circle ($r = r_b$). The multipole method is first used to obtain the thermal resistance between the pipes and the outer circle. The thermal resistance of the annular region ($r_b < r < r_c$) is then subtracted, and the remaining thermal resistance is attributed to the thermal process in the inner region.

In this symmetrical problem, the temperatures in the pipes are equal and the temperature at the outer boundary ($r = r_c$) is set to zero:

$$T_{f1} = T_f \qquad T_{f2} = T_f \qquad T_c = 0 \tag{8.54}$$

The resulting heat flows from the pipes will be of the same magnitude due to the symmetrical conditions:

$$q_1 = q_2 = q_s \tag{8.55}$$

The temperature field will exhibit symmetry with respect to the y-axis. This gives:

$$T(z) = T(-\bar{z}) \tag{8.56}$$

It can be shown that this implies that the strength of the first-order multipoles $j = 1$, ($P_{11} = P_1$, $P_{21} = P_2$) must satisfy:

$$P_1 = -\bar{P}_2 \tag{8.57}$$

The real and imaginary parts of P_1 and P_c ($= P_{c1}$) are denoted:

$$P_1 = N_1 + iM_1 \tag{8.58}$$

$$P_c = N_c + iM_c \tag{8.59}$$

The temperature in the pipes is given by eq. (C.1) in Appendix C ($N = 2$, $J = 1$):

$$\begin{aligned} T_f &= q_s R_{11}^{oc} + q_s R_{12}^{oc} + N_1 \frac{r_p}{2D} - N_1 \sigma \frac{r_p D}{r_b^2 - D^2} + N_1 \sigma \frac{r_p D}{r_b^2 + D^2} \\ &\quad - N_c (1 - \sigma) \frac{D}{r_c} \end{aligned} \tag{8.60}$$

The pipes are located on the real axis, which implies that we need only to solve the equations for the real parts of the multipole strengths (The imaginary parts are only required if we need an expression for the temperature field). We have an equation containing the two real-valued unknowns N_1 and N_c.

The boundary condition at the pipes (C.2) gives:

$$N_1 + \frac{1-\beta}{1+\beta}\left[\frac{q_s}{2\pi\lambda_b}\left(\frac{r_p}{2D} - \sigma\frac{r_p D}{r_b^2 - D^2} + \sigma\frac{r_p D}{r_b^2 + D^2}\right) + N_1\frac{r_p^2}{4D^2}\right.$$
$$+N_1\sigma\frac{r_p^2 D^2}{(r_b^2 - D^2)^2} + N_1\sigma\frac{r_p^2}{(r_b^2 - D^2)} + N_1\sigma\frac{r_p^2 D^2}{(r_b^2 + D^2)^2} - N_1\sigma\frac{r_p^2}{(r_b^2 + D^2)}$$
$$\left. + N_c(1-\sigma)\frac{r_p}{r_c}\right] = 0 \tag{8.61}$$

The boundary condition at the outer circle (C.3) gives:

$$N_c\left[1 - \sigma\left(\frac{r_b}{r_c}\right)^2\right] + (1+\sigma)\left[\frac{q_s}{2\pi\lambda_b}\left(\frac{-D}{r_c}\right) + \frac{q_s}{2\pi\lambda_b}\left(\frac{D}{r_c}\right)\right.$$
$$\left. + N_1\left(\frac{r_p}{r_c}\right) - N_1\left(\frac{r_p}{r_c}\right)\right] = 0 \tag{8.62}$$

,which implies that

$$N_c = 0 \tag{8.63}$$

The real part N_1 is now given by (8.61). The pipe temperature then becomes:

$$T_f = q_s(R_{11}^{oc} + R_{12}^{oc}) - \frac{q_s}{2\pi\lambda_b}\frac{\frac{r_p^2}{4D^2}\left[1 - \sigma\frac{4D^4}{(r_b^4 - D^4)}\right]^2}{\left\{\frac{1+\beta}{1-\beta} + \frac{r_p^2}{4D^2}\left[1 + \sigma\frac{16D^4 r_b^4}{(r_b^4 - D^4)^2}\right]\right\}} \tag{8.64}$$

The thermal resistances R_{11}^{oc} and R_{12}^{oc} are the line-source approximations of the resistance between T_f and T_c. We have from (8.8) and (8.35), or directly from (C.4) and (C.5), the following expressions:

$$R_{11}^{oc} = \frac{1}{2\pi\lambda_b}\left[\beta + \ln\left(\frac{r_b}{r_p}\right) + \sigma\ln\left(\frac{r_b^2}{r_b^2 - D^2}\right)\right] + \frac{1}{2\pi\lambda}\ln\left(\frac{r_c}{r_b}\right) \tag{8.65}$$

$$R_{12}^{oc} = \frac{1}{2\pi\lambda_b}\left[\ln\left(\frac{r_b}{2D}\right) + \sigma\ln\left(\frac{r_b^2}{r_b^2 + D^2}\right)\right] + \frac{1}{2\pi\lambda}\ln\left(\frac{r_c}{r_b}\right) \tag{8.66}$$

Our aim is to obtain a relation for the thermal resistance R_1^{Δ} given by:

$$T_f - T_b = q_s R_1^{\Delta} \tag{8.67}$$

The difference between the temperature T_b at the inner circle and the temperature $T_c = 0$ at the outer circle then becomes by (8.9):

$$T_b = 2q_s \cdot \frac{1}{2\pi\lambda}\ln\left(\frac{r_c}{r_b}\right) \tag{8.68}$$

Subtracting this expression from (8.64) and inserting the result in (8.67) yields the thermal resistance:

$$R_1^{\Delta} = \frac{1}{2\pi\lambda_b}\left[\beta + \ln\left(\frac{r_b}{r_p}\right) + \ln\left(\frac{r_b}{2D}\right) + \sigma\ln\left(\frac{r_b^4}{r_b^4 - D^4}\right)\right] - \frac{1}{2\pi\lambda_b}\frac{\frac{r_p^2}{4D^2}\left[1 - \sigma\frac{4D^4}{(r_b^4 - D^4)}\right]^2}{\left\{\frac{1+\beta}{1-\beta} + \frac{r_p^2}{4D^2}\left[1 + \sigma\frac{16D^4 r_b^4}{(r_b^4 - D^4)^2}\right]\right\}} \tag{8.69}$$

The first term within brackets on the right-hand side of (8.69) is equal to the line-source approximation (8.36). The second term is a correction originating from the first-order multipoles. The accuracy of this approximation will be demonstrated in section 8.4.5.

Asymmetric problem

In the asymmetric problem, the temperatures in the two pipes have the same magnitude, but opposite signs. The temperature at the outer boundary at $r = r_c$ is set to zero:

$$T_{f1} = T_a \qquad T_{f2} = -T_a \qquad T_c = 0 \tag{8.70}$$

The resulting heat flows from the pipes will be of the same magnitude but with opposite signs:

$$q_1 = q_a \qquad q_2 = -q_a \tag{8.71}$$

The temperature field will exhibit anti-symmetry with respect to the y-axis:

$$T(z) = -T(-\bar{z}) \tag{8.72}$$

This implies that the strength of the first-order multipoles must satisfy:

$$P_1 = \bar{P}_2 \tag{8.73}$$

The derivation for the asymmetrical problem is very similar to the one given for the symmetrical problem. We finally get a relation between the pipe temperature T_a and the heat flow q_a:

$$T_{f1} - T_{f2} = 2T_a = q_a R_a \tag{8.74}$$

The solution contains the thermal resistances R_{11}^{oc} and R_{12}^{oc}, which are given by (8.65-66). The thermal resistance for the asymmetrical case then becomes:

$$R_a = \frac{1}{\pi\lambda_b}\left[\beta + \ln\left(\frac{2D}{r_p}\right) + \sigma \ln\left(\frac{r_b^2 + D^2}{r_b^2 - D^2}\right)\right] - \frac{1}{\pi\lambda_b}\left\{\frac{\frac{r_p^2}{4D^2}\left[1 + \sigma\frac{4r_b^4D^2}{(r_b^4 - D^4)} - \xi\frac{2D^2}{r_c^2}\right]^2}{\left[\frac{1+\beta}{1-\beta} - \frac{r_p^2}{4D^2} + +\sigma\frac{2r_p^2r_b^2(r_b^4+D^4)}{(r_b^4-D^4)^2} - \xi\frac{r_p^2}{r_c^2}\right]} + \xi\frac{D^2}{r_c^2}\right\} \quad (8.75)$$

where

$$\xi = 2r_c^2\frac{1-\sigma^2}{r_c^2 - \sigma r_p^2} \quad (8.76)$$

There is an explicit dependence on the radius r_c in this formula. In the limit of large values of r_c, the terms containing ξ can be neglected. The thermal resistance R_{12}^{Δ} of the Δ-circuit is obtained from (8.19) and (8.21), where R_1^{Δ} is given by (8.69).

8.4.5 Accuracy of formulas for two pipes

The accuracy of the formulas given in section 8.4.2 and 8.4.4 for two pipes in a composite region will be demonstrated for a case with typical data. There are two identical plastic pipes placed symmetrically in a borehole. The distance between the center of the pipes and the center of the borehole is denoted D. The geometry of the two-dimensional heat flow problem in a plane perpendicular to the borehole axis is shown in figure 8.5. Let us take the following data:

$r_p = 0.016$ m	$r_b = 0.0575$ m	$r_c = 1.0$ m
$\lambda_b = 0.6$ W/mK	$\lambda = 3.5$ W/mK	
$R_p = 0.09$ K/(W/m)	$\Rightarrow \quad \beta = 0.34$	

We will compare the thermal resistances R_1^{Δ} and R_a for the line-source approximations (8.36, 8.37) and the first-order multipole approximations (8.69, 8.75) with the exact value obtained from the multipole method described in section 8.4.3. The exact value is calculated with use of the computer program developed by Bennet et al. (1987). Examples showing the sensitivity to the parameters r_c, D, r_p, λ_b/λ, and β will be given below.

We begin with the influence of the fictitious outer boundary at the radius r_c, which has been discussed in section 8.2.1. Figure 8.6 shows the thermal resistances R_1^{Δ} and R_a as a function of r_c.

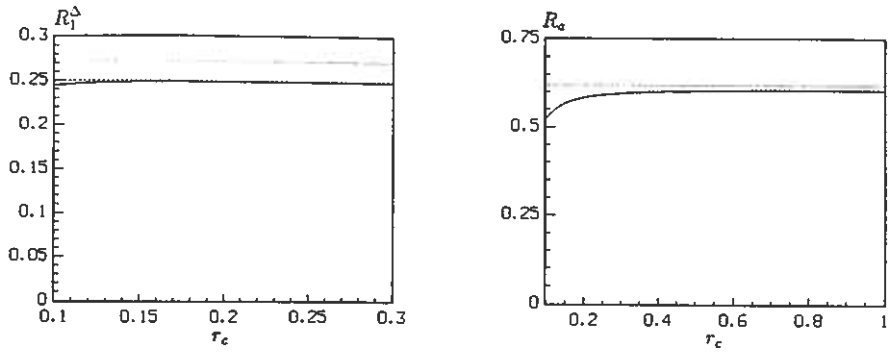

Figure 8.6. The thermal resistances R_1^Δ (left) and R_a (right) for the line-source approximation (dotted line), first-order multipole approximation (dashed-line), and the exact multipole solution (solid line) as a function of the radius r_c (m) of the fictitious outer boundary. Data according to the text.

The line-source approximation and the first-order multipole approximation for R_1^Δ do not depend on r_c. The exact value for R_1^Δ becomes constant for r_c >0.15 m. The value of the line-source approximation is then about 10 % higher, while the first-order multipole approximation only deviates by 0.4 %. The thermal resistance R_a between the pipes is more sensitive to the position of r_c. The exact value of r_c becomes constant for r_c >0.5 m. The relative error of the line-source approximation is then 2.5 %. The first-order multipole approximation, which represents the dependence on r_c accurately, gives an error of only 0.3 %.

The position of the pipes is given by the distance D, which ranges from 0.016 m for touching pipes at the center of the borehole to 0.0415 m for pipes in contact with the borehole wall. The relative error of the line-source approximation and the first-order multipole approximation in comparison with the exact solution is given in figure 8.7. The largest errors are found for the extreme positions (D=0.016 and D=0.0415). The error of the line-source approximation is here 5-10 %, while the first-order multipole method gives an error below 1 %. Both approximations result in very small errors for R_a when the pipes are in a position about halfway between the two extremes. For R_1^Δ, the line-source approximation gives a minimum error of about 3 %. The error is only 0.2 % or less for the first-order multipole approximation.

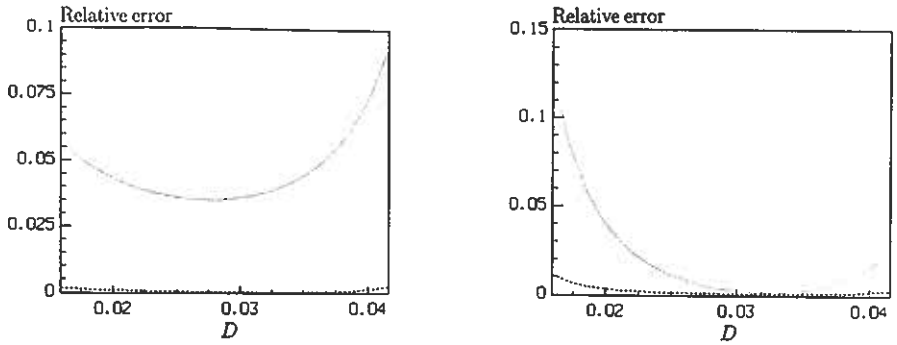

Figure 8.7. Relative errors of the thermal resistances R_1^{Δ} (left) and R_a (right) for the line-source approximation (dotted line) and first-order multipole approximation (dashed-line) as a function of the distance D (m) between the center of the borehole and the center of the pipes. Data according to the text.

The radius of the pipes is varied while keeping the pipes in contact with the borehole wall. The radius may take values up to 0.02875 m for which the pipes touch each other at the center of the borehole. The relative errors are shown in figure 8.8. The line-source approximation of R_1^{Δ} gives an error that increase from 7 % for a small pipe radius to 21 % for the largest pipe radius. The corresponding errors for the first-order multipole approximation are 0.3 % and 0.01 %, respectively. For R_a, the error of the line-source approximation varies in the range of 1.5 % to 3.5 %, while the error of the first-order multipole approximation increases from 0.25 % to 1 % in the given interval.

The accuracy is also influenced by the ratio λ_b/λ of the thermal conductivities. See figure 8.9, where the relative errors are shown for λ_b/λ with the value of β kept constant. The reference case gives a ratio of 0.17, which is at the low end of the range for ground heat storage applications. The relative error for R_1^{Δ} is small for large values of λ_b/λ. The errors of the first-order multipole approximation remain small in the whole interval $0.1 \leq \lambda_1/\lambda \leq 10$, while the errors for the line-source approximation increase gradually to 10-15 % for small values. For R_a, the line-source approximation has a minimum value around λ_b/λ=2. The error grows to about 8 % for λ_b/λ=0.1, and to 4 % for λ_b/λ=10. The error of the first-order multipole approximation is small in the whole interval. The maximum error is 0.5 % at λ_b/λ=0.

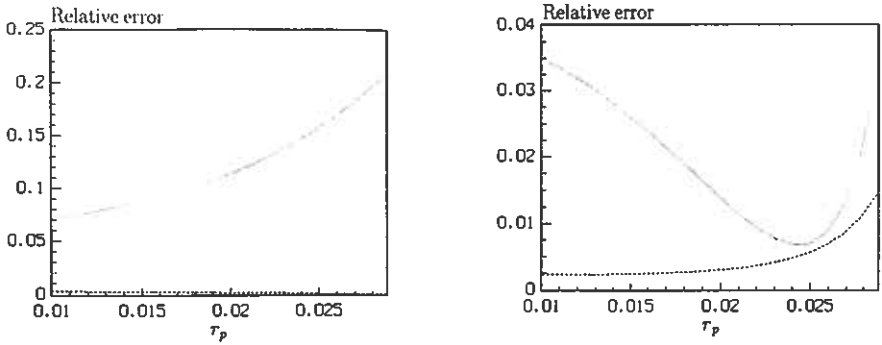

Figure 8.8. Relative errors of the thermal resistances R_1^{Δ} (left) and R_a (right) for the line-source approximation (dotted line) and first-order multipole approximation (dashed-line) as a function of the radius r_p (m) of the pipes. Data according to the text.

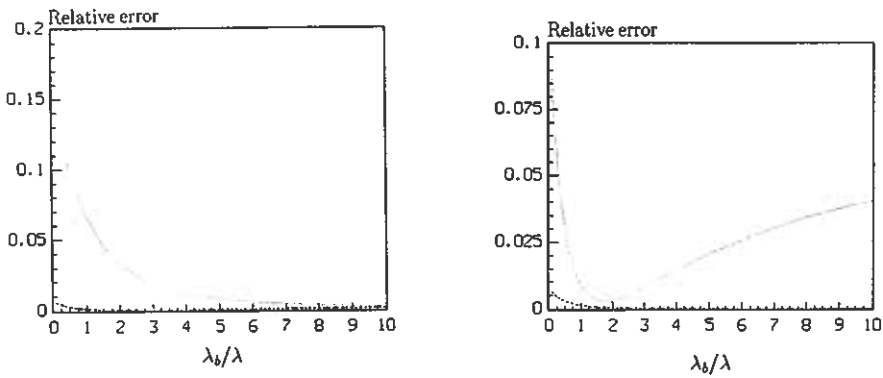

Figure 8.9. Relative errors of the thermal resistances R_1^{Δ} (left) and R_a (right) for the line-source approximation (dotted line) and first-order multipole approximation (dashed-line) as a function of the ratio between the thermal conductivity λ_b of the material in the borehole and the thermal conductivity λ of the surrounding ground. Data according to the text.

Finally, there is the important thermal resistance R_p at the pipes. It is here given by the dimensionless thermal resistance β ($= 2\pi\lambda_b R_p$), which is proportional to R_p and λ_b. The relative errors, see figure 8.10, for the line-source approximation become rather large for small values of β for both R_a

and, in particular, R_1^{Δ}. The errors grow towards smaller values of β also for the first-order multipole approximation. The largest error is 10 % at $\beta = 0$.

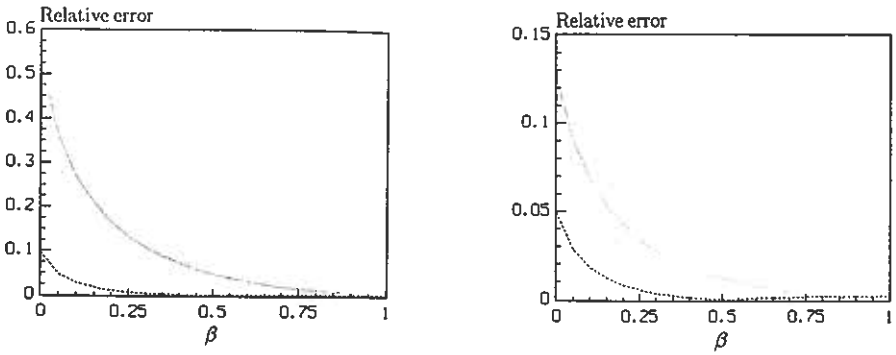

Figure 8.10. Relative errors of the thermal resistances R_1^{Δ} (left) and R_a (right) for the line-source approximation (dotted line) and first-order multipole approximation (dashed-line) as a function of the dimensionless thermal resistance β at the pipe wall. Data according to the text.

Let us summarize the sensitivity study for the reference case. The error of the line-source approximation is on the order of 10 %, while the first-order multipole approximation gives roughly 1 % deviation from the exact value. Factors that tend to increase the errors are: pipes close to each other or close to the borehole wall, large radius of the pipes, small values of the thermal conductivity ratio λ_b/λ, and small values of β.

8.5 Ducts with counterflow heat exchange

Heat exchanging boreholes in rock require a flow path by which the heat carrier fluid is transported to or from the bottom of the borehole. The simplest way to achieve this flow path is to insert a open-ended plastic tube that reaches the bottom of the borehole. The tube is preferably kept in a concentric position. See figure 2.4. This arrangement gives counterflow heat exchange between the inner circular flow channel and the outer annular flow channel.

An alternative is to insert two plastic tubes that are connected at the bottom of the borehole. The two pipes then form a closed circulation loop, a U-pipe, with counterflow heat exchange between the two shanks via the material that fills the borehole.

Ground heat exchangers in clay may be installed by driving down plastic tubes and refilling the hole with sand during extraction of the piling device.

Concrete piles containing plastic tubes have also been used. These designs are mathematically the same as the case of U-pipes in a borehole; the sand or concrete filling the borehole.

8.5.1 Counterflow heat balance equations

The fluid temperatures T_{f1} and T_{f2} will vary along the flow channels. The coordinate along the borehole is denoted z. The conductive heat transport along the flow channels can be neglected due to the comparatively small temperature gradients in this direction. The heat flow Δ-circuit, as shown in figure 8.2, is used to describe the local heat flow between the flow channels and the borehole wall. Formulas for the thermal resistances R_1^Δ, R_2^Δ, and R_{12}^Δ are presented in section 8.3-4. At steady-state condition, the convective heat transport in the fluid balances the transverse heat flows between the fluid channels and the borehole wall:

$$\begin{aligned} -C_f V_f \frac{\partial T_{f1}}{\partial z} &= q_1(z) = (T_{f1} - T_b)/R_1^\Delta + (T_{f1} - T_{f2})/R_{12}^\Delta \\ C_f V_f \frac{\partial T_{f2}}{\partial z} &= q_2(z) = (T_{f2} - T_b)/R_2^\Delta + (T_{f2} - T_{f1})/R_{12}^\Delta \\ & \qquad 0 \le z \le H \end{aligned} \tag{8.77}$$

The solution of this coupled equation can be derived by a straightforward use of Laplace transforms. The final expressions become (Eskilson and Claesson 1988):

$$\begin{aligned} T_{f1}(z,t) &= T_{f1}(0,t) f_1(z) + T_{f2}(0,t) f_2(z) + \int_0^z T_b(\zeta,t) f_4(z-\zeta)\, d\zeta \\ T_{f2}(z,t) &= -T_{f1}(0,t) f_2(z) + T_{f2}(0,t) f_3(z) - \int_0^z T_b(\zeta,t) f_5(z-\zeta)\, d\zeta \end{aligned} \tag{8.78}$$

The functions f_1, f_2, ..., f_5 are given by the expressions:

$$\begin{aligned} f_1(z) &= e^{\beta z}[\cosh(\gamma z) - \delta \sinh(\gamma z)] \\ f_2(z) &= e^{\beta z} \frac{\beta_{12}}{\gamma} \sinh(\gamma z) \\ f_3(z) &= e^{\beta z}[\cosh(\gamma z) + \delta \sinh(\gamma z)] \\ f_4(z) &= e^{\beta z}[\beta_1 \cosh(\gamma z) - (\delta\beta_1 + \frac{\beta_2\beta_{12}}{\gamma}) \sinh(\gamma z)] \\ f_5(z) &= e^{\beta z}[\beta_2 \cosh(\gamma z) + (\delta\beta_2 + \frac{\beta_1\beta_{12}}{\gamma}) \sinh(\gamma z)] \end{aligned} \tag{8.79}$$

$$\beta_1 = 1/(R_1^{\Delta} C_f V_f) \qquad \beta_2 = 1/(R_2^{\Delta} C_f V_f) \qquad \beta_{12} = 1/(R_{12}^{\Delta} C_f V_f)$$

$$\beta = \frac{\beta_2 - \beta_1}{2} \qquad \gamma = \sqrt{(\beta_1 + \beta_2)^2/4 + \beta_{12}(\beta_1 + \beta_2)}$$

$$\delta = \frac{1}{\gamma}\left(\beta_{12} + \frac{\beta_1 + \beta_2}{2}\right) \tag{8.80}$$

The condition that the two fluid channels are connected at the bottom gives:

$$T_{f1}(H,t) = T_{f2}(H,t) \tag{8.81}$$

The inlet fluid temperature $T_{f1}(0,t)$ will be written $T_{fin}(t)$. Finally, we get an expression for the outlet temperature $T_{fout}(t) = T_{f2}(0,t)$:

$$T_{fout}(t) = \frac{f_1(H) + f_2(H)}{f_3(H) - f_2(H)} T_{fin}(t) + \int_0^H \frac{T_b(\zeta,t)\,[f_4(H-\zeta) + f_5(H-\zeta)]}{f_3(H) - f_2(H)}\, d\zeta \tag{8.82}$$

Knowledge about the temperature $T_b(z,t)$ along the borehole wall is required in order to evaluate the integral. The case of a uniform borehole wall temperature will be solved in section 8.6.1.

8.6 Effective fluid-to-ground thermal resistance

Formulas for the fluid-to-ground thermal resistance R_b have been given in sections 8.1, 8.3, and 8.4. These resistances concern the local heat transfer at a given depth in the borehole. In this section an effective fluid-to-ground thermal resistance R_b^* will be derived for the cases of uniform temperature and uniform heat flux along the borehole. It includes the effect of varying fluid temperatures along the flow channels as well as the heat exchange between these channels.

The effective thermal resistance R_b^* for the ground heat exchanger is defined by:

$$(\bar{T}_f - \bar{T}_b) = \bar{q}\, R_b^* \tag{8.83}$$

where $\bar{T}_b$ is the average temperature of the borehole wall. The average fluid temperature $\bar{T}_f$ is:

$$\bar{T}_f = \frac{1}{2}(T_{fin} + T_{fout}) \tag{8.84}$$

It is perhaps more natural to define the effective thermal resistance with use of the inlet fluid temperature. However, the use of the arithmetic mean fluid

temperature $\bar{T}_f$ gives especially simple expression for the thermal resistance R_b^*.

The average heat injection rate $\bar{q}$ per meter borehole is simply the total heat injection rate divided the borehole length H:

$$\frac{1}{H}\int_0^L [q_1(z)+q_2(z)]\,dz = \bar{q}(t) = C_f V_f [T_{fin}(t) - T_{fout}(t)]/H \qquad \text{(W/m)} \tag{8.85}$$

8.6.1 Uniform borehole wall temperature

The integral of (8.78) can be solved for the case of a uniform borehole wall temperature $T_b(\zeta,t) = T_b(t)$. The outlet temperature then becomes:

$$T_{fout}(t) = \frac{1 - \frac{\beta_1+\beta_2}{2\gamma}\tanh(\gamma H)}{1 + \frac{\beta_1+\beta_2}{2\gamma}\tanh(\gamma H)} T_{fin}(t) + \frac{2\frac{\beta_1+\beta_2}{2\gamma}\tanh(\gamma H)}{1 + \frac{\beta_1+\beta_2}{2\gamma}\tanh(\gamma H)} T_b(t) \tag{8.86}$$

Insertion of (8.86) in (8.85) and (8.84) gives with (8.83) and (8.15) the following remarkably simple formula:

$$R_b^* = R_b\,\eta\coth(\eta) \tag{8.87}$$

where

$$\eta = \frac{H}{C_f V_f}\frac{1}{2R_b}\sqrt{1 + 4\frac{R_b}{R_{12}^{\Delta}}} \tag{8.88}$$

The factor $\eta\coth(\eta)$ gives the correction for the fluid temperature variation along the flow channels. It is shown figure 8.11. A series expansion for small values of η gives:

$$\eta\coth(\eta) \simeq 1 + \frac{\eta^2}{3} \qquad (\eta \le 1) \tag{8.89}$$

This yields the following interesting formula:

$$R_b^* \approx R_b + \frac{1}{3}\frac{1}{R_{12}^{\Delta}}\left(\frac{H}{C_f V_f}\right)^2 + \frac{1}{12}\frac{1}{R_b}\left(\frac{H}{C_f V_f}\right)^2 \qquad (\eta \le 1) \tag{8.90}$$

The value of (8.89) approaches 1 as η becomes small. The correction is less than 1.05 if $\eta < 0.4$. We get the following approximation:

$$R_b^* \approx R_b \qquad (\eta < 0.4) \tag{8.91}$$

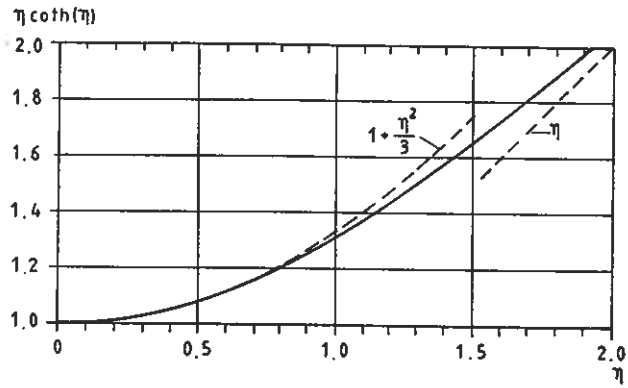

Figure 8.11. Correction term $\eta \coth(\eta)$ of eq. (8.87).

8.6.2 Uniform heat flux

In the case of uniform heat flux, the total heat flow q from the flow channels to the borehole wall is independent of the coordinate z along the borehole:

$$q_1(z) + q_2(z) = q \tag{8.92}$$

The steady-state heat balance equations (8.77) are then:

$$\begin{aligned} -C_f V_f \frac{\partial T_{f1}}{\partial z} &= q_1(z) \\ C_f V_f \frac{\partial T_{f2}}{\partial z} &= q_2(z) \qquad\qquad 0 \le z \le H \end{aligned} \tag{8.93}$$

The sum of these two equations are integrated with respect z. The requirement (8.81) that the flow channels are connected at the bottom gives:

$$T_{f1}(z) - T_{f2}(z) = \frac{qH}{C_f V_f}\left(1 - \frac{z}{H}\right) \tag{8.94}$$

The heat flows in the Δ-circuit satisfy (8.13). Then, with elimination of T_b and the use of (8.92) and (8.94), we get the heat flows:

$$\begin{aligned} q_1(z) &= \frac{R_2^\Delta}{R_1^\Delta + R_2^\Delta} q + \frac{1}{R_1^\Delta + R_2^\Delta} \frac{qH}{C_f V_f}\left(1 - \frac{z}{H}\right) + \frac{1}{R_{12}^\Delta} \frac{qH}{C_f V_f}\left(1 - \frac{z}{H}\right) \\ q_2(z) &= \frac{R_1^\Delta}{R_1^\Delta + R_2^\Delta} q - \frac{1}{R_1^\Delta + R_2^\Delta} \frac{qH}{C_f V_f}\left(1 - \frac{z}{H}\right) - \frac{1}{R_{12}^\Delta} \frac{qH}{C_f V_f}\left(1 - \frac{z}{H}\right) \end{aligned} \tag{8.95}$$

These relations are then inserted in the heat balance equations. The temperatures are obtained by integrating the resulting equations:

$$\begin{aligned} T_{f1}(z) &= T_H + \frac{R_2^\Delta}{R_1^\Delta + R_2^\Delta}\frac{qH}{C_f V_f}\left(1-\frac{z}{H}\right) + \frac{1}{R_a}\frac{qH^2}{2C_f^2V_f^2}\left(1-\frac{z}{H}\right)^2 \\ T_{f2}(z) &= T_H - \frac{R_1^\Delta}{R_1^\Delta + R_2^\Delta}\frac{qH}{C_f V_f}\left(1-\frac{z}{H}\right) + \frac{1}{R_a}\frac{qH^2}{2C_f^2V_f^2}\left(1-\frac{z}{H}\right)^2 \end{aligned} \tag{8.96}$$

where the temperature at the bottom ($z = H$) is denoted T_H ($= T_{f1}(H) = T_{f2}(H)$). The thermal resistance R_a is given by (8.18).

The borehole wall temperature $T_b(z)$ is now obtained from (8.13) and (8.94-96):

$$T_b(z) = T_H + \frac{R_2^\Delta - R_1^\Delta}{R_1^\Delta + R_2^\Delta}\frac{qH}{C_f V_f}\left(1-\frac{z}{H}\right) + \frac{1}{R_a}\frac{qH^2}{2C_f^2V_f^2}\left(1-\frac{z}{H}\right)^2 - R_b\, q \tag{8.97}$$

The average value $\bar{T}_b$ along the ground heat exchanger is:

$$\bar{T}_b = \frac{1}{H}\int_0^H T_b(z)\,dz \tag{8.98}$$

which becomes

$$\bar{T}_b = T_H + \frac{1}{2}\frac{R_2^\Delta - R_1^\Delta}{R_1^\Delta + R_2^\Delta}\frac{qH}{C_f V_f} + \frac{1}{3}\frac{1}{R_a}\frac{qH^2}{2C_f^2V_f^2} - R_b\, q \tag{8.99}$$

The average fluid temperature $\bar{T}_f = [T_{f1}(0) + T_{f2}(0)]/2$ is:

$$\bar{T}_f = T_H + \frac{1}{2}\frac{R_2^\Delta - R_1^\Delta}{R_1^\Delta + R_2^\Delta}\frac{qH}{C_f V_f} + \frac{1}{R_a}\frac{qH^2}{2C_f^2V_f^2} \tag{8.100}$$

The effective thermal resistance for the ground heat exchanger is defined by (8.83). Together with (8.99) and (8.100) we get:

$$R_b^* = R_b + \frac{1}{3}\frac{1}{R_a}\left(\frac{H}{C_f V_f}\right)^2 \tag{8.101}$$

Note that the flow rate enters as a quadratic term. Therefore, if the thermal resistances R_b and R_a are independent of the flow direction, it follows that the effective thermal resistance does not depend on the flow direction. This is true also for the case of uniform temperature, since $\eta\coth(\eta)$ is an even function of η or V_f.

Chapter 9

Steady-Flux Conditions

Heat injection or extraction pulses of long duration represent a fundamental particular process for the thermal analysis of a duct ground heat store. The thermal influence between adjacent ground heat exchangers is fully developed for such a pulse of constant heat injection rate during a longer time. The difference between the temperature of the heat carrier fluid and the local average temperature in the store is then constant. This process will be called the steady-flux regime.

The steady-flux solutions are derived for the two-dimensional thermal process in a plane perpendicular to the flow direction of the heat carrier fluid. A constant heat injection rate is prescribed from the pipes, or the boreholes, to the surrounding ground. The boreholes usually have inner pipes for the circulation of the fluid.

In section 9.1, a thermal resistance and a volumetric heat transfer capacity are defined for the heat flow between the heat carrier fluid and the store during steady-flux conditions. The time taken to attain the steady-flux situation is given.

Analytical solutions for the steady-flux process have been derived for several types of ground heat exchangers. Explicit, relatively simple formulas for the thermal resistance are obtained from these solutions. Ground heat exchangers where the heat transfer to surrounding ground takes place from a single pipe are treated in section 9.2. The solutions are also applicable for a borehole with inner pipes. Here, also, the ground is coupled to the fluid through the fluid-to-ground thermal resistance R_b. The ground interacts with a single *ground heat transfer channel*. The case when the ground interacts with more than one ground heat transfer channel is considered in section 9.3. Section 9.4 deals with the influence of a varying fluid temperature along the flow channels.

9.1 Introduction

9.1.1 Thermal resistance R_{sf}

Consider a ground heat exchanger in the inner part of the store. A certain part of the surrounding ground is, according to section 4.2, ascribed to the ground heat exchanger. See figure 9.1. The cross-sectional area of this ground region is denoted A_p. The analysis will be performed for ground regions with circular, hexagonal, and rectangular cross-sections. With regard to the thermal behavior of the ground heat exchanger, it will be shown that the circular and the hexagonal cross-sections are practically identical for equal cross-sectional area A_p. Thus, the results obtained for the circular cross-sections can be used for the hexagonal duct pattern of figure 4.3. The mean temperature T_m of the ground region is called the local average temperature.

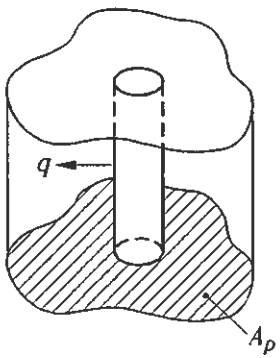

Figure 9.1. A ground heat exchanger with constant heat injection rate to the surrounding ground region.

The steady-flux analysis concerns the case with constant heat injection rate from the ground heat exchanger. There is no heat flow through the outer boundary of the surrounding ground region. After an initial transient period, a situation evolves where the *shape* of temperature field around the ground heat exchanger does not change with time. We call this basic situation the *steady-flux regime*. The heat flow is constant in time for each point in the ground region, and the temperature increases linearly with time, cf. section 6.1.2. The rate of increase is the same throughout the region. The difference between the fluid temperature T_f and the local average temperature T_m becomes constant. The difference is proportional to the heat injection rate. This proportionality may be written:

$$T_f - T_m = q\, R_{sf} \tag{9.1}$$

This is the fundamental formula for the analysis of heat injection and extraction pulses of long duration. Here, R_{sf} is a thermal resistance (K/(W/m)) between the temperature of the heat carrier fluid and the local average temperature in the store.

Let q_v be the heat injection rate per unit ground volume. The volumetric heat transfer capacity α_v (W/m^{3}K) is then defined by:

$$q_v = \frac{q}{A_p} = \alpha_v (T_f - T_m) \tag{9.2}$$

From (9.1-2) we obtain a relation between α_v and R_{sf}:

$$\alpha_v = \frac{1}{R_{sf} A_p} \tag{9.3}$$

The total heat transfer capacity (W/K) of the ground heat store is obtained by multiplying α_v with the storage volume V.

The steady-flux regime and the concept of a volumetric heat transfer capacity α_v are very useful for the thermal analyses of ground heat exchangers and the duct ground heat store. The complicated local thermal process is, on an appropriate time-scale, of a special character that is determined by a single parameter α_v.

9.1.2 Time-scale for the steady-flux regime

When a step change occurs in the heat injection rate $q(t)$ there will be a gradual change in the temperature profile until a new steady-flux situation is attained. It is shown in section 9.2.1 that the time t_{sf} to reach the steady-flux situation in the hexagonal duct pattern is given by:

$$\frac{a\, t_{sf}}{r_1^2} = 0.2 \qquad \frac{a\, t_{sf}}{A_p} = 0.065 \tag{9.4}$$

Here, a is the thermal diffusivity of the ground and r_1 is the radius of the equivalent circular region. The condition (9.4) is also valid for the rectangular duct pattern, figure 9.20, provided that the duct spacings B and B_1 are of about the same length, and that the cross-sectional area is the same ($A_p = \pi r_1^2 = B B_1$).

The transition period (9.4) is given in Table 9.1 for some different duct spacings B and thermal diffusivities a of the ground. The transition period is about one week for a duct spacing of 4 meters in granite ($a \simeq 1.6 \cdot 10^{-6}$ m^2/s) and 2 meters in clay ($a \simeq 0.4 \cdot 10^{-6}$ m^2/s).

TABLE 9.1. Duration (days) of the transition period t_{sf} (9.4) to attain the steady-flux regime for a hexagonal duct pattern as a function of the duct spacing B (or the corresponding cross-sectional area A_p).

		Thermal diffusivity a (m^2/s)		
B (m)	A_p (m^2)	$0.4 \cdot 10^{-6}$	$1.0 \cdot 10^{-6}$	$1.6 \cdot 10^{-6}$
0.5	0.22	0.40	0.16	0.10
1.0	0.87	1.6	0.6	0.4
1.5	1.95	3.6	1.4	0.9
2.0	3.46	6.4	2.6	1.6
2.5	5.4	10.0	4.0	2.5
3.0	7.8	14.4	5.7	3.6
3.5	10.6	19.5	7.8	4.9
4.0	13.8	25.5	10.2	6.4
4.5	17.5	32.3	12.9	8.1
5.0	21.6	39.0	16.0	10.0
5.5	26.2	48.2	19.3	12.1
6.0	31.2	57.4	23.0	14.4
6.5	36.6	67.4	27.0	16.8
7.0	42.4	78.2	31.3	19.5
7.5	48.7	89.7	35.9	22.4

9.2 Single ground heat transfer channel

The case where the heat transfer to surrounding ground takes place from a single channel in the ground heat exchanger is treated in this section. Examples are boreholes in rock and a single duct in soil. These ground heat exchangers may have inner pipes for the circulation of the fluid.

The steady-flux thermal resistance between the temperature T_b in the ground immediately outside the ground heat transfer channel and the local average temperature T_m is called R_g (ground). There is also the fluid-to-ground thermal resistance R_b, see chapter 8. The total thermal resistance R_{sf} is then:

$$R_{sf} = R_g + R_b \tag{9.5}$$

The formula gives the simple heat flow circuit of figure 9.2.

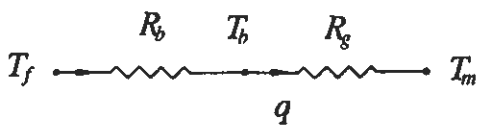

Figure 9.2. The steady-flux heat-flow circuit of a ground heat exchanger where the heat transfer to the surrounding ground takes place from only one ground heat exchanger channel.

9.2.1 Concentric pipe in a circular region

The thermal process around a concentric pipe in a cylindrical region is examined in this section. Let r be the radial distance from the center of a pipe and r_b the (outer) pipe radius. There is a local, radial thermal process around the pipe in the region $r_b \leq r \leq r_1$, where r_1 is the radius of the cylindrical ground region. The heat flux is zero at the outer boundary $r = r_1$. The pipe radius r_b is typically much smaller than r_1.

At the inner pipe radius $r = r_b$ there is a constant heat injection rate q that starts at $t = 0$. The initial temperature in the cylindrical region around the pipe is constant ($=T_m(0)$). Figure 9.3 shows the calculated the temperature field at different times from the solution below.

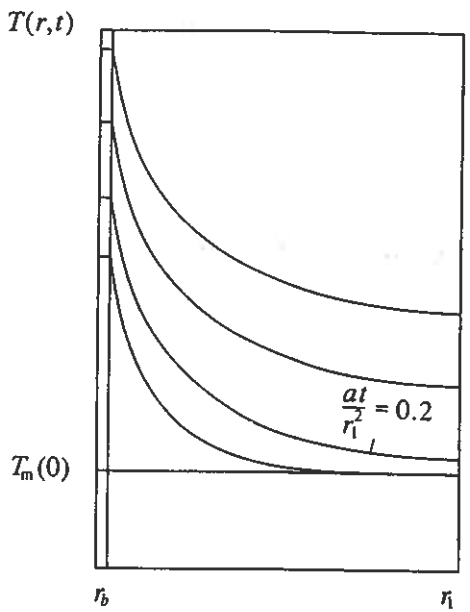

Figure 9.3. Temperature response to a constant heat injection rate.

The thermal conductivity is λ, the volumetric heat capacity C, and the thermal diffusivity $a = \lambda/C$. The fluid temperature is denoted $T_f(t)$.

The temperature in the ground satisfies (6.8):

$$\frac{\partial^2 T}{\partial r^2} + \frac{1}{r}\frac{\partial T}{\partial r} = \frac{1}{a}\frac{\partial T}{\partial t} \qquad (r_b < r < r_1, t > 0) \tag{9.6}$$

Initially the temperature is zero in the circular region:

$$T(r,0) = 0 \qquad (r_b < r < r_1) \tag{9.7}$$

Heat is injected at a constant rate q (W/m) at the pipe ($r = r_b$):

$$-2\pi r_b \lambda \left.\frac{\partial T}{\partial r}\right|_{r=r_b} = q \qquad (t > 0) \tag{9.8}$$

There is no heat flow through the outer boundary ($r = r_1$):

$$-2\pi r_1 \lambda \left.\frac{\partial T}{\partial r}\right|_{r=r_1} = 0 \qquad (t > 0) \tag{9.9}$$

The solution, which is obtained by use of the Laplace transformation method, is outlined by Carslaw and Jaeger (1959):

$$T(r,t) = \frac{q}{2\pi\lambda r_b}\left\{\frac{r_b r_1}{r_1^2 - r_b^2}\left[\frac{2a}{r_1}t + \frac{2r^2 - 3r_1^2 - r_b^2}{4r_1} + \frac{r_b^2 r_1}{r_1^2 - r_b^2}\ln\left(\frac{r_1}{r_b}\right) + r_1 \ln\left(\frac{r_1}{r}\right)\right] -\right.$$

$$\left. -\pi \sum_{n=1}^{\infty} \frac{e^{-a\alpha_n^2 t} J_1(\alpha_n r_b) J_1(\alpha_n r_1)\left[Y_1(\alpha_n r_1) J_0(\alpha_n r) - Y_0(\alpha_n r) J_1(\alpha_n r_1)\right]}{\alpha_n \left[J_1(\alpha_n r_1)^2 - J_1(\alpha_n r_b)^2\right]}\right\} \tag{9.10}$$

where α_n are the positive roots of the equation:

$$J_1(\alpha_n r_b) Y_1(\alpha_n r_1) - J_1(\alpha_n r_1) Y_1(\alpha_n r_b) = 0 \tag{9.11}$$

Here, J_0, J_1, Y_0, and Y_1 are Bessel functions of the first and second kind.

The solution may be divided into three parts, each with a characteristic time dependence. The first part gives the linear increase with time of the average temperature T_m in the circular region:

$$\begin{aligned} T_m(t) &= \frac{q}{2\pi\lambda}\frac{2at}{(r_1^2 - r_b^2)} = \frac{q\,t}{C\,\pi(r_1^2 - r_b^2)} \\ T_m(t) &= \frac{q\,t}{C\,\pi r_1^2} \qquad (r_1 \gg r_b) \end{aligned} \tag{9.12}$$

The second part includes the terms that do not depend on time. This part may be expressed as:

$$\frac{q}{2\pi\lambda} h_{sf}(r) \tag{9.13}$$

The dimensionless function $h_{sf}(r)$ gives the shape of the temperature profile after a certain initial period:

$$h_{sf}(r) = \frac{r_1^2}{(r_1^2 - r_b^2)} \left[\ln\left(\frac{r_1}{r}\right) - \frac{3}{4} + \frac{r^2}{2r_1^2} - \frac{r_b^2}{4r_1^2} + \frac{r_b^2}{r_1^2 - r_b^2} \ln\left(\frac{r_1}{r_b}\right) \right] \qquad (9.14)$$

The average value of this function, integrated over the annular region, is zero.

The remaining third part converges to zero with time. It gives the transient behavior of the temperature before the profile (9.13) is attained, namely:

$$-\frac{q}{2\pi\lambda}\pi \sum_{n=1}^{\infty} \frac{e^{-a\alpha_n^2 t} J_1(\alpha_n r_b) J_1(\alpha_n r_1) [Y_1(\alpha_n r_1) J_0(\alpha_n r) - Y_0(\alpha_n r) J_1(\alpha_n r_1)]}{\alpha_n r_b [J_1(\alpha_n r_1)^2 - J_1(\alpha_n r_b)^2]} \qquad (9.15)$$

The terms in the sum converges rapidly. The first (and smallest) root α_1 of (9.11) is given in Table 9.2. It is given as $\alpha_1 r_1$ for different values of r_b/r_1.

TABLE 9.2. The first root α_1 of eq. (9.11).

r_b/r_1	0.001	0.010	0.020	0.050	0.100	0.200
$\alpha_1 r_1$	3.832	3.832	3.836	3.860	3.941	4.236

The exponent $a\alpha_1^2 t$ of the first term in the sum may be used to derive a time-scale for the attenuation of the transient part. When the value of this exponent equals 3, the first term has been reduced to a fraction $e^{-3} \simeq 0.05$ of its initial value (at t=0). The other terms, for which the roots α_n are always greater than α_1, are of course attenuated even faster. Thus, the steady-flux regime prevails after an initial time period t_{sf} given by:

$$\frac{a\, t_{sf}}{r_1^2} = \frac{3}{\alpha_1^2 r_1^2} \simeq 0.2 \qquad (9.16)$$

Then, the temperature increases linearly with time. We will call this basic situation the *steady-flux regime*, since the heat flux is constant in time for each point in the ground. The shape of the temperature profile is given by (9.13):

$$T(r,t) - T_m(t) = \frac{q}{2\pi\lambda} h_{sf}(r) \qquad (9.17)$$

The function $h_{sf}(r)$ is shown in figure 9.4. The curves of figure 9.3 attain this shape after $at/r_1^2 = 0.2$.

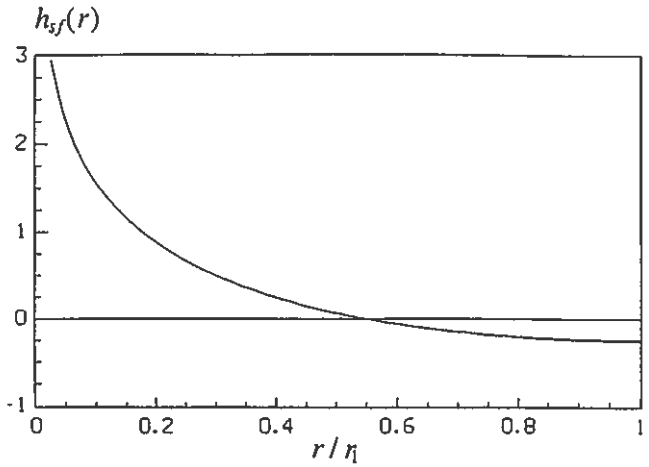

Figure 9.4. The dimensionless shape function $h_{sf}(r)$ for the steady-flux regime.

It can be seen that about half of the temperature drop between the pipe and the store occurs within $0.1r_1$ from the pipe during steady-flux conditions.

We will here give another, more direct derivation of the steady-flux formula (9.17) where the properties of linear temperature increase are utilized and the initial transient behavior is neglected. The temperature may be then be written as a sum of a temperature-dependent part and a part that takes care of the radial dependence:

$$T(r,t) = T_m(t) + T_{sf}(r) \tag{9.18}$$

The average temperature T_m increases linearly with time, so that:

$$T_m(t) = \beta\, t \tag{9.19}$$

where β is a constant to be determined by the heat injection rates. Inserting (9.18) and (9.19) in the partial differential equation (9.6) yields:

$$\frac{1}{r}\frac{\partial}{\partial r}\left(r\frac{\partial T_{sf}}{\partial r}\right) = \frac{1}{a}\beta \qquad (r_b < r < r_1,\, t > 0) \tag{9.20}$$

Straightforward integration shows that the solution has the following functional dependence:

$$T_{sf} = \beta_1\, r^2 + \beta_2 \ln(r) + \beta_3 \qquad \left(\beta_1 = \frac{\beta}{4a}\right) \tag{9.21}$$

The constants β_1, β_2, and β_3 are determined by the boundary conditions (9.8-9.9) and the requirement that the average value of the temperature profile T_{sf} is zero in the circular region:

$$\int_{r_b}^{r_1} T_{sf}\, 2\pi r\, dr = 0 \tag{9.22}$$

The solution (9.14) for $h_{sf}(r)$ is obtained.

In current heat storage applications, the ratio between r_1 and r_b, or, almost equivalently, between borehole spacing and borehole diameter, is roughly 20-40 (extreme values may be in the range of 10 to 60); boreholes with a diameter of 0.1 m and a spacing of 3 m give a ratio of 30. There is a larger variety of pipe dimensions available for heat stores in clay or soil, so the ratio may vary in the slightly wider range of 15-100; a pipe with a diameter of 32 mm and a spacing of 2 m gives a ratio of 62.5. For ratios in this range, the dimensionless shape function $h_{sf}(r)$ (9.14) can be approximated by:

$$h'_{sf}(r) = \ln\left(\frac{r_1}{r}\right) - \frac{3}{4} + \frac{r^2}{2r_1^2} \tag{9.23}$$

The value at the pipe ($r = r_b$) becomes:

$$h'_{sf}(r_b) \simeq \ln\left(\frac{r_1}{r_b}\right) - \frac{3}{4} \tag{9.24}$$

The relative error of the approximate dimensionless pipe temperature (9.24) compared with the exact value (9.14) is shown in figure 9.5. It is given as a function of r_1/r_b.

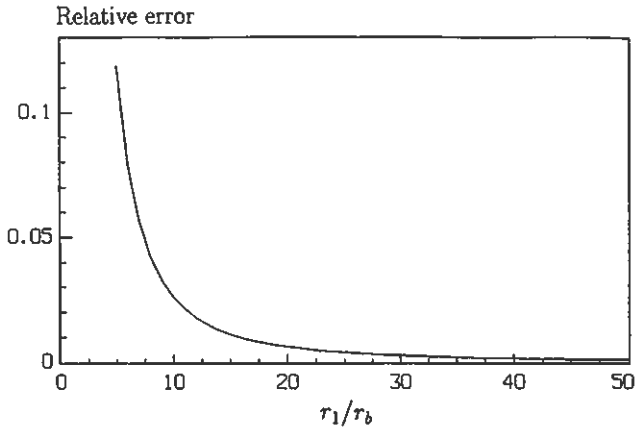

Figure 9.5. Relative error of the approximate dimensionless pipe temperature $h'_{sf}(r_b)$ (9.24) compared with the exact value $h_{sf}(r_b)$ (9.14) as a function of r_1/r_b.

The error is less than 1 % for $r_1/r_b > 15$ and less than 0.1 % for $r_1/r_b > 50$. Thus, the approximation (9.24) is appropriate for the analyses of ground heat exchangers.

The difference between the pipe temperature and the local average temperature during steady-flux conditions is now expressed by the simple formula:

$$T(r_b,t) - T_m(t) = \frac{q}{2\pi\lambda}\left[\ln\left(\frac{r_1}{r_b}\right) - \frac{3}{4}\right] \qquad r_1/r_b > 15 \qquad (9.25)$$

where the average temperature $T_m(t)$ is given by (9.12). Let us compare this formula with the exact transient time-dependent difference $T(r_b,t) - T_m(t)$, which is obtained by subtracting (9.12) from (9.10). The relative error, which is defined as the difference between the two formulas divided by the constant steady-flux value depends on at/r_1^2 and r_b/r_1. It is shown in figure 9.6 for $r_b/r_1 = 0.025$.

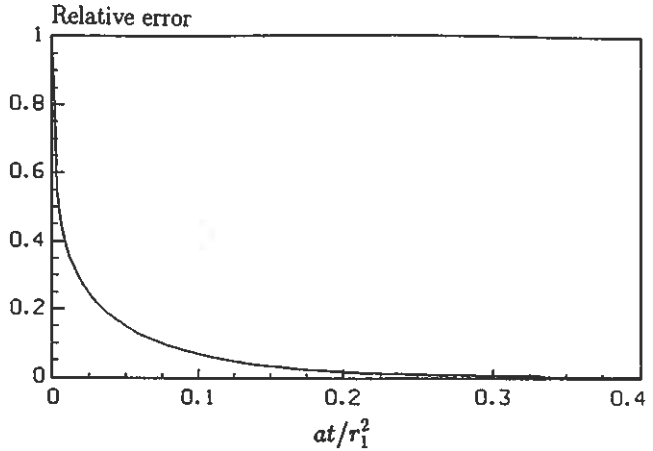

Figure 9.6. Relative error of the steady-flux solution for the difference between pipe temperature and local average temperature as a function of the dimensionless time at/r_1^2 for $r_b/r_1 = 0.025$.

The error amounts to 6.7 % at at/r_1^2=0.1 and 1.5 % at at/r_1^2=0.2, which is in accordance with the time criterion (9.16) and (9.4).

Figure 9.7 shows an example of the temperature response $T(r_b,t)$ for a step change in heat injection rate. The example concerns boreholes in granite, which has a thermal conductivity of 3.5 W/mK and a heat capacity of 2.2 MJ/m^{3}K. The borehole radius is 0.0575 m. The spacing between the boreholes is 4 m in a hexagonal duct pattern, so that the radius r_1 of the cross-sectional area becomes 2.1 m. The heat injection rate is 100 W/m.

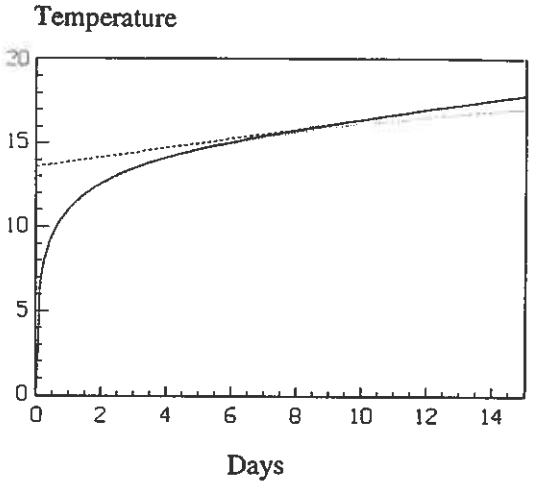

Figure 9.7. The temperature response at the pipe $r = r_b$ of a step change in heat injection rate for a insulated cylindrical region (solid line) and a semi-infinite region (dotted line). The steady-flux solution gives the temperature response of the dashed line. Data according to the text.

The borehole wall temperature T_b (at $r = r_b$) is given by the solid line. The influence of the outer boundary $r = r_1$ is negligible during a certain initial period. The growth of the borehole temperatures is the same as that of a single borehole in the ground (dotted line). The first part, before the transition time, may be approximated by the line source solution for a semi-infinite medium ($r_b < r < \infty$). The solution of this case is given in chapter 10. The pipe feels the presence of the outer boundary after a time $at_{sf}/r_1^2 \simeq 0.2$, and then the solution changes character. The temperature increases linearly with time, while the shape of the temperature curve becomes constant. The borehole temperature is now given by the steady-flux solution.

So far in the analysis of this fundamental problem, we have considered only the ground temperature at $r = r_b$, which has been called the pipe (or borehole wall) temperature. The fluid-to-ground thermal resistance R_b will give a temperature difference between the heat carrier fluid and the ground at $r = r_b$. The total difference between the fluid temperature T_f and the local average temperature T_m is then given by steady-flux solution (9.25) and the additional temperature difference due to the fluid-to-ground thermal resistance:

$$T_f(t) - T_m(t) \simeq \frac{q}{2\pi\lambda}\left[\ln(\frac{r_1}{r_b}) - \frac{3}{4}\right] + qR_b \qquad \text{for} \begin{cases} at_{sf}/r_1^2 > 0.2 \\ r_1/r_b > 15 \end{cases} \qquad (9.26)$$

The difference is proportional to the heat injection rate. This proportionality may be written:

$$T_f - T_m = q\, R_{sf} \tag{9.27}$$

This is the fundamental formula for the analysis of heat injection and extraction pulses of long duration. Here, R_{sf} (steady-flux) is a thermal resistance between the heat carrier fluid and the surrounding ground. From (9.25) we have for large values of r_1/r_b:

$$R_{sf} = \frac{1}{2\pi\lambda}\left[\ln\left(\frac{r_1}{r_b}\right) - \frac{3}{4}\right] + R_b \qquad r_1/r_b > 15 \tag{9.28}$$

The complete expression for the steady-flux thermal resistance that is valid for any value of r_1/r_b is:

$$R_{sf} = \frac{q}{2\pi\lambda}\left\{\left[\frac{r_1^2}{r_1^2 - r_b^2}\right]^2 \ln\left(\frac{r_1}{r_b}\right) - \frac{3}{4} - \frac{r_b^2}{2(r_1^2 - r_b^2)}\right\} + R_b \tag{9.29}$$

9.2.2 Comparison with steady-state solution

Let us compare the steady-flux solution with a steady-state solution for the same circular region $r_b < r < r_1$. There is a constant heat injection rate q at the pipe ($r = r_b$). The temperature at every point in the circular region will be constant during steady-state conditions. This implies that the temperature profile depends only on the radial coordinate:

$$T(r) = T_m + T_{ss}(r) \tag{9.30}$$

where T_m is the average temperature. The steady-state heat equation for the radial case yields the following functional dependence:

$$T_{ss} = \beta_1 \ln(r) + \beta_2 \tag{9.31}$$

The functional dependence of the steady-flux solution (9.21) has an additional term that is proportional to r^2. The constant β_1 is determined by the boundary condition at $r{=}r_b$. As a second requirement we prescribe that the average value of the temperature T_{ss} is zero. This gives the constant β_2. It should be noted that there is no condition at the outer boundary $r = r_1$, since it follows directly from the steady-state heat equation that the heat flow q passes through the outer boundary as well. The solution may be written:

$$T_{ss}(r) = \frac{q}{2\pi\lambda}\, h_{ss}(r) \tag{9.32}$$

The dimensionless function $h_{ss}(r)$ gives the shape of the steady-state temperature profile:

$$h_{ss}(r) = \ln\left(\frac{r_1}{r}\right) - \frac{1}{2} + \frac{r_b^2}{r_1^2 - r_b^2}\ln\left(\frac{r_1}{r_b}\right) = \frac{r_1^2}{r_1^2 - r_b^2}\left[\ln\left(\frac{r_1}{r}\right) + \frac{r_b^2}{r_1^2}\ln\left(\frac{r}{r_b}\right)\right] - \frac{1}{2} \tag{9.33}$$

The close similarities between (9.33) and (9.14) are clear from the second expression. The dimensionless shape function $h_{ss}(r)$ is shown in figure 9.8 together with the corresponding function $h_{sf}(r)$ for the steady-flux regime as a function of the dimensionless radial distance r/r_1.

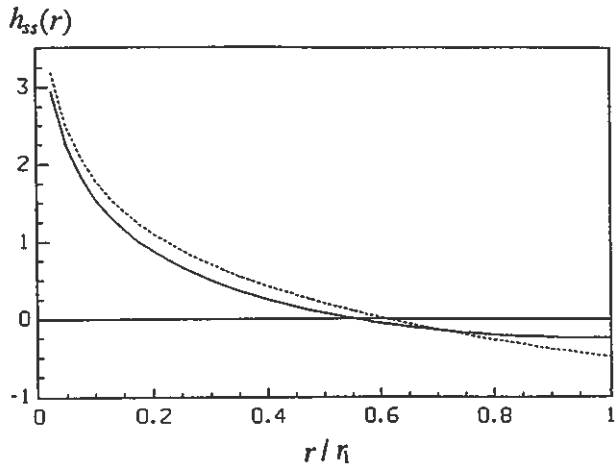

Figure 9.8. The dimensionless shape function $h_{ss}(r)$ (dashed line) for steady-state conditions and the dimensionless shape function $h_{sf}(r)$ (solid line) for the steady-flux regime as a function of r/r_1 (r_b/r_1=0.025).

The temperature at $r = r_b$ is slightly higher during steady-state conditions. The profiles are very similar for small values of r/r_1. In fact, if the curves are drawn so that the temperatures coincide at $r = r_b$, there will be virtually no difference between the curves for $r/r_1 < 0.25$.

For $r_1/r_b > 11$ the steady-state temperature $T_{ss}(r_b)$, (9.32-33), can be approximated with less than 1 % error by:

$$T_{ss}(r_b) = \frac{q}{2\pi\lambda}\left[\ln\left(\frac{r_1}{r_b}\right) - \frac{1}{2}\right] \qquad r_1/r_b > 11 \tag{9.34}$$

The important steady-flux thermal resistance R_{sf} is defined by (9.1). Let us also define a steady-state thermal resistance R_{ss} between the fluid temperature and the average ground temperature:

$$T_f - T_m = q\,R_{ss} \tag{9.35}$$

so that

$$R_{ss} = \frac{1}{2\pi\lambda}\left[\ln\left(\frac{r_1}{r_b}\right) - \frac{1}{2}\right] + R_b \qquad r_1/r_b > 11 \tag{9.36}$$

A comparison with (9.28) reveals that the steady-flux thermal resistance will be lower than (9.36) by only $1/(8\pi\lambda)$. The thermal resistances for steady-state and steady-flux conditions will be similar.

9.2.3 Eccentric pipe in circular region

The borehole drilling in rock and the insertion of plastic tubes in soil are always associated with some amount of deviation from the planned direction. The spacing between adjacent ground heat exchanger will not be uniform in the store.

Let us consider the case of pipe that is located a short distance $b\,r_1$ from the center of a cylinder region. See figure 9.9. There is no heat flow across the outer boundary at $r = r_1$.

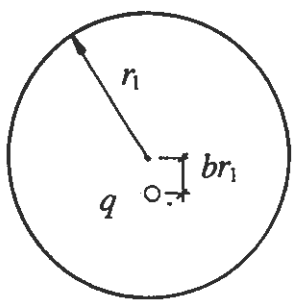

Figure 9.9. An eccentric pipe in a circular region.

The temperature field during steady-flux conditions consists of two parts:

$$T(x,y,t) = T_{sf}(x,y) + T_m(t) \tag{9.37}$$

The average temperature T_m increases linearly with time, (9.12):

$$T_m(t) = \frac{q\,t}{\pi r_1^2 C} \tag{9.38}$$

Carslaw and Jaeger (1959; p. 386) give a solution for an eccentric line source in a circular region. In our notation it becomes, when the pipe is displaced br_1 in the x-direction:

$$\begin{aligned} T_{sf}(x,y) \;=\; & \frac{q}{2\pi\lambda}\left\{\frac{x^2+y^2}{2r_1^2}+\frac{b^2}{2}-\frac{3}{4}+\right. \\ & \left.+\frac{1}{2}\ln\left[\frac{r_1^2}{(x-br_1)^2+y^2}\right]+\frac{1}{2}\ln\left[\frac{r_1^2}{(bx-r_1)^2+b^2y^2}\right]\right\} \end{aligned} \tag{9.39}$$

The pipe temperature T_b is to be evaluated on the circle:

$$(x-br_1)^2+y^2 = r_b^2 \tag{9.40}$$

The x and y coordinates of points on the periphery of the pipe are given by:

$$\begin{cases} x = br_1 + r_b\cos\phi \\ y = r_b\sin\phi \end{cases} \tag{9.41}$$

We rewrite the terms of (9.39) that contain x and y as functions of ϕ. We get:

$$\frac{x^2+y^2}{2r_1^2} = \frac{b^2}{2}+\frac{r_b^2}{2r_1^2}+b\frac{r_b}{r_1}\cos\phi \simeq \frac{b^2}{2} \qquad \text{if } r_b \ll r_1 \tag{9.42}$$

$$\frac{b^2}{r_1^2}\left[(x-r_1/b)^2+y^2\right] = (1-b^2)^2+\frac{b^2r_b^2}{r_1^2}+\frac{2r_bb^2}{r_1}(b-1/b)\cos\phi \simeq (1-b^2)^2 \tag{9.43}$$

Inserting these approximations in (9.39) yields, together (9.1) and (9.5), the thermal resistance:

$$R_{sf} = \frac{1}{2\pi\lambda}\left[\ln\left(\frac{r_1}{r_b}\right)-\frac{3}{4}+b^2-\ln(1-b^2)\right]+R_b \tag{9.44}$$

The influence of the eccentric position of the pipe is given by the two last terms within the brackets on the right-hand side.

The ratio between the thermal resistances for an eccentric pipe and a concentric pipe as a function of r_1/r_b and the eccentricity b is given in Table 9.3 for the case R_b=0.

TABLE 9.3. Ratio between the thermal resistances for an eccentric pipe (9.44) and a concentric pipe (9.28) as a function of r_1/r_b and the eccentricity b (R_b=0).

	b			
r_1/r_b	0.05	0.10	0.25	0.50
20	1.002	1.009	1.057	1.239
40	1.002	1.007	1.043	1.183
60	1.001	1.006	1.038	1.161
80	1.001	1.006	1.035	1.148

Apparently, the thermal resistance is quite insensitive to moderate deviations from a concentric position of the pipe in the cylindrical region.

9.2.4 Pipe in a rectangular region

The ground heat exchangers are often installed in a rectangular duct pattern. See figure 4.3. Figure 9.10 shows a line source q at the center of the corresponding rectangular region $-B/2 < x < B/2$, $-B_1/2 < y < B_1/2$. There is no heat flow across the four boundaries.

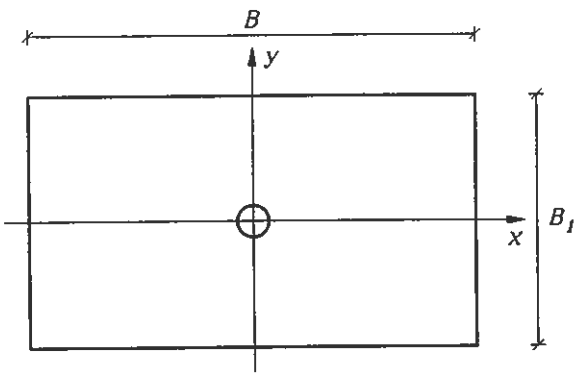

Figure 9.10. Line source in a rectangular area.

To derive the steady-flux solution for this case, we will start from the defining relation:

$$T(x,y,t) = T_m(t) + T_{sf}(x,y) \tag{9.45}$$

The linear increase of the mean temperature is:

$$T_m(t) = \frac{q\,t}{C\,B\,B_1} \tag{9.46}$$

A dimensionless steady-flux temperature u is defined by:

$$T_{sf}(x,y) = \frac{q}{\lambda} u(x,y) \tag{9.47}$$

It satisfies the equation:

$$\frac{\partial^2 u}{\partial x^2} + \frac{\partial^2 u}{\partial y^2} = \frac{1}{B\,B_1} \tag{9.48}$$

except in the origin (0,0), where there is the line source q. The normal derivative is zero at the boundaries. In order to fulfill the boundary conditions at $x = \pm B/2$ we use an infinite row of line sources q along the x-axis. The steady-state temperature distribution from such a row is well-known (Morse and Feshbach 1953; p. 1286):

$$\frac{q}{2\pi\lambda}\frac{-1}{2} \ln\left[\cosh(2\pi y/B) - \cos(2\pi x/B)\right] \tag{9.49}$$

The expression for $u(x,y)$ may be written in the following form:

$$\begin{aligned} u(x,y) \;=\; & -\frac{1}{4\pi} \ln\left[\cosh(2\pi y/B) - \cos(2\pi x/B)\right] + \frac{y^2}{2BB_1} + \\ & + \sum_{n=0}^{\infty} a_n \cos(2\pi n x/B)\, \cosh(2\pi n y/B) \end{aligned} \tag{9.50}$$

The term containing the y^2-dependence is a particular solution that takes care of the inhomogeneous right-hand side of (9.48). Each term in the infinite series satisfies the Laplace equation and the boundary condition at $x = \pm B/2$. The complete expression (9.50) satisfies the partial differential equation (9.48).

The boundary condition at $y = \pm B_1/2$ determines the coefficients a_n ($n = 1,2,3,\ldots$). The constant a_0 is chosen so that the mean value of $T_{sf}(x,y)$ in the rectangular region becomes zero.

The steady-flux solution becomes:

$$\begin{aligned} u(x,y) \;=\; & -\frac{1}{4\pi} \ln\{2\left[\cosh(2\pi y/B) - \cos(2\pi x/B)\right]\} + \frac{y^2}{2BB_1} + \frac{B_1}{12\,B} + \\ & + \frac{1}{2\pi} \sum_{n=1}^{\infty} \frac{1}{n} \cos(2\pi n x/B)\, \exp[-2\pi n(B_1 - y)/B]\, \frac{1 + \mathrm{e}^{-4\pi n y/B}}{1 - \mathrm{e}^{-2\pi n B_1/B}} \end{aligned} \tag{9.51}$$

The convergence of the series is very rapid due to the exponentials.

We are particularly interested in the temperature at the pipe radius:

$$x^2 + y^2 = r_b^2 \tag{9.52}$$

The radius r_b is usually small compared to the size of the rectangular region. The temperature at the pipe radius is then, with good approximation, obtained if we put $x = 0$ and $y = 0$ in all terms except in the logarithm, in which a Taylor expansion of the first two terms gives:

$$\ln\left[1 + \left(\frac{2\pi y}{B}\right)^2 - 1 + \left(\frac{2\pi y}{B}\right)^2\right] \simeq 2\ln\left(\frac{2\pi r_b}{B}\right) \tag{9.53}$$

The solution is then from (9.47), (9.51), and (9.53):

$$T_{sf}|_{r=r_b} = \frac{q}{\lambda}\left[\frac{1}{2\pi}\ln\left(\frac{B}{2\pi r_b}\right) + \frac{B_1}{12\,B} + \frac{1}{\pi}\sum_{n=1}^{\infty}\frac{1}{n}\frac{e^{-2\pi n B_1/B}}{1 - e^{-2\pi n B_1/B}}\right] \tag{9.54}$$

We can always choose the axes of the rectangle so that $B_1 \geq B$. Then the infinite series of (9.54) converges very rapidly. The first term is in fact so small ($e^{-2\pi}$=0.002), that the whole series can be neglected. We have with good accuracy:

$$T|_{r=r_b} - T_m = \frac{q}{2\pi\lambda}\left[\ln\left(\frac{B}{2\pi r_b}\right) + \frac{\pi B_1}{6B}\right] \qquad B_1 \geq B \tag{9.55}$$

By adding the fluid-to-ground thermal resistance, the thermal resistance R_{sf} becomes:

$$R_{sf} = \frac{1}{2\pi\lambda}\left[\ln\left(\frac{B}{2\pi r_b}\right) + \frac{\pi B_1}{6B}\right] + R_b \qquad B_1 \geq B \tag{9.56}$$

Table 9.4 gives the influence of the ratio B_1/B on the thermal resistance R_{sf} for the rectangular duct pattern compared to R_{sf} for the quadratic duct pattern ($B_1 = B$) at a given cross-sectional area A_p. The duct radius r_b is 0.0575 m and the fluid-to-ground thermal resistance R_b is 0 K/(W/m).

TABLE 9.4. Ratio of the thermal resistances for the rectangular duct pattern and the quadratic duct pattern ($B_1 = B$) for a given cross-sectional area A_p (m^2). r_b=0.0575 m and R_b=0 K/(W/m).

	B_1/B						
A_p	1.2	1.5	2.0	2.5	3.0	4.0	5.0
4.0	1.006	1.026	1.079	1.146	1.223	1.393	1.577
9.0	1.005	1.022	1.067	1.124	1.189	1.332	1.488
16.0	1.005	1.020	1.060	1.112	1.170	1.300	1.440

The variation of R_{sf} is less than 8 % for $1 \leq B_1/B \leq 2$. The shape of the rectangular duct pattern has a fairly weak influence on the thermal resistance.

Pipe in a hexagonal region

A hexagonal duct pattern with a duct spacing B, figure 4.3, can be considered as a superposition of two rectangular duct patterns with the spacings B and $B_1 = \sqrt{3}B$. The steady-flux temperature field due to one such rectangular duct pattern is obtained from (9.47) and (9.51). Eq. (9.55) gives the temperature of a pipe at the center of $(x = 0, y = 0)$ of the region. The influence of the other rectangular duct pattern is obtained by superimposing the temperature at $x = B/2$ and $y = \sqrt{3}B/2$. The thermal resistance becomes:

$$R_{sf} = \frac{1}{2\pi\lambda}\left[\ln\left(\frac{B}{2\pi r_b}\right) + \frac{\pi B_1}{6B} - \frac{1}{2}\ln\left\{2\left[\cosh(\pi\sqrt{3}) + 1\right]\right\} + \frac{5\pi\sqrt{3}}{12}\right] + R_b \tag{9.57}$$

The series of (9.51) can be neglected.

Comparison of circular, hexagonal and quadratic region

The influence of the shape of the surrounding ground region can be further illuminated by comparing the circular, hexagonal, and the quadratic region for the same cross-sectional area, so that:

$$A_p = B^2 = \pi r_1^2 \tag{9.58}$$

which implies

$$B = \sqrt{A_p} \qquad r_1 = \sqrt{A_p/\pi} \tag{9.59}$$

The thermal resistances for the circular, hexagonal, and quadratic region are given by the formulas (9.28), (9.57), and (9.56), respectively. We have:

Circular region:

$$R_{sf} = \frac{1}{2\pi\lambda}\left[\ln\left(\frac{\sqrt{A_p}}{\sqrt{\pi}r_b}\right) - 0.75\right] + R_b \tag{9.60}$$

Hexagonal region:

$$R_{sf} = \frac{1}{2\pi\lambda}\left[\ln\left(\frac{\sqrt{A_p}}{\sqrt{\pi}r_b}\right) - 0.7447\right] + R_b \tag{9.61}$$

Quadratic region:

$$R_{sf} = \frac{1}{2\pi\lambda}\left[\ln\left(\frac{\sqrt{A_p}}{\sqrt{\pi}r_b}\right) - 0.7419\right] + R_b \tag{9.62}$$

The three formulas (9.60-62) are practically identical; there is a mere difference of $0.0053/(2\pi\lambda)$ and $0.0081/(2\pi\lambda)$ compared with the expression for the circular region. If the infinite series of (9.51) were retained in the derivation of the thermal resistances for the hexagonal and the rectangular region, the differences would instead become $0.0010/(2\pi\lambda)$ and $0.0119/(2\pi\lambda)$. The hexagonal and the quadratic region give equal heat transfer properties provided that the cross-sectional areas are the same. Thus, taking the results of Table 9.3 for the eccentric pipe and Table 9.4 for the rectangular region into account, it must be concluded that within reasonable limits the *shape* of the cross-sectional area is of minor importance for the prediction of the fluid-to-ground thermal resistance.

Time-scale for steady-flux process in a rectangular region

The derivation of the steady-flux solution for the rectangular duct pattern did not include the initial transient process. However, an estimate of the time-scale for the attenuation of the transient part can be made from solutions of the transient heat equation for an arbitrary initial temperature distribution in a rectangular area (Carslaw and Jaeger 1959). These solutions typically consist of a series with the time dependence appearing in an exponential factor, which in the notation used here becomes:

$$\exp\left[-4\pi^2 at\left(\frac{m^2}{B^2}+\frac{n^2}{B_1^2}\right)\right] \qquad m,n = 0,1,2,\ldots \tag{9.63}$$

The first time-dependent terms, (m=1, n=0) and (m=0, n=1), will be attenuated by a factor $e^{-3} \simeq 0.05$ if the exponent equals 3. The time-scale is determined by the largest value of B and B_1. For a quadratic duct pattern (B=B_1, $A_p = B^2$) we then get:

$$\frac{at}{A_p} = \frac{at}{B^2} = \frac{3}{4\pi^2} \simeq 0.076 \tag{9.64}$$

The duration of the initial time period before steady-flux conditions are attained is given by this relation. This is roughly the same criterion as eq. (9.4) for the circular region.

9.2.5 Flat heat exchangers

The ground heat exchanger can be arranged by inserting flat (plate-type) heat exchangers in the ground or by using several parallel fractures in rock. We assume that the heat conduction takes place in a direction perpendicular to

the heat transfer surfaces. The distance between two heat transfer surfaces is B. See figure 9.11.

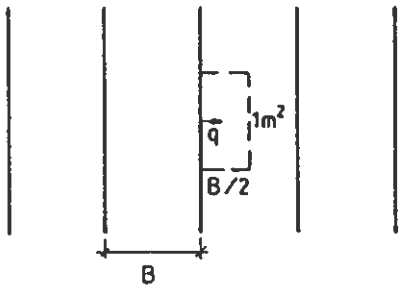

Figure 9.11. Parallel rows of flat heat exchangers.

The heat injection rate q is given per unit area (W/m^2). Note that each heat exchanger exposes two surfaces to the surrounding ground, so that the heat injection rate becomes $2q$ per unit area of heat exchanger.

We will first consider the steady-flux solution, which is the sum of the steady-flux temperature profile and the local average temperature:

$$T(x,t) = T_m(t) + T_{sf}(x) \tag{9.65}$$

The linear increase of the mean temperature is:

$$T_m(t) = \frac{2q\,t}{C\,B} \tag{9.66}$$

The steady-flux temperature satisfies:

$$\frac{d^2T_{sf}}{dx^2} = \frac{2q}{\lambda B} \tag{9.67}$$

It follows immediately by integration that the solution is:

$$T_{sf} = \frac{2q}{\lambda B}\frac{x^2}{2} + \beta_0 x + \beta_1 \tag{9.68}$$

The constants β_0 and β_1 are yet to be determined. We will assume that the heat injection occurs at $x = 0$. There is no heat flow through the boundary

at $x = B/2$. The average value of the steady-flux temperature is chosen to be zero. These conditions now give the solution:

$$T_{sf} = \frac{qB}{\lambda}\left(\frac{x^2}{B^2} - \frac{x}{B} + \frac{1}{6}\right) \tag{9.69}$$

The formulas given in sections 9.1.1-2 have to be slightly modified for this plane case. The heat flow q has the dimension $\mathrm{W/m^2}$ instead of W/m. The thermal resistance ($\mathrm{K/(W/m^2)}$) between the temperature of the heat carrier fluid and the mean storage temperature becomes:

$$R_{sf} = \frac{B}{6\lambda} + R_y \qquad (\mathrm{K/(W/m^2)}) \tag{9.70}$$

where R_y is a surface thermal resistance ($\mathrm{K/(W/m^2)}$) between the heat carrier fluid and the ground immediately outside the heat transfer surface at $x = 0$.

Finally, we will consider the initial transient process before the steady-flux temperature profile is attained. The transient temperature contribution T_{tr} will be added to the right side of (9.65). It will satisfy the heat equation:

$$\frac{\partial^2 T_{tr}}{\partial x^2} = \frac{1}{a}\frac{\partial T_{tr}}{\partial t} \tag{9.71}$$

The derivative of T_{tr} with respect to x is zero both at $x = 0$ and $x = B/2$. The total temperature is initially zero. This requires that:

$$T_{tr}(x, 0) = -T_{sf}(x) \tag{9.72}$$

The solution, which is outlined in Carslaw and Jaeger (1959; p. 101), becomes:

$$T_{tr}(x,t) = -\frac{qB}{\lambda}\frac{1}{\pi^2}\sum_{n=1}^{\infty}\frac{1}{n^2}\cos\left(\frac{2n\pi x}{B}\right)\exp\left(-\frac{4a\pi^2 n^2 t}{B^2}\right) \tag{9.73}$$

The sum converges rapidly. A characteristic time-scale for the transient process is obtained from the exponent of the first term. The transient part should be negligible after about three times the value of the exponent. Each term in the sum will then be less than a factor $\mathrm{e}^{-3} \simeq 0.05$ of its initial value (at t=0). Thus, the steady-flux solution is valid after an initial time period given by:

$$\frac{at}{B^2} = \frac{3}{4\pi^2} \simeq 0.076 \tag{9.74}$$

9.2.6 Concentric pipe in a composite circular region

The ground heat exchanger may be designed so that the pipe will be surrounded by a material that differs in thermal properties from the storage medium. This is sometimes done intentionally to reduce temperature gradients. Here, the case of a concentric pipe in a circular region composed of two layers with different thermal properties will be considered. See figure 9.12.

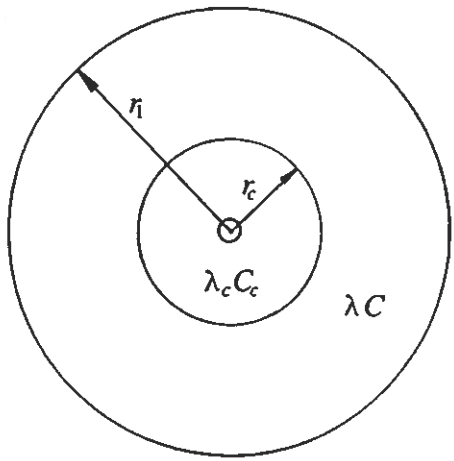

Figure 9.12. Concentric pipe in a composite circular region.

The interface between the inner circular region and the outer annular region is located at the radius r_c. The thermal constants of the inner region are denoted λ_c and C_c.

The steady-flux temperatures in the two regions have, according (9.21), the following functional dependence:

$$r_b < r < r_c : \qquad T_c(r) = \alpha_1 r^2 + \alpha_2 \ln r + \alpha_3 \tag{9.75}$$

$$r_c < r < r_1 : \qquad T(r) = \beta_1 r^2 + \beta_2 \ln r + \beta_3 \tag{9.76}$$

The constants α_1, α_2, α_3, β_1, β_2, and β_3 are to be determined by the boundary conditions and the requirement that the average value of the steady-flux profile in the whole region $r_b < r < r_1$ is zero.

There is constant heat injection rate q (W/m) at the pipe ($r = r_b$):

$$-2\pi r_b \lambda_c \left.\frac{\partial T_c}{\partial r}\right|_{r=r_b} = q \tag{9.77}$$

When the steady-flux regime is established, the rate of temperature increase will be the same in two regions. This requires that the heat flow q is absorbed in proportion to the heat capacity (J/K) of each region. Let q_c be the heat flow entering the outer region at $r = r_c$. Then

$$q_c = \frac{C\pi(r_1^2 - r_c^2)}{C_T} q \tag{9.78}$$

where C_T is the total heat capacity of the region:

$$C_T = C_c\pi(r_c^2 - r_b^2) + C\pi(r_1^2 - r_c^2) \tag{9.79}$$

The heat flow at interface $r = r_c$ becomes with (9.74):

$$-2\pi r_c \lambda_c \left.\frac{\partial T_c}{\partial r}\right|_{r=r_c} = q_c \tag{9.80}$$

Consequently, the heat flow to the annular region at $r = r_c$ becomes:

$$-2\pi r_c \lambda \left.\frac{\partial T}{\partial r}\right|_{r=r_c} = q_c \tag{9.81}$$

There is no heat flow through the outer boundary ($r = r_1$):

$$-2\pi r_1 \lambda \left.\frac{\partial T}{\partial r}\right|_{r=r_1} = 0 \tag{9.82}$$

The temperature at the interface $r = r_c$ must be continuous:

$$T_c(r_b) = T(r_b) \tag{9.83}$$

Finally, there is the requirement (6.13) that the average temperature, or to be more precise the heat content, is zero:

$$\left(C_c\, 2\pi \int_{r_b}^{r_c} T_c(r)\, r\, dr + C\, 2\pi \int_{r_c}^{r_1} T(r)\, r\, dr\right) / C_T = 0 \tag{9.84}$$

After straightforward, but rather lengthy, calculations we get the following expressions for the temperature:

$r_b < r < r_c$:

$$\begin{aligned} T_c(r) \;=\; & \frac{q}{2\pi\lambda}\left\{\frac{\lambda}{\lambda_c}\left[\left(1 + \frac{C_c\pi r_b^2}{C_T}\right)\left(\ln\left(\frac{r_c}{r}\right) + \frac{C_c\pi r_b^2}{C_T}\ln\left(\frac{r_c}{r_b}\right) - \frac{C_c\pi r_c^2}{C_T} + \right.\right. \\ & \left. + \frac{1}{2}\frac{C_c\pi r_b^2}{C_T}\right) + \frac{1}{2}\frac{C_c\pi r^2}{C_T} + \frac{1}{4}\left(\frac{C_c\pi r_c^2}{C_T}\right)^2 + \frac{1}{4}\left(\frac{C_c\pi r_b^2}{C_T}\right)^2\Bigg] + \\ & + \frac{1}{2}\left(\frac{C\pi r_1^2}{C_T}\right)^2\left[\ln\left(\frac{r_1^2}{r_c^2}\right) + \frac{r_c^2}{r_1^2} - 1\right] - \frac{1}{4}\left[\frac{C\pi(r_1^2 - r_c^2)}{C_T}\right]^2\Bigg\} \end{aligned} \tag{9.85}$$

$r_c < r < r_1$:

$$T(r) = \frac{q}{2\pi\lambda}\left\{\frac{\lambda}{\lambda_c}\left[\left(1+\frac{C_c\pi r_b^2}{C_T}\right)\left(\frac{C_c\pi r_b^2}{C_T}\ln\left(\frac{r_c}{r_b}\right)-\frac{C_c\pi r_c^2}{C_T}+\frac{1}{2}\frac{C_c\pi r_b^2}{C_T}\right)+\right.\right.$$
$$+\frac{1}{2}\frac{C_c\pi r_c^2}{C_T}+\frac{1}{4}\left(\frac{C_c\pi r_c^2}{C_T}\right)^2+\frac{1}{4}\left.\left(\frac{C_c\pi r_b^2}{C_T}\right)^2\right]+$$
$$+\frac{C\pi r_1^2}{C_T}\ln\left(\frac{r_c}{r}\right)+\frac{1}{2}\frac{C\pi r^2}{C_T}-\frac{1}{2}\frac{C\pi r_c^2}{C_T}+$$
$$\left.+\frac{1}{2}\left(\frac{C\pi r_1^2}{C_T}\right)^2\left[\ln\left(\frac{r_1^2}{r_c^2}\right)+\frac{r_c^2}{r_1^2}-1\right]-\frac{1}{4}\left[\frac{C\pi(r_1^2-r_c^2)}{C_T}\right]^2\right\} \qquad (9.86)$$

The thermal resistance is obtained by dividing the pipe temperature $T_c(r_b)$ with the heat flow q, and adding the fluid-to-ground thermal resistance R_b:

$$R_{sf} = \frac{1}{2\pi\lambda}\left\{\frac{\lambda}{\lambda_c}\left[\left(1+\frac{C_c\pi r_b^2}{C_T}\right)^2\ln\left(\frac{r_c}{r_b}\right)-\right.\right.$$
$$-\left(1+\frac{C_c\pi r_b^2}{C_T}\right)\left(\frac{C_c\pi r_c^2}{C_T}-\frac{C_c\pi r_b^2}{C_T}\right)+\frac{1}{4}\left(\frac{C_c\pi r_c^2}{C_T}\right)^2-$$
$$\left.-\frac{1}{4}\left(\frac{C_c\pi r_b^2}{C_T}\right)^2\right]+\frac{1}{2}\left(\frac{C\pi r_1^2}{C_T}\right)^2\left[\ln\left(\frac{r_1^2}{r_c^2}\right)+\frac{r_c^2}{r_1^2}-1\right]-$$
$$\left.-\frac{1}{4}\left[\frac{C\pi(r_1^2-r_c^2)}{C_T}\right]^2\right\}+R_b \qquad (9.87)$$

One may note that the steady-flux thermal process for the *inner* circular region may be regarded as a superposition of a steady-state component and a steady-flux component. In the steady-state part, there is a heat flow q_c (9.78) through the boundaries at $r = r_b$ and at $r = r_c$. The radial dependence of the steady-state temperature is of the type $\beta_4 \ln(r) + \beta_5$, where the constants β_4 and β_5 are determined by boundary conditions. For the steady-flux part, which has functional dependence like (9.75), the heat flow is $q - q_c$ at $r = r_b$ and there is no heat flow through the interface at $r = r_c$. The sum of the steady-flux and the steady-flux part fulfill the boundary conditions (9.77) and 9.80). The magnitude of the steady-state component is proportional to q_c, while the magnitude of the steady-flux component is proportional $q - q_c$. Stated differently, the steady-state component is proportional to the total heat capacity of the outer region and the steady-flux component is proportional to the total heat capacity of the inner region. Thus, the temperature profile and the thermal resistance of the *inner* region can be calculated at steady-state

conditions, if the heat capacity of the inner region ($C_c\pi(r_c^2 - r_b^2)$) is small compared to the heat capacity of the outer region ($C\pi(r_1^2 - r_c^2)$).

9.2.7 Eccentric pipe in a composite circular region

The temperature field from an eccentric line source forms the basis for the steady-flux analysis of arrangements with multiple flow channels. The eccentric pipe in a circular region composed of two layers with different thermal properties will be treated in this section. See figure 9.13.

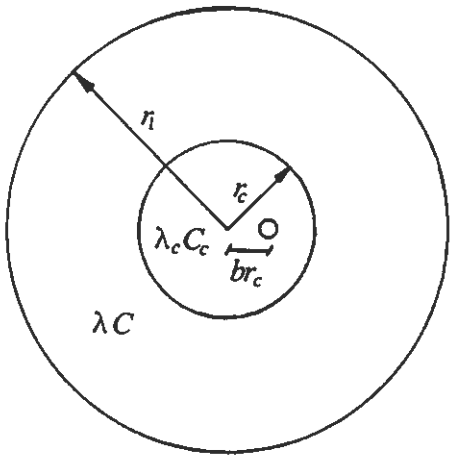

Figure 9.13. Eccentric pipe in a composite circular region.

The interface between the inner circular region and the outer annular region is located at the radius r_c. The thermal properties of the inner region are denoted λ_c and C_c.

If the total heat capacity of the inner region ($C_c\pi(r_c^2 - r_b^2)$) is small compared to the heat capacity of the outer region ($C\pi(r_1^2 - r_c^2)$), then the temperature field in the inner region is practically at steady-state conditions, cf. the discussion at the end of section 9.2.6. It is then preferable to use the method in section 8.4 to evaluate the thermal resistance of the inner region. The steady-flux thermal resistance of the outer region is obtained from the formulas for a concentric pipe in a circular region in section 9.2.1. The radius r_b of the concentric pipe must then be replaced by the radius r_c at the interface between the inner and the outer region.

Temperature field

The steady-flux temperature field for an eccentric pipe in a composite circular region will be derived in this section. The solution is approximate in the sense that the boundary condition at the outer boundary at $r = r_c$ is not exactly fulfilled. The total heat flow through this boundary is zero, but there is a slight variation around the periphery.

The temperature field is obtained by a superposition of three components. First we take the steady-state solution for an eccentric line-source in a circular region surrounded by an infinite region with different thermal conductivity. The solution is derived in Appendix B (Index b in the appendix corresponds to index c here). A line source located at the coordinates $x = br_c$ and $y = 0$ gives the following steady-state temperature field:

$x^2 + y^2 \leq r_c^2$:

$$u_1(x,y) = -\frac{q}{4\pi\lambda_c}\left\{\ln\left[\left(\frac{x}{r_c} - b\right)^2 + \frac{y^2}{r_c^2}\right] + \frac{\lambda_c - \lambda}{\lambda_c + \lambda}\ln\left[\left(\frac{bx}{r_c} - 1\right)^2 + \frac{b^2y^2}{r_c^2}\right]\right\} \tag{9.88}$$

$x^2 + y^2 \geq r_c^2$:

$$u_1(x,y) = -\frac{q}{4\pi\lambda_c}\frac{2\lambda_c}{\lambda_c + \lambda}\ln\left[\left(\frac{x}{r_c} - b\right)^2 + \frac{y^2}{r_c^2}\right] + \frac{q}{4\pi\lambda}\frac{\lambda_c - \lambda}{\lambda_c + \lambda}\ln\left(\frac{x^2 + y^2}{r_c^2}\right) \tag{9.89}$$

Polar coordinates will be used:

$$x = r\sin\varphi \qquad y = r\cos\varphi \tag{9.90}$$

It is shown in Appendix B that the temperature $u_1(x,y)$ fulfills the boundary conditions that the heat flows and the temperatures must be continuous at $r = r_c$:

$$-\lambda_c \left.\frac{\partial u_1}{\partial r}\right|_{r=r_c-0} = -\lambda \left.\frac{\partial u_1}{\partial r}\right|_{r=r_c+0} \qquad u_1|_{r=r_c-0} = u_1|_{r=r_c+0} \tag{9.91}$$

A second component, which satisfies the heat equation for the steady-flux regime, is:

$$u_2(x,y,t) = \frac{q}{C_T}\left(t + \frac{x^2 + y^2 - r_c^2}{4a_c}\right) \qquad x^2 + y^2 \leq r_c^2$$

$$u_2(x,y,t) = \frac{q}{C_T}\left(t + \frac{x^2 + y^2 - r_c^2}{4a}\right) \qquad x^2 + y^2 \geq r_c^2 \tag{9.92}$$

where C_T is the total heat capacity (9.79) of the region. This temperature is continuous at $r = r_c$, but it gives a net constant heat flux:

$$-\lambda_c \left.\frac{\partial u_2}{\partial r}\right|_{r=r_c-0} + \lambda \left.\frac{\partial u_2}{\partial r}\right|_{r=r_c+0} = \frac{q}{C_T} \cdot \frac{r_c}{2}(C - C_c) \tag{9.93}$$

We need a third solution u_3 that takes care of this boundary heat flow:

$$\begin{aligned} u_3(x,y) &= 0 && x^2 + y^2 \le r_c^2 \\ u_3(x,y) &= \frac{q}{4\pi\lambda} \frac{\pi r_c^2 (C_c - C)}{C_T} \ln\left(\frac{x^2+y^2}{r_c^2}\right) && x^2 + y^2 \ge r_c^2 \end{aligned} \tag{9.94}$$

The temperature field is the sum of the three components:

$$T(x,y,t) = u_1(x,y) + u_2(x,y,t) + u_3(x,y) \tag{9.95}$$

Finally, the expression for the temperature field becomes:

$x^2 + y^2 \le r_c^2$:

$$\begin{aligned} T(x,y,t) \;=\; & -\frac{q}{4\pi\lambda_c}\left\{\ln\left[\left(\frac{x}{r_c} - b\right)^2 + \frac{y^2}{r_c^2}\right]\right. \\ & \left. + \frac{\lambda_c - \lambda}{\lambda_c + \lambda} \ln\left[\left(\frac{bx}{r_c} - 1\right)^2 + \frac{b^2 y^2}{r_c^2}\right]\right\} + \\ & + \frac{q}{C_T}\left(t + \frac{x^2 + y^2 - r_c^2}{4a_c}\right) \end{aligned} \tag{9.96}$$

$x^2 + y^2 \ge r_c^2$:

$$\begin{aligned} T(x,y,t) \;=\; & -\frac{q}{4\pi\lambda_c}\frac{2\lambda_c}{\lambda_c + \lambda} \ln\left[\left(\frac{x}{r_c} - b\right)^2 + \frac{y^2}{r_c^2}\right] + \\ & + \frac{q}{4\pi\lambda}\left(\frac{\lambda_c - \lambda}{\lambda_c + \lambda} + \frac{\pi r_c^2 (C_c - C)}{C_T}\right) \ln\left(\frac{x^2+y^2}{r_c^2}\right) + \\ & + \frac{q}{C_T}\left(t + \frac{x^2 + y^2 - r_c^2}{4a}\right) \end{aligned} \tag{9.97}$$

The temperatures (9.96) and (9.97) satisfy the partial differential equation (6.10) for the steady-flux regime, the temperature and the heat flux are continuous at the boundary $r = r_c$, and there is the required line-source q at $(x,y) = (br_c, 0)$.

Finally, the condition of no heat flux through the outer boundary ($r = r_1$) requires that:

$$-\lambda \left.\frac{\partial T}{\partial r}\right|_{r=r_1} = 0 \tag{9.98}$$

A differentiation of (9.97) with respect to r for constant φ gives:

$$-\lambda \left.\frac{\partial T}{\partial r}\right|_{r=r_1} = \frac{q}{2\pi r_1}\frac{2\lambda}{\lambda_c+\lambda} f\left(\frac{br_c}{r_1},\varphi\right) \tag{9.99}$$

where

$$f\left(\frac{br_c}{r_1},\varphi\right) = \frac{\frac{br_c}{r_1}\cos\varphi - \left(\frac{br_c}{r_1}\right)^2}{1-2\frac{br_c}{r_1}\cos\varphi+\left(\frac{br_c}{r_1}\right)^2} \tag{9.100}$$

The total heat flow through the boundary becomes:

$$\frac{q}{2\pi}\frac{2\lambda}{\lambda_c+\lambda}\int_0^{2\pi} f\left(\frac{br_c}{r_1},\varphi\right)\,d\varphi = 0 \tag{9.101}$$

The integral value is given by Gradshteyn and Ryshik (1980; p.148). The total heat flow through the outer boundary is zero, but it varies with the angle φ around the periphery. This angular variation (9.100) has its maximum value at φ=0 and its minimum value at φ=π:

$$\begin{aligned} &\text{Maximum value:} && f\left(\frac{br_c}{r_1},0\right) = \frac{\frac{br_c}{r_1}}{1-\frac{br_c}{r_1}} \\ &\text{Minimum value:} && f\left(\frac{br_c}{r_1},\pi\right) = -\frac{\frac{br_c}{r_1}}{1+\frac{br_c}{r_1}} \end{aligned} \tag{9.102}$$

Note that the parameter br_c/r_1 is the distance between center of the region and the center of the pipe divided by the outer radius of the whole region.

Let us compare the amplitude of the heat flux variation (9.99) with the heat flux resulting from a hypothetical steady-state heat flow through the region. The thermal conductivities are set equal for simplicity. The steady-state heat flux would be $q/(2\pi\lambda r_1)$. A reasonable value of br_c/r_1 is about 0.1. The amplitude of the heat flux variation is from (9.99) and (9.102) about 10 % of the steady-state value, which must be regarded as relatively small.

A further remark concerns the superposition of eccentric line sources. If a pair of line sources of equal strength are placed symmetrically with respect to the center of the region, the heat fluxes from the two pipes balance each other to some extent on the periphery. The magnitude of the heat flux variation becomes smaller.

Pipe temperature

The temperature at the pipe is evaluated at:

$$(x - br_c)^2 + y^2 = r_b^2 \tag{9.103}$$

This expression is used for the first term of (9.96). The other terms are evaluated at the point $x = br_c$ and $y = 0$. This gives:

$$T_b(t) = \frac{q}{2\pi\lambda_c}\left[\ln\left(\frac{r_c}{r_b}\right) - \frac{\lambda_c - \lambda}{\lambda_c + \lambda}\ln(1-b^2) - \frac{C_c\pi r_c^2}{2C_T}(1-b^2)\right] + \frac{qt}{C_T} \tag{9.104}$$

Local average temperature

The average temperature in the region is by (6.13) obtained from:

$$T_m(t) = \left[C_1 \iint_{x^2+y^2\le r_c^2} T(x,y,t)\,dxdy + C\iint_{r_c^2\le x^2+y^2\le r_1^2} T(x,y,t)\,dxdy\right]/C_T \tag{9.105}$$

The integrations of the temperature fields (9.96-97) are rather lengthy but straightforward. The following integral (Gradshteyn and Ryzhik 1980; p. 541) is used:

$$\int_0^\pi \ln(a + b\cos\varphi)\,d\varphi = \pi\ln\left[\frac{1}{2}(a + \sqrt{a^2 - b^2})\right] \tag{9.106}$$

Finally, the average temperature in the ground becomes:

$$\begin{aligned} T_m(t) \;=\; & \frac{q}{4\pi\lambda_c}\left\{\frac{C_c\pi r_c^2}{C_T}(1-b^2) - \right. \\ & -\frac{C_c\pi r_b^2}{C_T}(1-b^2)\left[1 + \ln\left(\frac{r_c^2}{r_b^2}\right)\right] - \frac{1}{2}\left(\frac{C_c\pi r_c^2}{C_T}\right)^2\Bigg\} - \\ & -\frac{q}{4\pi\lambda}\left\{\left(\frac{C\pi r_1^2}{C_T}\right)^2\left[\ln\left(\frac{r_1^2}{r_c^2}\right) + \frac{r_c^2}{r_1^2} - 1\right] - \right. \\ & \left.-\frac{1}{2}\left(\frac{C\pi(r_1^2 - r_c^2)}{C_T}\right)^2\right\} + \frac{qt}{C_T} \end{aligned} \tag{9.107}$$

The heat capacity at the pipe $C_c\pi r_b^2$ is usually negligible in this application. The total heat capacity of the region is then:

$$C_T = \pi[Cr_1^2 + (C_c - C)r_c^2] \tag{9.108}$$

Thermal resistance

The temperature difference $T_b - T_m$ can be calculated by subtracting (9.107) from (9.104). Dividing by the heat flow q and adding the pipe thermal resistance R_b gives the thermal resistance between the fluid temperature and the average ground temperature:

$$\begin{aligned} R_{sf} &= \frac{1}{2\pi\lambda}\left\{\frac{\lambda}{\lambda_c}\left[\ln\left(\frac{r_c}{r_b}\right) - \frac{C_c\pi r_c^2}{C_T}(1-b^2) - \right.\right. \\ &\quad -\frac{\lambda_c-\lambda}{\lambda_c+\lambda}\ln(1-b^2) + \frac{1}{4}\left(\frac{C_c\pi r_c^2}{C_T}\right)^2\Bigg] + \\ &\quad \left.\left. +\frac{1}{2}\left(\frac{C\pi r_1^2}{C_T}\right)^2\left[\ln\left(\frac{r_1^2}{r_c^2}\right) + \frac{r_c^2}{r_1^2} - 1\right] - \frac{1}{4}\left(\frac{C\pi(r_1^2-r_c^2)}{C_T}\right)^2\right\} + R_b \\ &\qquad\qquad (C_c\pi r_b^2 \ll C_T) \end{aligned} \tag{9.109}$$

9.3 Multiple ground heat transfer channels

The ground heat exchanger consisting of multiple ground heat exchanger channels will be analyzed in this section. A general expression for the thermal resistance of N flow channels in a circular region with homogeneous thermal properties, see figure 9.14, is described in section 9.3.1.

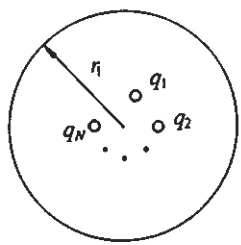

Figure 9.14. Ground heat exchanger with N parallel channels in a circular ground region with homogeneous thermal properties.

We will here present formulas for the steady-flux thermal resistance for symmetrically placed channels, corresponding to a single, double, or triple U-shaped pipe in a ground region with homogeneous thermal properties. The derivation of the temperature field for simplest case, the single U-pipe, will be presented in some detail. Finally, the multiple heat pipes in a composite region are dealt with.

The thermal process for the cases of two (figure 9.18), four (figure 9.19), and six symmetrical channels (figure 9.20) can be represented by the thermal circuits in figures 9.15, 9.16, and 9.17 respectively.

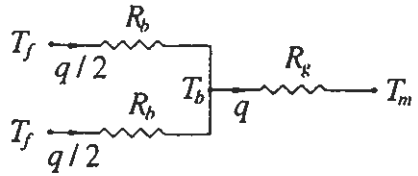

Figure 9.15. The thermal circuit of a ground heat exchanger with two symmetrical heat transfer channels.

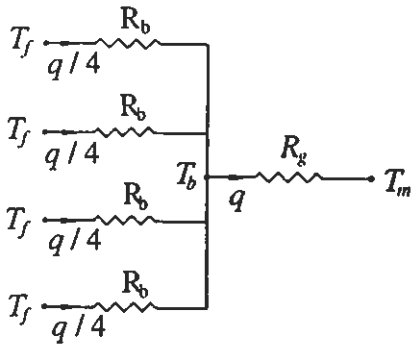

Figure 9.16. The thermal circuit of a ground heat exchanger with four symmetrical heat transfer channels.

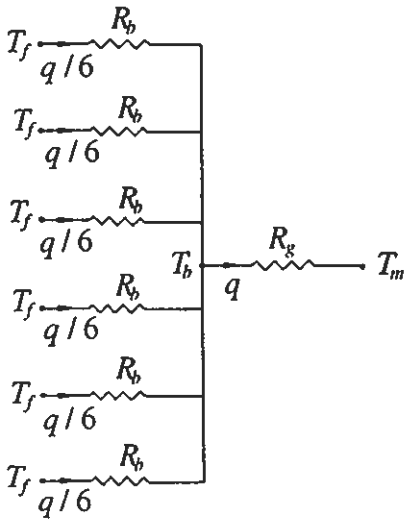

Figure 9.17. The thermal circuit of a ground heat exchanger with six symmetrical heat transfer channels.

The thermal resistance for a ground heat exchanger with N symmetrically placed heat transfer channels is given by:

$$R_{sf} = R_g + \frac{R_b}{N} \tag{9.110}$$

where R_b is the fluid-to-ground thermal resistance of the channels. The thermal resistance between the ground temperature T_b at the outer wall of the N pipes and the local average temperature T_m is denoted R_g, cf. section 9.2.

9.3.1 Multiple heat transfer channels in a homogeneous region

The thermal resistance for multiple flow channels in a circular region with homogeneous thermal properties can be obtained by superposing steady-flux solutions for the eccentric line source. The eccentric line-source solution is dealt with in section 9.2.3. The superposition method is essentially the same as the one used for the steady-state line-source approximation for multiple flow channels in a composite region. See section 8.4.1. The nomenclature differs slightly and the expressions for thermal resistances must be replaced by their steady-flux counterparts for a homogeneous region. For the sake of clarity, the method will be fully described also for this case.

The ground heat exchanger consists of N parallel channels in a circular ground region with homogeneous thermal properties. See figure 9.14. The heat injection rate at pipe i is q_i (W/m). The total heat injection rate is given by the sum:

$$q = \sum_{i=1}^{N} q_i \tag{9.111}$$

The center of the pipe i is located at the coordinates (x_i, y_i). The distance from the center of the circular region is given by $b_i r_1$, while the distance between two pipes i and j is $b_{ij} r_1$. Expressed in the coordinates of the pipes, we have:

$$\begin{aligned} b_i &= \frac{\sqrt{x_i^2 + y_j^2}}{r_1} \\ b_{ij} &= \frac{\sqrt{(x_i - x_j)^2 + (y_i - y_j)^2}}{r_1} \qquad \text{for } i, j = 1, \ldots, N \end{aligned} \tag{9.112}$$

Let R_{bi} denote the thermal resistance between the fluid and the ground immediately outside pipe i. Formulas for this resistance are found in chapter 8. The difference between the fluid temperature T_{fi} and the temperature T_{bi} in the ground immediately outside the channels becomes:

$$T_{fi} - T_{bi} = q_i R_{bi} \qquad i = 1, \ldots, N \tag{9.113}$$

Similar to the problem of steady-state heat flows between the fluid and the borehole wall in section 8.2.1, there are linear relations between the temperature differences $T_{fi} - T_m$ and the heat flows q_i:

$$T_{fi} - T_m = \sum_{j=1}^{N} R_{ij}\, q_j \qquad j = 1, \ldots, N \tag{9.114}$$

Note that T_m is the local average temperature in the ground.

The thermal resistances R_{ii} and R_{ij} are obtained from the expression (9.39) for the temperature field of an eccentric pipe in a circular region. See also the derivation of the thermal resistance for a single U-pipe in section 9.3.2. The fluid-to-ground thermal resistances R_{bi} are added to R_{ii}. We have:

$$\begin{aligned} R_{ii} &= \frac{1}{2\pi\lambda}\left[\ln\left(\frac{r_1}{r_{bi}}\right) - \frac{3}{4} + b_i^2 - \ln(1-b_i^2)\right] + R_{bi} \\ R_{ij} &= \frac{1}{2\pi\lambda}\left[\frac{1}{2}(b_i^2 + b_j^2) - \frac{3}{4} - \ln(b_{ij}) - \ln(b'_{ij})\right] \qquad \text{for } i \neq j \\ & b'_{ij} = \sqrt{(1-b_i^2)(1-b_j^2) + b_{ij}^2} \\ & b_i \ll 1 \qquad b_{ij} r_1 < 1.5(r_{bi} + r_{bj}) \end{aligned} \tag{9.115}$$

The thermal resistance matrix becomes symmetric, since the elements R_{ij} and R_{ji} are equal.

The heat flows q_i are given by the inverse of the equation system (9.114):

$$q_i = \sum_{j=1}^{N} (R_{ij})^{-1} (T_{fj} - T_m) \qquad i = 1, \ldots, N \tag{9.116}$$

where $(R_{ij})^{-1}$ are the matrix elements of the inverse to the matrix R_{ij}. The sum of q_i, $i = 1, \ldots, N$ gives the total heat flow q.

The thermal resistance R_{sf} for the steady-flux regime will be derived with all fluid temperatures T_{fi} set equal to T_f. Then we get:

$$q = \frac{T_f - T_m}{R_{sf}} \tag{9.117}$$

$$R_{sf} = \frac{1}{\sum_{i=1}^{N} \sum_{j=1}^{N} (R_{ij})^{-1}} \tag{9.118}$$

The general expression for R_{sf} concerning the case of N channels in a ground region with homogeneous thermal properties is given by (9.118). The matrix R_{ij} is defined by (9.115).

The formula (9.118) for the thermal resistance is further simplified in the completely symmetrical case. The heat injection rate at each pipe is equal, that is $q_i = q/N$. The thermal resistance R_{sf} is then by (9.114):

$$R_{sf} = \frac{1}{N}\sum_{j=1}^{N} R_{ij} = \frac{1}{N}\sum_{j=1}^{N} R_{1j} \tag{9.119}$$

9.3.2 Single U-pipe in a circular region

Figure 9.18 shows the positions of two pipes placed in opposite directions from the center of the circular region.

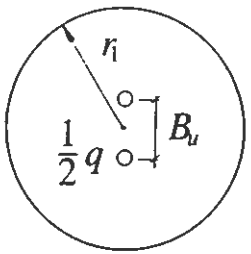

Figure 9.18. Single U-pipe in a circular region.

The distance between pipes, the shank spacing, is denoted B_u. The eccentricity parameter b is given by:

$$b = \frac{B_u}{2r_1} \tag{9.120}$$

Eq. (9.39) gives the temperature field of a line source placed at $x = br_1$ and $y = 0$. To obtain a solution for the two pipes we need to superpose the temperature field from a pipe placed at $x = -br_1$ and $y = 0$. The strength of the line sources are q_1 and q_2. The fluid-to-ground thermal resistance is R_b. From (9.39) and (9.42-43) we get:

$$\begin{aligned} T_{f1} - T_m &= \frac{q_1}{2\pi\lambda}\left[\ln\left(\frac{r_1}{r_b}\right) - \frac{3}{4} + b^2 - \ln(1-b^2)\right] + q_1 R_b + \\ &\quad + \frac{q_2}{2\pi\lambda}\left[b^2 - \frac{3}{4} - \ln[2b(1+b^2)]\right] \\ T_{f2} - T_m &= \frac{q_2}{2\pi\lambda}\left[\ln\left(\frac{r_1}{r_b}\right) - \frac{3}{4} + b^2 - \ln(1-b^2)\right] + q_2 R_b \\ &\quad + \frac{q_1}{2\pi\lambda}\left[b^2 - \frac{3}{4} - \ln[2b(1+b^2)]\right] \end{aligned} \tag{9.121}$$

The difference between the average fluid temperature T_f and the average ground temperature becomes:

$$T_f - T_m = \frac{q_1 + q_2}{2\pi\lambda}\left[\ln\left(\frac{r_1}{r_b}\right) - \frac{3}{4} + b^2 - \frac{1}{2}\ln(1-b^4) - \frac{1}{2}\ln\left(\frac{B_u}{r_b}\right)\right] + \\ + \frac{1}{2}(q_1 + q_2)R_b \qquad (9.122)$$

It is often convenient to use the heat injection rate q per meter of ground heat exchanger instead of the heat injection rates from the individual pipes. Here, the total heat injection rate q is $q_1 + q_2$. Finally, we get the thermal resistance for the single U-pipe of figure 9.18:

$$R_{sf} = \frac{1}{2\pi\lambda}\left[\ln\left(\frac{r_1}{r_b}\right) - \frac{3}{4} + b^2 - \frac{1}{2}\ln(1-b^4) - \frac{1}{2}\ln\left(\frac{B_u}{r_b}\right)\right] + \frac{R_b}{2} \qquad (9.123)$$

The derivation of this formula assumes that the pipe radius is small compared to the diameter of the circular region. The temperature on the pipe ($r = r_b$) should be constant. However, the eccentric position of the line source will give a variation of the temperature around the periphery of the pipe. The presence of the other line source will also disturb the temperature field. Our main concern is the average value on the pipe. If the pipes are too close to each other, the peripheral temperature variation will be large. This means that the line source approximation may not give the correct average pipe temperature. Another, quite obvious limitation is that the pipe must lie completely inside the circular region. The conditions are then:

$$r_b \ll r_1 \qquad B_u > 3r_b \qquad r_b < (1-b)r_1 \qquad (9.124)$$

9.3.3 Double U-pipe in a circular region

The derivation of the thermal resistance for the double U-pipe is carried out in the same way as for the single U-pipe. There are now four pipe in the circular region, as shown in figure 9.19.

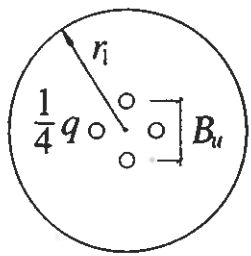

Figure 9.19. Double U-pipe in a circular region.

The shank spacing B_u refers to the distance between two opposing pipes. Eq. (9.120) defines the parameter b. The fluid-to-ground thermal resistance is R_b. The line sources have equal strength $q/4$ and are located at:

$$\begin{aligned} (x_1, y_1) &= (br_1, 0) & (x_2, y_2) &= (0, br_1) \\ (x_3, y_3) &= (-br_1, 0) & (x_4, y_4) &= (0, -br_1) \end{aligned} \tag{9.125}$$

The temperature field is obtained by superposing four contributions of the type (9.39). The expression for the thermal resistance is by (9.115) and (9.119):

$$\begin{aligned} R_{sf} &= \frac{1}{2\pi\lambda}\left[\ln\left(\frac{r_1}{r_b}\right) - \frac{3}{4} + b^2 - \frac{1}{4}\ln(1-b^8) - \right. \\ &\quad \left. -\frac{1}{2}\ln\left(\frac{\sqrt{2}br_1}{r_b}\right) - \frac{1}{4}\ln\left(\frac{2br_1}{r_b}\right)\right] + \frac{R_p}{4} \\ &\qquad r_b \ll r_1 \qquad B_u > 3r_b \qquad r_b < (1-b)r_1 \end{aligned} \tag{9.126}$$

The term containing $\ln(1-b^8)$ is usually negligible.

9.3.4 Triple U-pipe in a circular region

The triple U-pipe arrangement uses six pipes as shown in figure 9.20.

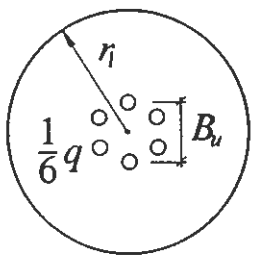

Figure 9.20. Triple U-pipe in a circular region.

The shank spacing B_u refers to the distance between two opposing pipes. Eq. (9.120) defines the parameter b. The fluid-to-ground thermal resistance is R_b. The line sources have equal strength $q/6$ and are located at:

$$\begin{aligned} (x_1, y_1) &= (br_1, 0) & (x_2, y_2) &= (br_1/2, \sqrt{3}br_1/2) \\ (x_3, y_3) &= (-br_1/2, \sqrt{3}br_1/2) & (x_4, y_4) &= (-br_1, 0) \\ (x_5, y_5) &= (-br_1/2, -\sqrt{3}br_1/3) & (x_6, y_6) &= (br_1/2, -\sqrt{3}br_1/2) \end{aligned} \tag{9.127}$$

The temperature field is composed of six contributions of the type (9.39). The expression for the thermal resistance is by (9.115) and (9.119):

$$R_{sf} = \frac{1}{2\pi\lambda}\left[\ln\left(\frac{r_1}{r_b}\right) - \frac{3}{4} + b^2 - \frac{1}{6}\ln(1-b^{12}) - \right. \tag{9.128}$$
$$\left. -\frac{1}{3}\ln\left(\frac{br_1}{r_b}\right) - \frac{1}{3}\ln\left(\frac{\sqrt{3}br_1}{r_b}\right) - \frac{1}{6}\ln\left(\frac{2br_1}{r_b}\right)\right] + \frac{R_p}{6}$$
$$r_b \ll r_1 \qquad B_u > 3r_b \qquad r_b < (1-b)r_1$$

The term containing $\ln(1-b^{12})$ is negligible.

9.3.5 Single U-pipe in a rectangular region

Figure 9.21 shows a single U-pipe in a rectangular region. The distance between the shanks is B_u.

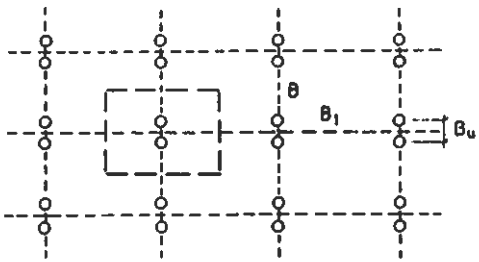

Figure 9.21. Single U-pipe in a rectangular region.

The steady-flux solution for a single U-pipe in a rectangular region can be derived by superposing two patterns with a single pipe in a rectangular region. It is obvious that the solution will fulfill the boundary conditions, due to the symmetry of the resulting pattern.

The heat injection rate from each of the two pipes is $q/2$. Eqs. (9.47) and (9.51) give the temperature field for the single pipe in a rectangular region. The influence from the other pipe is obtained by taking the temperature at a distance corresponding to the shank spacing B_u:

$$T(B_u,0) = \frac{q/2}{\lambda}\left[-\frac{1}{4\pi}\{2\ln[1-\cos(2\pi B_u/B)]\} + \frac{B_1}{12\,B} + \right. \tag{9.129}$$
$$\left. + \frac{1}{\pi}\sum_{n=1}^{\infty}\frac{1}{n}\cos(2\pi n B_u/B)\frac{\exp(-2\pi n B_1/B)}{1-\exp(-2\pi n B_1/B)}\right]$$

The series, which converges very rapidly, can be neglected if we choose $B_1 \geq B$. The influence (9.129) of the other pipe is added to the temperature (9.55, $q = q/2$) of a single pipe. Together with (9.110) and after some rearrangement we get:

$$R_{sf} = \frac{1}{4\pi\lambda}\left[\ln\left(\frac{B}{2\pi r_b}\right) + \frac{\pi B_1}{3B} + \ln\left(\frac{1}{2\sin(\pi B_u/B)}\right)\right] + \frac{1}{2}R_b \qquad (9.130)$$

$$B \leq B_1 \qquad r_b \ll B \qquad r_b \ll B_u$$

Let us compare the formulas for the single U-pipe in a circular region (9.123) and the quadratic region (9.130, $B = B_1$). The cross-sectional area A_p is equal for the two regions. The ratio of the thermal resistances is shown in Table 9.5 as a function of r_1/r_b and the shank spacing parameter b, which are defined for the circular region.

TABLE 9.5. Ratio between thermal resistance for a single U-pipe in a circular region (9.123) and quadratic region ((9.130), $B = B_1$) with the same cross-sectional area. The ratio is given as a function of r_1/r_b and the shank spacing parameter b (9.120), which are defined for the circular region.

	b			
r_1/r_b	0.05	0.10	0.20	0.40
20	0.9957	0.9946	0.9921	0.9851
60	0.9967	0.9960	0.9945	0.9902
100	0.9970	0.9964	0.9952	0.9916

As expected, the thermal resistances are practically the same for the circular and the quadratic region if the cross-sectional area is equal.

9.3.6 Single U-pipe in a composite circular region

Multiple heat transfer channels in a composite region can be handled by the superposition method presented in section 9.3.1 concerning the case of homogeneous thermal properties. The thermal resistances R_{ij} of (9.115) will of course be different. The temperature field from an eccentric pipe in a composite region, which is derived in section 9.2.7, is the starting point of the analyses. Here, we will only give the final expression for the thermal resistance R_{sf}.

Figure 9.22 shows the nomenclature used for a single U-pipe in a composite region.

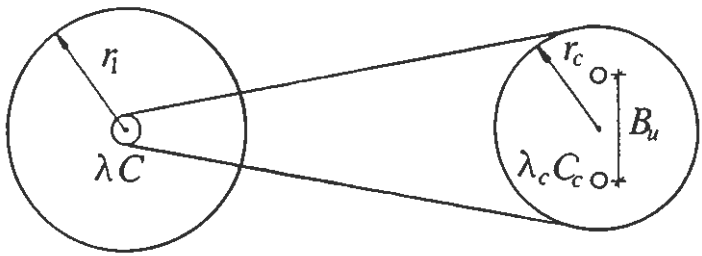

Figure 9.22. Single U-pipe in a composite circular region.

The distance between pipes, the shank spacing, is denoted B_u. The eccentricity parameter b is defined by:

$$b = \frac{B_u}{2r_c} \tag{9.131}$$

A superposition of two eccentric pipes (9.96-97) located at $x = -br_c$ and $x = br_c$ for $y = 0$ gives the temperature field. The heat injection rate is $q/2$ per pipe. The average temperature is given by (9.107). The temperature difference $T_f - T_m$ divided by the total heat flow q yields the thermal resistance:

$$\begin{aligned} R_{sf} \;=\; & \frac{1}{2\pi\lambda}\left\{\frac{\lambda}{\lambda_c}\left[\ln\left(\frac{r_c}{r_b}\right) - \frac{C_c\pi r_c^2}{C_T}(1-b^2) - \frac{1}{2}\ln\left(\frac{B_u}{r_b}\right) - \right.\right. \\ & -\frac{1}{2}\frac{\lambda_c-\lambda}{\lambda_c+\lambda}\ln(1-b^4) + \frac{1}{4}\left(\frac{C_c\pi r_c^2}{C_T}\right)^2\Bigg] + \\ & \left.\left. +\frac{1}{2}\left(\frac{C\pi r_1^2}{C_T}\right)^2\left[\ln\left(\frac{r_1^2}{r_c^2}\right) + \frac{r_c^2}{r_1^2} - 1\right] - \frac{1}{4}\left(\frac{C\pi(r_1^2-r_c^2)}{C_T}\right)^2\right\} + \frac{R_b}{2} \\ & C_c\pi r_b^2 \ll C_T \end{aligned} \tag{9.132}$$

Here, the total heat capacity C_T of the region is given by (9.79). The fluid-to-ground thermal resistance R_b has been added according to (9.110).

9.3.7 Double U-pipe in a composite circular region

The nomenclature used for the double U-pipe in a composite circular region is shown in figure 9.23.

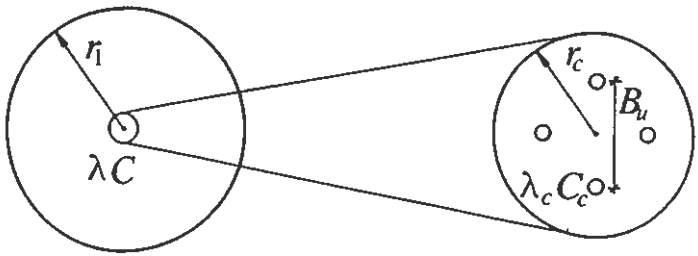

Figure 9.23. Double U-pipe in a composite circular region.

The four pipes are located at the coordinates given by (9.125). The distance between two opposing pipes is denoted B_u. Eq. (9.131) defines the eccentricity parameter b. The heat injection rate is $q/4$ per pipe. Each pipe has a fluid-to-ground thermal resistance R_b.

A superposition of the four eccentric pipes (9.96-97) yields the temperature field. The temperatures on the four pipes are equal. The average ground temperature is given by (9.107). The temperature difference $T_f - T_m$ divided by the total heat flow q yields the thermal resistance:

$$
\begin{aligned}
R_{sf} \;=\; & \frac{1}{2\pi\lambda}\left\{\frac{\lambda}{\lambda_c}\left[\ln\left(\frac{r_c}{r_b}\right) - \frac{C_c\pi r_c^2}{C_T}(1-b^2) - \frac{1}{2}\ln\left(\frac{\sqrt{2}br_c}{r_b}\right) - \right.\right. \\
& -\frac{1}{4}\ln\left(\frac{2br_c}{r_b}\right) - \frac{1}{4}\frac{\lambda_c-\lambda}{\lambda_c+\lambda}\ln(1-b^8) + \frac{1}{4}\left(\frac{C_c\pi r_c^2}{C_T}\right)^2\Bigg] + \\
& \left.\left. +\frac{1}{2}\left(\frac{C\pi r_1^2}{C_T}\right)^2\left[\ln\left(\frac{r_1^2}{r_c^2}\right) + \frac{r_c^2}{r_1^2} - 1\right] - \frac{1}{4}\left(\frac{C\pi(r_1^2-r_c^2)}{C_T}\right)^2\right\} + \frac{R_b}{4} \\
& C_c\pi r_b^2 \ll C_T
\end{aligned}
\qquad (9.133)
$$

where the total heat capacity C_T is given by (9.79).

9.3.8 Triple U-pipe in a composite circular region

The nomenclature used for the triple U-pipe in a composite circular region is shown in figure 9.24.

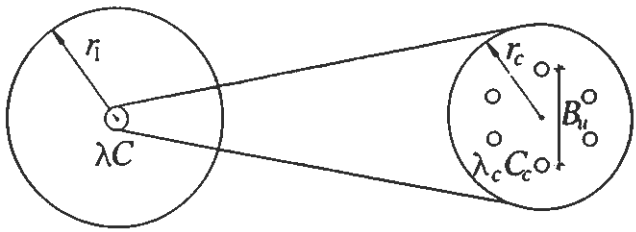

Figure 9.24. Triple U-pipe in a composite circular region.

The six pipes are located at the coordinates given by (9.127). The distance between two opposing pipes is denoted B_u. Eq. (9.131) defines the eccentricity parameter b. The heat injection rate is $q/6$ per pipe. Each pipe has a fluid-to-ground thermal resistance R_b.

The temperatures on the four pipes are obtained by superposing the temperature field from the six eccentric pipes (9.96-97). The average ground temperature is given by (9.107). The temperature difference $T_f - T_m$ divided by the total heat flow q yields the thermal resistance:

$$
\begin{aligned}
R_{sf} \;=\; & \frac{1}{2\pi\lambda}\left\{\frac{\lambda}{\lambda_c}\left[\ln\left(\frac{r_c}{r_b}\right) - \frac{C_c\pi r_c^2}{C_T}(1-b^2) - \frac{1}{3}\ln\left(\frac{br_c}{r_b}\right) - \right.\right. \\
& -\frac{1}{3}\ln\left(\frac{\sqrt{3}br_c}{r_b}\right) - \frac{1}{6}\ln\left(\frac{2br_c}{r_b}\right) - \frac{1}{6}\frac{\lambda_c-\lambda}{\lambda_c+\lambda}\ln(1-b^{12}) + \frac{1}{4}\left(\frac{C_c\pi r_c^2}{C_T}\right)^2\Big] \\
& \left.\left. +\frac{1}{2}\left(\frac{C\pi r_1^2}{C_T}\right)^2\left[\ln\left(\frac{r_1^2}{r_c^2}\right) + \frac{r_c^2}{r_1^2} - 1\right] - \frac{1}{4}\left(\frac{C\pi(r_1^2-r_c^2)}{C_T}\right)^2\right\} + \frac{R_b}{6} \\
& C_c\pi r_b^2 \ll C_T
\end{aligned}
\qquad (9.134)
$$

where the total heat capacity C_T is given by (9.79).

9.4 Varying temperature along the flow channels

The heat exchange with the surrounding ground causes the fluid temperature to vary along the flow channels. At a given depth in the ground heat exchanger, the temperatures in the upwards and downwards flow channeis will differ. The resulting heat flow between these channels may reduce the efficiency of

the ground heat exchanger. The influence on ground heat exchangers with boreholes or closely spaced pipes, i.e. a single ground heat transfer channel, may be analyzed by the methods presented in sections 8.5 and 8.6, where the concept of an effective fluid-to-ground thermal resistance is defined. In a similar manner, we will define an effective thermal resistance for the steady-flux regime that includes the effects of varying fluid temperatures along the flow channels.

Formulas for the effective steady-flux thermal resistance of multiple ground heat transfer channels in a homogeneous region, and multiple channels in a composite region are given in section 9.4.2. The flow channels are assumed to be arranged symmetrically.

9.4.1 Single ground heat transfer channel

The problem of varying fluid temperatures along the flow channels of a single ground heat transfer channel has been studied in sections 8.5. The analyses is applicable to single flow channels, boreholes with annular flow channels or U-pipes, or similar ground heat exchangers in soil. In these arrangements, the total heat capacity of the borehole, or the corresponding volume in soil, is small compared with heat capacity of the ground volume ascribed to each ground heat exchanger. Therefore, the heat flow in the small region containing the flow channels is essentially in steady-state conditions (see sections 9.2.2 and 9.2.6). The thermal resistance of the small region can then be included in the fluid-to-ground thermal resistance, while there is a steady-flux process to be accounted for in the surrounding volume.

In section 8.6, formulas are given for the effective fluid-to-ground thermal resistance R_b^*, which includes the effect of varying fluid temperatures along the flow channels. The heat flux q to the ground is *constant* along the channel. The simple formula (8.101) is then applicable. The steady-flux thermal resistance is $R_{sf} = R_g + R_b$ according (9.5), where R_g is the thermal resistance of the ground. An effective thermal resistance for the steady-flux regime is obtained by replacing R_b with the effective fluid-to-ground thermal resistance R_b^*. We have from (8.101):

$$R_{sf}^* = R_g + R_b^* = R_g + R_b + \frac{1}{3}\frac{1}{R_a}\left(\frac{H}{C_f V_f}\right)^2 \tag{9.135}$$

The sum $R_g + R_b$ is the ordinary steady-flux thermal resistance R_{sf}. Eq. (9.135) then becomes:

$$R_{sf}^* = R_{sf} + \frac{1}{3}\frac{1}{R_a}\left(\frac{H}{C_f V_f}\right)^2 \tag{9.136}$$

The formulas in section 9.2 give R_{sf}, while R_a is obtained from the formulas in section 8.4.2 or 8.4.4.

9.4.2 Heat balance equations for multiple ground heat transfer channels

The influence of temperature variations along the flow channels on the steady-flux heat flow between the fluid and the store will be treated by analogy with the steady-state problem of the fluid-to-ground thermal resistance in chapter 8. The analysis concerns the case of two pipes in the ground and arrangements with multiple flow channels that can be described by the same type of equations. It is required that the temperature in the downflow channels at a certain depth is given by a single temperature $T_{f1}(z)$. For the upward channels we have similarly the temperature $T_{f2}(z)$. The heat injection rate from the channels with downwards and upwards flow is denoted $q_1(z)$ and $q_2(z)$, respectively. The total heat flow is constant along the ground heat exchanger:

$$q_1(z) + q_2(z) = q \tag{9.137}$$

The thermal Δ-circuit introduced in section 8.2.2 will be used to represent the relations between heat flows and temperature differences. See figure 8.2. The borehole temperature $T_b(z)$ referred in 8.2.2 should here be replaced by the local average temperature $T_m(z)$. The thermal resistances of the Δ-circuit are then given by (8.14), where the steady-flux thermal resistances R_{mn} given in section 9.3.1 take the place of the resistances R^o_{mn}.

The steady-flux thermal resistance R_{sf}, which is obtained by setting $T_{f1} = T_{f2} = T_f$, becomes by (8.15):

$$R_{sf} = \frac{R_1^\Delta R_2^\Delta}{R_1^\Delta + R_2^\Delta} \tag{9.138}$$

The steady-flux thermal resistance R_a between the flow channels is by (8.18):

$$R_a = \frac{R_{12}^\Delta (R_1^\Delta + R_2^\Delta)}{R_1^\Delta + R_2^\Delta + R_{12}^\Delta} = R_{11} + R_{22} - 2R_{12} \tag{9.139}$$

The counterflow heat exchange between the flow channels gives by analogy with the analysis in section 8.6.2 an effective steady-flux thermal resistance R^*_{sf}. We have from (8.101):

$$R^*_{sf} = R_{sf} + \frac{1}{3}\frac{1}{R_a}\left(\frac{H}{C_f V_f}\right)^2 \tag{9.140}$$

Expressions for the thermal resistances R_{11}, R_{12}, and R_a are presented for the single, double, and triple U-pipe below. In the case of single, double, and

triple U-pipe U-pipes in a composite region we will, for the sake of brevity, give only the thermal resistance R_a. It is assumed that the pipes are arranged symmetrically, so that $R_{11} = R_{22}$. The formulas (9.138-139) for R_{sf} and R_a are then, by (8.20-21), simplified to:

$$R_{sf} = \frac{1}{2}(R_{11} + R_{12}) \qquad R_a = 2(R_{11} - R_{12}) \tag{9.141}$$

Single U-pipe

The arrangement of the flow channels for the single U-pipe is shown in figure 9.25.

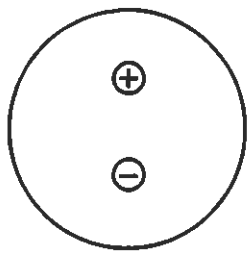

Figure 9.25. Single U-pipe; one channel with upward flow (+) and one channel with downward flow (-).

The thermal resistances R_{11} and R_{12} are obtained with use of the superposition method described in section 9.3.1. From (9.115) we get:

$$\begin{aligned} R_{11} &= \frac{1}{2\pi\lambda}\left[\ln\left(\frac{r_1}{r_b}\right) - \frac{3}{4} + b^2 - \ln(1-b^2)\right] + R_p \\ R_{12} &= \frac{1}{2\pi\lambda}\left[\ln\left(\frac{1}{2b}\right) - \frac{3}{4} + b^2 - \ln(1+b^2)\right] \end{aligned} \tag{9.142}$$

where b is defined by (9.120).

The total resistance R_a, (9.141), between the upward and downward flow channel becomes:

$$R_a = 2 \cdot \frac{1}{2\pi\lambda}\left[\ln\left(\frac{2br_1}{r_b}\right) - \ln\left(\frac{1-b^2}{1+b^2}\right)\right] + 2R_p \tag{9.143}$$

The steady-flux thermal resistance R_{sf} is given by (9.123).

Double U-pipe

The arrangement of the flow channels for the double U-pipe is shown in figure 9.26.

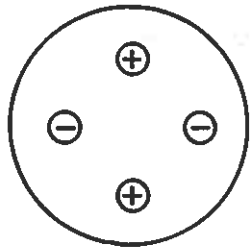

Figure 9.26. Double U-pipe; two channels with upward flow (+) and two channels with downward flow (-).

The thermal resistances R_{11} and R_{12} are:

$$\begin{aligned} R_{11} &= \frac{1}{2\pi\lambda}\left[\ln\left(\frac{r_1}{r_b}\right) - \frac{3}{4} + b^2 - \frac{1}{2}\ln(1-b^2) - \right. \\ &\quad \left. -\frac{1}{2}\ln(1+b^2) - \frac{1}{2}\ln\left(\frac{2br_1}{r_b}\right)\right] + \frac{R_p}{2} \\ R_{12} &= \frac{1}{2\pi\lambda}\left[\ln\left(\frac{1}{\sqrt{2}b}\right) - \frac{3}{4} + b^2 - \frac{1}{2}\ln(1+b^4)\right] \end{aligned} \tag{9.144}$$

where b is defined by (9.120).

The total resistance R_a between the upwards and downwards flow channels becomes:

$$R_a = 2 \cdot \frac{1}{2\pi\lambda}\left[\ln\left(\frac{\sqrt{2}br_1}{r_b}\right) - \frac{1}{2}\ln\left(\frac{2br_1}{r_b}\right) - \frac{1}{2}\ln\left(\frac{1-b^4}{1+b^4}\right)\right] + R_p \tag{9.145}$$

The steady-flux thermal resistance R_{sf} is given by (9.126).

Triple U-pipe

The arrangement of the flow channels for the triple U-pipe is shown in figure 9.27.

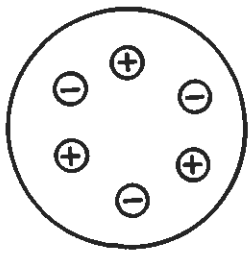

Figure 9.27. Triple U-pipe; three channels with upward flow (+) and three channels with downward flow (-).

The thermal resistances R_{11} and R_{12} are:

$$\begin{aligned} R_{11} &= \frac{1}{2\pi\lambda}\left[\ln\left(\frac{r_1}{r_b}\right) - \frac{3}{4} + b^2 - \frac{2}{3}\ln\left(\frac{\sqrt{3}br_1}{r_b}\right) - \frac{1}{3}\ln(1-b^6)\right] + \frac{R_p}{3} \\ R_{12} &= \frac{1}{2\pi\lambda}\left[\frac{1}{3}\ln\left(\frac{1}{2b}\right) + \frac{2}{3}\ln\left(\frac{1}{b}\right) - \frac{3}{4} + b^2 - \frac{1}{3}\ln(1+b^6)\right] \end{aligned} \qquad (9.146)$$

where b is defined by (9.120).

The total resistance R_a between the upwards and downwards flow channels becomes:

$$\begin{aligned} R_a = 2\cdot\frac{1}{2\pi\lambda}\Bigg[&\frac{2}{3}\ln\left(\frac{br_1}{r_b}\right) + \frac{1}{3}\ln\left(\frac{2br_1}{r_b}\right) - \\ &-\frac{2}{3}\ln\left(\frac{\sqrt{3}br_1}{r_b}\right) - \frac{1}{3}\ln\left(\frac{1-b^6}{1+b^6}\right)\Bigg] + \frac{2}{3}R_p \end{aligned} \qquad (9.147)$$

The steady-flux thermal resistance R_{sf} is given by (9.128).

Single U-pipe in a composite region

The case of U-pipes in a composite region will be dealt with more briefly than U-pipes in a homogeneous region. We will only present formulas for the total thermal resistance R_a between the upwards and the downwards channels. The thermal resistances R_{11} and R_{12} can be calculated from (9.141) when R_{sf} and R_a are known.

The single U-pipe in a composite region is shown in figure 9.22. There is one channel with upwards flow and one channel with downwards flow. The nomenclature used for this problem is specified in section 9.3.6.

The total resistance R_a between the upwards and downwards flow channels is:

$$R_a = 2 \cdot \frac{1}{2\pi\lambda} \left\{ \frac{\lambda}{\lambda_c} \left[\ln\left(\frac{2br_c}{r_b}\right) - \frac{\lambda_c - \lambda}{\lambda_c + \lambda} \ln\left(\frac{1-b^2}{1+b^2}\right) \right] \right\} + 2R_p \qquad (9.148)$$

where b is defined by (9.131). The steady-flux thermal resistance R_{sf} is given by (9.132).

Double U-pipe in a composite region

The double U-pipe in a composite region is shown in figure 9.23. The relative positions of the upwards and downwards flow channels are the same as for the double U-pipe in a homogeneous region. See figure 9.26. The nomenclature used for this problem is specified in section 9.3.7.

The total resistance R_a between the upwards and downwards flow channels is:

$$R_a = 2 \cdot \frac{1}{2\pi\lambda} \left\{ \frac{\lambda}{\lambda_c} \left[\ln\left(\frac{\sqrt{2}br_c}{r_b}\right) - \frac{1}{2}\ln\left(\frac{2br_c}{r_b}\right) - \frac{1}{2}\frac{\lambda_c - \lambda}{\lambda_c + \lambda} \ln\left(\frac{1-b^4}{1+b^4}\right) \right] \right\} + R_p \qquad (9.149)$$

where b is defined by (9.131). The steady-flux thermal resistance R_{sf} is given by (9.133).

Triple U-pipe in a composite region

The triple U-pipe in a composite region is shown in figure 9.24. The relative positions of the upwards and downwards flow channels are the same as for the triple U-pipe in a homogeneous region. See figure 9.27. The nomenclature used for this problem is specified in section 9.3.8.

The total resistance R_a between the upwards and downwards flow channels is:

$$\begin{aligned} R_a \;=\; & 2 \cdot \frac{1}{2\pi\lambda} \left\{ \frac{\lambda}{\lambda_c} \left[\frac{2}{3}\ln\left(\frac{br_1}{r_b}\right) + \frac{1}{3}\ln\left(\frac{2br_1}{r_b}\right) - \right. \right. \\ & \left. \left. -\frac{2}{3}\ln\left(\frac{\sqrt{3}br_1}{r_b}\right) - \frac{1}{3}\frac{\lambda_c - \lambda}{\lambda_c + \lambda} \ln\left(\frac{1-b^6}{1+b^6}\right) \right] \right\} + \frac{2}{3}R_p \end{aligned} \qquad (9.150)$$

where b is defined by (9.131). The steady-flux thermal resistance R_{sf} is given by (9.134).

Chapter 10

Step-Pulse Analysis

The heat exchange between the fluid and the store varies in time. There are short-term fluctuations superimposed on the seasonal variation. One example is the storage of solar heat with its swift changes in heat injection during day. On this time-scale, the thermal influence between adjacent ground heat exchangers due to the superimposed variations is negligible.

The basic assumption for the analysis is that the short-term variations in heat injection rate can be represented by a sequence of piece-wise constant values. Any such short-term variation becomes a superposition of step changes in heat injection rate. See section 6.5 and figures 6.1 and 6.2. The fundamental case of the thermal response to such a step change in heat injection rate will be treated in section 10.1. A method for step-pulse analysis is developed from the basic cases of a single pulse, two balanced pulses, and a sequence of balanced pulses. These are discussed in section 10.2.

If the ground heat exchanger consists of multiple flow channels, such as U-pipes in clay, there will be a thermal influence between these channels. This problem can be handled with use of the superposition techniques described in section 10.3.

When a step change occurs in the heat supply to a ground heat store, the fluid temperature increases rapidly during the first few hours. A large fraction of the supplied heat is then absorbed by the fluid. After this initial phase, the capacitive effect of the fluid is practically negligible, and almost all of the supplied heat is transferred to the ground. A few estimates of this effect are made in section 10.4.

A further complication is the thermal process along the flow channel. The evolution of the fluid temperature along the flow channel is given in section 10.5 for the case of a step change in inlet temperature.

10.1 Heat injection step

A step change in heat injection rate is a fundamental case in the analysis of the short-term response of a ground heat exchanger. Any variation $q(t)$ can be obtained by superposing the response from a sequence of such step changes. The heat extraction step may be expressed by use of the Heaviside-function:

$$q(t) = q_1 \; He(t) \qquad He(t) = \begin{cases} 1 & t > 0 \\ 0 & t \leq 0 \end{cases} \tag{10.1}$$

The temperature increase associated with the step change in heat extraction rate is denoted T^q. The boundary condition at the pipe radius $r = r_b$ becomes:

$$-2\pi r_b \lambda \left. \frac{\partial T^q}{\partial r} \right|_{r=r_b} = q_1 \qquad (t > 0) \tag{10.2}$$

Initially, the temperature disturbance due to the step change is zero in the infinite surrounding region ($r_b \leq r \leq \infty$):

$$T^q(r, 0) = 0 \qquad (r_b > 0) \tag{10.3}$$

The temperature T^q satisfies the heat equation (6.8).

10.1.1 Integral solution

The problem of a step change in heat injection rate can be solved with use of the Laplace transform method. The solution in the Laplace domain becomes (Carslaw and Jaeger 1959; p. 338):

$$\tilde{T}^q(r, p) = \frac{q_1}{2\pi r_b \lambda} \frac{1}{p} \frac{\mathrm{K}_0(\omega r)}{\omega \mathrm{K}_1(\omega r_b)} \tag{10.4}$$

where $\omega = \sqrt{p/a}$.

The inversion theorem gives, after a suitable choice of integration contour, a real-valued integral solution for the temperature:

$$T^q(r, t) = \frac{q_1}{2\pi\lambda} \cdot \left[-\frac{1}{r_b} \frac{2}{\pi} \int_0^\infty (1 - \mathrm{e}^{-au^2 t}) \frac{\mathrm{J}_0(ur)\mathrm{Y}_1(ur_b) - \mathrm{Y}_0(ur)\mathrm{J}_1(ur_b)}{u^2[\mathrm{J}_1^2(ur_b) + \mathrm{Y}_1^2(ur_b)]} \, du \right] \tag{10.5}$$

Here, J_0, J_1, Y_0, and Y_1 are Bessel functions of the first and second kind.

The oscillatory behavior of the Bessel functions and the limits the integration interval make the integral (10.5) difficult and time-consuming to evaluate (Baudoin 1988).

10.1.2 Numerical Inversion of Laplace Transform Solution

Baudoin (1988) recommends the following method, which is particularly attractive for a fast and easily programmable numerical solution. A numerical inversion of the complex-valued solution in the Laplace domain yields the following real-valued solution (Veillon 1972):

$$T^q(r,t) = \frac{q_1}{2\pi r_b \lambda} \sum_{j=1}^{j=10} \frac{V_j}{j} \frac{\mathrm{K}_0(\omega_j r)}{\omega_j \mathrm{K}_1(\omega_j r_b)} \tag{10.6}$$

where

$$\omega_j = \sqrt{\frac{j \ln(2)}{at}} \tag{10.7}$$

and

$$V_j = \sum_{k=\mathrm{Int}((j-1)/2)}^{min(j,5)} \frac{(-1)^{j-5} k^5 (2k)!}{(5-k)!(k-1)!k!(j-k)!(2k-j)!} \tag{10.8}$$

The lower bound of the summation index should be taken as the integer part of $(j-1)/2$.

10.1.3 Line source approximation

An alternative to the solutions (10.5) and (10.6-8) is obtained by approximating the heat injection from the pipe by a line source starting at $t = 0$. The temperature in the ground becomes (Carslaw and Jaeger 1959; p. 261):

$$T^q(r,t) = \frac{q_1}{4\pi\lambda} \int_0^t \mathrm{e}^{-r^2/4a(t-t')} \frac{dt'}{t-t'} = \frac{q_1}{4\pi\lambda} \int_{r^2/4at}^{\infty} \frac{\mathrm{e}^{-u}}{u} du = \frac{q_1}{4\pi\lambda} E_1(r^2/4at) \tag{10.9}$$

Here, E_1 is the so-called exponential integral. Tables and formulas pertaining to this function are given by Abramowitz and Stegun (1964). The function is shown in figure 10.1.

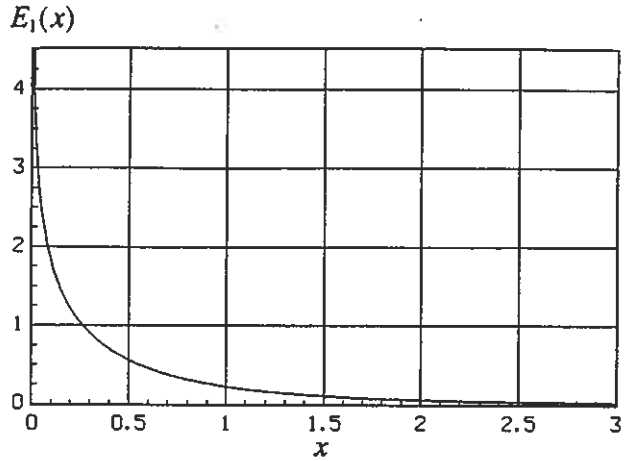

Figure 10.1. The exponential integral $E_1(x)$.

The temperature T^q becomes a function of a single parameter $r/\sqrt{at}$. The length $\sqrt{at}$ is a measure of the range of thermal influence around the pipe. The temperature change is extremely small for $r/\sqrt{at} > 3$. The thermal influence range $\sqrt{at}$ is given in Table 10.1 for some different time periods and thermal diffusivities.

TABLE 10.1. Thermal influence range $\sqrt{at}$ (m) for some different times t and thermal diffusivities a.

	t						
a	1 min	15 min	1 h	6 h	12 h	24 h	1 week
$0.4{\cdot}10^{-6}$	0.005	0.019	0.038	0.062	0.13	0.19	0.49
$1.0{\cdot}10^{-6}$	0.008	0.030	0.060	0.098	0.21	0.29	0.78
$1.6{\cdot}10^{-6}$	0.010	0.038	0.076	0.124	0.26	0.37	0.98

For large values of the parameter at/r^2, the exponential integral E_1 can be approximated by:

$$E_1(r^2/4at) = \ln\left(\frac{4at}{r^2}\right) - \gamma - \frac{1}{4}\left[r^2/at - (r^2/4at)^2\right] \qquad \frac{at}{r^2} \geq 0.5 \quad (10.10)$$

where $\gamma = 0.57722\ldots$ is Euler's constant. The maximum error is 1 % for $at/r^2 \geq 0.5$.

There is also the following simple and useful relation:

$$E_1(r^2/4at) = \ln\left(\frac{4at}{r^2}\right) - \gamma \qquad \frac{at}{r^2} \geq 5 \quad (10.11)$$

with a maximum error of 2 % for $at/r^2 \geq 5$. One may note that this approximation is valid when the thermal process in the region within the radius r is roughly at a steady-state condition.

The temperature T_b^q at the pipe radius is of special interest. It is obtained by setting $r = r_b$ in the formulas given above. Let us compare the different expressions for the temperature T_b^q: the exact solution obtained from the numerical inversion of the Laplace solution (10.6-8), the line-source solution (10.9), and the simple approximation (10.11). Figure 10.2 shows the dimensionless temperature change $4\pi\lambda T_b^q/q_1$ as a function of the dimensionless time at/r_b^2.

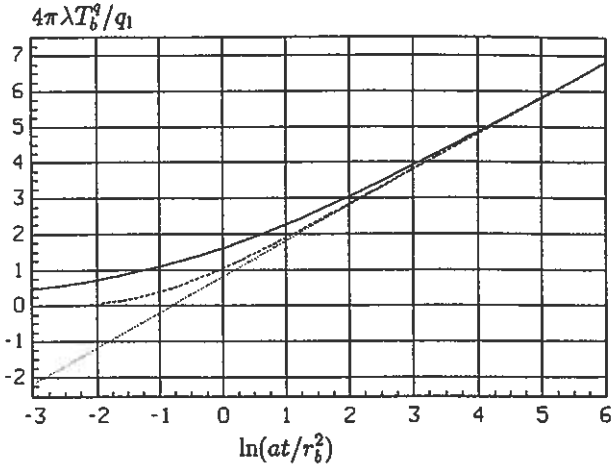

Figure 10.2. Comparison of the expressions for the temperature change T_b^q at the pipe: the numerical inversion of the Laplace solution (10.6-8) (solid line), the line-source solution (10.9) (dashed line), and the simple approximation (10.11) (dotted line). The dimensionless temperature change $4\pi\lambda T_b^q/q_1$ as a function of the dimensionless time at/r_b^2.

The exact solution gives a prompt increase of the pipe temperature, while the response of the line-source (at $r = 0$) is delayed at the pipe radius $r = r_b$.

The relative error of the line source solution (10.9) at the pipe $r = r_b$ compared to the exact solution (10.6-8) is given in Table 10.2 for some values of the dimensionless time at/r_b^2.

TABLE 10.2. The relative error of the line source solution (10.9) at the pipe $r = r_b$.

at/r_b^2	5	10	20	50	100
Error (%)	10.5	5.3	2.5	1.0	0.5

Let t_b denote the time taken from the start of a pulse until the error of the line-source solution is less than about 10 %. Hence from Table 10.2:

$$t_b = \frac{5r_b^2}{a} \tag{10.12}$$

Thus, when the line source solution gives an acceptable accuracy for the temperature at $r = r_b$, the exponential integral can be approximated by the simple relation (10.11).

The fluid-to-ground thermal resistance R_b determines the temperature difference between the fluid and the ground at $r = r_b$. The change in fluid temperature $T_f^q(t)$ due to a step change in heat injection rate is then given by:

$$T_f^q(t) = \frac{q_1}{4\pi\lambda}\left[\ln\left(\frac{4at}{r_b^2}\right) - \gamma\right] + R_b = q_1\, R'_q(t) \qquad t \geq t_b \tag{10.13}$$

where the time-dependent thermal resistance for a heat injection step is:

$$R'_q(t) = \frac{1}{4\pi\lambda}\left[\ln\left(\frac{4at}{r_b^2}\right) - \gamma\right] + R_b \qquad t \geq t_b \tag{10.14}$$

The prime ($'$) indicates that R'_q is a thermal resistance between the fluid and the initial (undisturbed) temperature level $T^q = 0$.

10.1.4 Local average temperature

The increase in fluid temperature may be related to the ensuing increase in the average temperature of the surrounding ground. The local average temperature within a circular region with the radius $r = r_1$ is given by a simple heat balance:

$$C\,\pi(r_1^2 - r_b^2)T_m^q(t) = C\,2\pi\int_{r_b}^{r_1} T^q(r,t)\,r\,dr \tag{10.15}$$

Inserting the line source approximation (10.9) gives:

$$\begin{aligned} T_m^q(t) &= \frac{1}{\pi(r_1^2 - r_b^2)}\frac{q_1}{2\lambda}\int_{r_b}^{r_1} E_1(r^2/4at)\,r\,dr \\ &= \frac{1}{\pi(r_1^2 - r_b^2)}\frac{q_1 t}{C}\int_{r_b^2/4at}^{r_1^2/4at} E_1(u)\,du \end{aligned} \tag{10.16}$$

By use of the derivative

$$\frac{dE_2(x)}{dx} = -E_1(x) \tag{10.17}$$

and the recurrence relation (Abramowitz and Stegun 1964):

$$E_2(x) = e^{-x} - xE_1(x) \tag{10.18}$$

we have finally:

$$\begin{aligned} T_m^q(t) &= \frac{q_1}{4\pi\lambda}\frac{1}{(r_1^2 - r_b^2)}\left[r_1^2 E_1(r_1^2/4at) - r_b^2 E_1(r_b^2/4at)\right] + \\ &\quad + \frac{q_1 t}{C}\frac{1}{\pi(r_1^2 - r_b^2)}\left[\exp(-r_b^2/4at) - \exp(-r_1^2/4at)\right] \end{aligned} \tag{10.19}$$

Let us define a R_q by:

$$T_f^q - T_m^q = q_1 R_q(t) \tag{10.20}$$

The thermal resistance between the fluid temperature T_f^q and the average ground temperature T_m^q becomes by (10.9) and (10.18):

$$\begin{aligned} R_q(t) &= \frac{1}{4\pi\lambda}\frac{r_1^2}{(r_1^2 - r_b^2)}\left[E_1(r_b^2/4at) - E_1(r_1^2/4at)\right] - \\ &\quad -\frac{t}{C}\frac{1}{\pi(r_1^2 - r_b^2)}\left[\exp(-r_b^2/4at) - \exp(-r_1^2/4at)\right] + R_b \end{aligned} \tag{10.21}$$

The fluid-to-ground thermal resistance R_b has been added on the right hand side.

10.2 Step pulse analysis

This section presents a method for the analysis of a sequence of step changes in heat injection rate. The method, which has been developed by Claesson and Eskilson (1988), concerns the case of deep heat extraction boreholes. The spacing between these boreholes is such that the thermal influence becomes negligible with respect to variations around the mean heat extraction rate. However, the thermal influence between adjacent ground heat exchangers in a ground heat store is usually fully developed after a week. The thermal response of a step change is after this period of time given by the steady-flux solutions presented in chapter 9. The step pulse method will here be used for the analysis of short-term variations when the thermal influence between adjacent ground heat exchangers can be neglected.

It is convenient to define a dimensionless temperature increase:

$$\Delta T' = T_f^q \cdot \frac{4\pi\lambda}{q_1} \tag{10.22}$$

10.2.1 Superposition of heat extraction steps

The heat injection function $q(t)$ is represented by a sequence of N piece-wise constant values, so that $q(t)$ equals 0 for $t \leq t_1$, q_n for $t_n < t < t_{n+1} (n = 1, \ldots, N-1)$, and q_N for $t > t_N$. See figure 6.2. The heat injection function may then be written as a sum of step changes in heat injection rate:

$$q(t) = \sum_{n=1}^{N} (q_n - q_{n-1}) \cdot He(t - t_n) \qquad (q_0 = 0) \tag{10.23}$$

The general expression for the fluid temperature may be written:

$$T_f(t) = T_m(t) + \sum_{n=1}^{N}(q_n - q_{n-1})R(t - t_n) \cdot He(t - t_n) \qquad (q_0 = 0) \quad (10.24)$$

Here, R denotes the step-change thermal resistance between the fluid temperature and the average ground temperature.

For pulses that have lasted longer than the steady-flux time t_{sf} (9.4), we have the steady-flux thermal resistance, which is independent of time:

$$R(t) = R_{sf} \qquad t - t_n > t_{sf} \qquad (10.25)$$

Let N_{sf} be the last pulse to have reached steady-flux conditions, so that $(t - t_{N_{sf}}) > t_{sf}$ and $(t - t_{N_{sf}+1}) < t_{sf}$. See figure 10.3.

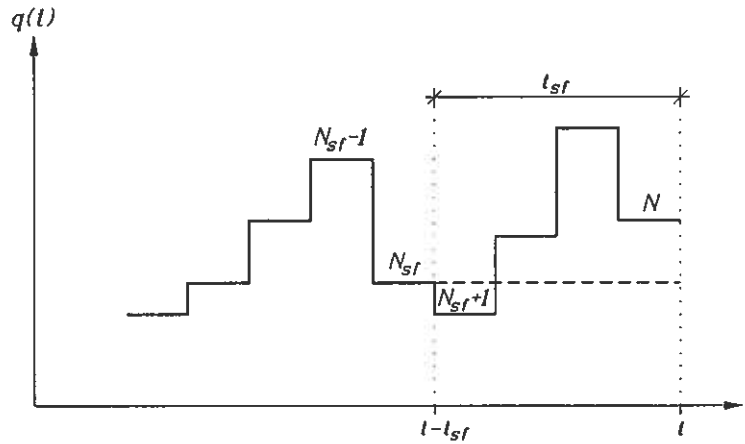

Figure 10.3. A sequence of heat extraction pulses. The nomenclature is explained in the text.

The part of the fluid temperature that is due to the steady-flux component becomes by (9.12), (9.27), and (10.24):

$$\begin{aligned} T_{sf}(t) &= T_m(t_1) + \frac{1}{C\pi(r_1^2 - r_b^2)} \sum_{n=1}^{N_{sf}}(q_n - q_{n-1})(t - t_n) \\ &\quad + \sum_{n=1}^{N_{sf}}(q_n - q_{n-1})R_{sf} \qquad (q_0 = 0) \end{aligned} \qquad (10.26)$$

The second term on the right-hand side of (10.26) gives the increase in the local average temperature due to the pulses $q_1, \ldots, q_{N_{sf}}$. The first two terms are the

current local average temperature $T_m(t)$ when the steady-flux contribution has been included. Since R_{sf} is constant, the last term simply becomes $q_{N_{sf}} R_{sf}$. Eq. (10.26) then reduces to:

$$T_{sf}(t) = T_m(t) + q_{N_{sf}} R_{sf} \qquad t - t_n > t_{sf} \tag{10.27}$$

Note that there is no influence from the pulses preceding the pulse N_{sf}. This is an important result, which has been discussed in chapter 9. The thermal response of a heat extraction rate $q(t)$ at the time t can be determined from the variation of $q(t)$ since the time $t - t_{sf}$. In the remaining part of this section we will consider only the superimposed short-term variation on a time-scale shorter than t_{sf}.

The thermal resistance R for pulses with a duration $t - t_n$ that is longer than t_b (10.12), but shorter than the steady-flux time t_{sf}, is given by:

$$R(t) = R'_q(t) \qquad t_b < t - t_n < t_{sf} \tag{10.28}$$

The thermal resistance $R'_q(t)$ is given by (10.14). It should be emphasized that this is a thermal resistance between the fluid temperature and an average ground temperature that is not influenced by these superimposed pulses. See section 10.1.4. The temperature increase for the superimposed short-term variation is:

$$T_f^q = \sum_{n=1}^{N} (q_n - q_{n-1}) R'_q(t - t_n) \cdot He(t - t_n) \qquad (q_0 = 0)$$
$$t_b < t - t_n < t_{sf} \tag{10.29}$$

The formula requires a value of q_0, which is here set to zero.

10.2.2 Single pulse

Any sequence of pulses can be expressed as superposition of single pulses. A single pulse with the length t_1 is shown in figure 10.4.

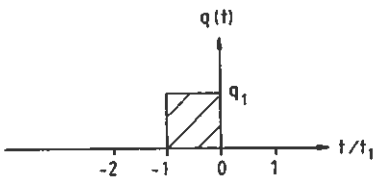

Figure 10.4. A single heat extraction pulse.

The temperature increase at the end of the pulse at the time $t = 0$, is from (10.13-14):

$$T_f^q = q_1 R_q'(t_1) = q_1 \left\{ \frac{1}{4\pi\lambda} \left[\ln\left(\frac{4at_1}{r_b^2}\right) - \gamma \right] + R_b \right\} \qquad (t_b < t_1 < t_{sf}) \tag{10.30}$$

Example 10.1. A ground heat store in granite with the following data:

$$a = 1.6{\cdot}10^{-6}\ \mathrm{m^2/s} \qquad \lambda = 3.5\ \mathrm{W/mK} \qquad r_b = 0.0575\ \mathrm{m}$$

The approximate formula (10.13-14) for a heat extraction step is valid after a time:

$$t_b = \frac{5r_b^2}{a} \approx 2.9\ \text{hours}$$

A few values of the dimensionless temperature increase $\Delta T'$ are given below for different values of t_1 and a fluid-to-ground thermal resistance R_b equal to 0.01 K/(W/m) and 0.10 K/(W/m).

t_1	3h	6h	12h	24h	48h
R_b=0.01	2.9	3.6	4.3	5.0	5.7
R_b=0.10	6.9	7.6	8.3	9.0	9.7

Example 10.2. A ground heat store in clay with the following data:

$$a = 0.4{\cdot}10^{-6}\ \mathrm{m^2/s} \qquad \lambda = 1.0\ \mathrm{W/mK}$$
$$r_b = 0.016\ \mathrm{m} \qquad R_b = 0.10\ \mathrm{K/(W/m)}$$

The approximate formula (10.13-14) is valid after a time:

$$t_b = \frac{5r_b^2}{a} \approx 0.9\ \text{hours}$$

A few values of the dimensionless temperature increase $\Delta T'$ are given below for different values of t_1.

t_1	1h	3h	6h	12h	24h	48h
R_b=0.10	3.8	4.9	5.6	6.3	7.0	7.7

When the pulse is completed at $t = 0$, we have to superimpose a step-change of $-q_1$, so that the heat injection rate becomes zero for $t > 0$. The temperature is by (10.29):

$$T_f^q = q_1 R_q'(t + t_1) - q_1 R_q'(t) = \frac{q_1}{4\pi\lambda} \ln\left(\frac{t + t_1}{t}\right) \qquad t_b < t < t_{sf} \tag{10.31}$$

The logarithmic term is the dimensionless temperature increase $\Delta T'$, which only depends on the ratio t/t_1. A few values are given in Table 10.3.

TABLE 10.3. Dimensionless temperature increase $\Delta T'$ after a single pulse.

t/t_1	0.1	0.25	0.5	1	3	5	10
$\Delta T'$	2.4	1.6	1.1	0.69	0.29	0.18	0.10

The values in Table 10.3 should be compared with those for the temperature increase at the end of the pulse given in examples 10.1 and 10.2. The remaining temperature increase after one pulse length ($t = t_1$) is about 25 % for a pulse length of 3 hours and about 10 % for a pulse length of 24 hours. After three pulse lengths ($t = 3t_1$) the corresponding values are about 10 % and 4 %.

10.2.3 Two balanced pulses

The variable heat extraction rate may be represented by the average component and balanced pairs of pulses. A single balanced pair of pulses is shown in figure 10.5.

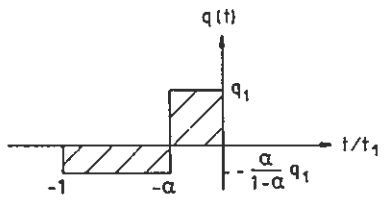

Figure 10.5. A balanced pair of heat extraction pulses.

The balanced pair consists of an extraction and an injection pulse containing the same amount of energy. The length of the pulses is $(1-\alpha)t_1$ and αt_1, and the heat extraction and injection rates are q_1 and $-\alpha q_1/(1-\alpha)$, respectively. The temperature at the end (t=0) of the two balanced pulses, which follows from a superposition of two step changes (10.29; 10.13-14), becomes:

$$T_f^q(0) = \underset{(t_b < \alpha t_1)}{\frac{q_1}{4\pi\lambda}\left[\ln\left(\frac{4at_1}{r_b^2}\right) - \gamma\right]} + \underset{(t_1 < t_{sf})}{q_1 R_b - \frac{q_1}{4\pi\lambda}\left[\frac{1}{1-\alpha}\ln\left(\frac{1}{\alpha}\right)\right]} \qquad (10.32)$$

The first two terms on the right are identical to the temperature increase of a single pulse with length t_1 (10.30) and the strength q_1. The last term gives

the difference between the single pulse and two balanced pulses. Expressed in dimensionless temperature increase $\Delta T'$, it is a function of α. Table 10.4 gives a few values.

TABLE 10.4. Difference in dimensionless temperature increase $\Delta T'$ at the end of a single pulse and two balanced pulses.

α	0.25	0.5	0.75
$\ln(1/\alpha)/(1-\alpha)$	1.84	1.39	1.15

The temperature recovery after the two balanced pulses is according to (10.31):

$$T_f^q = \frac{q_1}{4\pi\lambda}\left[\ln\left(\frac{t+\alpha t_1}{t}\right) - \frac{\alpha}{1-\alpha}\ln\left(\frac{t+t_1}{t+\alpha t_1}\right)\right] \qquad (10.33)$$
$$(t_b < \alpha t) \qquad (t_1 + t < t_{sf})$$

The dimensionless temperature increase $\Delta T'$, i.e. the factor between the brackets, becomes a function of t/t_1 and α. A few values are given in Table 10.5.

TABLE 10.5. Dimensionless temperature increase $\Delta T'$ after a balanced pair of pulses.

	t/t_1						
α	0.1	0.25	0.5	1	2	5	10
0.25	0.87	0.39	0.17	0.07	0.02	0.004	0.001
0.50	1.2	0.59	0.29	0.12	0.04	0.008	0.002
0.75	1.4	0.72	0.37	0.16	0.06	0.010	0.003

The values of Table 10.5 should be compared with temperature increase at the end of the pulse. From (10.32) and with values from examples 10.1-2 and Table 10.4, the increase in dimensionless temperature at the end of a 24-hour pulse is about 4. After one pulse length ($t = t_1$) the remaining temperature increase, given in Table 10.5, is less 0.2. The attenuation of balanced variations around the average component is evidently very rapid.

10.2.4 Pulsated versus constant extraction

In many applications, such as storage of solar heat, the heat injection rate often exhibit large diurnal variations. Consequently, the fluid temperature will vary with time. During some periods, the fluid temperature will be higher than if the heat were injected at a constant average rate. High fluid temperatures often lead to a reduced thermal performance. Thus, it is of interest to compare the pulsated and the constant heat extraction. Figure 10.6 shows a pulsated heat injection.

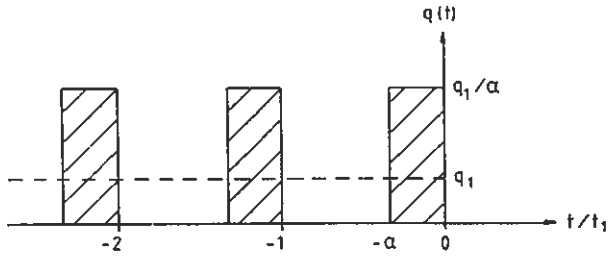

Figure 10.6. Sequence of heat extraction pulses.

Let us begin with the two balanced pulses in figure 10.5. It will be superposed on the average heat injection rate, which is denoted q_1 in accordance with the notation used in figure 10.6. The total heat injection rate, which is given by the sum of the two balanced pulses and the constant heat injection rate, is taken to be 0 for $-t_1 < t < -\alpha t_1$ and q_1/α for $-\alpha t_1 < t < 0$. With this new notation, the additional temperature increase due to the two balanced pulses becomes by (10.32) or (10.29):

$$T_f^q(0) = \frac{q_1}{4\pi\lambda}\left\{\left(\frac{1}{\alpha}-1\right)\left[\ln\left(\frac{4a\alpha t_1}{r_b^2}\right)-\gamma\right]+\ln(\alpha)\right\}$$
$$+q_1\left(\frac{1}{\alpha}-1\right)R_b \qquad (\alpha t_1 > t_b) \qquad (t_1 < t_{sf}) \qquad (10.34)$$

The problem of an infinite sequence of balanced pulses yields to a rather simple solution. It should be remembered that this solution presupposes that eqs. (10.13-14) can be used. This is, according to section 10.3.2, not the case for pulses that have lasted longer than the steady-flux time t_{sf}. Thus, the infinite sequence is not applicable in a strict sense. However, the solution gives a good approximation for a sequence of 10 or more balanced pulses.

The temperature increase due to a sequence of N pulses is given by the sum of the temperature increase at the end of the last pulse and the contributions from the preceding $N-1$ pulses. To obtain the expression for N of *balanced* pulses we must also subtract the temperature increase of the average heat injection rate of these pulses. See figure 10.6. The temperature increase is then by (10.30) and (10.31):

$$T_f^q(0) = \frac{q_1/\alpha}{4\pi\lambda}\left[\ln\left(\frac{4a\alpha t_1}{r_b^2}\right)-\gamma\right]+\frac{q_1}{\alpha}R_b+$$
$$\frac{q_1/\alpha}{4\pi\lambda}\sum_{n=2}^{N}\ln\left[\frac{(n-1)t_1+\alpha t_1}{(n-1)t_1}\right]- \qquad (10.35)$$
$$-\frac{q_1}{4\pi\lambda}\left[\ln\left(\frac{4aNt_1}{r_b^2}\right)-\gamma\right]-q_1R_b \qquad (t_b < \alpha t_1) \qquad (10.36)$$

This can be rewritten as:

$$T_f^q(0) = \frac{q_1}{4\pi\lambda}\left\{\left(\frac{1}{\alpha}-1\right)\left[\ln\left(\frac{4a\alpha t_1}{r_b^2}\right)-\gamma\right]+\ln\left(\frac{\alpha}{N}\right)+ \right.$$
$$\left. +\frac{1}{\alpha}\sum_{n=2}^{N}\ln\left[\frac{n-1+\alpha}{n-1}\right]\right\}+q_1\left(\frac{1}{\alpha}-1\right)R_b \qquad (10.37)$$
$$(t_b < \alpha t_1) \qquad (Nt_1 < t_{sf})$$

The two terms containing the number N become:

$$\ln(\alpha)-\frac{1}{\alpha}\left[\alpha\ln(N)+\sum_{n=2}^{N}\ln\left(\frac{n-1}{n-1+\alpha}\right)\right] \qquad (10.38)$$

The expression within the brackets is:

$$\ln\left[\frac{N^\alpha\cdot 1\cdot 2\cdot\ldots\cdot(N-1)}{(1+\alpha)\cdot\ldots\cdot(N-1+\alpha)}\right]= \qquad (10.39)$$
$$\ln\left[\frac{N^\alpha\cdot 1\cdot 2\cdot\ldots\cdot(N-1)\cdot N}{\alpha\cdot(1+\alpha)\cdot\ldots\cdot(N-1+\alpha)\cdot(N+\alpha)}\right]-\ln\left[\frac{1}{\alpha}\frac{N}{(N+\alpha)}\right]$$

When $N\to\infty$, we get with the use of Euler's formula (Abramowitz and Stegun 1964; p. 255):

$$\ln[\Gamma(\alpha)]-\ln\left(\frac{1}{\alpha}\right)=\ln[\alpha\Gamma(\alpha)]=\ln[\Gamma(1+\alpha)] \qquad (10.40)$$

where the last step involves a recurrence relation for the Gamma function Γ. The Gamma function is tabulated in (Abramowitz and Stegun 1964). The temperature increase for an infinite sequence of pulses above the effect of the average pulse becomes by (10.37) and (10.40):

$$T_f^q(0) = \frac{q_1}{4\pi\lambda}\left\{\left(\frac{1}{\alpha}-1\right)\left[\ln\left(\frac{4a\alpha t_1}{r_b^2}\right)-\gamma\right]+\ln(\alpha)-\frac{\ln[\Gamma(1+\alpha)]}{\alpha}\right\}+$$
$$+q_1\left(\frac{1}{\alpha}-1\right)R_b \qquad (t_b<\alpha t_1) \qquad (10.41)$$

One part of the formulas (10.37) and (10.41) represent the temperature increase of the superposed pulse $q_1/\alpha - q_1$ during the time $-\alpha t_1 < t < 0$. The remaining part is a small correction that depends on α. Table 10.6 gives the correction term (10.38) for a few values of α and N. The correction term in (10.41) is obtained from the values for $N=\infty$.

TABLE 10.6. Correction term (10.38) in eq. (10.37). The value for $N = \infty$ is obtained from (10.38-10.40).

	α									
N	0.1	0.2	0.3	0.4	0.5	0.6	0.7	0.8	0.9	1.0
2	-2.04	-1.39	-1.02	-0.77	-0.58	-0.42	-0.29	-0.18	-0.09	0.00
3	-1.96	-1.32	-0.96	-0.72	-0.53	-0.39	-0.27	-0.17	-0.08	0.00
4	-1.92	-1.28	-0.93	-0.69	-0.51	-0.37	-0.26	-0.16	-0.07	0.00
5	-1.90	-1.26	-0.91	-0.68	-0.50	-0.36	-0.25	-0.15	-0.07	0.00
10	-1.85	-1.22	-0.88	-0.65	-0.48	-0.34	-0.23	-0.14	-0.07	0.00
20	-1.83	-1.20	-0.86	-0.63	-0.46	-0.33	-0.23	-0.14	-0.06	0.00
50	-1.81	-1.19	-0.85	-0.62	-0.46	-0.33	-0.22	-0.14	-0.06	0.00
∞	-1.80	-1.18	-0.84	-0.62	-0.45	-0.32	-0.22	-0.13	-0.06	0.00

Example 10.3. A ground heat store in granite with the following data:

$a = 1.6{\cdot}10^{-6}$ m^2/s $\quad \lambda = 3.5$ W/mK
$B = 4$ m $\quad r_b = 0.0575$ m $\quad R_b = 0.01$ K/(W/m)

For the hexagonal duct pattern this gives r_1=2.1 m.

The approximate formula (10.13-14) for a heat extraction step is valid after a time:

$$t_b = \frac{5r_b^2}{a} \approx 2.9 \text{ hours}$$

The pulsated heat extraction is given by:

$$q_1 = 100 \text{ W/m} \qquad t_1 = 24 \text{ hours} \qquad \alpha = 1/3$$

The constant average component gives a temperature difference $T_f - T_m$ between the fluid and the store. We have from (9.27-28):

$$T_f - T_m = 100 \cdot (0.13 + 0.01) = 14.0 \ ^\circ\text{C}$$

The superposed balanced pulse gives according to (10.34) an additional increase:

$$T_f^q = 2.27 \cdot (2 \cdot 3.44 - 1.10) + 100 \cdot 2 \cdot 0.01 = 13.1 + 2.0 = 15.1 \ ^\circ\text{C}$$

Added to the temperature of the constant component we get a maximum temperature of 29.1 °C at the end of the balanced pulse.
If we instead use (10.41) for a sequence of pulses we get:

$$T_f^q = 2.27 \cdot (2 \cdot 3.44 - 0.76) + 100 \cdot 2 \cdot 0.01 = 13.9 + 2.0 = 15.9 \ ^\circ\text{C}$$

This gives a maximum temperature difference of 29.9 °C for the pulsated heat injection.
In order to have the same temperature difference for the pulsated and the constant heat injection, the average component of the pulsated heat injection rate has to be reduced by 50-60%.

With the exception of very small values of α, the correction is rather small compared with dimensionless temperature increase due to the last two balanced pulses. Thus, the additional temperature increase due to the pulsation is approximately equal to the temperature increase due to two balanced pulses (10.34). It should also be noted that the difference between $N = 2$ and any higher value including $N = \infty$ is quite small.

10.3 Superposition method for multiple channels

Some types of ground heat exchangers make use of multiple flow channels in a homogeneous ground region. U-pipes in clay is an example. The distance between the flow channels may be such that thermal influence between the channels must be accounted for. The thermal influence is analyzed with use of a superposition technique similar to those described in chapter 8.2.1 and 9.3.1.

There are N flow channels in the ground heat exchanger. The center of pipe i with the radius r_{bi} is located at the coordinates (x_i, y_i). There is also the fluid-to-ground thermal resistance R_{bi}. The total heat injection rate, which has a contribution q_i from pipe i, is given by:

$$q = \sum_{i=1}^{N} q_i \tag{10.42}$$

The temperature increase T_{fi}^q in pipe i is:

$$T_{fi}^q(t) = \sum_{j=1}^{N} R_{ij}^q q_i(t) \qquad i = 1, \ldots, N \tag{10.43}$$

where the thermal resistances are:

$$\begin{aligned} R_{ii}^q(t) &= \frac{1}{4\pi\lambda} E_1\left(\frac{r_{bi}^2}{4at}\right) + R_{bi} \\ R_{ij}^q(t) &= \frac{1}{4\pi\lambda} E_1\left(\frac{b_{ij}^2 r_1^2}{4at}\right) \qquad i \neq j \end{aligned} \tag{10.44}$$

The exponential integral in the formula for R_{ii}^q may be approximated by the simpler relation (10.11). The resistances R_{ij}^q and R_{ji}^q are equal by reciprocity. The factor b_{ij} are defined by (9.112).

In the case of identical pipes, i.e. pipes with equal pipe radius r_{bi} and equal fluid-to-ground thermal resistances R_{bi}, the thermal resistances R_{ii}^q will be the same for all pipes i. When there is also equal heat injection rates $q_i = q/N$ from the pipes, the temperature increases in the pipes become same,

i.e. $T^q_{fi}(t) = T^q_f(t)$. The thermal resistance R'_q is then from (10.43-44) given by:

$$R'_q(t) = \frac{1}{N}\sum_{j=1}^{N} R_{1j} \qquad j = 1, \ldots, N \tag{10.45}$$

The temperature increase due to the pulsated heat injection of figure 10.5 can, according to section 10.2.4, be approximated by the response from two balanced pulses. The temperature increase at the end of such a pulse is obtained by superimposing two step changes (10.30):

$$T^q_f(0) = -qR'_q(t_1) + \frac{q}{\alpha}R'_q(\alpha t_1) \tag{10.46}$$

The definitions of α and t_1 are given in section 10.2.4.

10.3.1 Single U-pipe

The single U-pipe will be taken as an application of (10.45-46). The properties of the two shanks are equal, so that $R_{b1} = R_{b2} = R_b$ and $r_{b1} = r_{b2} = r_b$. The shank spacing $b_{12}r_1$ is denoted B_u. The thermal resistance R'_q for the symmetrical case with equal heat injection rate ($q_1 = q_2 = q/2$) at the two pipes becomes by (10.45):

$$R'_q(t) = \frac{1}{2}\left[\frac{1}{4\pi\lambda}E_1\left(\frac{r_b^2}{4at}\right) + R_b + \frac{1}{4\pi\lambda}E_1\left(\frac{B_u^2}{4at}\right)\right] \tag{10.47}$$

The last term gives the influence of the other shank of the U-pipe. The response from two balanced pulses can be obtained from (10.46).

10.4 Effect of fluid heat capacity

The influence of the fluid heat capacity on the thermal processes has been neglected so far in the analysis. In this section we will make a few simple estimates of the influence on the thermal response for a step change in heat injection rate.

Estimate of heat absorbed by the fluid

Consider a case where a constant heat injection rate q_1 is supplied to a pipe. The heat carrier fluid has the volumetric heat capacity C_f (J/m^{3}K), while the heat capacity of the surrounding ground is denoted C. The heat rate q_1 is supplied to the fluid. When the fluid temperature increases, heat starts to flow from the pipe to the surrounding ground.

The fluid temperature for the case where the fluid heat capacity can be neglected is given by (10.13-14). The formula gives an upper limit for the temperature increase in the fluid, since part of the heat injection rate is actually consumed for heating of the fluid. The ratio between the amount of energy that has been absorbed by the fluid, $\pi r_b^2 C_f [T_f^q(t) - T_f^q(0)]$, and the total injected amount of heat $q_1 t$ becomes:

$$\frac{C_f}{C} \frac{\ln(4at/r_b^2) - \gamma + 4\pi\lambda R_b}{4at/r_b^2} \qquad t > t_b = \frac{5r_b^2}{a} \tag{10.48}$$

This ratio is a measure of the influence of the fluid heat capacity on the temperature evolution.

Example 10.4. A ground heat store in granite with the following data:

$C_f = 4.2$ MJ/m^{3}K	$C = 2.2$ MJ/m^{3}K	$\lambda = 3.5$ W/mK
$B = 4$ m	$r_b = 0.0575$ m	$R_b = 0.01$ K/(W/m)

For the hexagonal duct pattern of figure 4.? this gives r_1=2.1 m.

The approximate formula (10.13-14) for a heat extraction step is valid after a time:

$$t_b = \frac{5r_b^2}{a} \approx 2.9 \text{ hours}$$

At this time the ratio (10.48) equals 0.27. The ratio is 0.10 after about 12 hours.

The steady-flux analysis in chapter 9 is valid after a time:

$$t_{sf} = \frac{0.2r_1^2}{a} \approx 6.4 \text{ days}$$

The ratio (10.48) is then 0.012.

If the fluid-to-ground thermal resistance R_b is 0.10 K/(W/m), the ratio becomes 0.65 after 2.9 hours, 0.10 after 25 hours, and 0.02 after 6.4 days.

Example 10.5. A ground heat store in clay with the following data:

$C_f = 4.2$ MJ/m^{3}K $\quad C = 3.4$ MJ/m^{3}K $\quad \lambda = 1.0$ W/mK
$B = 2$ m $\quad r_b = 0.02$ m $\quad R_b = 0.10$ K/(W/m)

For the hexagonal duct pattern this gives r_1=1.05 m.

The approximate formula (10.13-14) is valid after a time:

$$t_b = \frac{5r_b^2}{a} \approx 1.9 \text{ hours}$$

The ratio (10.48) then equals 0.23. It becomes 0.10 after 5.4 hours.

The steady-flux analysis is valid after a time:

$$t_{sf} = \frac{0.2r_1^2}{a} \approx 8.7 \text{ days}$$

The ratio (10.48) is then 0.005.

These examples show that short-term pulses sometimes require that the influence of the fluid heat capacity is accounted for. This is especially important if the pipe radius and the fluid-to-ground thermal resistance is large. For heat injection pulses of longer duration, the influence of the fluid heat capacity can usually be neglected.

The formula (10.13-14) can still be used if q_1 is taken to be the heat injection rate from the pipe to the surrounding ground. The total heat injection rate q_1', supplied to both the ground and the fluid, is then given by q_1 and the additional contribution required to heat the fluid. We get the following general formula:

$$q_1' = q_1 + C_f \pi r_b^2 \frac{dT_f}{dt} \tag{10.49}$$

Derivation of (10.13-14) then gives:

$$q_1' = q_1 \left(1 + \frac{C_f}{C} \frac{r_b^2}{4at} \right) \qquad t > t_b = \frac{5r_b^2}{a} \tag{10.50}$$

The right term in the parenthesis gives the ratio between the heat injection rate supplied to the fluid and the constant heat injection rate from the pipe to the ground. The magnitude of this ratio for typical ground heat storage applications is:

$$\frac{C_f}{C} < 2 \qquad \frac{4at}{r_b^2} > 20 \qquad \Rightarrow \qquad \frac{C_f}{C} \frac{r_b^2}{4at} < \frac{1}{10} \tag{10.51}$$

The ratio between the heat absorbed by the fluid and the heat supplied to the surrounding ground at the time $t = t_b = 5r_b^2/a$ is by (10.48):

$$\frac{\pi}{5}\frac{C_f}{C}(\lambda R_b + 0.2) \tag{10.52}$$

Approximate formula for fluid temperature

Carslaw and Jaeger (1959; p. 345) gives the following solution for the fluid temperature when the fluid heat capacity taken into account. There is a step change in heat injection rate at $t = 0$. The solution, which is valid for large values of at/r_b^2, is:

$$\begin{aligned} T_b^q &= \frac{q_1}{4\pi\lambda}\left\{\left(1+\frac{2(1-C_f/C)}{4at/r_b^2}\right)\left[\ln\left(\frac{4at}{r_b^2}\right)-\gamma\right]-\right. \\ &\left.-\left(\frac{8\pi\lambda R_b C_f/C-2}{4at/r_b^2}\right)\right\}+q_1 R_b \end{aligned} \tag{10.53}$$

This formula resembles (10.13-14). For the parameter values applicable to ground heat stores, the influence of the fluid heat capacity is essentially given the term $[2(1-C_f/C)]/(4at/r_b^2)]$ that appears on the right side. Let us require that the absolute value of this term is less than 0.1. This gives the following criterion:

$$\frac{at}{r_b^2} > 5|1-\frac{C_f}{C}| \tag{10.54}$$

The ratio C_f/C is typically in the range from 1.2 to 2.5. The factor on the right side is then 1 to 7.5.

Time-scale

These estimates indicate that the influence of the fluid capacity is small and can be neglected after the time $t > t_b = 5r_b^2/a$. We then have:

$$q_1' \simeq q_1 \qquad t > t_b = \frac{5r_b^2}{a} \tag{10.55}$$

It should be observed, however, that a relatively large fraction of the supplied heat is absorbed in the fluid during the initial time period $0 < t < t_b = 5r_b^2/a$.

10.5 Thermal process along the flow channel

An analytical solution for the case of convective heat flow in a circular pipe with radial heat conduction in the ground outside the pipe is derived in this section. The fluid in the pipe and the surrounding ground are initially at a constant temperature, which is here set to zero. At a certain time, the inlet fluid temperature is raised instantly to a constant value T_1. The heat flow between the fluid and the surrounding ground takes place via the fluid-to-ground thermal resistance R_b. The situation is shown in figure 10.7, which gives the conditions of the thermal problem in dimensionless form.

The ground temperature $T(r,z,t)$ satisfies the heat equation (6.8). The fluid temperature T_f along the flow channel becomes a function of the axial coordinate z and the time t. The fluid flow rate is denoted V_f.

The boundary condition along the flow channel is:

$$-2\pi r_b \lambda \left.\frac{\partial T(r,z,t)}{\partial r}\right|_{r=r_b} = \frac{1}{R_b}[T_f(z,t) - T(r_b,z,t)] \tag{10.56}$$

Heat conduction is neglected in the fluid. A heat balance for the fluid then gives:

$$C_f \pi r_b^2 \frac{\partial T_f}{\partial t} = 2\pi r_b \lambda \left.\frac{\partial T}{\partial r}\right|_{r=r_b} - C_f V_f \frac{\partial T_f}{\partial z} \tag{10.57}$$

Let us introduce the dimensionless fluid-to-ground thermal resistance β, the characteristic length z_f for the convective process, and the average flow velocity v:

$$\beta = 2\pi\lambda R_b \qquad z_f = \frac{C_f V_f}{2\pi\lambda} \qquad v = \frac{V_f}{\pi r_b^2} \tag{10.58}$$

Then we have at $r = r_b$:

$$\frac{1}{v}\frac{\partial T_f}{\partial t} + \frac{\partial T_f}{\partial z} = \frac{1}{z_f}\frac{T - T_f}{\beta} = \frac{\partial T}{\partial r} \tag{10.59}$$

The fluid moves with the velocity v in the pipe. A temperature change at inlet at $t = 0$ does not influence T_f or T before $vt > z$.

If the fluid heat capacity is neglected, then the term $\partial T_f/\partial t$ vanishes:

$$\frac{\partial T_f}{\partial z} == \frac{1}{z_f}\frac{T - T_f}{\beta} = \left.\frac{\partial T}{\partial r}\right|_{r=r_b} \tag{10.60}$$

10.5.1 Step change of injection temperature

We will consider the case of a step change for the inlet temperature. The initial temperature is taken to be zero.

$$\begin{aligned} T_f(0,t) &= T_1 \qquad t > 0 \\ T_f(z,0) &= 0 \qquad z > 0 \\ T(r,z,0) &= 0 \qquad r > r_b, z > 0 \end{aligned} \tag{10.61}$$

The temperature disturbance moves with a velocity v, so that:

$$T_f(z,t) = 0 \qquad T(r,z,t) = 0 \qquad \text{for } z > vt \tag{10.62}$$

Our main interest is the fluid temperature $T_f(z,t)$.

10.5.2 Convection time

Let us introduce the convective time τ:

$$\tau = t - \frac{z}{v} \tag{10.63}$$

It gives the time elapsed since the moment a temperature disturbance reaches the axial distance z in the flow channel. The temperature is, by (10.62), zero for negative values of τ.

The dimensionless temperature as a function of τ is denoted T' and T'_f:

$$\begin{aligned} T_1 \cdot T'(r,z,\tau) &= T(r,z,t) \\ T_1 \cdot T'_f(z,\tau) &= T_f(z,t) \end{aligned} \tag{10.64}$$

Inserting the convective time in the heat balance equation (10.59) for the fluid gives:

$$\frac{\partial T'_f}{\partial z} = \frac{1}{T_1}\left[\frac{\partial T}{\partial z} + \frac{1}{v}\frac{\partial T}{\partial z}\right]$$

or

$$\frac{\partial T'_f}{\partial z} = \frac{1}{z_f}\frac{T' - T'_f}{\beta} = \frac{\partial T'}{\partial r} \qquad r = r_b \tag{10.65}$$

This is the same type of equation as (10.60), which is valid when the fluid heat capacity is neglected.

10.5.3 Dimensionless formulation

The following choice of dimensionless parameters gives the simple forms of the equations illustrated in figure 10.7:

$$r' = \frac{r}{r_b} \qquad \tau' = \frac{a\tau}{r_b^2} \qquad z' = \frac{z}{z_f} \tag{10.66}$$

The dimensionless temperatures T and T_f as a function of the parameters r', z', and τ' are denoted U and U_f. The heat equation, the boundary condition, and the initial conditions for the dimensionless ground temperature becomes by (6.8), (10.65), and (10.61):

$$\frac{\partial^2 U}{\partial (r')^2} + \frac{1}{r'}\frac{\partial U}{\partial r'} = \frac{\partial U}{\partial \tau'} \qquad r' > 1 \tag{10.67}$$

$$\frac{\partial U}{\partial r'} = \frac{U - U_f}{\beta} \qquad r' = 1 \tag{10.68}$$

$$U(r', z', 0) = 0 \qquad r' > 1 \quad z' > 0 \tag{10.69}$$

For the dimensionless fluid temperature we have from (10.65), (10.56), (10.58), and (10.61):

$$\frac{\partial U_f}{\partial z'} = \frac{U - U_f}{\beta} \qquad r' = 1 \tag{10.70}$$

$$\frac{\partial U_f}{\partial \tau'} = \frac{U - U_f}{\beta} \qquad r' = 1 \tag{10.71}$$

$$U_f(z', 0) = 0 \qquad z' > 0 \tag{10.72}$$

$$U_f(0, \tau') = 1 \qquad \tau' > 0 \tag{10.73}$$

The conditions (10.76-73) that define our basic problem are illustrated in figure 10.7.

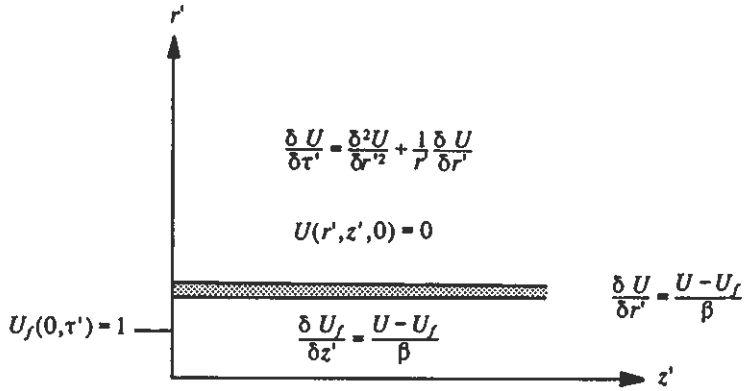

Figure 10.7. Basic problem for convective heat flow in the pipe with radial heat conduction in the ground outside the pipe.

10.5.4 Laplace transform

The Laplace transform is taken with respect to τ'. The solution in the Laplace domain for the ground temperature becomes (Carslaw and Jaeger 1959; p. 335):

$$\tilde{U}(r',z',p) = \tilde{U}(1,z',p)\,\frac{K_0(\sqrt{p}r')}{K_0(\sqrt{p})} \tag{10.74}$$

The boundary condition (10.68) at $r' = 1$ gives:

$$\tilde{U}(1,z',p)\,\frac{-\sqrt{p}K_1(\sqrt{p})}{K_0(\sqrt{p})} = \frac{1}{\beta}[\tilde{U}(1,z',p) - \tilde{U}_f(z',p)] \tag{10.75}$$

where K_0 is a modified Bessel function. Let us use the notation:

$$\rho(p) = \frac{K_0(\sqrt{p})}{\sqrt{p}K_1(\sqrt{p})} \tag{10.76}$$

Then we get:

$$\tilde{U}(1,z',p) = \frac{\rho}{\rho+\beta}\tilde{U}_f(z',p) \tag{10.77}$$

Insertion of this relation in the heat balance equation (10.70) for the fluid gives together with (10.73):

$$\tilde{U}_f(z',p) = \frac{1}{p}\exp\left(-\frac{z'}{\rho+\beta}\right) \tag{10.78}$$

The Laplace transform of the temperature U in the ground becomes from (10.74) and (10.77):

$$\tilde{U}(r',z',p) = \frac{1}{p}\frac{K_0(\sqrt{p}r')}{K_0(\sqrt{p})}\frac{\rho}{\rho+\beta}\exp\left(-\frac{z'}{\rho+\beta}\right) \tag{10.79}$$

10.5.5 Inversion of the Laplace transform

The fluid temperature U_f will be determined by the use of the inversion theorem of the Laplace transformation:

$$U_f(z',\tau') = \frac{1}{2\pi i}\int_{\gamma_0-i\infty}^{\gamma_0+i\infty} e^{p\tau'}\frac{1}{p}e^{-\frac{z'}{\rho+\beta}}\,dp \tag{10.80}$$

where ρ is given by (10.76).

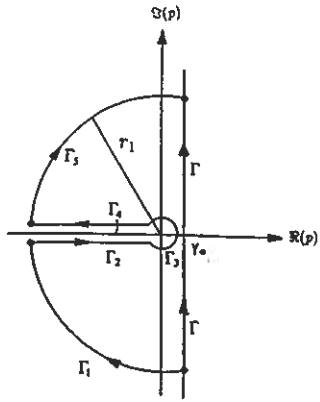

Figure 10.8. Contour used for evaluation of the inversion integral (10.80).

The integral is evaluated by use of the contour shown in figure 10.8. We make a cut along the negative p-axis. The argument $\sqrt{p}$ in $K_0(\sqrt{p})$ and $K_1(\sqrt{p})$ then falls in the right half-plane, where K_0 and K_1 do not have any zeros (Abramowitz and Stegun 1964; p. 377). The function $\rho(p)$ is then regular, except at the point p=0. The contour circumvents this point, so the integrand of (10.80) has no poles within the contour. We have:

$$U_f = \frac{1}{2\pi i}\int_{\Gamma} e^{p\tau'}\frac{1}{p}e^{-\frac{z'}{\rho+\beta}}\,dp = \frac{1}{2\pi i}\int_{\Gamma_1+\Gamma_2+\Gamma_3+\Gamma_4+\Gamma_5} e^{p\tau'}\frac{1}{p}e^{-\frac{z'}{\rho+\beta}}\,dp \tag{10.81}$$

The integrals along Γ_1 and Γ_5 tends to zero for $r_1 \to \infty$, since $\rho(p)$ behaves as $1/\sqrt{p}$ for large values of p (Abramowitz and Stegun 1964; p. 378):

$$\int_{\Gamma_1} \ldots\, dp \to 0 \qquad \int_{\Gamma_5} \ldots\, dp \to 0 \qquad r_1 \to \infty \tag{10.82}$$

For the integral along Γ_3 we have:

$$\Gamma_3 : \qquad \rho = \varepsilon \cdot e^{i\varphi} \qquad -\pi \leq \varphi \leq \pi \qquad dp = i\,p\,d\varphi$$

From a series expansion of $\rho(p)$ we have (Abramowitz and Stegun 1964; p. 375):

$$\rho(p) \to \infty \qquad p \to 0 \tag{10.83}$$

The integral then becomes:

$$\frac{1}{2\pi i}\int_{\Gamma_3} \ldots\, dp = \frac{1}{2\pi i}\int_{-\pi}^{\pi} \frac{1}{p} e^{p\tau'} e^{-\frac{z'}{\rho+\beta}}\, ip\, d\varphi \to 1 \qquad \varepsilon \to \infty \tag{10.84}$$

For Γ_2 we have:

$$\Gamma_2 : \qquad p = -s \qquad s : \infty \to 0 \qquad \sqrt{p} = -i\sqrt{s}$$

$$\begin{aligned}\frac{1}{2\pi i}\int_{\Gamma_2} \ldots\, dp &= \frac{1}{2\pi i}\int_{\infty}^{0} \frac{1}{-s} e^{-s\tau'} e^{-\frac{z'}{\rho(-i\sqrt{s})+\beta}}\,(-ds) = \\ &= -\frac{1}{2\pi i}\int_{0}^{\infty} \frac{1}{s} e^{-s\tau'} e^{-\frac{z'}{\rho(-i\sqrt{s})+\beta}}\, ds\end{aligned} \tag{10.85}$$

For the integration along Γ_4 we have:

$$\Gamma_4 : \qquad p = -s \qquad s : 0 \to \infty \qquad \sqrt{p} = i\sqrt{s}$$

$$\frac{1}{2\pi i}\int_{\Gamma_4} \ldots\, dp = \frac{1}{2\pi i}\int_{0}^{\infty} \frac{1}{-s} e^{-s\tau'} e^{-\frac{z'}{\rho(i\sqrt{s})+\beta}}\,(-ds) \tag{10.86}$$

The fluid temperature is now:

$$U_f(z',\tau') = 1 - \frac{1}{2\pi i}\int_{0}^{\infty} \frac{1}{s} e^{-s\tau'} \left[e^{-\frac{z'}{\rho(-i\sqrt{s})+\beta}} - e^{-\frac{z'}{\rho(i\sqrt{s})+\beta}} \right] ds \tag{10.87}$$

The exponential terms within the brackets are each others complex conjugate, which gives:

$$U_f(z',\tau') = 1 - \frac{1}{\pi}\int_{0}^{\infty} \frac{1}{s} e^{-s\tau'} \Im \left[e^{-\frac{z'}{\rho(-i\sqrt{s})+\beta}} \right] ds \tag{10.88}$$

The function $\rho(-i\sqrt{s})$, which is eq. (10.76) with a complex-valued argument, can be expressed as (Abramowitz and Stegun 1964; pp. 358, 375):

$$\rho(-i\sqrt{s}) = \frac{1}{\sqrt{s}} \frac{J_0(\sqrt{s}) + iY_0(\sqrt{s})}{J_1(\sqrt{s}) + iY_1(\sqrt{s})} \tag{10.89}$$

Inserting this relation in (10.88), we get a real-valued expression for the temperature U_f:

$$U_f = 1 - \frac{1}{\pi}\int_0^\infty \frac{1}{s} e^{-s\tau'} e^{-z' f_2(s)} \sin\left(\frac{2z'}{\pi f_1(s)}\right) ds \tag{10.90}$$

where

$$\begin{aligned} f_1(s) &= J_0^2(\sqrt{s}) + Y_0^2(\sqrt{s}) + \beta^2 s[J_1^2(\sqrt{s}) + Y_1^2(\sqrt{s})] \\ &\quad +2\beta\sqrt{s}[J_0(\sqrt{s})J_1(\sqrt{s}) + Y_0(\sqrt{s})Y_1(\sqrt{s})] \\ f_2(s) &= \left\{\sqrt{s}[J_0(\sqrt{s})J_1(\sqrt{s}) + Y_0(\sqrt{s})Y_1(\sqrt{s})] + \beta s[J_1^2(\sqrt{s}) + Y_1^2(\sqrt{s})]\right\}/f_1 \end{aligned} \tag{10.91}$$

10.5.6 Numerical integration procedure

The integral (10.90) is evaluated numerically. This has to be done with some care due to the oscillatory behavior of the Bessel functions and the rather poor convergence as $s \to 0$. The integral is split into three parts:

$$\int_0^\infty \ldots ds = \int_0^\varepsilon \ldots ds + \int_\varepsilon^R \ldots ds + \int_R^\infty \ldots ds \tag{10.92}$$

The second part is solved numerically, while the integration limit R is chosen large enough so that the last part can be neglected:

$$\int_R^\infty \ldots ds \simeq 0 \tag{10.93}$$

The first part of (10.92) is evaluated analytically by use of suitable approximations of the integrand for small values of s. These approximations give sufficient accuracy for $s < \varepsilon$. The value of ε is determined by a procedure described below. The Bessel functions exhibit the following dependence for small values s,:

$$\begin{aligned} J_0(\sqrt{s}) &\sim 1 & J_1(\sqrt{s}) &\sim \frac{1}{2}\sqrt{s} \\ Y_0(\sqrt{s}) &\sim \tfrac{2}{\pi}\left[\ln\left(\tfrac{1}{2}\sqrt{s}\right) + \gamma\right] & Y_1(\sqrt{s}) &\sim -\frac{1}{\pi}\frac{2}{\sqrt{s}} \end{aligned} \tag{10.94}$$

Insertion of these expression in (10.91) gives the behavior of the functions $f_1(s)$ and $f_2(s)$ for small values of s:

$$f_1(s) \sim \frac{1}{\pi^2}\left\{[\ln(s/4) + 2(\gamma - \beta)]^2 + \pi^2\right\} \tag{10.95}$$

$$f_2(s) \sim -\frac{2[\ln(s/4) + 2(\gamma - \beta)]}{\{[\ln(s/4) + 2(\gamma - \beta)]^2 + \pi^2\}} \tag{10.96}$$

The parts of the integrand may now be approximated as:

$$e^{-s\tau'} \simeq 1 \qquad \sin\left(\frac{2z'}{\pi f_1(s)}\right) \simeq \frac{2z'}{\pi f_1(s)} \tag{10.97}$$

For $z' < 3$ the exponent $-z' f_2(s)$ is usually small, so that:

$$e^{-z' f_2(s)} \simeq 1 - z' f_2(s) \tag{10.98}$$

The first part of the integral (10.92) is then:

$$\begin{aligned} \int_0^\varepsilon \ldots ds \;\sim\; & \int_0^\varepsilon \frac{1}{s} \frac{2\pi z'}{[\ln(s/4) + 2(\gamma - \beta)]^2 + \pi^2}\, ds + \\ & + \int_0^\varepsilon \frac{1}{s} \frac{4\pi (z')^2}{[\ln(s/4) + 2(\gamma - \beta)]^3}\, ds \end{aligned} \tag{10.99}$$

The π^2-term has been removed in the second integral in order to obtain a closed-form solution. We finally get:

$$\begin{aligned} \int_0^\varepsilon \ldots ds \;\simeq\; & 2\pi z' \left\{ \frac{1}{2} + \frac{1}{\pi} \arctan\left[\frac{1}{\pi} (\ln(\varepsilon/4) - 2(\gamma - \beta)) \right] \right\} - \\ & - \frac{2\pi (z')^2}{[\ln(\varepsilon/4) + 2(\gamma - \beta)]^2} \end{aligned} \tag{10.100}$$

For $z' \geq 3$ we will retain the exponential term in the integrand. The approximate expressions (10.95-96) for the functions $f_1(s)$ and $f_2(s)$ are used without the π^2-term. We get:

$$\begin{aligned} \int_0^\varepsilon \ldots ds \;&\simeq\; \int_0^\varepsilon \frac{1}{s} \exp\left[\frac{2z'}{\ln(s/4) + 2(\gamma - \beta)} \right] \frac{2\pi z'}{[\ln(s/4) + 2(\gamma - \beta)]^2}\, ds \\ &=\; \pi \left\{ 1 - \exp\left[\frac{2z'}{\ln(\varepsilon/4) + 2(\gamma - \beta)} \right] \right\} \end{aligned} \tag{10.101}$$

The main integral $\int_\varepsilon^R \ldots ds$ is solved with use of a cubic spline quadrature. At first the integral is calculated for the range $[R_1, R]$. The evaluation proceeds towards smaller values of s for the interval $[R_2, R_1]$ where $R_2 = R_1/2$. The value of the integral is compared with the approximate value for the same range $\int_0^{R_1} \ldots ds - \int_0^{R_2} \ldots ds$, which can be obtained from (10.100-101). The procedure is repeated until the numerical value and the approximate value agree within a given tolerance. We then have the value $\int_\varepsilon^R \ldots ds$. Since the integration limit ε is now known, the integral $\int_0^\varepsilon \ldots ds$ can be calculated.

10.5.7 Fluid temperature

The calculated dimensionless fluid temperature U_f is shown in figures 10.9-14 as a function of the dimensionless axial length z' for some values of the dimensionless convective time τ' and the dimensionless fluid-to-ground thermal resistance β. These parameters are defined by (10.63) and (10.58).

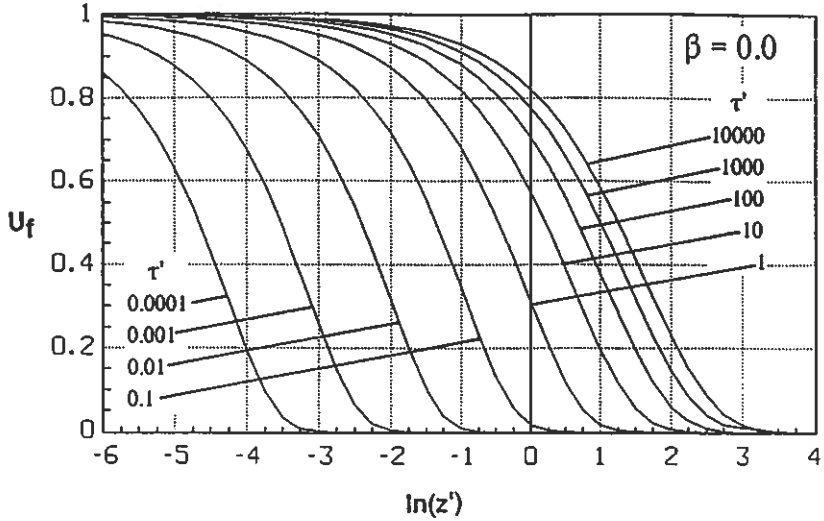

Figure 10.9. Dimensionless fluid temperature U_f as a function of the dimensionless axial length z' for some values τ'. β=0. The parameters are defined by (10.63) and (10.58).

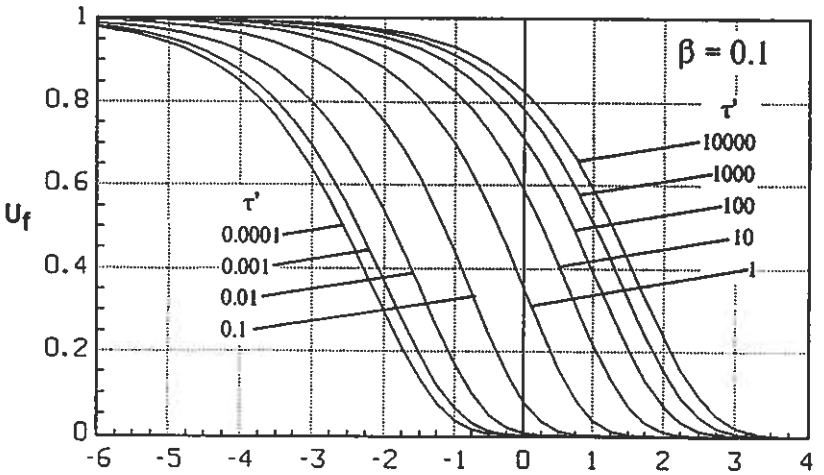

Figure 10.10. Dimensionless fluid temperature U_f as a function of the dimensionless axial length z'. β=0.1.

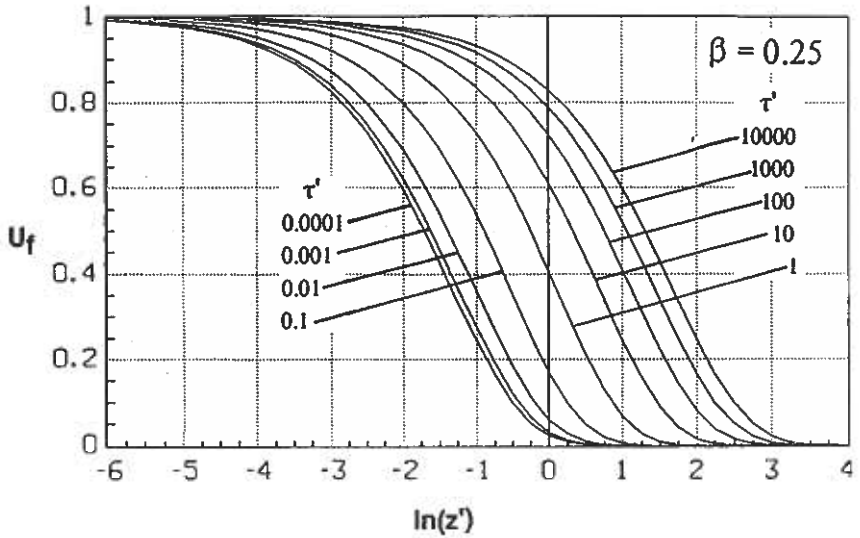

Figure 10.11. Dimensionless fluid temperature U_f as a function of the dimensionless axial length z'. β=0.25.

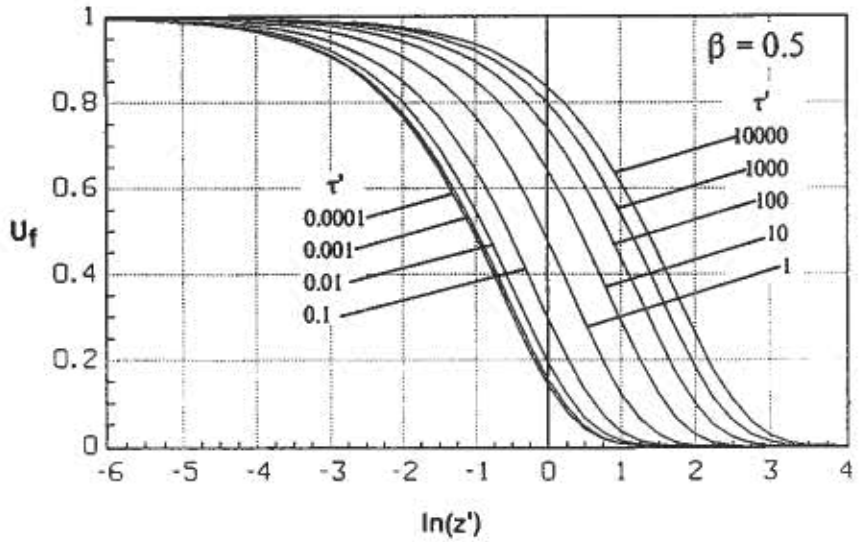

Figure 10.12. Dimensionless fluid temperature U_f as a function of the dimensionless axial length z'. β=0.5.

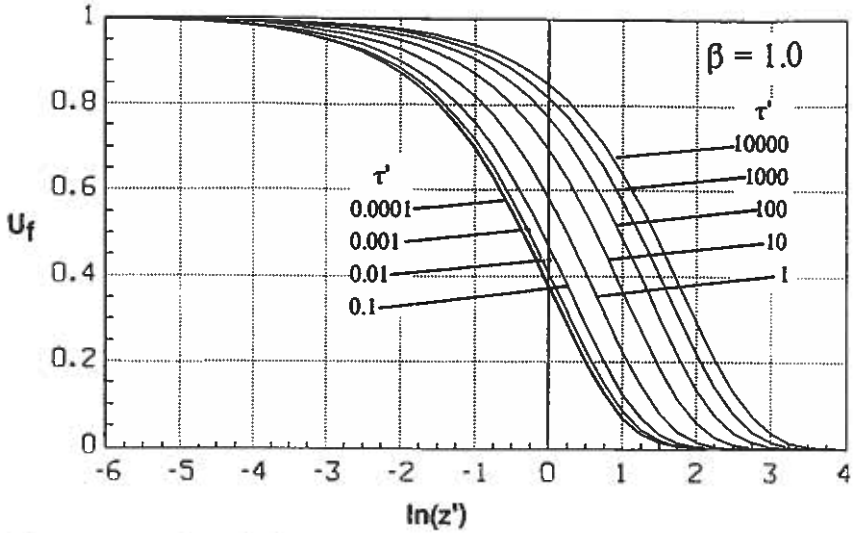

Figure 10.13. Dimensionless fluid temperature U_f as a function of the dimensionless axial length z'. β=1.0.

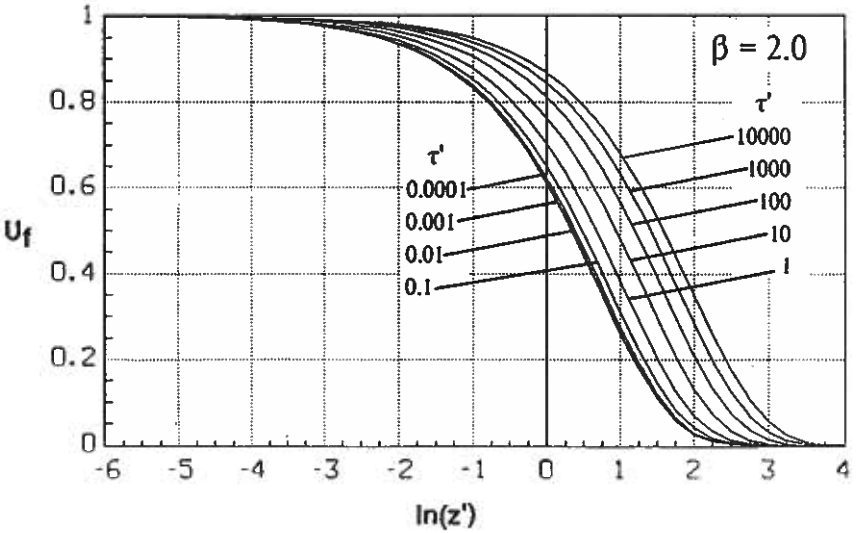

Figure 10.14. Dimensionless fluid temperature U_f as a function of the dimensionless axial length z'. β=2.0.

Chapter 11

Periodic Processes

The thermal process in the ground around each ground heat exchanger can be separated into simpler particular processes. The total thermal process may be composed of a steady-flux component (see chapter 9) and a number of superposed periodical components. In this chapter we will treat the regular periodic variation discussed section 6.1.3.

Basic relations for the periodic processes are given in section 11.1. The thermal influence between adjacent heat transfer channels is treated in 11.2. Periodic processes for the cases of a circular duct and multipole heat transfer channels are dealt with in sections 11.3 and 11.4, respectively. Finally, the problem of varying fluid temperatures along the flow channels is analyzed in section 11.5.

11.1 Basic relations

11.1.1 Complex temperatures and heat flows

The periodic temperature in the ground outside a circular pipe is a function the radial distance r and the time t. With use of the complex notation explained in section 6.1.3, the ground temperature can be expressed as:

$$T(r,t) = \hat{T}(r)e^{i2\pi t/t_p} \tag{11.1}$$

where the period length is denoted t_p. The temperature T_b at the pipe is of special interest:

$$T_b(t) = \hat{T}_b e^{i2\pi t/t_p} \tag{11.2}$$

There is a periodic heat injection rate at the pipe:

$$q(t) = \hat{q}\, e^{i2\pi t/t_p} \tag{11.3}$$

Note that the symbol ˆ indicates that a parameter is complex-valued. The amplitude of the heat injection rate is given by the absolute value $|\hat{q}|$, whereas the phase time is obtained from the argument $\arg(\hat{q})$.

11.1.2 Penetration depth

A characteristic length for the periodic variations in the ground is the penetration depth d_p. The definition of d_p is from (6.23):

$$d_p = \sqrt{\frac{at_p}{\pi}} \tag{11.4}$$

The concept of a penetration depth d_p is further explained in section 12.4.1, where d_p is given for some different values of a and t_p in Table 12.5.

11.1.3 Dimensionless parameters

The lengths that appear in the periodic problem are scaled with the penetration depth according to:

$$r' = \frac{r\sqrt{2}}{d_p} \qquad r'_b = \frac{r_b\sqrt{2}}{d_p} \qquad r'_1 = \frac{r_1\sqrt{2}}{d_p} \tag{11.5}$$

11.2 Thermal influence

The thermal influence between adjacent ground heat exchangers becomes negligible when the penetration depth d_p (11.4) is small compared to the spacing between the ground heat exchanger. The periodical process is then the same as for a single ground heat exchanger in an infinite surrounding.

The thermal influence has to be accounted for if the spacing between the ground heat exchangers is small. If the ground heat exchangers are placed in a regular duct pattern as described in section 4.2, then a cylindrical ground region may be ascribed to each ground heat exchanger. The conditions for the local thermal process require that the heat flow is zero at the outer boundary $r = r_1$.

It will be shown in section 11.3.2 that the thermal influence between adjacent ground heat exchanger in a *hexagonal* duct pattern, figure 4.3, can be classified by the following criteria:

$$\begin{aligned} &\text{Negligible influence:} && r'_1 = r_1\sqrt{\frac{2\pi}{at_p}} \geq 3 \\ &\text{Moderate influence:} && 0.8 < r'_1 < 3 \\ &\text{Strong influence:} && r'_1 \leq 0.8 \end{aligned} \tag{11.6}$$

For a *quadratic* duct pattern, figure 4.3, with a spacing B between the ground heat exchanger the criteria become:

$$\begin{aligned} &\text{Negligible influence:} && B \geq 2\sqrt{at_p} \\ &\text{Moderate influence:} && 0.6\sqrt{at_p} < B < 2\sqrt{at_p} \\ &\text{Strong influence:} && B \leq 0.6\sqrt{at_p} \end{aligned} \tag{11.7}$$

Example 11.1. A ground heat store in granite with the following data:

$\lambda = 3.5$ W/mK $\quad C = 2.2$ MJ/m^{3}K

Quadratic duct pattern $\quad B = 4$ m

$$\begin{aligned} &\text{Negligible influence:} && t_p \leq 1 \text{ month} \\ &\text{Moderate influence:} && 1 \text{ month} < t_p < 11 \text{ months} \\ &\text{Strong influence:} && t_p \geq 11 \text{ months} \end{aligned}$$

Example 11.2. A ground heat store in clay with the following data:

$\lambda = 1.0$ W/mK $\quad C = 3.4$ MJ/m^{3}K

Quadratic duct pattern $\quad B = 2$ m

$$\begin{aligned} &\text{Negligible influence:} && t_p \leq 40 \text{ days} \\ &\text{Moderate influence:} && 40 \text{ days} < t_p < 14 \text{ months} \\ &\text{Strong influence:} && t_p \geq 14 \text{ months} \end{aligned}$$

These two examples, with typical values on the spacing between the ground heat exchangers, show that the thermal influence can be neglected for period lengths shorter than 1 month.

11.3 Circular duct

11.3.1 Duct with negligible thermal influence

In this section we will treat a circular duct where the thermal influence from other ground heat exchangers can be neglected. Criteria for the thermal influence are given by (11.6) and (11.7).

The relation between the ground temperature (11.1) at a radius r and the period line source $\hat{q}_1 e^{-i2\pi t/t_p}$ is from (Carslaw and Jaeger 1959) given by:

$$\hat{T}(r') = \frac{1}{2\pi\lambda} \cdot \mathrm{K}_0\left(\sqrt{i}r'\right) \cdot \hat{q}_1 \tag{11.8}$$

where K_0 is a modified Bessel function. The argument $\sqrt{i}r'$ can also be expressed as $(1+i)r/d_p$. The temperature variation at the pipe radius r_b becomes:

$$\hat{T}_b = \hat{T}\left(r_b'\right) = \frac{1}{2\pi\lambda} \cdot \mathrm{K}_0\left(\sqrt{i}r_b'\right) \cdot \hat{q}_1 \tag{11.9}$$

We can now eliminate the line source strength q_1 in (11.8) and express the ground temperature as a function of temperature variation at the pipe:

$$\hat{T}\left(r'\right) = \frac{\mathrm{K}_0\left(\sqrt{i}r'\right)}{\mathrm{K}_0\left(\sqrt{i}r_b'\right)} \cdot \hat{T}_b \tag{11.10}$$

The complex-valued Bessel functions may be expressed in the real and the imaginary parts, or in polar form:

$$\mathrm{K}_0\left(\sqrt{i}r'\right) = \mathrm{ker}_0\left(r'\right) + i \cdot \mathrm{kei}_0\left(r'\right) = N_0\left(r'\right) e^{i\phi_0(r')} \tag{11.11}$$

The functions N_0 and ϕ_0 give the modulus and the phase of the Kelvin functions ker_0 and kei_0 (Abramowitz and Stegun 1964). The solution (11.10) may then be written as:

$$\hat{T}\left(r'\right) = \frac{N_0\left(r'\right)}{N_0\left(r_b'\right)} \cdot e^{i\left[\phi_0(r') - \phi_0\left(r_b'\right)\right]} \cdot \hat{T}_b \tag{11.12}$$

The functions N_0 and ϕ_0 are given in figure 11.1 and Table 11.1.

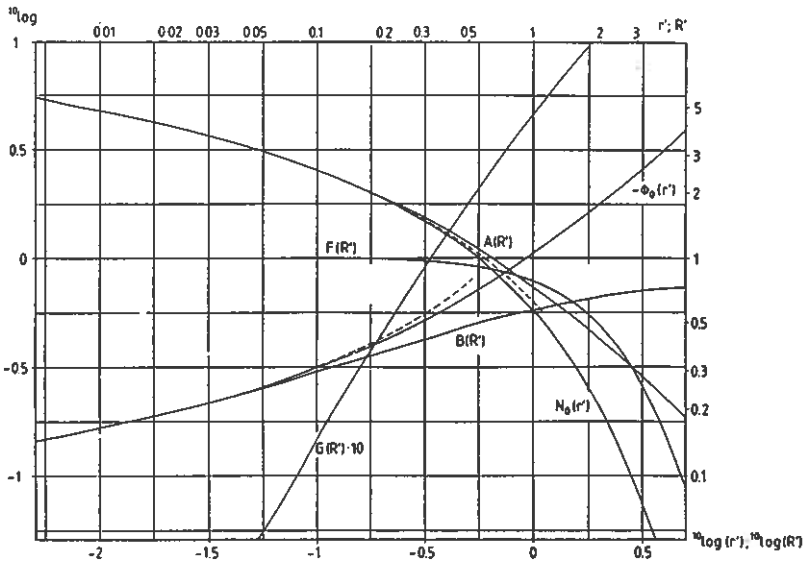

Figure 11.1. Functions used for evaluation at the periodic process around a circular duct. The dashed lines give the approximations (11.13).

For small arguments there are the following approximate expressions:

$$\begin{aligned} N_0(r') &\approx \sqrt{[\ln(2/r') - \gamma]^2 + \pi^2/16} \\ \phi_0(r') &\approx -\arctan\left[\frac{\pi/4}{\ln(2/r') - \gamma}\right] \\ & r' < 0.1 \qquad \gamma = 0.5772\ldots \end{aligned} \tag{11.13}$$

The error is less than 1% for $r' < 0.1$. These approximations are shown by the dashed lines in figure 11.1. For large arguments we have:

$$\begin{aligned} N_0(r') &\approx \sqrt{\frac{\pi}{2r'}} e^{-r'/\sqrt{2}} \qquad (r' > 7) \\ \phi_0(r') &\approx -\left(\frac{r'}{\sqrt{2}} + \frac{\pi}{8}\right) \end{aligned} \tag{11.14}$$

TABLE 11.1. Functions used for evaluation of the periodic process around a circular duct.

$r'; R'$	$N_0(r')$	$-\phi_0(r')$	$F(R')$	$G(R')$	$A(R')$	$B(R')$	$1/A(R')$
0.001	7.067	0.111	1	0	7.067	0.111	0.142
0.002	6.379	0.123	1	0	6.379	0.123	0.157
0.003	5.977	0.132	1	0	5.977	0.132	0.167
0.004	5.692	0.138	1	0	5.692	0.138	0.176
0.005	5.471	0.144	1	0	5.471	0.144	0.183
0.006	5.291	0.149	1	0	5.291	0.149	0.189
0.007	5.138	0.153	1	0	5.138	0.153	0.195
0.008	5.006	0.158	1	0	5.006	0.158	0.200
0.009	4.890	0.161	1	0	4.890	0.161	0.204
0.01	4.786	0.165	1	0.000	4.786	0.165	0.209
0.02	4.104	0.193	1	0.001	4.104	0.192	0.244
0.03	3.707	0.214	1.000	0.002	3.707	0.212	0.270
0.04	3.426	0.231	0.999	0.003	3.429	0.228	0.292
0.05	3.209	0.247	0.999	0.005	3.212	0.242	0.311
0.06	3.033	0.261	0.999	0.006	3.036	0.255	0.329
0.07	2.884	0.276	0.998	0.008	2.890	0.268	0.346
0.08	2.756	0.289	0.998	0.010	2.762	0.279	0.362
0.09	2.643	0.302	0.997	0.012	2.651	0.290	0.377
0.1	2.542	0.311	0.996	0.015	2.552	0.296	0.392
0.2	1.892	0.412	0.986	0.045	1.919	0.367	0.521
0.3	1.525	0.501	0.971	0.086	1.571	0.415	0.637
0.4	1.275	0.585	0.949	0.131	1.344	0.454	0.744
0.5	1.088	0.665	0.925	0.181	1.176	0.484	0.850
0.6	0.942	0.744	0.899	0.235	1.048	0.509	0.954
0.7	0.823	0.820	0.870	0.291	0.946	0.529	1.057
0.8	0.725	0.896	0.840	0.349	0.863	0.547	1.16
0.9	0.643	0.971	0.810	0.408	0.794	0.563	1.26
1	0.572	1.046	0.779	0.469	0.734	0.577	1.36
2	0.207	1.774	0.489	1.119	0.423	0.655	2.36
3	0.084	2.490	0.284	1.800	0.296	0.690	3.38
4	0.036	3.202	0.158	2.492	0.228	0.710	4.39
5	0.0161	3.913	0.086	3.189	0.187	0.724	5.35
10	0.00034	7.463	0.0035	6.712	0.0965	0.751	10.36
20	0.00000	14.53	0.0000	13.77	0.0491	0.768	20.35
50	0.00000	35.74	0.0000	34.97	0.0199	0.778	50.35

The radial heat flow (W/m) at a distance r' is by (11.8):

$$-2\pi r'\lambda\frac{\partial\hat{T}}{\partial r'} = \sqrt{i}r'\mathrm{K}_1\left(\sqrt{i}r'\right)\cdot\hat{q}_1 \tag{11.15}$$

At the pipe radius r'_b we have:

$$\hat{q} = \sqrt{i}r'_b\mathrm{K}_1\left(\sqrt{i}r'_b\right)\cdot\hat{q}_1 \tag{11.16}$$

We can now replace the line source strength $\hat{q}_1$ in (11.8) with the heat injection rate $\hat{q}$ at the pipe radius r'_b:

$$\hat{T}(r) = \frac{1}{2\pi\lambda}\frac{1}{\sqrt{i}r'_b}\frac{\mathrm{K}_0\left(\sqrt{i}r'\right)}{\mathrm{K}_1\left(\sqrt{i}r'_b\right)}\cdot\hat{q} \tag{11.17}$$

The temperature at the pipe radius becomes:

$$\hat{T}_b = \frac{1}{2\pi\lambda}\frac{1}{\sqrt{i}r'_b}\frac{\mathrm{K}_0\left(\sqrt{i}r'_b\right)}{\mathrm{K}_1\left(\sqrt{i}r'_b\right)}\cdot\hat{q} \tag{11.18}$$

The Bessel function $\mathrm{K}_0\left(\sqrt{i}r'_b\right)$ is expressed in polar form by (11.11). For the Bessel function $\mathrm{K}_1\left(\sqrt{i}r'_b\right)$ we have from Abramowitz and Stegun (1964):

$$\mathrm{K}_1\left(\sqrt{i}r'_b\right) = iN_1\left(r'_b\right)e^{i\phi_1(r'_b)} \tag{11.19}$$

The denominator of (11.18) becomes in polar form:

$$\sqrt{i}r'_b\mathrm{K}_1\left(\sqrt{i}r'_b\right) = F\left(r'_b\right)e^{-iG(r'_b)} \tag{11.20}$$

where F and G by (11.19) are:

$$\begin{aligned} F\left(r'_b\right) &= r'_bN_1\left(r'_b\right) \\ G\left(r'_b\right) &= -\phi_1\left(r'_b\right) - 3\pi/4 \end{aligned} \tag{11.21}$$

The functions F and G are given in figure 11.1 and Table 11.1. For small r'_b we have:

$$F\left(r'\right) \approx 1 \qquad G\left(r'\right) \approx 0 \qquad \left(r' < 0.1\right) \tag{11.22}$$

The temperature at the pipe radius (11.18) may now by (11.11) and (11.20) be written:

$$\hat{T}_b = \frac{1}{2\pi\lambda}\cdot\frac{N_0\left(r'_b\right)}{F\left(r'_b\right)}e^{i\left[\phi_0\left(r'_b\right)+G\left(r'_b\right)\right]}\cdot\hat{q} \tag{11.23}$$

If we introduce $A\left(r'_b\right) = N_0\left(r'_b\right)/F\left(r'_b\right)$ and $B\left(r'_b\right) = -\phi_0\left(r'_b\right) - G\left(r'_b\right)$, eq. (11.23) takes the form:

$$\hat{T}_b = \frac{1}{2\pi\lambda}\cdot A\left(r'_b\right)e^{-iB\left(r'_b\right)}\cdot\hat{q} \tag{11.24}$$

The functions A and B are given in figure 11.1 and Table 11.1. For small values we have from (11.22) that $F \approx 1$ and $G \approx 0$, which implies that $A \approx N_0$ and $B \approx -\phi_0$. The approximations (11.13) for N_0 and ϕ_0 can then be used.

11.3.2 Concentric pipe in a circular region

For the hexagonal duct pattern, the ground volume assigned to each ground heat exchanger is approximately a cylindrical region with the radius r_1. See section 4.2.

At the pipe radius $r = r_b$ there is a periodical heat injection rate $q(t) = \hat{q}\, e^{i2\pi t/t_p}$. There is no heat flow through the outer boundary at $r = r_1$.

Pipe temperature

The temperature $\hat{T}(r)$ is a complex-valued function of the type:

$$\hat{T}(r) = C_1 I_0\left(\sqrt{i}r'\right) + C_2 \mathrm{K}_0\left(\sqrt{i}r'\right) \tag{11.25}$$

where C_1 and C_2 are constant to be determined by the boundary conditions. The heat flow is $\hat{q}$ at $r = r_b$ and 0 at $r = r_1$, which finally gives:

$$\hat{T}(r) = \frac{1}{2\pi\lambda}\,\frac{1}{\sqrt{i}\,r_b}\,\frac{\mathrm{I}_1(\sqrt{i}\,r_1')\mathrm{K}_0(\sqrt{i}\,r) + \mathrm{K}_1(\sqrt{i}\,r_1')\mathrm{I}_0(\sqrt{i}\,r)}{\mathrm{I}_1(\sqrt{i}\,r_1')\mathrm{K}_1(\sqrt{i}\,r_b') - \mathrm{K}_1(\sqrt{i}\,r_1')\mathrm{I}_1(\sqrt{i}\,r_b')} \cdot \hat{q} \tag{11.26}$$

Let us introduce:

$$A(r_b', r_1')e^{-iB(r_b', r_1')} = \frac{1}{\sqrt{i}\,r_b'}\,\frac{\mathrm{I}_1(\sqrt{i}\,r_1')\mathrm{K}_0(\sqrt{i}\,r_b') + \mathrm{K}_1(\sqrt{i}\,r_1')\mathrm{I}_0(\sqrt{i}\,r_b')}{\mathrm{I}_1(\sqrt{i}\,r_1')\mathrm{K}_1(\sqrt{i}\,r_b') - \mathrm{K}_1(\sqrt{i}\,r_1')\mathrm{I}_1(\sqrt{i}\,r_b')} \tag{11.27}$$

The temperature at the pipe is then:

$$\hat{T}_b = \frac{1}{2\pi\lambda} \cdot A(r_b', r_1')e^{-iB(r_b', r_1')} \cdot \hat{q} \tag{11.28}$$

The amplitude function $A(r_b', r_1')$ and the phase function $B(r_b', r_1')$ are shown in figure 11.2-4.

Eq. (11.28) gives the temperature variation when the heat injection rate $\hat{q}$ is known. The reverse relationship is simply:

$$\hat{q} = 2\pi\lambda \cdot \frac{1}{A(r_b', r_1')} e^{iB(r_b', r_1')} \cdot \hat{T}_b \tag{11.29}$$

The eq. (11.28) is analogous to (11.24) given previously for the pipe in an infinite surrounding. The functions $A(r_b')$ and $B(r_b')$ used for the infinite case are obtained by setting $r_1' = \infty$ in (11.27).

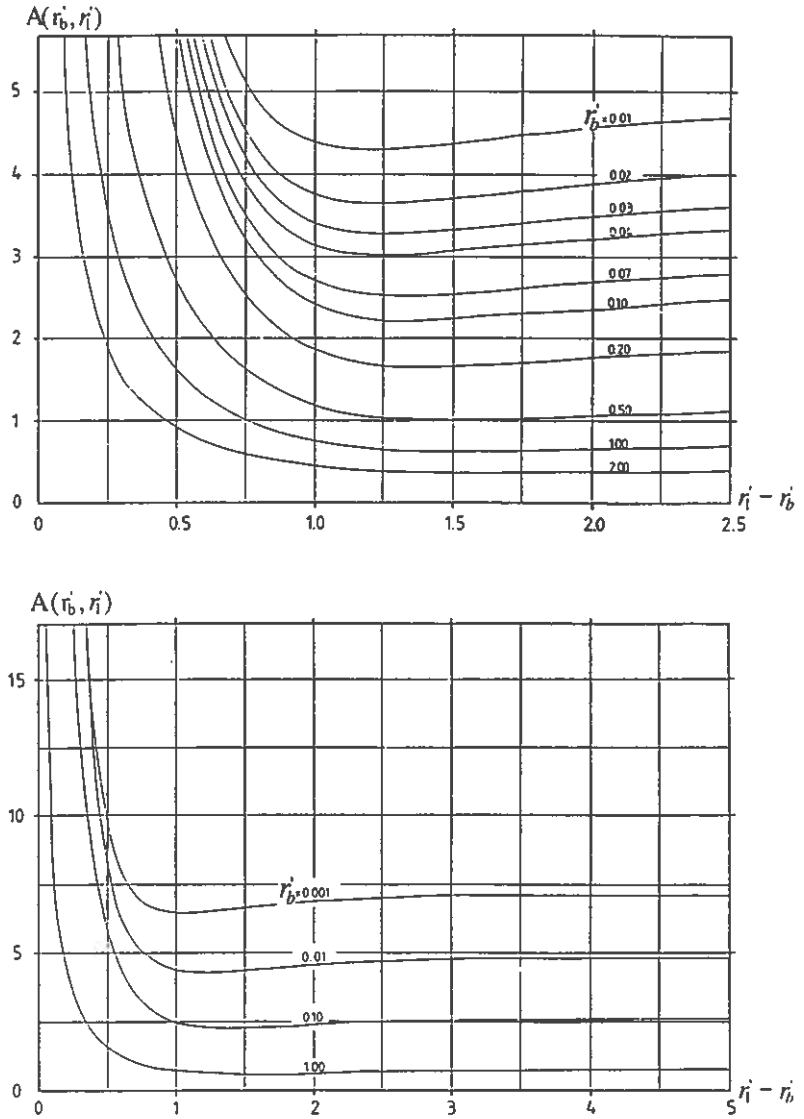

Figure 11.2. Amplitude function $A(r'_b, r'_1)$ for the temperature at the pipe radius $r' = r'_b$; eqs. (11.27-28).

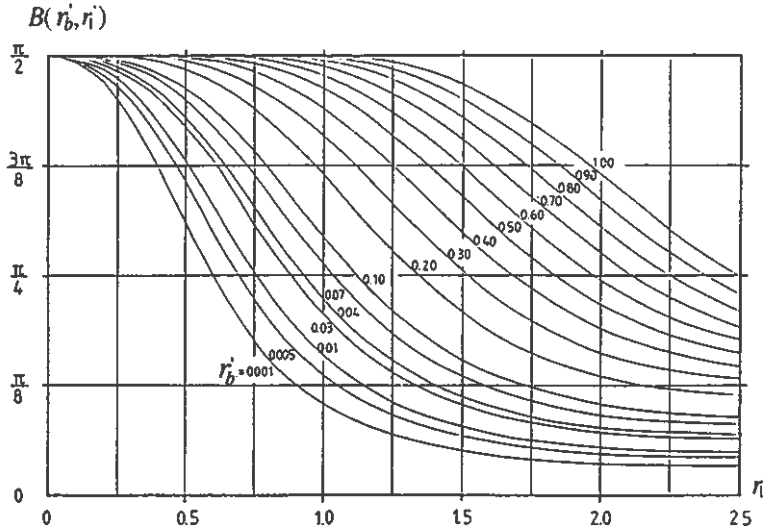

Figure 11.3. Phase function $B(r'_b, r'_1)$ for the temperature at the pipe radius $r' = r'_b$; eqs. (11.27-28).

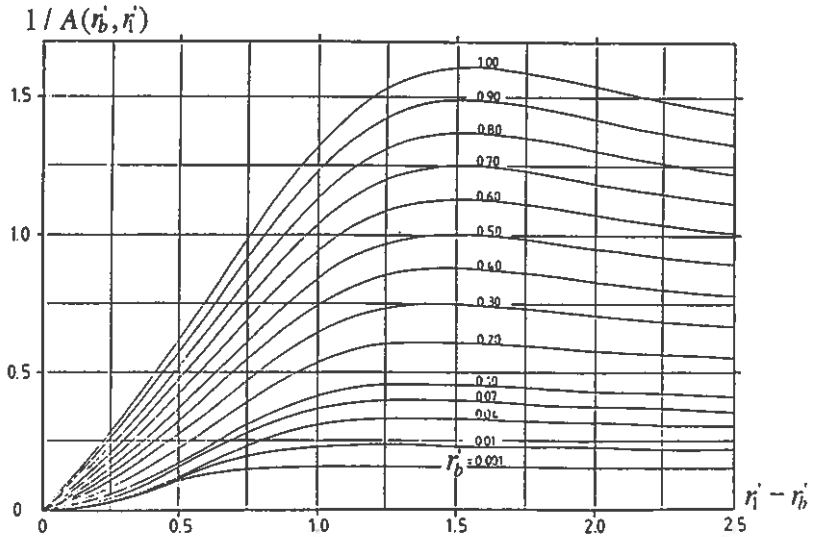

Figure 11.4. Amplitude function $1/A(r'_b, r'_1)$ for the heat flow at the pipe radius $r' = r'_b$; eqs. (11.27) and (11.29).

Optimum spacing

It is interesting to note that the curves in figure 11.2 for the amplitude function A have a minimum value for a certain $r_1' - r_b'$. In figure 11.4, this corresponds to a maximum for $1/A$ for a certain $r_1' - r_b'$. For given values of the pipe radius r_b and the penetration depth d_p, the maximum occurs for a certain value of the radius r_1 of the cylindrical region. This may be considered to represent an optimum, since it gives the maximum heat injection rate for a given amplitude of the temperature. Conversely, it gives the minimum amplitude of the temperature for a given heat injection rate. Figure 11.5 shows the relation between r_1' and r_b' for this optimum.

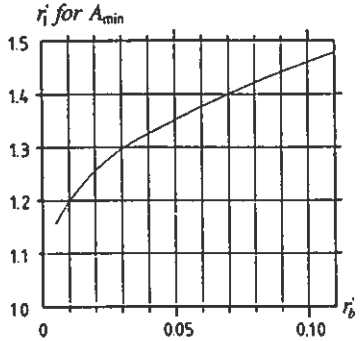

Figure 11.5. Relation between r_1' and r_b' at the minimum of the function A.

Thermal influence

The thermal influence between adjacent ducts can be estimated by comparing the temperature amplitude (11.24) for a pipe in a circular region with the amplitude (11.28) for a pipe in an infinite region. The values of the radius r_1' that give a relative difference in amplitude of 1, 2, 5 %, and 10 % are given in Table 11.2 for some values of r_b'.

TABLE 11.2. Radius r_1' that gives a relative difference between $A(r_b', r_1')$ and $A(r_b')$ of 1, 2, 5 % and 10 %. Eqs. (11.24) and (11.28).

	r_b'					
Difference	0.01	0.02	0.05	0.1	0.2	0.3
1 %	2.79	2.85	2.95	3.05	3.19	3.31
2 %	2.51	2.59	2.71	2.83	2.98	3.11
5 %	2.01	2.12	2.27	2.42	2.61	2.75
10 %	0.72	0.76	0.85	0.94	1.07	1.19

The relative difference in amplitude between adjacent pipes becomes negligible (<1 %) for $r_1' > 3$. The amplitude $A(r_b', r_1')$ can then be approximated by $A(r_b')$ for an infinite region (or spacing). Below $r_1' \approx 3$, the thermal influence

gradually increases as r_1' gets smaller until $r_1' \approx 0.8$, below which the thermal influence becomes strong (>10 %). In the intermediate interval $0.8 < r_b' < 3$ we have moderate thermal influence.

Approximate relations

The pipe radius r_b is much smaller than the penetration depth d_p in many applications. For small values of the dimensionless pipe radius r_b' (11.5) we get the following approximation:

$$A(r_b', r_1')e^{-iB(r_b', r_1')} \approx \ln\left(\frac{2}{r_b'}\right) - \gamma - i\frac{\pi}{4} - \mathrm{KI}\,(r_1')$$
$$\gamma = 0.5722\ldots \qquad (r_b' < 0.3) \qquad (11.30)$$

The error is less than 1% for $r_b' < 0.3$. The complex-valued function $\mathrm{KI}(r_1')$ is given by:

$$\mathrm{KI}\,(r_1') = -\frac{\mathrm{K}_1(\sqrt{i}\,r_1')}{\mathrm{I}_1(\sqrt{i}\,r_1')} \qquad (11.31)$$

The real and imaginary parts of KI are shown in figure 11.6 and Table 11.3. A few values are also given in Table 11.3.

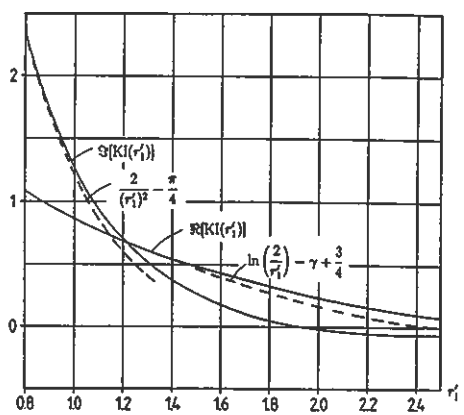

Figure 11.6. Function $\mathrm{KI}(r_1')$ (11.31).

TABLE 11.3. Function $\mathrm{KI}(r_1')$ (11.31).

r_1'	$\Re[\mathrm{KI}(r_1')]$	$\Im[\mathrm{KI}(r_1')]$	r_1'	$\Re[\mathrm{KI}(r_1')]$	$\Im[\mathrm{KI}(r_1')]$
0.1	3.17	199	3.4	$-7.4\cdot10^{-3}$	$-2.9\cdot10^{-2}$
0.2	2.48	49.2	3.6	$-1.1\cdot10^{-2}$	$-1.9\cdot10^{-2}$
0.3	2.07	21.4	3.8	$-1.2\cdot10^{-2}$	$-1.2\cdot10^{-2}$
0.4	1.78	11.7	4.0	$-1.1\cdot10^{-2}$	$-5.9\cdot10^{-3}$
0.5	1.56	7.23	4.2	$-9.1\cdot10^{-3}$	$-2.0\cdot10^{-3}$
0.6	1.38	4.80	4.4	$-7.0\cdot10^{-3}$	$4.2\cdot10^{-4}$
0.7	1.22	3.33	4.6	$-5.0\cdot10^{-3}$	$1.7\cdot10^{-3}$
0.8	1.09	2.39	4.8	$-3.2\cdot10^{-3}$	$2.3\cdot10^{-3}$
0.9	0.97	1.74	5.0	$-1.9\cdot10^{-3}$	$2.3\cdot10^{-3}$
1.0	0.87	1.29	5.2	$-8.6\cdot10^{-4}$	$2.1\cdot10^{-3}$
1.1	0.78	0.96	5.4	$-2.0\cdot10^{-4}$	$1.7\cdot10^{-3}$
1.2	0.69	0.71	5.6	$2.0\cdot10^{-4}$	$1.2\cdot10^{-3}$
1.3	0.62	0.52	5.8	$4.0\cdot10^{-4}$	$8.5\cdot10^{-4}$
1.4	0.55	0.38	6.0	$4.7\cdot10^{-4}$	$5.3\cdot10^{-4}$
1.5	0.48	0.27	6.2	$4.5\cdot10^{-4}$	$2.9\cdot10^{-4}$
1.6	0.42	0.18	6.4	$3.8\cdot10^{-4}$	$1.1\cdot10^{-4}$
1.7	0.37	0.11	6.6	$3.0\cdot10^{-4}$	$2.9\cdot10^{-6}$
1.8	0.32	$5.9\cdot10^{-2}$	6.8	$2.2\cdot10^{-4}$	$-6.0\cdot10^{-5}$
1.9	0.28	$2.0\cdot10^{-2}$	7.0	$1.5\cdot10^{-4}$	$-8.9\cdot10^{-5}$
2.0	0.23	$-9.8\cdot10^{-3}$	7.5	$2.6\cdot10^{-5}$	$-7.9\cdot10^{-5}$
2.2	0.17	$-4.7\cdot10^{-2}$	8.0	$-1.5\cdot10^{-5}$	$-3.8\cdot10^{-5}$
2.4	0.11	$-6.3\cdot10^{-2}$	8.5	$-1.8\cdot10^{-5}$	$-9.3\cdot10^{-6}$
2.6	$6.8\cdot10^{-2}$	$-6.6\cdot10^{-2}$	9.0	$-9.6\cdot10^{-6}$	$2.2\cdot10^{-6}$
2.8	$3.6\cdot10^{-2}$	$-6.0\cdot10^{-2}$	9.5	$-2.9\cdot10^{-6}$	$3.9\cdot10^{-6}$
3.0	$1.5\cdot10^{-2}$	$-5.0\cdot10^{-2}$	10.0	$1.4\cdot10^{-7}$	$2.4\cdot10^{-6}$
3.2	$6.1\cdot10^{-3}$	$-3.9\cdot10^{-2}$			

Series expansions of K_1 and I_1 give the following approximations for small values of r_1' (Abramowitz and Stegun 1964):

$$\mathrm{KI}(r_1') = \ln\left(\frac{2}{r_1'}\right) - \gamma + \frac{3}{4} + i\left[\frac{2}{(r_1')^2} - \frac{\pi}{4}\right] \qquad (r_1' < 1) \qquad (11.32)$$

The maximum error is a few percent for $r_1' < 1$. The approximation is shown by the dashed line in figure 11.6.

For large values of r_1' we have:

$$\mathrm{KI}(r_1') = \pi e^{-\sqrt{2}r_1'(1+i)}\left[1 + \frac{3}{4\sqrt{2}r_1'}(1+i)\right] \qquad (r_1' > 3) \qquad (11.33)$$

with a maximum error of a few percent for $r_1' > 3$.

The approximations (11.30) and (11.32) taken together give the simple relation:

$$A(r_b', r_1')e^{-iB(r_b', r_1')} \approx \ln\left(\frac{r_1}{r_b}\right) - \frac{3}{4} + \frac{2}{i(r_1')^2} \qquad (r_b' < 0.3, r_1' < 1) \qquad (11.34)$$

The average temperature $T_m(t)$ in the circular region is:

$$T_m = \frac{1}{\pi(r_1 - r_b)} \int_{r_b}^{r_1} 2\pi r\, T(r,t)\, dr \tag{11.35}$$

The integration of the ground temperature (11.26) gives for $r_b \ll r_1$:

$$\hat{T}_m = \frac{1}{2\pi\lambda} \cdot \frac{2}{i(r_1')^2} \cdot \hat{q} \tag{11.36}$$

Eqs. (11.28), (11.34), and (11.36) now give

$$\hat{T}_b - \hat{T}_m \simeq \frac{1}{2\pi\lambda} \left[\ln\left(\frac{r_1}{r_b}\right) - \frac{3}{4} \right] \hat{q} \qquad (r_1' < 1.8, r_1/r_b > 15) \tag{11.37}$$

We recognize the steady-flux thermal resistance (9.25) on the right-hand side. The range of validity of (11.34) is based on the accuracy of the real and the imaginary parts of (11.30) and (11.32) taken separately. A direct comparison of the approximation (11.34) and the exact solution (11.28) reveals that the error is less than 1% for $r_1' < 1.8$, less than 2% for $r_1' < 2.2$, and less than 5% for $r_1' < 2.7$. A further condition is that $r_1/r_b > 15$, which holds also for the steady-flux solution (11.37). The condition that $r_b' < 0.3$ is no longer needed.

11.3.3 Periodic thermal resistance of the ground

The factor in front of $\hat{q}$ in (11.24) and (11.28) can be interpreted as a complex-valued periodic thermal resistance for the temperature $\hat{T}_b$ at the pipe radius. This thermal resistance will be denoted $\hat{R}_g$, so that

$$\hat{R}_g = \frac{1}{2\pi\lambda} A e^{-iB} \tag{11.38}$$

where the suitable version of A and B is taken from either (11.24) or (11.28).

11.3.4 Fluid-to-ground thermal resistance

The formulas (11.24) and (11.28) relate the heat injection rate $\hat{q}$ to the temperature $\hat{T}_b$ at the pipe radius $r = r_b$. We are also interested in the fluid temperature variation $\hat{T}_f$. The fluid-to-ground thermal resistance is R_b. We have from (4.1):

$$\hat{T}_f - \hat{T}_b = \hat{q} \cdot R_b \tag{11.39}$$

The fluid temperature variation is then from (11.28), (11.38), and (11.39):

$$\hat{T}_f = \left(\hat{R}_g + R_b\right) \cdot \hat{q} \tag{11.40}$$

11.3.5 Influence of fluid heat capacity

In section 10.4 it was observed that a relatively large fraction of the injected heat may be absorbed by the fluid during short-term variations.

The heat injection rate $\hat{q}$ used earlier in this chapter concerns the heat that flows into the ground. Let us here denote this heat flow by $\hat{q}_g$. The corresponding variation of the fluid temperature is from (11.40):

$$T_f(t) = \hat{T}_f \cdot e^{i2\pi t/t_p} = \left(\hat{R}_g + R_b\right) \cdot \hat{q}_g e^{i2\pi t/t_p} \tag{11.41}$$

The variation of the fluid temperature means that the energy content of the fluid also varies. The heating of the fluid requires an additional heat injection rate $q_f(t)$:

$$q_f(t) = \pi r_b^2 C_f \frac{dT_f}{dt} \tag{11.42}$$

where C_f is the volumetric heat capacity ($\mathrm{J/m^3K}$) of the fluid. From (11.41) we have:

$$q_f(t) = \pi r_b^2 C_f \cdot \frac{2\pi i}{t_p} \cdot \hat{T}_f \cdot e^{i2\pi t/t_p} \tag{11.43}$$

or with (11.3-5):

$$\hat{q}_f = \lambda\pi \cdot \frac{C_f}{C} \left(r_b'\right)^2 \cdot i\hat{T}_f \tag{11.44}$$

The factor in front of $\hat{T}_f$ is the inverse of an equivalent thermal resistance $\hat{R}_f$ for the influence of the fluid heat capacity:

$$\hat{R}_f = \frac{1}{2\lambda\pi} \frac{2C}{C_f i (r_b')^2} \tag{11.45}$$

The total heat injection rate $\hat{q}$ to the fluid is then given by $\hat{q}_g + \hat{q}_f$, which by (11.40), (11.44), and (11.45) becomes

$$\hat{q} = \left(\frac{1}{\hat{R}_f} + \frac{1}{\hat{R}_g + R_b}\right) \cdot \hat{T}_f \tag{11.46}$$

The influence of the fluid heat capacity is roughly given by the ratio $\hat{R}_g/\hat{R}_f$. If we consider short-term variations without thermal influence with other ground heat exchangers, the ratio is from (11.38) and (11.45):

$$\frac{\hat{R}_g}{\hat{R}_f} = \frac{C_f}{2C} \left(r_b'\right)^2 \cdot A\left(r_b'\right) e^{-i[B(r_b')+\pi/2]} \tag{11.47}$$

The factor $C_f/(2C)$ is typically about one. The amplitude is then given by $(r_b')^2 \cdot A(r_b')$. With values from Table 11.1, we find that the influence is less than a few percent if $r_b' < 0.1$.

11.4 Multiple heat transfer channels

A ground heat exchanger may consist of two or more heat transfer channels that lie close to each other. See figure 9.14. Although the thermal influence between adjacent ground heat exchangers is negligible, it is often necessary to consider the thermal influence between the different heat transfer channels. In this section, however, we will assume that the thermal influence between adjacent ground heat exchangers is negligible.

11.4.1 Superposition method

The ground heat exchanger consists of N parallel ducts. The temperature in the ground is obtained by superimposing the temperature fields from the different ducts. The periodic heat injection rate at pipe i is $\hat{q}_i$ (W/m). The total heat injection rate is given by the sum:

$$\hat{q} = \sum_{i=1}^{N} \hat{q}_i \tag{11.48}$$

The center of a pipe is located at (x_i, y_i). A dimensionless distance between two pipes i and j is:

$$b_{ij} = \frac{\sqrt{(x_i - x_j)^2 + (y_i - y_j)^2}}{\sqrt{2}d_p} \qquad \text{for} \quad i,j = 1,\ldots,N \tag{11.49}$$

The fluid-to-ground thermal resistance R_{bi} at pipe i is given by the formulas in Chapter 8. The difference between the fluid temperature $\hat{T}_{fi}$ and the temperature $\hat{T}_{bi}$ in the ground immediately outside the ducts becomes:

$$\hat{T}_{fi} - \hat{T}_{bi} = \hat{q}_i R_{bi} \tag{11.50}$$

The fluid temperature $\hat{T}_{fi}$ is obtained by a superposition of the temperature fields due to the heat flows $\hat{q}_i$:

$$\hat{T}_{fi} = \sum_{j=1}^{N} \hat{R}_{ij}\hat{q}_j \qquad i = 1,\ldots,N \tag{11.51}$$

where the thermal resistances $\hat{R}_{ii}$ and $\hat{R}_{ij}$ are obtained from (11.40), (11.38), (11.17), (11.11), and (11.20):

$$\begin{aligned} \hat{R}_{ii} &= \frac{1}{2\pi\lambda} A\left(r'_{bi}\right) e^{-iB\left(r'_{bi}\right)} + R_{bi} \\ \hat{R}_{ij} &= \frac{1}{2\pi\lambda} \frac{N_0\left(b_{ij}\right)}{F\left(r'_{bi}\right)} e^{i\left[\phi_0(b_{ij}) + G\left(r'_{bi}\right)\right]} \qquad b_{ij}\sqrt{2}d_p \gg r_{bi} \end{aligned} \tag{11.52}$$

Thus, there are linear relations between the fluid temperatures and the heat flows. The functions A, B, N_0, F, ϕ_0, and G are given in figure 11.1 and Table 11.1.

For the symmetrical case with equal heat injection rates $\hat{q}_i = \hat{q}/N$ and fluid temperatures $\hat{T}_{fi} = \hat{T}_f$, the eq. (11.51) takes the simpler form:

$$\hat{T}_{fi} = \hat{T}_f = \hat{q} \cdot \frac{1}{N} \sum_{j=1}^{N} \hat{R}_{ij} = \hat{q} \cdot \frac{1}{N} \sum_{j=1}^{N} \hat{R}_{1j} \tag{11.53}$$

The thermal influence from adjacent ground heat exchangers may be accounted for by including these heat transfer channels in the superposition (11.51). According to the criteria (11.7) for negligible thermal influence, it is necessary to include channels within $3.5d_p$ from the channel under consideration. See Table 12.5.

11.4.2 Symmetrical heat transfer channels

The superposition method presented in section 11.4.1 will here be applied to a single, double, and triple U-pipe in a homogeneous region. The heat transfer channels have equal radius r_b, fluid-to-ground thermal resistance R_b, and heat injection rate $\hat{q}$ per unit length of ground heat exchanger.

The spacing between the two opposing shanks of a U-pipe is denoted B_u. We will use a dimensionless shank spacing defined by:

$$b_u = \frac{B_u\sqrt{2}}{d_p} \tag{11.54}$$

The penetration depth d_p is given by (11.4).

Single U-pipe

Figure 9.18 shows a single U-pipe in a circular region. The heat injection rate is $\hat{q}/2$ from each shank of the U-pipe. The complex-valued fluid temperature becomes by (11.53):

$$\hat{T}_f = \frac{1}{2}\left\{\frac{1}{2\pi\lambda}\left[A\left(r_b'\right)e^{-iB(r_b')} + \frac{N_0\left(b_u\right)}{F\left(r_b'\right)} \cdot e^{i\left[\phi_0(b_u)+G(r_b')\right]}\right] + R_b\right\} \cdot \hat{q} \tag{11.55}$$

Double U-pipe

Figure 9.19 shows a double U-pipe in a circular region. The heat injection rate is $\hat{q}/4$ from each shank of the double U-pipe. The fluid temperature is by (11.53):

$$\hat{T}_f = \frac{1}{4}\left\{\frac{1}{2\pi\lambda}\left[A\left(r_b'\right)e^{-iB(r_b')} + \frac{N_0\left(b_u\right)}{F\left(r_b'\right)}\cdot e^{i[\phi_0(b_u)+G(r_b')]} + \right.\right.$$
$$\left.\left. + \frac{2N_0\left(b_u/\sqrt{2}\right)}{F\left(r_b'\right)}\cdot e^{i[\phi_0(b_u/\sqrt{2})+G(r_b')]}\right] + R_b\right\}\cdot\hat{q} \qquad (11.56)$$

Triple U-pipe

Figure 9.20 shows a double U-pipe in a circular region. The heat injection rate is $\hat{q}/6$ from each shank of the triple U-pipe. The fluid temperature is by (11.53):

$$\hat{T}_f = \frac{1}{6}\left\{\frac{1}{2\pi\lambda}\left[A\left(r_b'\right)e^{-iB(r_b')} + \frac{N_0\left(b_u\right)}{F\left(r_b'\right)}\cdot e^{i[\phi_0(b_u)+G(r_b')]} + \right.\right.$$
$$+\frac{2N_0\left(b_u/2\right)}{F\left(r_b'\right)}\cdot e^{i[\phi_0(b_u/2)+G(r_b')]} +$$
$$\left.\left. + \frac{2N_0\left(\sqrt{3}b_u/2\right)}{F\left(r_b'\right)}\cdot e^{i[\phi_0(\sqrt{3}b_u/2)+G(r_b')]}\right] + R_b\right\}\cdot\hat{q} \qquad (11.57)$$

11.5 Varying fluid temperature along the flow channels

The problem of a temperature variation along the flow channels in a ground heat exchanger will be treated in this section. We will consider the cases of a single duct, an annular duct, and multiple flow channels in a homogeneous ground region.

11.5.1 Basic relations

The complex-valued representation is used for all temperatures:

$$\begin{array}{lll}
\text{Ground:} & T_g(r,z,t) = \hat{T}_g(r,z)\,e^{i2\pi t/t_p} \\
\text{Borehole wall:} & T_b(z,t) = \hat{T}_b(z)\,e^{i2\pi t/t_p} \\
\text{Fluid:} & T_f(z,t) = \hat{T}_f(z)\,e^{i2\pi t/t_p} \\
\text{Fluid inlet:} & T_{fin}(t) = \hat{T}_{fin}(z)\,e^{i2\pi t/t_p} \\
\text{Fluid outlet:} & T_{fout}(t) = \hat{T}_{fout}(z)\,e^{i2\pi t/t_p}
\end{array} \qquad (11.58)$$

The heat flows are denoted similarly:

$$\begin{array}{lll} \text{Total heat injection rate (W):} & Q(t) & = \hat{Q}\, e^{i2\pi t/t_p} \\ \text{Heat injection rate per unit length (W/m):} & q(z,t) & = \hat{q(z)}\, e^{i2\pi t/t_p} \\ \text{Heat injection rate to the ground (W/m):} & q_g(z,t) & = \hat{q_g(z)}\, e^{i2\pi t/t_p} \end{array} \tag{11.59}$$

Conductive heat transport in the axial direction of the flow channels is neglected both in the flow channels and in the surrounding ground. The partial differential equation (6.22) for the periodic thermal process in the ground becomes:

$$\frac{\partial^2 \hat{T}_g}{\partial r^2} + \frac{1}{r}\frac{\partial \hat{T}_g}{\partial r} = \frac{2\pi i}{a t_p}\hat{T}_g \tag{11.60}$$

11.5.2 Single duct

The heat balance for the fluid in a single circular duct with a radius r_b is:

$$C_f \pi r_b^2 \frac{\partial T_f}{\partial t} = -q_g - C_f V_f \frac{\partial T_f}{\partial z} \tag{11.61}$$

The term on the left-hand side is the rate of increase in energy content of the fluid. The first term on the right ($-q_g$) is the heat flow from the ground to the fluid. These two terms are given by (11.46), hence when the time factor $e^{i2\pi t/t_p}$ is deleted:

$$-C_f V_f \frac{\partial \hat{T}_f}{\partial z} = \left[\frac{1}{\hat{R}_f} + \frac{1}{\hat{R}_g + R_b}\right] \cdot \hat{T}_f \tag{11.62}$$

The total thermal resistance for the fluid will be denoted $\hat{R}_0$. It is given by:

$$\frac{1}{\hat{R}_0} = \frac{1}{\hat{R}_f} + \frac{1}{\hat{R}_g + R_b} \tag{11.63}$$

Let us introduce a complex-valued length $\hat{z}_f$ defined by:

$$\hat{z}_f = C_f V_f \hat{R}_0 \tag{11.64}$$

The solution of the differential equation for the fluid temperature becomes:

$$\hat{T}_f(z) = \hat{T}_f(0) \cdot \exp(-z/\hat{z}_f) \tag{11.65}$$

The length $\hat{z}_f$ is evidently a characteristic length for the attenuation of the amplitude of the periodic temperature variation along the duct. Expressed in thermal resistances, (11.64) is by (11.63) and (11.62):

$$\hat{T}_f(z) = \hat{T}_f(0) \cdot \exp\left(-\frac{z}{C_f V_f \hat{R}_f}\right) \cdot \exp\left[-\frac{z}{C_f V_f (\hat{R}_g + R_b)}\right] \tag{11.66}$$

The factor containing the thermal resistance of fluid capacity $\hat{R}_f$ can, with use of (11.45), be written:

$$\exp\left(-i2\pi \cdot \frac{\pi r_b^2 C_f z}{t_p C_f V_f}\right) = \exp\left(-i2\pi \cdot \frac{z}{v_f t_p}\right) \tag{11.67}$$

where $v_f = V_f/(\pi r_b^2)$ is the fluid velocity. Taken together with the time factor we get:

$$\exp\left(i2\pi \cdot \frac{t}{t_p}\right) \cdot \exp\left(-i2\pi \cdot \frac{z}{v_f t_p}\right) = \exp\left(i2\pi \cdot (t - z/v_f)/t_p\right) \tag{11.68}$$

This means that the fluid capacity factor only gives a phase-lag z/v_f.

The heat injection rate from the duct with its length H is:

$$Q(t) = C_f V_f [T_{fin}(t) - T_{fout}(t)] \tag{11.69}$$

where $T_{fin}(t)$ is the fluid temperature at the inlet ($z = 0$), and T_{fout} is the outlet temperature at $z = H$. From (11.65) we then have:

$$\hat{Q} = C_f V_f [1 - \exp(-H/\hat{z}_f)] \cdot \hat{T}_f(0) \tag{11.70}$$

The average fluid temperature $\bar{T}_f$, defined as the arithmetic mean value of the inlet and the outlet temperature, becomes:

$$\bar{\hat{T}}_f = \frac{1}{2}(\hat{T}_{fin} + \hat{T}_{fout}) = \frac{1}{2}[1 + \exp(-H/\hat{z}_f)] \cdot \hat{T}_f(0) \tag{11.71}$$

Combining (11.70) and (11.71) gives a relation between the heat injection rate and the average fluid temperature:

$$\hat{q} = \frac{\hat{Q}}{H} = \frac{2C_f V_f}{H} \frac{1 - \exp(-H/\hat{z}_f)}{1 + \exp(-H/\hat{z}_f)} \cdot \bar{\hat{T}}_f \tag{11.72}$$

where $\hat{q}$ is the average heat injection rate per meter duct. The eq. (11.72) may be rewritten as:

$$\bar{\hat{T}}_f = \hat{R}_0 \cdot \hat{\eta} \coth(\hat{\eta}) \cdot \hat{q} \tag{11.73}$$

where

$$\hat{\eta} = \frac{H}{2C_f V_f \hat{R}_0} \tag{11.74}$$

The correction factor for the axial temperature variation is $\hat{\eta}\coth(\hat{\eta})$. A series expansion of this factor for small values of $\hat{\eta}$ gives:

$$\hat{\eta}\coth(\hat{\eta}) \approx 1 + (\hat{\eta})^2/3 \tag{11.75}$$

The correction factor is roughly equal to unity, if $|\hat{\eta}| < 0.4$.

11.5.3 Ducts with counterflow heat exchange

The ground heat exchanger consists of one channel with upwards flow and one with downwards flow. The heat flows to the ground from the channels with fluid temperatures $\hat{T}_{f1}$ and $\hat{T}_{f2}$ are denoted $\hat{q}_{g1}$ and $\hat{q}_{g2}$ respectively. The heat exchange between the ducts will be described with use of the heat flow Δ-circuit presented in section 8.2.2. By analogy with (8.77), the heat balance for the two flow channels becomes with complex notation:

$$\begin{aligned} -C_f V_f \frac{\partial \hat{T}_{f1}}{\partial z} &= \hat{T}_{f1}/\hat{R}_1^{\Delta} + (\hat{T}_{f1} - \hat{T}_{f2})/\hat{R}_{12}^{\Delta} \\ C_f V_f \frac{\partial \hat{T}_{f2}}{\partial z} &= \hat{T}_{f2}/\hat{R}_2^{\Delta} + (\hat{T}_{f2} - \hat{T}_{f1})/\hat{R}_{12}^{\Delta} \end{aligned} \tag{11.76}$$

The thermal resistances $\hat{R}_1^{\Delta}$, $\hat{R}_2^{\Delta}$, and $\hat{R}_{12}^{\Delta}$ are complex-valued:

$$\begin{aligned} \frac{1}{\hat{R}_1^{\Delta}} &= \frac{1}{\hat{R}_{f1}} + \frac{1}{\hat{R}_{g1} + R_{b1}} \\ \frac{1}{\hat{R}_2^{\Delta}} &= \frac{1}{\hat{R}_{f2}} + \frac{1}{\hat{R}_{g2} + R_{b2}} \end{aligned} \tag{11.77}$$

where we have introduced the thermal resistances (11.43) for the fluid heat capacity:

$$\hat{R}_{f1} = \frac{t_p}{C_f A_1 2\pi i} \qquad \hat{R}_{f2} = \frac{t_p}{C_f A_2 2\pi i} \tag{11.78}$$

where A_1 and A_2 are the cross-sectional areas of the two ducts.

The solution of (11.76) follows from the procedures presented in sections 8.5-6.2. By comparing the heat balance equations (8.77) and (11.76) we find that they become identical if we set the borehole wall temperature T_b in (8.77) equal to zero. The relation between the average fluid temperature $\bar{\hat{T}}_f$ and the heat injection rate $\hat{q}$ per unit length of the ground heat exchanger becomes by (8.83), (8.87), and (8.88):

$$\bar{\hat{T}}_f = \hat{R}_0 \cdot \hat{\eta} \coth(\hat{\eta}) \cdot \hat{q} \tag{11.79}$$

where

$$\hat{\eta} = \frac{H}{2C_f V_f} \frac{1}{\hat{R}_0} \sqrt{1 + 4\frac{\hat{R}_0}{\hat{R}_{12}^{\Delta}}} \tag{11.80}$$

and

$$\frac{1}{\hat{R}_0} = \frac{1}{\hat{R}_1^{\Delta}} + \frac{1}{\hat{R}_2^{\Delta}} \tag{11.81}$$

The term $\hat{\eta}\coth(\hat{\eta})$ gives the correction for the fluid temperature variation along the flow channels. For small values of $\hat{\eta}$ we have the series expansion (11.75). The influence of the temperature variation can be neglected, $\hat{\eta}\coth(\hat{\eta}) \approx 1$, when $|\hat{\eta}_0| < 0.4$.

Chapter 12

Global Thermal Processes

The large-scale thermal process in the store and the surrounding ground consists of three fundamental components. There is a steady-state part, a superimposed periodic variation during an annual cycle, and an initial transient thermal build-up of the temperature field around the store.

The periodic component gives a pulsating thermal process with a limited range of influence around the storage region. The net heat flow through the storage boundaries becomes zero for an annual cycle.

The transient thermal build-up of the temperature field around the store may, for large storage volumes, be important during the first years or even decades. The transient process gradually approaches a steady-state condition. There is then a time-independent, or steady-state, temperature distribution in the surrounding ground and a superimposed periodical variation during the storage cycle.

The annual heat losses from the store can be calculated without taking the periodic component into account, since the net heat flow of this component is zero. The seasonal variations of the heat transfer rates to the store and the temperature at the ground surface may be important for the heat loss distribution during the cycle, but they do not influence the annual heat loss. The heat loss is then determined by the average temperatures during the annual cycle. The ground surface temperature should be taken as the annual mean temperature at the site. At the storage boundary, i.e. the interface between the storage volume and the surrounding ground, we will use a suitable constant temperature that represents an annual average value.

The transient thermal build-up begins from the undisturbed ground temperature. The basic case with a constant average temperature on the storage boundary is treated in section 12.3. The steady-state thermal process determines the annual heat losses when transient part has become negligible. This important process is dealt with in section 12.2.

12.1 Thermal interaction between local and global process

The global process is coupled to the local process around each ground heat exchanger. The local process, which has been treated in chapters 7-11, can be represented by a single parameter in the analyses of the global process. Eq. (9.2) gives the following relation between the heat injection rate q_v (W/m^3) and the difference between the fluid temperature T_f and the local average temperature T_m around a ground heat exchanger:

$$q_v = \alpha_v (T_f - T_m) \tag{12.1}$$

The local average temperature will vary in the storage volume. This variable average temperature in the store gives the global temperature distribution.

The volumetric heat transfer capacity α_v (W/m^{3}K)can be expressed as:

$$\alpha_v = \frac{\lambda}{\ell^2} \tag{12.2}$$

Here, the thermal conductivity of the ground is denoted λ. The parameter ℓ has the dimension of a length. Inserting (12.2) in (12.1) gives:

$$q_v = \lambda \frac{T_f - T_m}{\ell^2} \quad \text{W/m}^3 \tag{12.3}$$

The length ℓ is a *characteristic heat transfer length* for the ground heat exchanger.

Eqs. (9.3) and (12.2) yield a relation between the heat transfer length ℓ and the steady-flux thermal resistance R_{sf}:

$$\ell = \sqrt{\lambda R_{sf} A_p} \tag{12.4}$$

The steady-flux thermal resistance R_{sf} is dealt with in chapter 9. The cross-sectional area A_p around the ground heat exchanger is discussed in section 4.2.

The volume of the store is denoted V. The vertical extension H of the store is, for the case of vertical ground heat exchangers, equal to length for which there is heat exchange between a ground heat exchanger and the ground. The number of ground heat exchangers in the store is N_p. The storage volume is then given by:

$$V = N_p A_p H \tag{12.5}$$

The radius R of a cylindrical storage volume is given by:

$$\pi R^2 = N_p A_p \tag{12.6}$$

Ground heat stores with the upper boundary at the ground surface are supposed to be thermally insulated on the entire upper boundary and to a depth D_i on the vertical sides.

12.2 Steady-state thermal process

The steady-state component of the total heat loss is analyzed in this section. The steady-state heat flow gives the heat loss during a storage cycle when the transient component has become negligible. Claesson et al. (1985) give formulas, figures, and tables by which the steady-state heat loss can be calculated for several basic geometries. Here, we will give the results pertaining to cylindrical and parallelepipedical storage volumes with the upper boundary at or close to the ground surface. The situation is shown in figure 12.1.

Figure 12.1. Steady-state thermal process around a ground heat store with constant temperature T_m at the storage boundary. The temperature at the ground surface is T_0.

The temperature at the storage boundary has a constant value T_m. This boundary temperature is discussed in section 12.2.6. The constant ground surface temperature is T_0. The steady-state heat flow from the store will be denoted Q_m (W).

12.2.1 Dimensionless formulation

The steady-state temperature field in the ground, $T(x, y, z)$, can be expressed in dimensionless form by:

$$T(x, y, z) = T_0 + (T_m - T_0) \cdot u\,(x/L_s, y/L_s, z/L_s) \tag{12.7}$$

The dimensionless temperature u is zero at the ground surface and $+1$ on the storage boundary. The spatial coordinates of u are dimensionless by the scaling with the length L_s, which could be taken as the vertical extension H or some horizontal width of the store.

The heat loss Q_m is directly proportional to the temperature difference $T_m - T_0$ and to the thermal conductivity λ of the ground:

$$Q_m = \lambda\,(T_m - T_0)\,L_s \cdot h \quad \text{(W)} \tag{12.8}$$

where h denotes a *dimensionless heat loss factor.*

The dimension of the heat store is characterized by the lengths L_s, L_1, L_2, etc. The heat loss factor becomes a function of the scaled lengths, i.e. of the shape and the position of the store:

$$h = h\,(L_1/L_s, L_2/L_s, \ldots) \tag{12.9}$$

The surrounding ground may consist of regions with different thermal conductivities $\lambda, \lambda_1, \lambda_2$, etc. The heat loss factor will then also depend on the relative thermal conductivities λ_1/λ etc.:

$$h = h(L_1/L_s, \ldots, \lambda_1/\lambda, \ldots) \tag{12.10}$$

A particular complication is the scaling of the thermal insulation of the store. Figure 12.2 shows an example, where the store is fitted with an insulation that extends downwards a length D_i on the vertical side. The insulation sheet has a thickness d_i and a thermal conductivity λ_i.

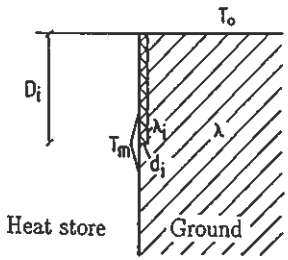

Figure 12.2. Insulation on the vertical side of a store.

The insulation gives the three dimensionless parameters $d_i/L_s, D_i/L_s$, and λ_i/λ. Usually the insulation is treated only as a thermal resistance between the storage temperature T_m and the ground just outside the insulation. The thermal resistance d_i/λ_i of the insulation should then be scaled by the thermal resistance L_s/λ, cf. (6.30). The insulation then results in two dimensionless parameters for the heat loss factor:

$$h(L_1/L_s, \ldots, D_i/L_s, (d_i\lambda)/(L_s\lambda_i)) \tag{12.11}$$

12.2.2 Heat loss from a store at the ground surface

In this section we will analyze the different components of the heat loss from a store with the upper boundary at the ground surface. The entire upper boundary and the upper part of the vertical sides are thermally insulated. The effect of the vertical insulation will be treated in detail.

Figure 12.3 shows the considered type of heat store. The store reaches a depth H. The insulation extends a length D_i down the vertical side. The temperature is T_0 at the ground surface and T_m on storage boundary within the insulation.

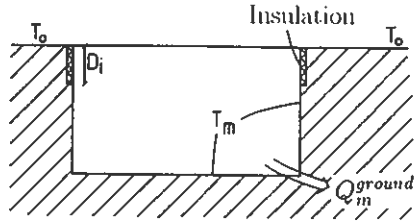

Figure 12.3. Heat store with thermal insulation on the upper boundary and on the vertical side.

The steady-state heat loss Q_m has three contributions: through the insulation on the upper boundary, through the insulation on the vertical side, and directly to the ground through the uninsulated part of the store:

$$Q_m = Q_m^{upper} + Q_m^{side} + Q_m^{ground} \tag{12.12}$$

The first two parts are fairly simple to estimate. The third part is more difficult, since it requires a calculation of the multidimensional, steady-state temperature field in the ground. Here, the influence of the vertical insulation is a special complication.

Heat loss through the upper boundary

The thermal insulation on the upper boundary has the thickness d_i, the thermal conductivity λ_i and the horizontal area A_i. The heat loss is:

$$Q_m^{upper} = (T_m - T_0)\frac{\lambda_i}{d_i}A_i \tag{12.13}$$

Heat loss through the insulation on the vertical side

Let L_i denote the length of the store's horizontal periphery. The total area of the vertical insulation is then $D_i L_i$. The temperature will vary in the ground outside the insulation. The value is T_0 at the ground surface, while it is T_m at the lower tip of the insulations. Let T_{m0} be a suitable average temperature over the depth D_i. The heat loss through the vertical insulation then becomes:

$$Q_m^{side} = (T_m - T_{m0})\frac{\lambda_i}{d_i}D_i L_i \tag{12.14}$$

A reasonable estimate of T_{m0} is:

$$T_{m0} \approx \frac{T_m + T_0}{2} \tag{12.15}$$

An estimate of heat loss through the vertical side is then from (12.14-15):

$$Q_m^{side} \approx (T_m - T_0)\frac{\lambda_i}{d_i} \cdot \frac{D_i}{2} L_i \tag{12.16}$$

The total heat loss through the horizontal and vertical insulation may now be written, by (12.13) and (12.16):

$$Q_m^{insulation} = Q_m^{upper} + Q_m^{side} \approx \frac{\lambda_i (T_m - T_0)}{d_i} \cdot \left(A_i + \frac{1}{2} L_i D_i \right) \qquad D_i/\lambda < d_i/\lambda_i \tag{12.17}$$

Heat losses through the uninsulated part

The heat loss through the uninsulated part of the ground, Q_m^{ground} in (12.12), depends on the geometry of the store, the thermal conductivity of the ground, and the insulation on the vertical side. See figure 12.3. The functional dependence is given by (12.8) and (12.11).

It is usually acceptable to make the following simplification. The ground outside the insulation will offer an additional thermal resistance on the order of $D_i/(2\lambda)$. The thermal resistance of the insulation is usually much larger. The conditions for the heat flow through the uninsulated part are then approximately the same as for the case of no heat flow through the vertical insulation. By that the number of dependent parameters in (12.11) is be reduced by one. This approximation will be applied in the following.

Formula for small insulation depth

Figure 12.4 shows a plane, vertical cross-section of the region around the insulation on the vertical side. The vertical extension H of the store is supposed to be large compared with the insulation depth D_i.

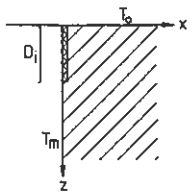

Figure 12.4. Vertical cross-section of the region around the insulation on the vertical side.

Let us assume that the vertical extension of the store is very large. The plane problem of figure 12.4 with zero heat flow through the insulation ($0 < z < D_i, x = 0$) can then be solved by analytical methods.

Our main interest is the heat flux $q_x(z)$ (W/m^2) through the storage boundary ($x = 0, z > D_i$). This problem can be solved with the use of the conformal mapping technique. The solution becomes (Hagentoft 1988):

$$q_x(z) = \lambda (T_m - T_0) \frac{2}{\pi \sqrt{z^2 - D_i^2}} \tag{12.18}$$

An integration of (12.18) in the z-direction gives the heat flow per meter in a plane perpendicular to the (x, z)-plane. However, the integral diverges as the upper integration limit approaches infinity.

Consider two cases with different insulation depths D_i and D_i^o, other properties being equal. The difference in heat flux is given by two terms of the type (12.18). The integral of this difference over $D_i < z < \infty$ converges, so that:

$$q_m(D_i) - q_m(D_i^o) = \lambda (T_m - T_0) \cdot \frac{2}{\pi} \ln \left(\frac{D_i^o}{D_i} \right) \quad (D_i, D_i^o < H/2) \tag{12.19}$$

Here, $q_m(D_i)$ (W/m) is the heat loss per meter along the periphery of the store for the insulation depth D_i. It is assumed that D_i^o and D_i are relatively small compared with the storage depth H. It can be proved that it suffices for D_i and D_i^o to be smaller than $H/2$.

The heat loss directly to the ground for two different insulation depths is by (12.19) related by the following formula:

$$Q_m^{ground}(D_i) = Q_m^{ground}(D_i^o) + \lambda (T_m - T_0) L_i \cdot \frac{1}{\pi} \ln \left(\frac{D_i^o}{D_i} \right) \quad (D_i, D_i^o < H/2) \tag{12.20}$$

Here, L_i denotes the total length of the insulation in the horizontal plane. Eqs. (12.19-20) imply that the calculations of Q_m^{ground} need only to be done for one insulation depth.

Formula for an arbitrary insulation depth

The validity of (12.19) can be extended to an arbitrary insulation depth $0 < D_i \leq H$. The geometry of the heat conduction problem for the vertical cross-section is shown in figure 12.5.

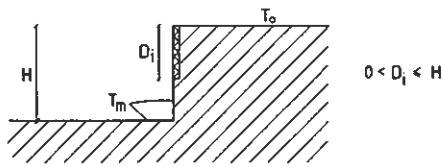

Figure 12.5. Geometry of the heat conduction problem for a vertical cross-section around the vertical insulation.

The difference in heat loss for two different relative insulation depths D_i/H and D_i^o/H is now (Claesson et al. 1985):

$$q_m\,(D_i/H) - q_m\,(D_i^o/H) = \lambda\,(T_m - T_0) \cdot \frac{1}{\pi} \ln\left(\frac{1-\xi_i^o}{1-\xi_i}\right) \tag{12.21}$$

where the functions ξ_i and ξ_i^o are given by the equations:

$$\frac{D_i}{H} = f\,(\xi_i) \quad \frac{D_i^o}{H} = f\,(\xi_i^o) \tag{12.22}$$

$$f(\xi) = \frac{1}{\pi} \cdot \left[\sqrt{1-\xi^2} + \operatorname{arccot}\left(\frac{\xi}{\sqrt{1-\xi^2}}\right)\right] \quad (0 \le \xi \le 1) \tag{12.23}$$

The function $f(\xi)$ is shown in figure 12.6. Approximations for certain values of ξ are also given. If D_i/H and D_i^o/H are less than 0.5, then (12.21) becomes equal to (12.19).

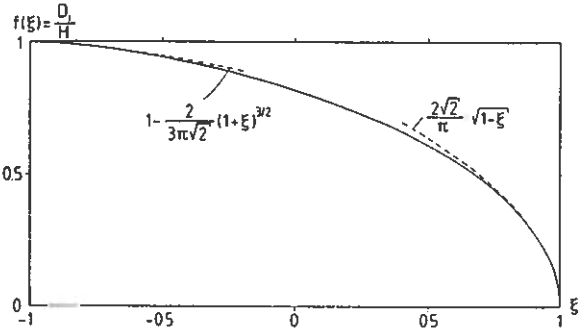

Figure 12.6. The function $f(\xi)$ of eq. (12.23).

The derivation of the solution (12.21-23) is not given here. The technique of conformal transformations is used (Carslaw and Jaeger 1959; section 16.6). The boundary of figure 12.5 is mapped on to the real axis, and then to a semi-infinite rectangle where the short side corresponds to the total insulation.

In the remainder of this section we will present calculations of the steady-state heat loss where the insulation depth often is taken to be $H/10$. We have:

$$\frac{D_i^o}{H} = 0.1 \qquad \xi_i^o = 0.988 \tag{12.24}$$

The heat loss for this case is by (12.21):

$$q_m\,(D_i/H) = q_m(0.1) + \lambda\,(T_m - T_0) \cdot g\,(D_i/H)$$

The function g is given in figure 12.7.

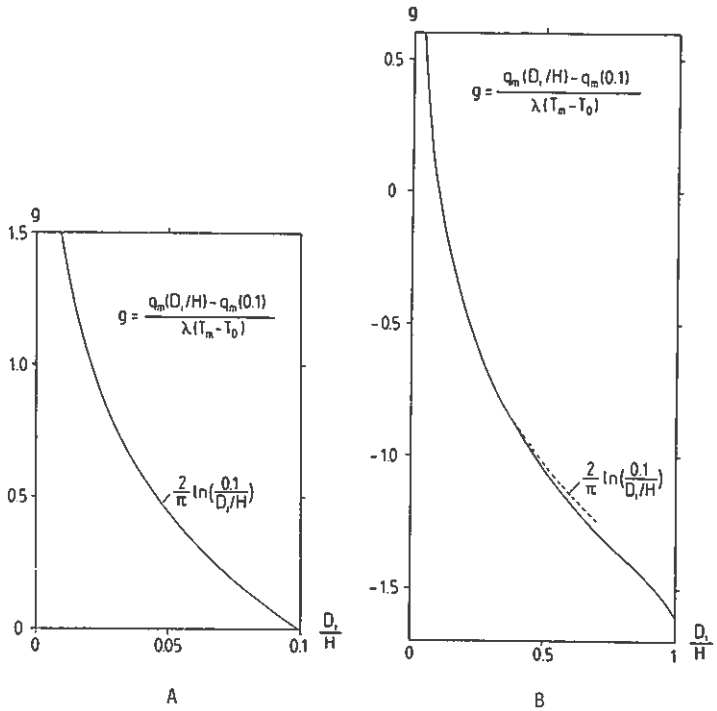

Figure 12.7. The function $g\,(D_i/H)$ that gives the heat loss relative to the heat loss for the insulation depth $D_i^o/H = 0.1$.

The heat loss from the uninsulated part of the store is now:

$$Q_m^{ground}\,(D_i/H) = Q_m^{ground}(0.1) + \lambda\,(T_m - T_0)\,L_i \cdot g\,(D_i/H) \qquad (12.25)$$

The function g is given in figure 12.7.

Vertical versus horizontal insulations at the side

The thermal insulation of the upper part of the vertical side of the store has been assumed to be in a vertical position. An alternative is to put the insulation on the ground surface, so that it extends horizontally from the side of the store. The two alternatives are shown in figure 12.8.

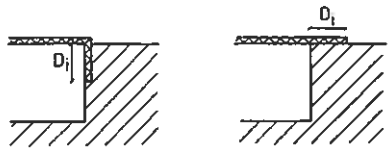

Figure 12.8. Vertical versus horizontal insulation of the upper side of the store.

The analyses presented above for the vertical case can be carried out in a similar way for the horizontal case. If the width of the insulations in the horizontal case is set equal to the depth D_i in the vertical case, we find that the heat flows from the store are the same for both cases. The formula (12.20) is still valid.

The conclusion is that, with regard to the steady-state heat losses, it does not matter if the thermal insulation of the upper part of the store is realized by putting the insulation vertically or horizontally.

12.2.3 Cylindrical heat store at the ground surface

The heat store has the shape of a cylinder with vertical symmetry axis. The upper boundary is located at the ground surface. The store reaches to the depth H and the radius of the cylindrical volume is R. The entire upper surface is thermally insulated. The insulation extends down a length D_i on the vertical side of the store. The insulation thickness is d_i and its thermal conductivity is λ_i. The temperature on the surface of the cylindrical volume is T_m, while the temperature at the ground surface is T_0. The temperature difference through the horizontal insulation is then $T_m - T_0$. Figure 12.9 shows a vertical cross-section through the store.

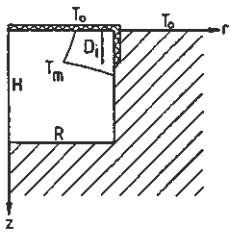

Figure 12.9. Cylindrical storage volume at the ground surface. The upper boundary and the upper part of the vertical side are thermally insulated.

Temperature field

The dimensionless steady-state temperature u is given by (12.7). It is zero at the ground surface and +1 on the cylindrical storage boundary. The radius of

the store is used as a scaling length: $L_s = R$. The dimensionless coordinates then become r/R and z/R. The temperature field in the ground is:

$$u(r/R, z/R) = \frac{T(r,z) - T_0}{T_m - T_0} \tag{12.26}$$

The dimensionless temperature field depends on the shape H/R and the relative depth D_i/H of the totally insulated part. The solution u has been calculated numerically for a large number of parameter values.

Figure 12.10 shows the isotherms for the case a cylindrical store with equal length and diameter, i.e. $H/R = 2$ (and $D_i/H = 0.1$).

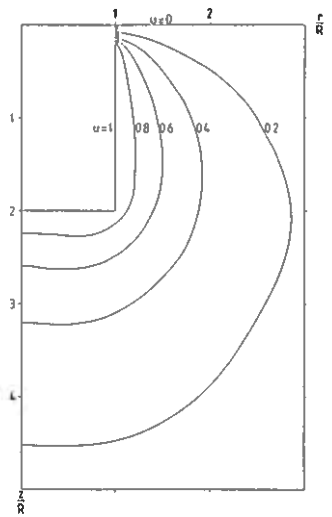

Figure 12.10. Isotherms for the dimensionless temperature u for the case of $H/R = 2$.

Total heat loss

The total steady-state heat loss from the cylindrical store consists, according to (12.12), of three components. Two components concern the heat loss through the insulated part, while the third part comes from the heat loss directly to the ground below the level $z = D_i$. The total heat loss may be written:

$$Q_m = Q_m^{insulation} + Q_m^{ground} \tag{12.27}$$

Heat loss through the insulated part of the store

The area A_i of the upper insulation and length of L_i of insulation on the side of the store becomes:

$$A_i = \pi R^2 \qquad L_i = 2\pi R \tag{12.28}$$

The heat loss through the insulated upper part of the store is by (12.17):

$$Q_m^{insulation} \approx \frac{\lambda_i (T_m - T_0)}{d_i} \cdot \left(\pi R^2 + \pi R D_i\right) \tag{12.29}$$

Heat loss from the uninsulated part of the store

General relations for the heat loss directly to the ground are discussed in section 12.2.1. The heat loss is obtained from a numerical calculation of the steady-state temperature field. It is assumed that there is no heat flow through the insulation on the vertical side. The remaining parameters of the problem are then the lengths R, H, and D_i. If the parameters are scaled with R, we have from (12.8-9):

$$Q_m^{ground} = \lambda (T_m - T_0)\, R \cdot h\,(H/R, D_i/H) \tag{12.30}$$

The heat loss factor h becomes a function of H/R and D_i/R, or H/R and D_i/H.

Insulation depth D_i = 2m

A reasonable value of the insulation depth is 2 meters. The heat loss directly to the ground is given as a function of R and H in figure 12.11, which shows $Q_m^{ground}/\lambda (T_m - T_0)$ or $R \cdot h\,(H, R, D_i = 2)$.

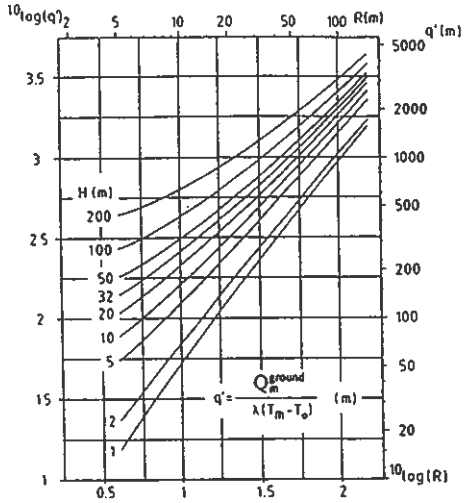

Figure 12.11. Heat loss directly to the ground as a function of radius R and depth H of a cylindrical heat store. The insulation depth D_i equals 2 m.

Insulation depth $D_i = H/10$

The heat loss factor h in (12.30) is shown in figure 12.12 as a function of the form factor H/R in the case of $D_i/H = 0.1$. It is also given in Table 12.1.

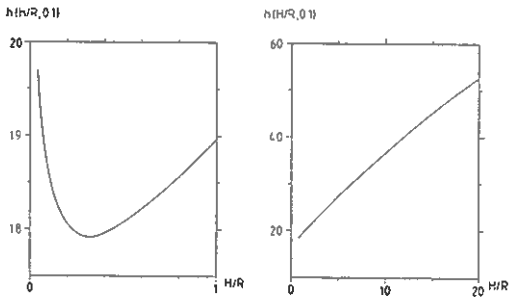

Figure 12.12. The heat loss factor h in (12.30) for a cylindrical store for $D_i/H = 0.1$.

TABLE 12.1. The heat loss factor h in (12.30) for a cylindrical store $D_i/H = 0.1$.

H/R	.04	.08	0.2	0.6	0.8	2	6	10	20
$h(H/R, 0.1)$	19.7	18.7	18.1	18.2	18.6	21.2	29.2	36.6	52.5

Arbitrary insulation depth D_i

The influence of the insulation depth is analyzed in section 12.2.2. It is demonstrated that the heat loss can be calculated from (12.18-25) for any insulation depth D_i, provided that the heat loss is known for one value of D_i.

For $D_i < H/2$ we have from (12.19) and (12.30) ($L_i = 2\pi R$):

$$Q_m^{ground} = \lambda (T_m - T_0) R \cdot [h(H/R, 0.1) + 4 \cdot \ln(0.1H/D_i)] \quad (0 < D_i < H/2) \tag{12.31}$$

For larger insulation depths, eq. (12.24) should be used instead:

$$Q_m^{ground} = \lambda (T_m - T_0) R \cdot [h(H/R, 0.1) + 2\pi g(D_i/H)] \quad (0 < D_i/H \leq 1) \tag{12.32}$$

The function g is given by figure 12.7.

12.2.4 Parallelepipedical heat store at the ground surface

The heat store has the shape of a parallelepiped with the upper boundary at the ground surface. See figure 12.13. The depth of the store is denoted H, while the length and the width are L and B, respectively. We will assume that $L \geq B$. The entire upper boundary is thermally insulated. The vertical

side of the store is insulated to the depth D_i. The temperature on storage boundary is T_m, and the temperature at the ground surface is T_0.

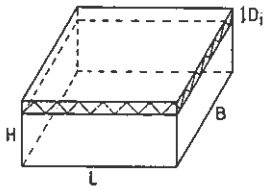

Figure 12.13. Parallelepipedical storage volume at the ground surface. The upper boundary and the upper part of the vertical side are thermally insulated.

Total heat loss

The heat loss through the thermally insulated parts is given by (12.17). The area of the upper surface and the length of insulation on the sides become:

$$A_i = L \cdot B \qquad L_i = 2L + 2B \tag{12.33}$$

The total heat loss from store is obtained from (12.17), (12.12), and (12.8). Using H as the scaling length yields:

$$\begin{aligned} Q_m &= (T_m - T_0)\{\lambda H \cdot h(L/H, B/H, D_i/H) + \\ &+ \frac{\lambda_i}{d_i}[LB + (L+B)\,D_i]\Big\} \end{aligned} \tag{12.34}$$

Heat loss from the uninsulated part of the store

Heat loss from the uninsulated part of the ground is determined by the heat loss factor, which is given in Table 12.2 for different parallelepipedical shapes of the store. The insulation depth D_i equals $H/10$.

TABLE 12.2. Heat loss factor $h(L/H, B/H, D_i/H)$ for a parallelepipedical heat store with $D_i/H = 0.1$.

B/H \ L/H	1/5	1/2	1	2	5	10
10						110
5					53.6	80.3
2				22.2	37.0	61.5
1			12.2	17.1	31.2	54.5
1/2		7.17	9.64	14.4	28.1	50.9
1/5	3.99	5.54	7.92	12.5	25.8	48.0

Comparison between cylindrical and parallelepipedical store

It is of interest to compare the heat loss from a parallelepipedical heat store with that of a cylindrical store. The depth of the store is H in both cases. The insulation depth D_i is taken to be $H/10$. The radius of the cylindrical store is chosen so that the volumes become equal:

$$\pi R^2 H = L\,B\,H \qquad R = \sqrt{\frac{LB}{\pi}} \tag{12.35}$$

We will only consider the heat loss through the uninsulated part of the store. The ratio between heat loss for the parallelepiped and the cylinder is denoted f. From (12.34) and (12.30) we then get:

$$f = \frac{Q_m^{ground}(parallelepiped)}{Q_m^{ground}(cylinder)} = \frac{H \cdot h^p(L/H, B/H, 0.1)}{R \cdot h^c(H/R, 0.1)} \tag{12.36}$$

where R is given by (12.35). The heat loss factors are given in Table 12.2 (h^p) and Table 12.1 (h^c). The ratio f is given in Table 12.3 for different shapes of the store.

TABLE 12.3. The ratio f defined by (12.36) between the heat loss for a parallelepipedical and a cylindrical store with the same volume and height.

B/H \ L/H	1/5	1/2	1	2	5	10
10						1.08
5					1.06	1.12
2				1.05	1.14	1.36
1			1.05	1.10	1.33	1.68
1/2		1.05	1.08	1.24	1.64	2.18
1/5	1.02	1.09	1.25	1.53	2.22	3.08

The heat losses through the uninsulated part are rather similar for the parallelepipedical and the cylindrical heat store provided that the length L and the width B do not differ too much. The difference is less than 8% for $L = B$. If the store is relatively deep, so that L/H and B/H become small, the difference is even smaller.

12.2.5 Cylindrical heat store below ground surface

The heat store has the shape of cylinder with vertical symmetry axis. The upper boundary of the store is at a depth D below the ground surface. The temperature is T_m on the storage boundary, and T_0 at the ground surface. See figure 12.14.

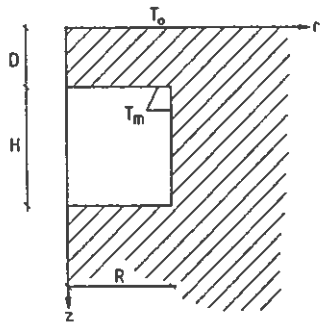

Figure 12.14. Cylindrical heat store at a depth D below the ground surface.

Temperature field

The dimensionless temperature u, which is defined by 12.7, is $+1$ on the storage boundary and zero at the ground surface. All lengths are scaled with the depth D to the upper storage boundary. The temperature field will depend on the two dimensionless parameters R/D and H/D. The heat flow problem has been solved numerically (Eftring and Claesson 1978). The results for three cases with different geometries are shown in figure 12.15. The three figures give a good picture of the thermal influence around a ground heat store. The range of influence depends on the linear dimensions of the store.

The ground is assumed to be homogeneous with constant thermal conductivity in these three examples. Figure 12.16 shows a case where the ground consists of three layers. The thermal conductivities of the three layers are

given in the figure. The geometry is the same as for figure 12.15:A.

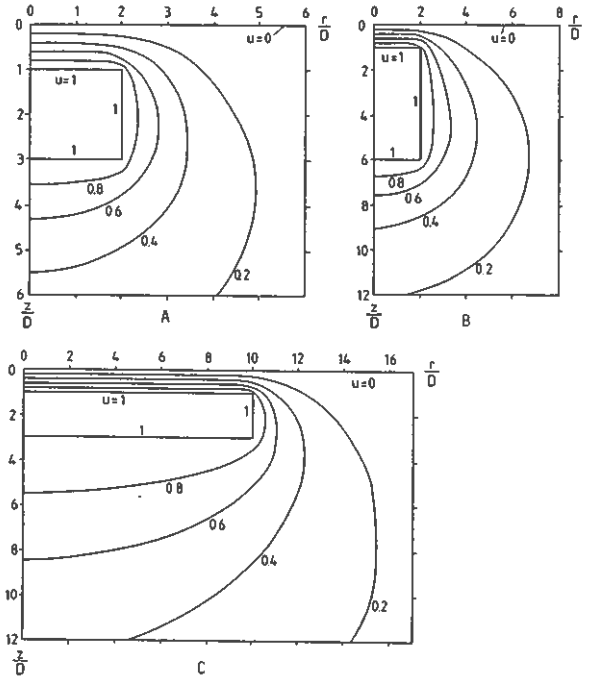

Figure 12.15. Dimensionless temperature field around a cylindrical heat store below the ground surface. A: $R/D = 2, H/D = 2$. B: $R/D = 2, H/D = 5$. C: $R/D = 10, H/D = 2$.

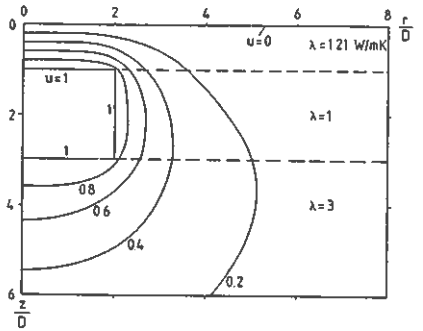

Figure 12.16. Dimensionless temperature field around a cylindrical heat store below the ground surface. There are three ground layers with different thermal conductivity $R/D = 2, H/D = 2$.

The temperature fields of figure 12.16 and 12.15A are similar in appearance. The isotherms in the heterogeneous case are just slightly more spread

out, even though the thermal conductivity of the lowest layer is considerably higher.

Heat losses

The heat losses from the cylindrical store below the ground surface are of the type (12.7). Using the depth D as the scaling length yields:

$$Q_m = \lambda (T_m - T_0) D \cdot h(R/D, H/D) \tag{12.37}$$

The heat loss factor h is given in Table 12.4 for some values of R/D and H/D. Each value is obtained from a numerical calculation of the steady-state temperature field.

TABLE 12.4. Heat loss factor h for a cylindrical store below the ground surface. Eq. (12.37).

	R/D						
H/D	1	2	3	5	10	15	20
20	63			230	569	1064	1716
15	54			213	547	1038	1686
10	43			194	521	1006	1649
5	31	57	89	171			
4	28	53	84	165			
2	21	44	73	150	456	923	1549
1	17	32	66	140			

12.2.6 Temperature on and near the storage boundary

The temperature difference $T_m - T_0$ must be estimated in order to calculate the steady-state heat loss.

The temperature T_0 at the ground surface may be obtained from meteorological data. Usually, the annual average values of the air temperature and the ground surface differ by a few degrees. This difference depends mainly on the amount of snow and the duration of the snow cover. The snow has an insulating effect during the cold part of the year, thus the average temperature at the ground surface will be slightly higher than in the air. The temperature of ground water at a depth of 5-10 meters, where seasonal variations are small, can also be used. The best value of T_0 is to use a measured average value during the year in the ground at, say, 1 m depth. For heat stores that reaches a large depth, it may be necessary to account for the increase of the ground temperature with depth. The average of the undisturbed ground temperature at the mean storage depth is an appropriate estimate.

It is more difficult to make an estimate of the average temperature T_m on the storage boundary. The value of T_m will usually increase during the

period of thermal build-up. It should be an average value that represents the long-term storage conditions.

Areskoug and Claesson (1981) present a method by which the temperature T_m may be calculated. It is assumed that the spatial variation of the fluid temperatures between different ground heat exchangers is small. There is one average temperature $T_m^{insulation}$ for the insulated part of the storage boundary, and one average temperature T_m^{ground} for the part that is exposed directly to the surrounding ground.

The method uses a one-dimensional approximation of the thermal process at the storage boundary. It is assumed that the heat flow both on the inside and on the outside of the store is in a direction perpendicular to the storage boundary. The uninsulated boundary is shown in figure 12.17.

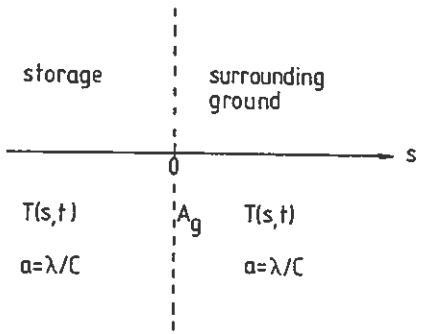

Figure 12.17. One-dimensional approximation of the thermal process at the storage boundary.

The coordinate along an axis perpendicular to the storage boundary is denoted s. The area of the uninsulated part of the storage boundary is A_g.

The heat injection from the ground heat exchangers is treated like a source term. The steady-state heat equation (6.9) becomes with (12.3):

$$\lambda \frac{d^2T}{ds^2} + \frac{\lambda}{\ell^2}[T_{f0} - T(s)] = 0 \quad (s < 0) \tag{12.38}$$

where T_{f0} is the average fluid temperature during the cycle. The heat transfer length ℓ is determined by the properties of the ground heat exchanger. See eq. (12.4) and chapter 9. The solution is

$$T(s) = T_{f0} - \beta_1 \cdot e^{+s/\ell} \tag{12.39}$$

The heat loss q_m (W/m^2) at the boundary is

$$q_m = -\lambda \frac{dT}{ds}|_{s=0} \tag{12.40}$$

which gives

$$\beta_1 = \frac{\ell}{\lambda} q_m$$

Thus we have

$$T(s) = T_{f0} - \frac{\ell}{\lambda} q_m e^{+s/\ell} \quad (s < 0) \tag{12.41}$$

This equation offers an interpretation of the heat transfer length. At the storage boundary, $s = 0$, (12.41) yields:

$$q_m = \lambda \frac{T_{f0} - T_m^{ground}}{\ell} \tag{12.42}$$

The heat transfer length ℓ corresponds to the thickness of a surface insulation between the fluid and the boundary. The heat loss through the uninsulated part of the ground becomes:

$$Q_m^{ground} = \lambda \frac{T_{f0} - T_m^{ground}}{\ell} \cdot A_g \tag{12.43}$$

The heat loss through the insulated part may be derived in a similar way (Areskoug and Claesson 1981). The final expression is:

$$Q_m^{insulation} = \frac{T_{f0} - T_0}{\frac{\ell}{\lambda} + \frac{d_i}{\lambda_i}} \cdot A_i \tag{12.44}$$

where the insulation has a thickness d_i and a thermal conductivity λ_i.

Eq. (12.30) gives an expression for the steady-state heat loss from a cylindrical heat store based on the temperature difference $T_m^{ground} - T_0$. The temperature on the storage boundary can be eliminated by use of (12.43), which implies:

$$Q_m^{ground} = \lambda \frac{T_{f0} - T_0}{\ell + \ell_g} \cdot A_g \tag{12.45}$$

where

$$\ell_g = \frac{A_g}{R \cdot h(H/R, D_i/H)} \tag{12.46}$$

The steady-state loss can now be calculated from eqs. (12.43-46) if the average fluid temperature during the cycle is known. The total steady-state heat loss is, by (12.27), simply the sum of the two components (12.44) and (12.45-46).

It is sometimes of interest to know mean temperature *in* the storage volume during a cycle. Eq. (12.3) gives a relation between the fluid mean temperature and this mean storage temperature T_{ms}. Inserting the steady-state heat loss gives:

$$T_{ms} = T_{f0} - \frac{Q_m \ell^2}{\lambda V} \tag{12.47}$$

12.3 Transient thermal build-up process

The temperature in the ground is essentially at its undisturbed level T_0 when the heat storage process begins. The storage temperature is then raised to its operational level. The heat flow from the store to surrounding ground gives a transient *thermal build-up* of the temperature field during the initial years. We will consider the case the temperature on the storage region boundary instantly increased to T_m at the time $t = 0$. The ensuing transient heat flow from the store is denoted Q_{tr} (W). The heat flow gradually approaches steady-state conditions. The steady-state thermal process has been treated in section 12.2.

12.3.1 Temperature on storage boundary

The temperature on the storage boundary determines the heat loss to the surrounding ground. This temperature varies in time and space on the surfaces of the store. In the analysis presented here, the boundary temperature is represented by a suitable average value T_m during the considered time period, cf. section 12.2.6.

12.3.2 Transient temperature field

Figure 12.18 illustrates the transient thermal build-up process for a cylindrical heat store at the ground surface.

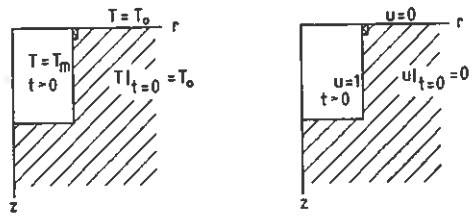

Figure 12.18. Transient thermal process for a cylindrical heat store at the ground surface. The temperature on the storage boundary is increased to T_m at $t = 0$. The dimensionless formulation of the problem is shown on the right.

The dimensionless temperature u is defined by

$$u = \frac{T - T_0}{T_m - T_0} \tag{12.48}$$

It will be +1 on the storage boundary and 0 at the ground surface. The initial value of u is zero. The conditions valid for u is illustrated on the right-hand side of figure (12.18).

The temperature u depends on the spatial coordinates and the time. A length L_s is used for scaling of the spatial coordinates in the dimensionless formulation. The dimensionless time becomes at/L_s^2, where a is the thermal diffusivity of the ground. The functional dependence of the dimensionless temperature is:

$$u = u\left(\frac{x}{L_s}, \frac{y}{L_s}, \frac{z}{L_s}, \frac{at}{L_s^2}\right) \tag{12.49}$$

Figure 12.19 shows the transient process in the ground outside a cylindrical heat store at the ground surface. The store reaches a depth H and has the diameter $2R$. The thermal insulation extends to the depth $D_i = 0.1\,H$. This calculation presupposes that there is no heat flow through the thermal insulation. The influence of the insulation is rather local. It does not affect the thermal process on a global scale.

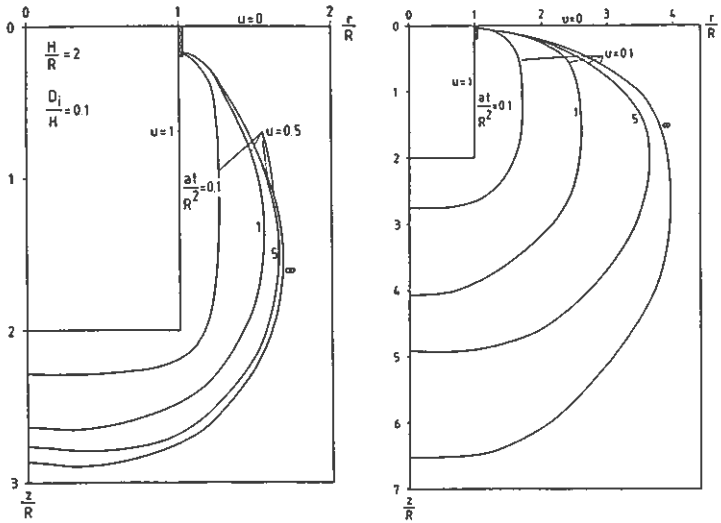

Figure 12.19. Transient thermal process outside a cylindrical heat store. Left: the isotherm $u = 0.5$, right: the isotherm $u = 0.1$. The isotherms are given for different dimensionless times at/R^2.

The radius R of the store is used as a scaling length. The dimensionless temperature becomes a function of $r/R, z/R$, and at/R^2. Figure 12.19 (left) shows the isotherm $u = 0.5$ at different times, while the evolution of the isotherm $u = 0.1$ is shown on the right. The isotherm $u = 0.5$ approaches the steady-state value at $at/R^2 = \infty$ much faster than the isotherm $u = 0.1$.

Let us consider three storages of different size in order to quantify the time-scale of transient process. The thermal diffusivity a is taken to be $1.0 \cdot 10^{-6}$ m^2/s.

Size	Time-scale
R = 10 m (H = 20 m)	R^2/a = 3.2 years
R = 20 m (H = 40 m)	R^2/a = 13 years
R = 50 m (H = 100 m)	R^2/a = 79 years

The smallest store gives a time-scale of 3 years for the transient process. The time-scale for the largest store is almost 100 years.

12.3.3 Transient heat loss

The transient heat loss through the storage boundary is denoted $Q_{tr}(t)$ (W). The subscript tr will be used for this type of transient process. In a plane cross-section, the heat flow per unit length perpendicular to the plane is $q_{tr}(t)$. We also use $q_{tr}(t)$ to denote the heat flow per unit length of a cylinder. In the plane, one-dimensional case, $q_{tr}(t)$ is the heat flow per unit area. The dimension of $q_{tr}(t)$ is either W/m or W/m^2.

Dimensionless formulation

The transient heat loss is directly proportional to the thermal conductivity λ in the ground and to the temperature difference $T_m - T_0$. The transient heat loss is, just as the steady-state heat loss, proportional to the scaling length L_s. The heat loss becomes a function of dimensionless time at/L_s^2 and scaled parameters like L_1/L_s, etc. We have:

$$Q_{tr}(t) = \lambda (T_m - T_0) L_s \cdot h_{tr} \left(at/L_s^2, L_1/L_s, \ldots \right) \quad \text{(W)} \tag{12.50}$$

where h_{tr} is the dimensionless heat loss factor. The value approaches the steady-state heat loss factor h as time goes to infinity.

In a plane cut we get:

$$q_{tr}(t) = \lambda (T_m - T_0) \cdot h_{tr} \left(at/L_s^2, \ldots \right) \quad \text{(W/m)} \tag{12.51}$$

It should be noted that there is no multiplicative length factor L_s in a two-dimensional case.

The one-dimensional case gives:

$$q_{tr}(t) = \frac{\lambda (T_m - T_0)}{L_s} \cdot h_{tr} \left(at/L_s^2, \ldots \right) \quad \text{(W/m}^2\text{)} \tag{12.52}$$

The accumulated heat loss E_{tr} expressed in dimensionless form becomes:

$$E_{tr} = C\,(T_m - T_0)\,L_s^3 \cdot e_{tr}\left(at/L_s^2, \ldots\right) \quad \text{(J)} \tag{12.53}$$

Here, e_{tr} denotes the dimensionless accumulated heat loss. The volumetric heat capacity in the ground is C ($a = \lambda/C$). In the two-dimensional case we have:

$$E_{tr} = C\,(T_m - T_0)\,L_s^2 \cdot e_{tr}\left(at/L_s^2, \ldots\right) \quad \text{(J/m)} \tag{12.54}$$

Finally, the plane, one-dimensional case gives:

$$E_{tr} = C\,(T_m - T_0)\,L_s \cdot e_{tr}\left(at/L_s^2, \ldots\right) \quad \text{J/m}^2 \tag{12.55}$$

The heat loss approaches the constant steady-state value as time goes to infinity. The accumulated heat loss then increases as $Q_m \cdot t$ or $q_m \cdot t$, i.e. a linear increase with time.

Cylindrical heat store at the ground surface

The heat store has the shape of a cylinder with upper boundary at the ground surface. The depth of store is H, and its radius is R. The vertical side is fitted with thermal insulation to a depth D_i. We will only consider the case where $D_i = 0.1H$. There is no heat flow through the thermal insulation.

The radius R is used as scaling length L_s. The accumulated, dimensionless heat flow e_{tr} becomes a function of the dimensionless time at/R^2. The shape factor H/R is the only other parameter, since there is no heat flow through the insulation, and the insulation depth D_i is equal to the depth $0.1H$. We have from (12.53):

$$E_{tr} = C\,(T_m - T_0)\,R^3 \cdot e_{tr}\left(\frac{at}{R^2}, \frac{H}{R}\right) \tag{12.56}$$

Numerically computed values of e_{tr} are shown in figure 12.20. The increase becomes linear after some time. The thermal process is then essentially in steady-state conditions.

The graphs are valid for an insulation depth $D_i = 0.1H$. However, the results may be used for other insulation depths as well. The steady-state heat flow Q_m varies with the insulation depth according to the formulas given in section 12.2.2. The difference between Q_{tr} and Q_m becomes approximately independent of D_i, since the insulation depth only influences a small region near the side. We have the following approximation:

$$(Q_{tr} - Q_m)|_{D_i} \approx (Q_{tr} - Q_m)|_{D_i = 0.1H} \tag{12.57}$$

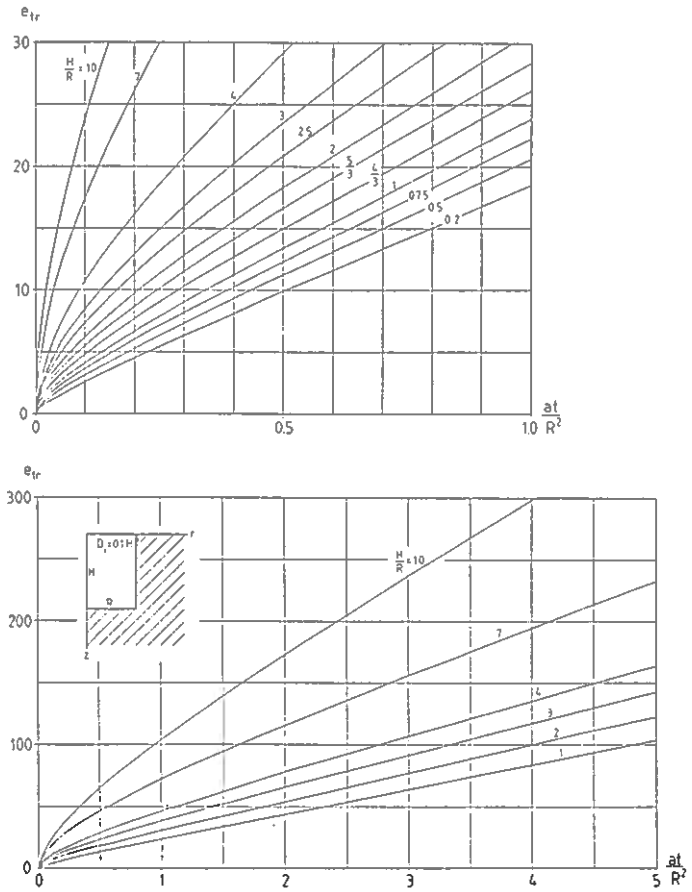

Figure 12.20. Transient, accumulated heat loss from a cylindrical store at the ground surface. Eq. (12.56).

Inserting eq. (12.25) then gives:

$$Q_{tr}|_{D_i} \approx Q_{tr}|_{D_i=0.1H} + \lambda\,(T_m - T_0)\,L_i \cdot g\,(D_i/H) \tag{12.58}$$

Therefore, it is sufficient to perform the calculations for $D_i = 0.1H$. The factor g is shown in figure 12.7. The length of the insulation around the store is L_i.

Plane, one-dimensional case

The plane, one-dimensional case for a semi-infinite region is illustrated in figure 12.21.

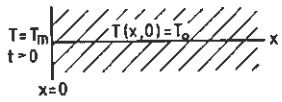

Figure 12.21. Plane, one-dimensional case.

The solution is given by the well-known error function:

$$u = \operatorname{erfc}\left(\frac{x}{\sqrt{4at}}\right) \tag{12.59}$$

The heat flow through the boundary $x = 0$ with an area A becomes:

$$Q_{tr}(t) = A \cdot q_{tr}(t) = A \cdot \frac{\lambda (T_m - T_0)}{\sqrt{\pi at}} \qquad \text{(W)} \tag{12.60}$$

These formulas are quite useful, since the thermal process often is essentially plane during the initial time period.

The accumulated heat flow is given by:

$$E_{tr}(t) = C\,(T_m - T_0)\sqrt{\frac{4at}{\pi}} \quad \text{(J/m}^2\text{)} \tag{12.61}$$

Cylindrical surface

The transient thermal process in the region bounded internally by a cylindrical surface is an important case. The surface is at the radius R. The thermal process takes place in the transverse direction from the cylinder axis. This problem has been treated in section 10.1.

The heat flow per unit length of the cylinder axis is:

$$q_{tr} = \lambda (T_m - T_0) \cdot h_{tr}\left(at/R^2\right) \quad \text{(W/m)} \tag{12.62}$$

The heat loss factor h_{tr} is shown in figure 12.22.

For small values of time there is the approximation:

$$h_{tr}(t) \approx 2\pi\left(\frac{1}{\sqrt{\pi\tau}} + \frac{1}{2} - \frac{1}{4}\sqrt{\frac{\tau}{\pi}} + \frac{\tau}{8}\right) \qquad \left(\tau = \frac{at}{R^2} < 0.5\right) \tag{12.63}$$

The error is less 2% for the specified range of validity.

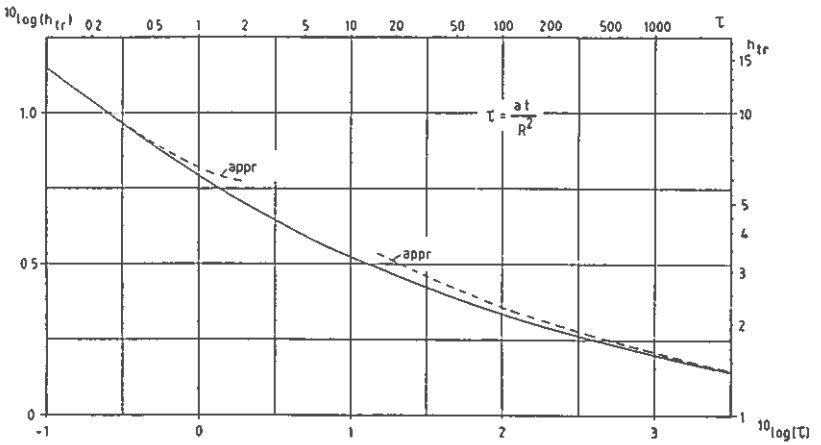

Figure 12.22. Transient heat loss factor for a cylindrical surface. Eq. (12.62) with the approximations (12.63) and (12.64).

The heat loss factor for large times is approximately

$$h_{tr}(\tau) \approx \frac{4\pi(\ln\tau - 0.345)}{(\ln\tau + 0.232)^2} \qquad \left(\tau = \frac{at}{R^2} > 1500\right) \tag{12.64}$$

The error is less than 2% in the given interval.

12.4 Periodic thermal process

In this section we will treat the periodic part of the thermal process. The general equations for periodic processes are given in section 6.1.3. The period time is denoted t_p. Any periodic variation can be expanded in Fourier series, so that regular harmonic components are obtained. These components will have the period time $t_p, t_p/2, t_p/3$, etc.

12.4.1 Plane surface

The periodic process at a plane boundary is the simplest case, yet applicable to many situations. See figure 12.23.

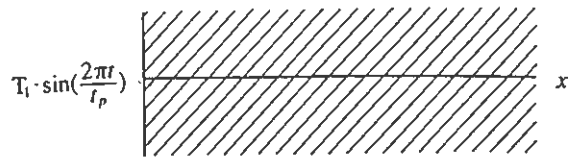

Figure 12.23. Periodic variation in the plane, semi-infinite case.

The plane surface is located at $x = 0$, and the ground extends to infinity in the positive x-direction. The temperature in the ground is given by (Carslaw and Jaeger 1959; p. 65):

$$T(x,t) = T_1 \cdot e^{-x/d_p} \cdot \sin\left(\frac{2\pi t}{t_p} - \frac{x}{d_p}\right) \tag{12.65}$$

where the depth d_p is:

$$d_p = \sqrt{\frac{at_p}{\pi}} \tag{12.66}$$

We will also give the complex-valued solution, cf. section 6.1.3. The complex temperature at $x = 0$ is:

$$T(0,t) = \hat{T}_1 \cdot e^{2\pi i t/t_p} \tag{12.67}$$

Here, $\hat{T}_i$ is a complex number. The complex-valued solution becomes (Carslaw and Jaeger 1959; p. 65):

$$T(x,t) = \hat{T}_1 \cdot e^{-(1+i)x/d_p} \cdot e^{2\pi i t/t_p} \tag{12.68}$$

The real-valued solutions are given by the real and imaginary parts, cf. section 6.1.3. The solution (12.65) is obtained by setting $\hat{T}_1 = T_1$ and taking the imaginary part of (12.68). The absolute value of the temperature (12.68) is:

$$|T| = |\hat{T}_1| \cdot e^{-x/d_p} \tag{12.69}$$

The periodic temperature variation is attenuated by the exponential factor e^{-x/d_p}. The amplitude is $|\hat{T}_1|$ at $x = 0$. The length d_p will be called the *penetration depth* for the periodic variation. At the depth d_p, the amplitude

has been diminished to $e^{-1} = 0.37$ of the amplitude $|\hat{T}_1|$. Only 5% of the amplitude remains at a depth $3d_p$ from the boundary.

The phase of the periodic variation is given by the factor

$$e^{i\left(2\pi t/t_p + \arg(\hat{T}_1) - x/d_p\right)} \tag{12.70}$$

The term $-x/d_p$ results in an increasing phase lag away from the boundary. The variation is in anti-phase in relation to the boundary temperature when $x/d_p = \pi$.

The penetration depth d_p depends on the thermal diffusivity a and the period time t_p. The penetration depth is given for three values of a and several period times in Table 12.5.

TABLE 12.5. Penetration depth d_p for different period times t_p.

	t_p							
a (m^2/s)	1 sec	1 min	1 h	24 h	1 week	1 month	1 y	5 y
$1.6{\cdot}10^{-6}$	0.0007	0.006	0.043	0.21	0.55	1.16	4.0	9.0
$1.0{\cdot}10^{-6}$	0.0006	0.004	0.034	0.17	0.44	0.91	3.2	7.1
$0.4{\cdot}10^{-6}$	0.0004	0.003	0.021	0.10	0.28	0.58	2.0	4.5

The heat flow (W/m^2) at the boundary becomes with (12.68):

$$-\lambda \left.\frac{\partial T}{\partial x}\right|_{x=0} = -\lambda \cdot \hat{T}_1 \cdot (-)\frac{1+i}{d_p} e^{2\pi i t/t_p} \tag{12.71}$$

which may be expressed as a complex-valued heat flow:

$$\hat{q}_1 = \frac{\lambda(1+i)}{d_p}\hat{T}_1 \tag{12.72}$$

The relation between the amplitude of heat flow and temperature is then:

$$|\hat{q}_1| = \frac{\lambda\sqrt{2}}{d_p}\left|\hat{T}_1\right| \tag{12.73}$$

The argument of $1 + i$ is $\pi/4$. The maximum temperature occurs at a time $t_p/8$ after the maximum heat flow.

The heat flow is also the time derivative of the accumulated amount energy $\hat{e}_1$ that pulsates through the boundary, hence

$$\hat{e}_1 = \frac{t_p}{2\pi i}\hat{q}_1 \tag{12.74}$$

The accumulated amount of energy is then from (12.72) and (12.74):

$$\hat{e}_1 = \frac{C d_p}{1+i}\hat{T}_1 \quad (\mathrm{J/m^2}) \tag{12.75}$$

By taking, for instance, the imaginary part of (12.72) and (12.75) we get the following real valued expressions:

$$\begin{aligned} &\text{Boundary temperature:} && T_1 \cdot \sin\left(\frac{2\pi t}{t_p}\right) \\ &\text{Boundary heat flow:} && T_1 \cdot \frac{\lambda\sqrt{2}}{d_p} \cdot \sin\left(\frac{2\pi t}{t_p} + \frac{\pi}{4}\right) \\ &\text{Accumulated heat:} && T_1 \cdot \frac{C d_p}{\sqrt{2}} \cdot \sin\left(\frac{2\pi t}{t_p} - \frac{\pi}{4}\right) \end{aligned} \tag{12.76}$$

12.4.2 Cylindrical surface

The radius of the cylindrical surface is R. At the boundary $r = R$ there is a periodical temperature variation, which in complex notation is expressed by:

$$T(R,t) = \hat{T}_1 \cdot e^{2\pi i t/t_p} \tag{12.77}$$

The analytical solution that gives the temperature field in the ground $r \geq R$ is treated in section 11.3. Here, we will assume that the radius R is large compared to the penetration depth d_p defined by (12.66). The approximations (11.14) can then be used. The temperature is then:

$$T(r,t) \approx \hat{T}_1 \cdot \sqrt{\frac{R}{r}} \cdot e^{-(r-R)/d_p} \cdot e^{i(2\pi t/t_p - (r-R)/d_p)} \quad (R \geq 5d_p) \tag{12.78}$$

The maximum error for $r \geq R \geq 5d_p$ is 1%. Eq. (12.78) has, with $x = r - R$, the same form as (12.68) for the plane case. The only difference is the additional factor $\sqrt{R/r}$.

The amplitude is attenuated by the factor:

$$\sqrt{\frac{R}{r}} e^{-(r-R)/d_p} \quad (R > d_p) \tag{12.79}$$

with a maximum error of 4% for $r \geq R > d_p$.

The complex-valued relation between the temperature and the heat flow at the boundary $r = R$ is from (11.24) for any radius R given by:

$$\hat{T}_1 = \frac{1}{2\pi\lambda} A(R') e^{-iB(R')} \cdot \hat{q}_1 \tag{12.80}$$

where $A(R')$ and $B(R')$ are shown in figure 11.1 and Table 11.1. The dimensionless radius R' is defined by $R\sqrt{2}/d_p$ in accordance with (11.5). Note that $\hat{q}_1$ is the heat flow per unit axial length of the cylindrical surface.

For large values of R', eq. (12.80) can be approximated by:

$$\hat{T} \cdot 2\pi\lambda R \left(\frac{1+i}{d_p} + \frac{1}{2R} \right) \approx \hat{q}_1 \quad (R < d_p) \tag{12.81}$$

The maximum error of the absolute value is a few percent. The maximum error of the argument, or the phase time, is slightly larger.

Real-valued expressions may be obtained by taking the imaginary part of (12.77) and (12.80)

$$\text{Boundary temperature:} \quad T_1 \cdot \sin\left(\frac{2\pi t}{t_p}\right) \tag{12.82}$$

$$\text{Boundary heat flow:} \quad T_1 \cdot \frac{2\pi\lambda}{A(R')} \cdot \sin\left[\frac{2\pi t}{t_p} + B(R')\right]$$

12.4.3 Heat store at the ground surface

In this section we will give the periodic heat flow through the boundary of a ground heat store. The store has its upper boundary at the ground surface. There is thermal insulation on the entire upper surface and to a depth D_i on the vertical side.

The periodic temperature on the storage boundary is denoted $\hat{T}_1$. Above the insulation on the ground surface, there is the periodic temperature $\hat{T}_a$. The situation is depicted in figure 12.24.

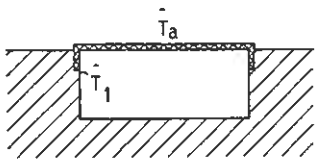

Figure 12.24. Periodic thermal process for a heat store at the ground surface.

The periodic heat flow $\hat{Q}_1$ through the storage boundary has two components; the heat flow through the insulated part and the heat flow directly to the ground in the uninsulated part:

$$\hat{Q}_1 = \hat{Q}_1^{insulation} + \hat{Q}_1^{ground} \tag{12.83}$$

The temperature difference over the insulating layer is $\hat{T}_1 - \hat{T}_a$. The insulation covers an area A_i on the storage boundary. The periodic heat flow through the insulation is then:

$$\hat{Q}_1^{insulation} = A_i \cdot \left(\hat{T}_1 - \hat{T}_a\right) \frac{\lambda_i}{d_i} \tag{12.84}$$

The temperature difference over the insulation on the vertical sides will be slightly lower, due to the influence of the ground. This can be neglected if D_i is just a few meters and if the insulation is relatively thick. The thermal resistance of the ground is then small compared with that of the insulation. Eq. (12.84) can then be used for the whole insulated surface of the storage boundary.

The uninsulated parts of the storage boundary have a surface area A_g. The heat loss from plane surfaces has been treated in section 12.4.1, and the heat loss from a cylindrical surface in section 12.4.2. These expressions may be used provided that the extension of the surfaces are large compared to the penetration depth so that the periodic thermal process becomes essentially one-dimensional in the direction perpendicular to the surface. This will not be true near the edges of plane and cylindrical surfaces, where the process becomes two-dimensional, or even three-dimensional near corners.

The extra heat loss due to the two-dimensional process perpendicular to an edge line, where two plane surfaces meet at right angle may be accounted for by a simple formula (Claesson et al. 1985). We will not give any details here but just use the result. The extra heat loss is $\lambda \hat{T}_1 \cdot 0.602$ (W/m). This value is multiplied by the total length L_e (edge) of the edge.

For a *cylindrical* heat store with the radius R and the depth H, we have:

$$\begin{aligned} A_i &= \pi R^2 + 2\pi R D_i \\ L_e &= 2\pi R \end{aligned}$$

There are four contributions to the total heat flow: 1. Heat flow through the insulation; 2. Heat flow through the lower horizontal boundary with area πR^2; 3. Additional heat flow due to the effect of the lower circular edge of the cylindrical store ; 4. Heat flow through the cylindrical surface with the length $H - D_i$. The total heat flow becomes from (12.84), (12.72), and (12.80):

$$\hat{Q}_1 = \left(\hat{T}_1 - \hat{T}_a\right) \frac{A_i \lambda_i}{d_i} + \hat{T}_1 \cdot \lambda \left[\pi R^2 \cdot \frac{1+i}{d_p} + 2\pi R \cdot 0.6 + (H - D_i) \frac{2\pi}{A(R')} e^{iB(R')} \right] \tag{12.85}$$

The corresponding relations for a *parallelepipedical* heat store with the length L, the width B, and the depth H become:

$$\begin{aligned} A_i &= LB + 2(B+L)D_i \\ A_g &= LB + 2(B+L)(H - D_i) \\ L_e &= 2L + 2B + 4(H - D_i) \end{aligned} \tag{12.86}$$

The total heat flow is then from (12.84) and (12.72):

$$\hat{Q}_1 = \left(\hat{T}_1 - \hat{T}_a\right) \frac{A_i \lambda_i}{d_i} + \hat{T}_1 \cdot \lambda \left(A_g \frac{1+i}{d_p} + L_e \cdot 0.6 \right) \tag{12.87}$$

The last term is the additional heat loss due to the influence of the edges between the plane surfaces (Claesson et al. 1985).

12.5 Model with steady-state and periodic components

Areskoug and Claesson (1981) have developed a model of the thermal process in a ground heat store. The results of the model are presented here without derivation and detailed explanations. The thermal process has a steady-state and periodic component.

Figure 12.25 gives a schematic picture of the heat store. The upper boundary of the heat store is at the ground surface. There is thermal insulation on the upper surface and down to a depth D_i on the vertical side of the store. The insulation has a thickness d_i and its thermal conductivity is λ_i. The insulated part of the store has an area A_i, while the area of uninsulated part is A_g. In the ground, the thermal conductivity and the volumetric heat capacity is λ and C, respectively.

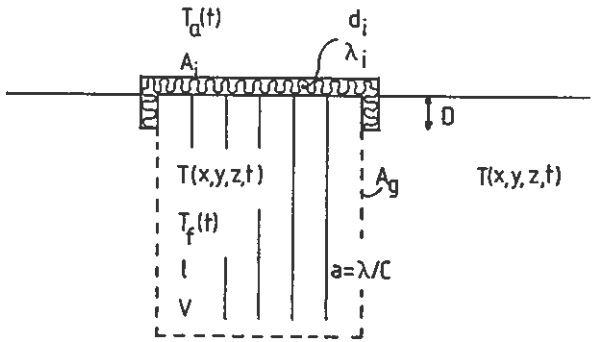

Figure 12.25. Ground heat store at the ground surface. Nomenclature according to the text.

12.5.1 Relation between heat injection rate and fluid temperature

The temperature is a superposition of a steady-state and a periodic component. Using complex rotation, the fluid temperature T_f in the ground heat exchangers and ground surface temperature T_a may be written:

$$\begin{aligned} T_f(t) &= T_{f0} + T_{f1} \cdot e^{i\phi_f} \cdot e^{i2\pi t/t_p} \\ T_a(t) &= T_{a0} + T_{a1} \cdot e^{i\phi_a} \cdot e^{i2\pi t/t_p} \end{aligned} \qquad (12.88)$$

where T_{f1} and T_{a1} are the amplitudes of the periodic parts. The relative phase lags are ϕ_f and ϕ_a. The period time is t_p.

The fluid temperature T_f is defined by (6.33) as the average of the inlet temperature $T_{fin}(t)$ and the outlet temperature $T_{fout}(t)$:

$$T_f = \frac{1}{2}(T_{fin} + T_{fout}) \tag{12.89}$$

The inlet and outlet temperature at a given time are, according to (6.35), given by

$$\begin{aligned} T_{fin}(t) &= T_f(t) + \frac{Q(t)}{2C_f V_f} \\ T_{fout}(t) &= T_f(t) + \frac{Q(t)}{2C_f V_f} \end{aligned} \tag{12.90}$$

The expressions contain the total heat injection rate $Q(t)$, the volumetric heat capacity C_f of the fluid, and the flow rate V_f (m^3/s). The total heat injection rate is given by the steady-state component and a periodic variation:

$$Q(t) = Q_m + Q_1 \cdot e^{i\phi_q} e^{i2\pi t/t_p} \tag{12.91}$$

The heat equations for the global thermal process are solved with use of one-dimensional approximations. The heat flow around the storage boundaries is assumed to be in the normal direction to the boundary surface. The influence of edges is neglected. The thermal interaction between different boundary surfaces has a small influence on the temperature distribution in the store. The heat flows through the insulated and uninsulated parts of the storage boundary are treated separately. The model assumes that the linear dimensions of store correspond to a couple of penetration depths d_p.

The following notations are used:

$$\begin{aligned} d_0 &= \sqrt{\frac{at_p}{2\pi}} \quad (= d_p/\sqrt{2}) \\ \beta &= \sqrt{d_0^2 + i\ell^2} = be^{i\psi} \\ \gamma &= \frac{1}{\sqrt{1/\ell^2 + i/d_0^2}} \quad (\Re\gamma \geq 0) \\ m^1 &= \frac{\lambda}{d_0} \cdot \frac{d_i}{\lambda_i} \end{aligned} \tag{12.92}$$

Note that d_p is here defined with a factor 2 in the denominator. The heat transfer length ℓ is given by (12.4) and the formulas presented in chapter 9.

The heat transfer between the heat carrier fluid and the store has five contributions. A derivation of these contributions is found in (Areskoug and Claesson 1981). The steady-state part is given in section 12.2.6. The five contributions are:

1. Steady-state heat loss through the insulated part of the storage boundary (12.44):

$$Q_{0i} = \frac{T_{f0} - T_{a0}}{\ell/\lambda + d_i/\lambda_i} \cdot A_i \tag{12.93}$$

2. Steady-state heat loss Q_{0g} through the uninsulated part of the store according to eqs. (12.45-46) in section 12.2.6 for a cylindrical heat store.

3. Periodic component for the heat transfer between the fluid and the storage volume:

$$Q_{1v}e^{i\phi_{qv}} = V\lambda\frac{i}{\beta^2}T_{f1}e^{i\phi_f} \tag{12.94}$$

4. Periodic component from the insulated part of the storage boundary:

$$Q_{1i}e^{i\phi_{qi}} = A_i\lambda\frac{d_0}{\beta}\frac{1}{\ell + m^1\beta}\left(\frac{d_0^2}{\beta^2}T_{f1}e^{i\phi_f} - T_{a1}e^{i\phi_a}\right) \tag{12.95}$$

5. Periodic component through the uninsulated storage boundary:

$$Q_{1g}e^{i\phi_{qg}} = A_g\lambda\left(\frac{d_0}{\beta}\right)^3\frac{\sqrt{i}}{\ell\sqrt{i} + \beta} \cdot T_{f1}e^{i\phi_f} \tag{12.96}$$

The heat transfer between the fluid and the store is then:

$$\begin{aligned} Q &= Q_0 + Q_1 \cdot e^{i\phi_q} \cdot e^{i2\pi t/t_p} \\ Q_0 &= Q_{0i} + Q_{0g} \\ Q_1 \cdot e^{i\phi_q} &= Q_{1v} \cdot e^{i\phi_{qv}} + Q_{1i} \cdot e^{i\phi_{qi}} + Q_{1g} \cdot e^{i\phi_{qg}} \end{aligned} \tag{12.97}$$

The periodic parts of the thermal process can be evaluated with use of diagrams. The eqs. (12.94-96) is then rewritten in the following way (the scaling length b is by (12.92) the absolute value of β):

$$\begin{aligned} Q_{1v}e^{i\phi_{qv}} &= \lambda b \cdot \frac{V}{b^3} \cdot z_v \cdot T_{f1}e^{i\phi_f} \\ Q_{1i}e^{i\phi_{qi}} &= \lambda b \cdot \frac{A_i}{b^2}\left(z_i T_{f1}e^{i\phi_f} - z_a T_{a1}e^{i\phi_a}\right) \\ Q_{1g}e^{i\phi_{qg}} &= \lambda b \cdot \frac{A_g}{b^2} z_g \cdot T_{f1}e^{i\phi_f} \end{aligned} \tag{12.98}$$

The sum of these components gives the total periodic heat injection rate (12.97). We now have a relation between the periodic heat injection rate and the fluid temperature.

Any periodic process can, by use of Fourier series expansion, be represented by sine and cosine terms with the period times $t_p, t_p/2, t_p/3 \ldots$. Eq. (12.97) can be applied to each such component. There is, however, one restriction that must be observed. The model presupposes that the coupling between the fluid and the store is given by a single real-valued parameter ℓ. According to section 11, this is true if the criteria of (11.37) are met. Periodic variations with shorter time periods do not interact with the ground surrounding the store. These variations may then be superimposed on the solutions given by (12.97).

The parameters z_v, z_i, z_g, and z_a are dimensionless complex numbers. They may be expressed as functions of ψ and m^1. From (12.92) we have:

$$be^{i\psi} = \beta = \sqrt{d_0^2 + i\ell^2} \tag{12.99}$$

This implies:

$$\begin{aligned} b &= \sqrt[4]{d_0^4 + \ell^4} \\ \psi &= \frac{1}{2}\arctan\left(\ell^2/d_0^2\right) \quad \left(0 \le \psi \le \frac{\pi}{4}\right) \\ \frac{d_0}{b} &= \sqrt{\cos 2\psi} \\ \frac{\ell}{b} &= \sqrt{\sin 2\psi} \end{aligned} \tag{12.100}$$

The dimensionless numbers z_v, z_i, z_g, and z_a then becomes:

$$\begin{aligned} z_v &= \frac{i}{e^{i2\psi}} \\ z_i &= (\cos 2\psi)^{3/2} e^{-i3\psi} \frac{1}{\sqrt{\sin 2\psi} + m^1 e^{i\psi}} \\ z_g &= (\cos 2\psi)^{3/2} e^{-i3\psi} \frac{1}{\sqrt{\sin 2\psi} + e^{-i\pi/4} \cdot e^{i\psi}} \\ z_a &= \sqrt{\cos 2\psi} \cdot e^{-i\psi} \frac{1}{\sqrt{\sin 2\psi} + m^1 e^{i\psi}} \end{aligned} \tag{12.101}$$

The real and imaginary parts of z_v, z_i, and z_g are presented as functions of ψ in figures 12.26-29. In the case of z_a, it is more suitable to give the absolute value and the argument. See figure 12.30-31.

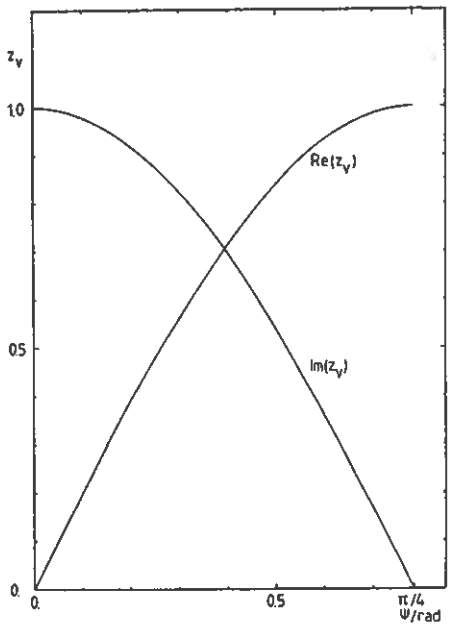

Figure 12.26.
z_v as a function of ψ.

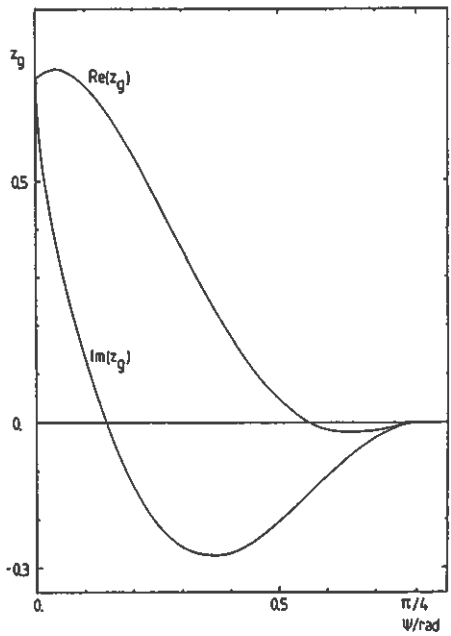

Figure 12.27.
z_g as a function of ψ.

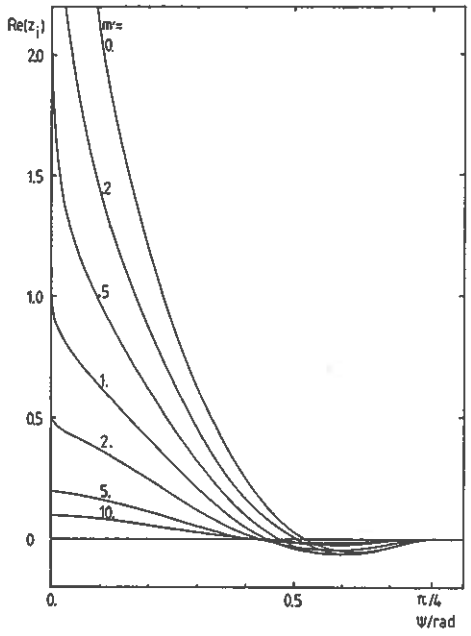

Figure 12.28.
Real part of z_i as a function of ψ and m^1.

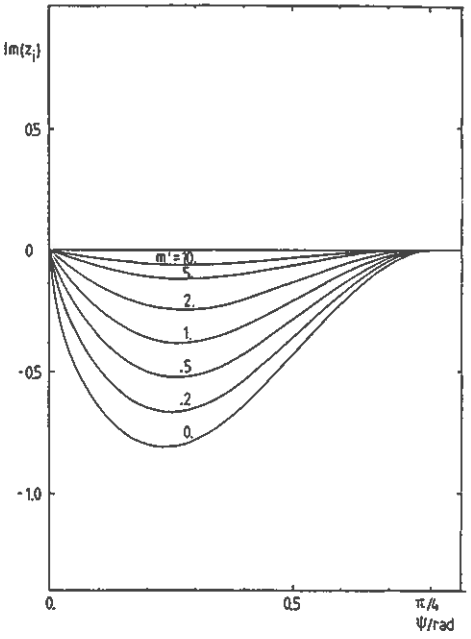

Figure 12.29.
Imaginary part of z_i as a function of ψ and m^1.

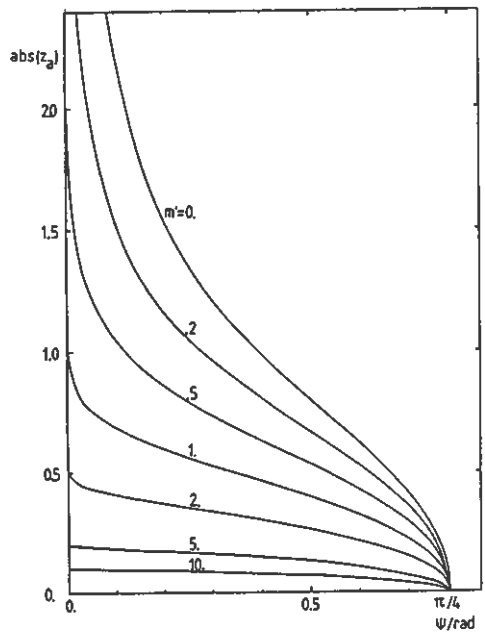

Figure 12.30.
Absolute value of z_a as a function of ψ and m^1.

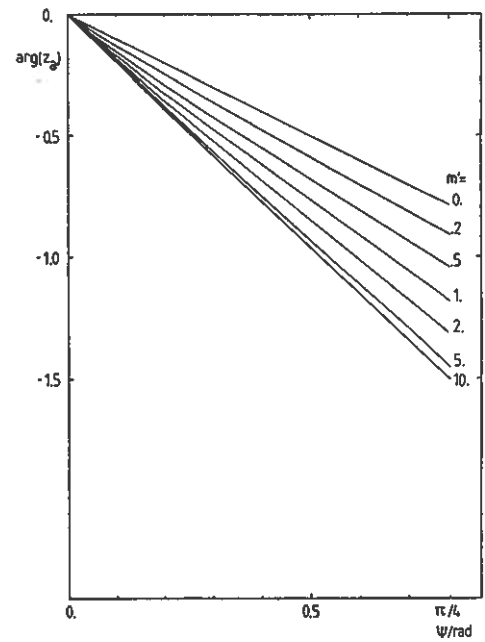

Figure 12.31.
Argument of z_a as a function of ψ and m^1.

12.5.2 Heat balance during a cycle

The heat balance during a storage cycle can be calculated from the expression (12.91) for the total heat flow rate $Q(t)$. An integration over the time period during which $Q(t)$ is positive gives the injected amount of energy E_{in}, while the period with negative values of $Q(t)$ gives the extracted energy E_{out}:

$$\begin{aligned} E_{in} &= \frac{Q_1 t_p}{\pi} \cdot \cos(\varphi_1) + \frac{Q_m t_p}{\pi} \left(\frac{\pi}{2} + \varphi_1 \right) \\ E_{out} &= \frac{Q_1 t_p}{\pi} \cdot \cos(\varphi_1) - \frac{Q_m t_p}{\pi} \left(\frac{\pi}{2} - \varphi_1 \right) \\ \varphi_1 &= \arcsin(Q_m/Q_1) \qquad (Q_m \leq Q_1) \end{aligned} \tag{12.102}$$

If the steady-state heat loss Q_m is lower than the amplitude Q_1 of the periodic component there is, of course, no heat extraction from the store.

The recovery factor η_E is defined as the ratio between the injected and the extracted amount of energy. From (12.102) we get:

$$\eta_E = \frac{E_{out}}{E_{in}} = \frac{\cos\varphi_1 - (\frac{\pi}{2} - \varphi_1) \cdot Q_m/Q_1}{\cos\varphi_1 + (\frac{\pi}{2} + \varphi_1) \cdot Q_m/Q_1} \tag{12.103}$$

The recovery factor becomes a function of the ratio Q_m/Q_1. A few values are given in Table 12.5.

TABLE 12.5. Recovery factor η_E as a function of the ratio Q_m/Q_1.

Q_m/Q_1	0.0	0.05	0.1	0.22	0.25	0.5	0.75	1.0
η_E	1.0	0.86	0.73	0.50	0.45	0.18	0.05	0.0

From Table 12.5, we can see that to achieve a recovery factor above 50%, the ratio of Q_m/Q_1 must be less than 0.22.

Appendix A

Thermal Properties of Soils and Rocks

The thermal properties of soils and rocks in Sweden have been investigated by Sundberg (1988). The rocks are organized in agreement with the classification used by the Swedish Geological Survey.

A.1 Crystalline rock

The majority of crystalline rocks in Sweden is granite-granodiorite and different kinds of gneiss. A representative mean value of the thermal conductivity for these rocks is 3.5 W/mK, and for which about 90 % of all samples exceeds a value just below 3.0 W/mK. Table A.1 gives the thermal conductivity for some types of crystalline rock.

TABLE A.1. Thermal conductivity (W/(mK)) of crystalline rocks. Mean value and interval containing 90 % of measured samples are given.

Type of rock	Mean value	90 % within interval
Granite	3.47	2.85–4.15
Granodiorite	3.34	2.85–3.85
Tonalite	3.16	2.70–3.65
Aplite, Pegmatite	3.31	2.45–4.35
Quartzdiorite	2.87	2.50–3.30
Syenite, diorite	2.67	2.15–3.25
Porphyry	3.55	2.65–4.50
Porphyrite	2.54	1.70–3.60
Ryolite, dacite	3.37	2.70–4.20
Trachyte, basalt	2.83	2.25–3.55
Quartzite	6.62	5.35–8.10
Other quartzite	4.65	3.55–6.00
Other metamorphic sediment	3.58	2.75–4.55
Metamorph. sed. unspecified	3.54	2.45–4.90
Metamorph. basic rocks	2.56	2.05–3.15
Gneiss, unspec.	3.47	2.70–4.40
Leptite, leptite gneiss	3.58	2.65–4.70

The volumetric heat capacity of most types of crystalline rock is about 0.6 kWh/(m^{3}K) or 2.2 MJ/(m^{3}K).

A.2 Sedimentary rock

Table A.2 gives some values of thermal properties, which have been calculated based assumed porosity and mineral content.

TABLE A.2. Thermal conductivity λ (W/(mK)) and specific heat capacity c (J/(kgK)) of sedimentary rocks.

Type of rock	λ (W/(mK))	c (J/(kgK))
Sandstone (Mesozoic)	2.3–4.5	2000– 950
Sandstone (Cambro-silur)	4.0–6.0	1000– 900
Sandstone (Pre-cambrium)	4.0–6.5	1000– 850
Shale (Mesozoic)	1.5–3.0	2200–1100
Shale (Cambro-silur)	2.0–3.5	1600– 950
Limestone (Mesozoic)	1.5–2.8	2200– 950
Limestone (Cambro-silur)	2.8–3.3	1150– 850

A.3 Soil

The thermal properties of soils are given in Table A.3. They are based on over 900 field and laboratory measurements.

TABLE A.3. Thermal conductivity λ (W/(mK)) and volumetric heat capacity C (MJ/(m^{3}K)) of soils (gw-table = ground water table).

Type of soil	λ (W/(mK))	C (MJ/(m^{3}K))
Clay with clay content	0.85–1.1	3.0–3.6
Silty clay/silt layer	1.1–1.5	2.9–3.3
Silt	1.2–2.4	2.4–3.3
Sand, gravel below gw-table	1.6–2.0	2.9
Sand, gravel above gw-table	0.7–0.9	1.4
Till below gw-table	1.5–2.5	2.2–3.0
Sandy till above gw-table	0.6–1.8	1.3–1.9
Peat below gw-table	0.6	4.0
Peat above gw-table	0.2–0.5	0.7–3.2

Appendix B

Line Sources in a Composite Circular Region

Figure B.1 shows the considered two-dimensional, steady-state heat conduction problem. The inner circular region $0 \leq r \leq r_b$ has the thermal conductivity λ_b, while the outer infinite region $r_b \leq r \leq \infty$ has the thermal conductivity λ. There is a line source with the strength q_n at the point (x_n, y_n), which lies in the inner region.

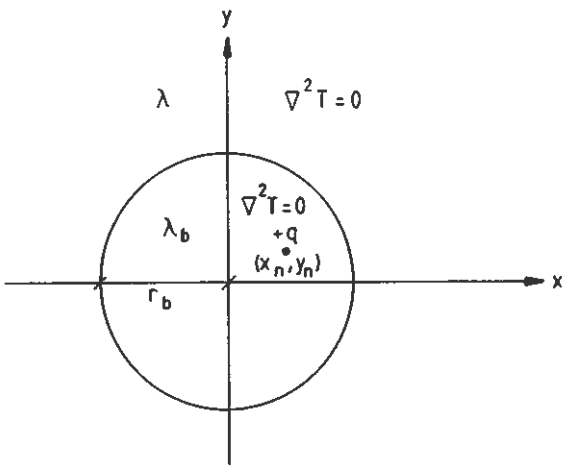

Figure B1. Fundamental line source problem for a composite circular region.

The solution $T(x, y)$ satisfies Laplace equation $\nabla^2 T = 0$ in both regions except at the point (x_n, y_n). The temperature and the normal heat flux are contiuous at the circle $r = r_b$:

$$T|_{r_b-0} = T|_{r_b+0} \qquad \lambda_b \left.\frac{\partial T}{\partial r}\right|_{r_b-0} = \lambda \left.\frac{\partial T}{\partial r}\right|_{r_b+0} \tag{B.1}$$

The exact solution, which is determined except for an arbitrary constant temperature level, is:

$r \leq r_b$:

$$T(x,y) = \frac{q_n}{2\pi\lambda_b}\left\{\ln\left[\frac{r_b}{\sqrt{(x-x_n)^2+(y-y_n)^2}}\right] + \sigma \cdot \ln\left[\frac{r_b/b_n}{\sqrt{(x-x'_n)^2+(y-y'_n)^2}}\right]\right\} \tag{B.2}$$

$r_b \leq r \leq \infty$:

$$T(x,y) = \frac{q_n}{2\pi\lambda}\left\{(1-\sigma)\cdot \ln\left[\frac{r_b}{\sqrt{(x-x_n)^2+(y-y_n)^2}}\right] + \sigma \cdot \ln\left[\frac{r_b}{\sqrt{x^2+y^2}}\right]\right\} \tag{B.3}$$

The conductivity parameter σ is defined by:

$$\sigma = \frac{\lambda_b - \lambda}{\lambda_b + \lambda} \tag{B.4}$$

The following geometrical parameters are used:

$$b_n = \frac{\sqrt{x_n^2+y_n^2}}{r_b} \qquad x'_n = \frac{x_n}{b_n^2} \qquad y'_n = \frac{y_n}{b_n^2} \tag{B.5}$$

The point (x'_n, y'_n) is the harmonic mirror point to (x_n, y_n) relative to the circle $r = r_b$. This means that the two points lie on the same radius, and that the product of the distances to the center is r_b^2:

$$\sqrt{(x'_n)^2+(y'_n)^2}\cdot\sqrt{x_n^2+y_n^2} = r_b^2 \tag{B.6}$$

An arbitrary constant temperature level may be added to the solution (B.2-3). The solution has a simple form. For $r \leq r_b$, where the thermal conductivity is λ_b, it is given by two line sinks:

$$0 \leq r \leq r_b : \qquad q_n \text{ at } (x_n, y_n) \qquad \sigma \cdot q_n \text{ at } (x'_n, y'_n) \tag{B.7}$$

For $r_b \leq r < \infty$, where the thermal conductivity is λ, the solution is given by the two line sinks outside the region:

$$r_b \leq r < \infty : \qquad (1-\sigma)\cdot q_n \text{ at } (x_n, y_n) \qquad \sigma \cdot q_n \text{ at } (0,0) \tag{B.8}$$

The solution (B.2-3) was derived in the following way. In $r \leq r_b$, the solution consisted of the line source, i.e. the first term of (B.2) and an infinite sum to account for any variation on $r = r_b$:

$$\sum_n a_n e^{in\varphi} \left(\frac{r}{r_b}\right)^n \tag{B.9}$$

The solution in the outer region $r_b \leq r \leq \infty$ is:

$$\sum_n b_n e^{in\varphi} \left(\frac{r_b}{r}\right)^n + \frac{q_n}{2\pi\lambda} \ln\left(\frac{r_b}{\sqrt{x^2+y^2}}\right) \tag{B.10}$$

The logarithmic term accounts for the injected heat q_n so that the remaining part, i.e. the infinite sum, is finite when r tends to infinity.

It is clear that the solution satisfies all conditions of figure B.1 for any a_n and b_n, except for the boundary conditions at $r = r_b$. These two boundary conditions determine the coefficients of a_n and b_n. The calculations, which are somewhat lengthy but straightforward, are not given here. It turned out that the obtained infinite sums may be summed. The compact expressions (B.2) and (B.3) were finally obtained.

A direct verification that (B.2) and (B.3) indeed are the solution is straightforward, but also somewhat lengthy. The temperature T is then expressed in polar coordinates in order to verify the boundary conditions (B.1).

Let us now consider the problem of section 8.4. There are N *ducts in a composite region.* See figure 8.1 and 8.4. We will here derive the expressions in subsection 8.4.1 for the line-source approximation.

We now have N line sinks in the inner region $r < r_b$. The strength of the line-source at (x_n, y_n) is q_n. The temperature field is obtained as a sum of (B.2) and (B.3) for $n = 1, 2, ..., N$.

We are interested in the fluid temperatures T_{fm} and the temperature T_c at a large outer circle $r = r_c, r_c \gg r_b$. The fluid temperature T_{fm} is related to the temperature in the ground at the pipe by:

$$T_{fm} - T_{pm} = q_m \cdot R_{pm} \tag{B.11}$$

The temperature T_{pm} at the pipe is obtained by inserting $x = x_m + r_{pm} \cdot \cos(\varphi_n)$ and $y = y_m + r_{pm} \cdot \sin(\varphi_n)$ in the sum of (B.2). We assume that r_{pm} is much smaller than the distances to the other sources and mirror sources. Then we may insert $x = x_m$ and $y = y_m$ for all terms except for the contribution from q_m itself. We get:

$$T_{pm} \simeq \frac{q_m}{2\pi\lambda_b} \left\{ \ln\left[\frac{r_b}{r_{pm}}\right] + \sigma \cdot \ln\left[\frac{r_b/b_m}{\sqrt{(x_m - x'_m)^2 + (y_m - y'_m)^2}}\right] \right\} +$$

$$\sum_{n\neq m}^{N} \frac{q_n}{2\pi\lambda_b} \left\{ \ln\left[\frac{r_b}{\sqrt{(x_m-x_n)^2+(y_m-y_n)^2}}\right] + \sigma\cdot\ln\left[\frac{r_b/b_n}{\sqrt{(x_m-x'_m)^2+(y_m-y'_m)^2}}\right]\right\} \tag{B.12}$$

The temperature T_c at a large outer circle $r = r_c$, $r_c \gg r_b$, is obtained from (B.3). The distance from the circle to all sources is approximately r_c. We get in this approximation:

$$T_c \simeq \sum_{n=1}^{N} \frac{q_n}{2\pi\lambda} \left\{ (1-\sigma)\ln\left[\frac{r_b}{r_c}\right] + \sigma\ln\left[\frac{r_b}{r_c}\right]\right\} \tag{B.13}$$

We define in accordance with (8.9) the average temperature T_b at $r = r_b$ by:

$$T_b = T_c + q\cdot\frac{1}{2\pi\lambda}\ln\left(\frac{r_c}{r_b}\right) \simeq 0 \tag{B.14}$$

The temperature T_b becomes in this cases zero. This is due to the choice of temperature level for (B.2-3).

Let b_{mn} give the distance between (x_m, y_m) and (x_n, y_n) as in (8.26):

$$\sqrt{(x_m-x_n)^2+(y_m-y_n)^2} = b_{mn}r_b \tag{B.15}$$

In the same way we define the dimensionless parameter b'_{mn} for the distance between (x_m, y_m) and (x'_n, y'_n):

$$\sqrt{(x_m-x'_n)^2+(y_m-y'_n)^2} = b'_{mn}r_b/b_n \tag{B.16}$$

A straightforward calculation gives the relation (8.29):

$$b'_{mn} = \sqrt{(1-b_m^2)(1-b_n^2)+b_{mn}^2} \tag{B.17}$$

From (B.12), (B.11), and (B.15) we get the relations between $T_{fm} - T_b$ and q_n:

$$T_{fm} - T_b = \sum_{n=1}^{N} R^o_{mn}\, q_n \qquad m = 1,\ldots,N \tag{B.18}$$

$$\begin{aligned} R^o_{mm} &= \frac{1}{2\pi\lambda_b}\left[\ln\left(\frac{r_b}{r_{pm}}\right) - \sigma\ln(1-b_m^2)\right] + R_{pm} \\ R^o_{mn} &= -\frac{1}{2\pi\lambda_b}\left[\ln(b_{mn}) + \sigma\ln(b'_{mn})\right] \qquad \text{for } m\neq n \end{aligned} \tag{B.19}$$

These are the expressions (8.28).

Appendix C

Final Equations for Multipole Method

A complete description of the multipole method is given by Claesson and Bennet (1987) and Bennet, Claesson, and Hellström (1987). A brief review of the method is found in section 8.4.3, where the thermal problem is defined and the nomenclature used in this appendix is explained.

The final equations for the heat flows q_n and the complex-valued strengths of the multipoles P_{nj} and P_{cj} are given below. Multipoles of all orders are needed in an exact solution. In the numerical solution, we truncate the equation system and consider multipoles up to order J at each pipe and at infinity. The sine and cosine variation around the pipes and around the outer circle can then be satisfied up to order J only.

We have the following final equations:

$m = 1, ..., N$:

$$
\begin{aligned}
T_{fm} - T_c \;=\; & \sum_{n=1}^{N} q_n \cdot R^{oc}_{mn} \\
& + \Re \left[\sum_{\substack{n=1 \\ n \neq m}}^{N} \sum_{j=1}^{J} P_{nj} \left(\frac{r_{pn}}{z_m - z_n} \right)^j + \sum_{n=1}^{N} \sum_{j=1}^{J} P_{nj} \sigma \left(\frac{r_{pn} \bar{z}_m}{r_b^2 - z_n \bar{z}_m} \right)^j \right. \\
& \left. + \sum_{j=1}^{J} P_{cj} (1 - \sigma) \left(\frac{z_m}{r_c} \right)^j \right] \qquad \text{(C.1)}
\end{aligned}
$$

$m = 1, ..., N \quad ; \quad k = 1, ..., J :$

$$\bar{P}_{mk} + \frac{1 - k\beta_m}{1 + k\beta_m} \left[\sum_{\substack{n=1 \\ n \neq m}}^{N} \frac{q_n}{2\pi\lambda_b} \frac{1}{k} \left(\frac{r_{pm}}{z_n - z_m} \right)^k + \sum_{n=1}^{N} \frac{q_n}{2\pi\lambda_b} \sigma \frac{1}{k} \left(\frac{r_{pm}\bar{z}_n}{r_b^2 - z_m\bar{z}_n} \right)^k \right.$$
$$+ \sum_{\substack{n=1 \\ n \neq m}}^{N} \sum_{j=1}^{J} P_{nj} \binom{j+k-1}{j-1} \left(\frac{r_{pn}}{z_m - z_n} \right)^j \left(\frac{r_{pm}}{z_n - z_m} \right)^k$$
$$+ \sum_{n=1}^{N} \sum_{j=1}^{J} \sum_{j'=0}^{min(j,k)} \bar{P}_{nj} \sigma \binom{j}{j'} \binom{j+k-j'-1}{j-1} \cdot \frac{r_{pn}^j r_{pm}^k z_m^{j-j'} \bar{z}_n^{k-j'}}{(r_b^2 - \bar{z}_n z_m)^{j+k-j'}}$$
$$\left. + \sum_{j=k}^{J} P_{cj}(1 - \sigma) \binom{j}{k} \frac{z_m^{j-k} r_{pm}^k}{r_c^j} \right] = 0 \qquad \text{(C.2)}$$

$k = 1, ..., J:$

$$\bar{P}_{ck} \cdot \left[1 - \sigma \frac{1 - k\beta_c}{1 + k\beta_c} \left(\frac{r_b}{r_c} \right)^{2k} \right] \qquad \text{(C.3)}$$
$$+ (1 + \sigma) \frac{1 - k\beta_c}{1 + k\beta_c} \cdot \left[\sum_{n=1}^{N} \frac{q_n}{2\pi\lambda_b} \frac{1}{k} \left(\frac{z_n}{r_c} \right)^k + \sum_{n=1}^{N} \sum_{j=1}^{k} P_{nj} \binom{k-1}{j-1} \frac{r_{pn}^j z_n^{k-j}}{r_c^k} \right] = 0$$

Here, $\bar{z}$, $\bar{P}_{nj}$, and $\bar{P}_{ck}$ denote the complex conjugate of z, P_{nj}, and P_{ck}. The parameter σ is defined by (8.30).

The thermal resistances R_{mn}^{oc} consist of two parts. There are the line-source approximations for the resistance between T_f and T_b given in Appendix B, and the thermal resistance of the annular region $r_b < r < r_c$. Hence,

$m = 1, ..., N:$

$$R_{mm}^{oc} = \frac{1}{2\pi\lambda_b} \left[\beta_m + \ln \left(\frac{r_b}{r_{pm}} \right) + \sigma \cdot \ln \left(\frac{r_b^2}{r_b^2 - |z_m|^2} \right) \right] + \frac{1}{2\pi\lambda} \left[\ln \left(\frac{r_c}{r_b} \right) + \beta_c \right] \qquad \text{(C.4)}$$

$m, n = 1, ..., N \; ; \; m \neq n:$

$$R_{mn}^{oc} = \frac{1}{2\pi\lambda_b} \left[\ln \left(\frac{r_b}{r_{mn}} \right) + \sigma \cdot \ln \left(\frac{r_b^2}{|r_b^2 - z_n\bar{z}_m|} \right) \right] + \frac{1}{2\pi\lambda} \left[\ln \left(\frac{r_c}{r_b} \right) + \beta_c \right] \qquad \text{(C.5)}$$

There are N real-valued equations (C.1) and $N \cdot J + J$ complex-valued ones (C.2-3). This corresponds to the N line sources q_n and the $N \cdot J + J$ complex-valued multipoles P_{nj} and P_{cj}. A numerical method, where the equation system (C.1-3) is solved iteratively, is described by Bennet et al. (1987).

References

Chapter 1

Dalenbäck JO. 1990. Central Solar Heating Plants with Seasonal Storage — Status Report, International Energy Agency, Solar Heating and Cooling Programme, Task VII, Document D14:1990, Swedish Council for Building Research.

Duffie JA, Beckman WA. 1975. *Solar Energy Thermal Processes*, Wiley, New York.

Lund P, Östman B. 1985. A Numerical Model for Seasonal Storage of Solar Heat in the Ground by Vertical Pipes, Solar Energy, Vol. 34, No. 4/5, pp. 351-366.

Margen P. 1983. State-of-the-Art and System Aspects: Storage of High Temperature Heat in Channeled Rock, Proceedings from International Conference on Subsurface Heat Storage, Stockholm, June 6-8, 1983, Swedish Council for Building Research, Document D16:1983.

Margen P. 1985. The Role and Economics of Different Types of Energy Storage, Swedish Council for Building Research, Document D5:1985.

Chapter 2

Eskilson P. 1987. Thermal Analyses of Heat Extraction Boreholes, thesis, Dept. of Mathematical Physics, Lund Institute of Technology, Box 118,
S-221 00 Lund, Sweden.

Nordell B. 1987. The Borehole Heat Store in Rock at the Luleå University of Technology, Constructional and Operational Experience, The Lulevärme project 1982-1985, Document D6:1985, Swedish Council for Building Research.

Nordell B. 1990. A Borehole Heat Store in Rock at the University of Luleå, The Lulevärme project 1982-1988, Document D12:1990, Swedish Council for Building Research.

Chapter 3

Adolfsson K, Lindblom U, Rhen I. 1983. Geotechnical Consequences of Heating/-Cooling and Freezing/Thawing of Clay, Proceedings from International Conference on Subsurface Heat Storage, Stockholm, June 6-8, 1983, Swedish Council for Building Research, Document D16:1983.

Agence Francaise pour la Maitrise de l'Energie. 1988. Proceedings of JIGASTOCK'88, 18-21 October, 1988, Versailles, France.

Andersson S, Johansson A, Nordell B, Åbyhammar T. 1983. A Borehole Heat Store in Rock, Pilot Trials in Luleå and Preliminary Design of a Full-Scale Installation, BFR-Document D6:1983.

Aranovitz E, Hardy M, Esposito L, Rizzi G, Soma L. 1985. Performance and Analysis of a Seasonal Heat Storage with Vertical Tubes in the Ground, Second Workshop on Solar Assisted Heat Pumps with Ground-Coupled Storage, Proceedings, Vienna, Austria: Commission of the European Communities.

Areskoug M, Wigström P. 1980. Förberedande försök med långtidslagring av överskottssolvärme från växthus, Sveriges Lantbruksuniversitet, Institutionen för lantbrukets byggnadsteknik, Lund, Rapport 11.

Ausseur JY, Vachaud G. 1978. Le système "soltherm", fonctionnement et dimensionnement d'unmode de stockage de chaleur intersaisonnier pour l'habitat individuel, Institut de mécanique, B.P. 53, Grenoble, France.

Bankston CA. 1988. The Status and Potential of Central Solar Heating Plants with Seasonal Storage: An International Report, Advances in Solar Energy, Vol. 4, Plenum Publishing Company.

Baudoin A. 1988. Stockage intersaisonnier de chaleur dans le sol par batterie d'échangeurs baionnette verticaux; modèle de prédimensionnement, thesis, L'Université de Reims Champagne-Ardenne, France.

Brun G. 1965. La régularisation de l'ènergie solaire par le stockage thermique dans le sol, Revue Générale de Thermique, n°44, France.

Brun G. 1967. Le stockage thermique dans le sol en vue de la régularisation de l'ènergie solaire, Conference prononcée le 20 Avril 1967 au Centre de Perfectionnement Technique, France.

Chuard P, Chuard D, van Gilst J, Hadorn JC, Mercier. 1983. The IEA Task VII Swiss Project in Vaulruz, Design and First Experience, Proceedings from International Conference on Subsurface Heat Storage, Stockholm, June 6-8, 1983, Swedish Council for Building Research, Document D16:1983.

Claesson, Eftring, Eskilson, Hellström. 1985. Markvärme – En handbok om termiska analyser, (Ground Heat Systems – A handbook on thermal analyses, in Swedish), Report T16-18:1985, Swedish Council for Building Research, Stockholm, Sweden.

Claesson J, Hellström G. 1988. Theoretical and Experimental Study of the Local Heat Transfer in Exchanger Pipes, Proceedings of JIGASTOCK'88, 18-21 October, 1988, Versailles, France, Agence Francaise pour la Maitrise de l'Energie.

Dalenbäck JO. 1990. Central Solar Heating Plants with Seasonal Storage — Status Report, International Energy Agency, Solar Heating and Cooling Programme, Task VII, Document D14:1990, Swedish Council for Building Research.

Eskilson P, Claesson J. 1988. Simulation Model for Thermally Interacting Heat Extraction Boreholes, Numerical Heat Transfer, vol. 13, pp. 149-165.

Givoni. 1977. Underground Long-Term Storage of Solar Energy, A Review, Solar Energy, Vol. 19, pp. 617-623.

Guimbal. 1976. Lotissement de 16 villas a chauffage solaire integral, Société Générale d'Etudes et Construction, Saint-Etienne, France.

Guison O, Lachal B, Mathey B, Mermoud A, Pahud D. 1990. A 20,000 m^3 Solar Seasonal Heat Store under an Industrial Building at Meyrin-Geneva — Measurements and Calculations, Zeitschrift für angewandte Geowissenschaften, Heft 9, pp. 35-55.

Hadorn JC. 1981. Stockage souterrain de chaleur en terre humide, Developpement d'un modéle de calcul et comparaison avec des mesures in situ, Institut d'Economie et Aménagements Energétiques, Départment de Génie Civil, Ecole Polytechnique Fédérale de Lausanne, Suisse.

Hadorn JC, Chuard P. 1983. Heat Storage Models, Evaluation and Selection, IEA Task VII report, Distribution: EDMZ, 3000 Berne, Switzerland.

Hadorn JC, Chuard P, Chuard D. 1985. The Vaulruz Project – First Experimental Results, Second Workshop on Solar Assisted Heat Pumps with Ground-Coupled Storage, Proceedings, Vienna, Austria: Commission of the European Communities.

Hellström. 1982. Duct Storage Model, Manual for Computer Code, Department of Mathematical Physics, Lund Institute of Technology, Box 118, S-221 00 Lund, Sweden.

Hellström G, Palmgren C, Rydell B. 1985. Heat Storage in Clay – A Technical and Economical Evaluation of Vertical Earth Heat Exchangers, Proceedings of III International Conference on Energy Storage for Building Heating and Cooling, September 22-26, 1985, Toronto, Canada.

Hultmark G. 1981. Sunclay Project – First Year Operation with a Seasonal Storage of 80,000 m^3 Clay, Proceedings of International Conference on Seasonal Thermal Energy Storage and Compressed Air Storage, October 19-21, 1981, Seattle, U.S.A.

Hydén H, Mattson, Rune. 1983. Säsongslagring av solenergi genom borrhålslager i berg, förprojektering av Stora Skuggan, Stockholm, BFR-rapport R14:1983.

Jigastock'88. 1988. Proceedings, A.F.M.E, Agence Francaise pour la Maîtrise del l'Energie, 27 rue L. Vicat, 75015 Paris, France.

Lahtinen. 1983. Kerava Solar Village Project, Proceedings from International Conference on Subsurface Heat Storage, Stockholm, June 6-8, 1983, Swedish Council for Building Research, Document D16:1983.

Landtechnik Weihenstephan. 1990. Proceedings of the Workshop on Seasonal Thermal Energy Storage in Duct Systems, Landtechnik Weihenstephan, Freising, Germany, Zeitschrift für angewandte Geowissenschaften, Heft 9.

Lawrence Berkeley Laboratory. 1978. Proceedings of Thermal Energy Storage in Aquifers Workshop, May 10-12, 1978, Lawrence Berkeley Laboratory, Berkeley, U.S.A.

Lund P, Östman B. 1985. A Numerical Model for Seasonal Storage of Solar Heat in the Ground by Vertical Pipes, Solar Energy, Vol. 34, No. 4/5, pp. 351-366.

Lundin SE. 1985. Thermal Energy Storage Programme in Sweden, Proceedings of III International Conference on Energy Storage for Building Heating and Cooling, September 22-26, 1985, Toronto, Canada.

Magnusson C, Sundberg J. 1990. Markvärmeteknik, Handledning för planering och projektering, Swedish Council for Building Research, Report T6:1990.

de Marsily G. 1978. Peut-on stocker de l'ènergie dans le sol? Annales des Mines, Avril 1978, Ecole nationale supérieure des mines de Paris, France.

Mathey B, Pilonel B. 1985. Solar Assisted Gas Heat Pump with Ground Coupled Storage for Twelwe Family Houses, Second Workshop on Solar Assisted Heat Pumps with Ground-Coupled Storage, Proceedings, Vienna, Austria: Commission of the European Communities.

Mazzarella. 1990. The MINSUN Simulation and Optimization Program. User's manual. Dipartimento di Energetica, Polytecnico di Milano, Piazza Leonardo da Vinci 32, I-20133 Milano, Italy.

van Meurs GAM. 1986. Seasonal Heat Storage in the Soil, thesis, Department of Applied Physics, University of Technology Delft, P.O.Box 5046, 2600 GA Delft, Netherlands.

Modin B. 1977. Ackumulering av lågvärdigt värme i mark, Avdelningen för installationsteknik, Chalmers University of Technology, Gothenburg.

Nir A. 1983. Heat Storage in Unsaturated Soils: From Theory to Application, Proceedings from International Conference on Subsurface Heat Storage, Stockholm, June 6-8, 1983, Swedish Council for Building Research, Document D16:1983.

Nordell B. 1987. The Borehole Heat Store in Rock at the Luleå University of Technology, Constructional and Operational Experience, The Lulevärme project 1982-1985, Document D6:1985 Swedish Council for Building Research.

Nordell B. 1990. A Borehole Heat Store in Rock at the University of Luleå, The Lulevärme project 1982-1988, Document D12:1990, Swedish Council for Building Research.

Olsson. 1983. Kullavik Project – Ground Heat Storage with High Temperatures, Proceedings from International Conference on Subsurface Heat Storage, Stockholm, June 6-8, 1983, Swedish Council for Building Research, Document D16:1983.

Platell O, Wikström H. 1981. Sunstore-projektet 1977-1980, Solvärmesystem med låg temperatur och säsongslagring för uppvärmning av lokaler, mätning och utvärdering 1981-82, Report R100:1981, Swedish Council for Building Research.

Public Works of Canada. 1985. Proceedings of III International Conference on Energy Storage for Building Heating and Cooling, September 22-26, 1985, Toronto, Canada.

Puntilla A, Saastamoinen J. 1983. Annular Solar Heat Storage in the Bedrock, Proceedings from International Conference on Subsurface Heat Storage, Stockholm, June 6-8, 1983, Swedish Council for Building Research, Document D16:1983.

Rosenblad G. 1983. Seasonal Heat Storing 1979-83 in Utby Ground Heat Pump Project, Proceedings from International Conference on Subsurface Heat Storage, Stockholm, June 6-8, 1983, Swedish Council for Building Research,
Document D16:1983.

Schunnesson H. 1983. Borrning av värmelager, En studie av borrningsarbetena för projekt Lulevärme, på Porsön i Luleå, Examensarbete 1983:073E, Avd. f. Bergmaskinteknik, Luleå University of Technology, Sweden.

Shelton J. 1975. Underground Storage of Heat in Solar Heating Systems, Solar Energy, Vol. 17, pp. 137-143.

Sundberg J. 1990. Högtemperaturalager i lera, Geoteknik, systemteknik och kostnadskalkyler, Swedish Council for Building Research, Rapport R40:1990.

Swedish Council for Building Research. 1983. Proceedings from International Conference on Subsurface Heat Storage, Stockholm, June 6-8, 1983, Swedish Council for Building Research, Document D16:1983.

Wijsman A. 1983. The Groningen Project. 100 Houses with Seasonal Solar Heat Storage in the Soil Using a Vertical Heat Exchanger, Proceedings from International Conference on Subsurface Heat Storage, Stockholm, June 6-8, 1983, Swedish Council for Building Research, Document D16:1983.

Wijsman A, van Meurs GAM. 1985. Validation of "Duct-Store" Models with Experimental Data from the Gronningen Project, Proceedings of III International Conference on Energy Storage for Building Heating and Cooling, September 22-26, 1985, Toronto, Canada.

Wilén P, Rhen I, Bäckström B. 1985. Development of Heat Storage Systems with Vertical Pipes in Earth and Rock, Proceedings of III International Conference on Energy Storage for Building Heating and Cooling, September 22-26, 1985, Toronto, Canada.

Chapter 5

Brehm DR. 1989. Entwicklung, Validierung und Anwendung eines dreidimensionalen, strömungsgekoppelten finite Differenzen Wärmetransportmodells, Giessener Geologische Schriften, Nr. 43, Giessen, Germany.

Hellström G, Tsang CF, Claesson J. 1988. Buoyancy Flow at a Two-Fluid Interface in a Porous Medium: Analytical Studies, Water Resources Research, Vol. 24, No. 4, pp.493-506.

Lund P. 1985. Effect of Ground Water Flow on the Performance of Long-Term Pipe Heat Storage in the Ground. Report TKK-F-A586(1985), Helsinki University of Technology, Finland, 1985.

van Meurs GAM. 1986. Seasonal Heat Storage in the Soil, thesis, Department of Applied Physics, University of Technology Delft, P.O.Box 5046, 2600 GA Delft, Netherlands.

Sundberg J. 1988. Thermal Properties of Soils and Rocks, thesis, Publ. A57, Department of Geology, Chalmers University of Technology and University of Gothenburg, S-412 96 Gothenburg, Sweden.

Sundberg J. 1990. Högtemperaturalager i lera, Geoteknik, systemteknik och kostnadskalkyler, Swedish Council for Building Research, Rapport R40:1990.

Chapter 6

Carslaw HS, Jaeger JC. 1959. *Conduction of Heat in Solids*, Second ed., Oxford University Press, Great Britain.

Chapter 7

Bennet CO, Myers JE. 1962. *Momentum, Heat, and Mass Transfer*, McGraw-Hill, New York, U.S.A.

Chiou JP. 1987. Experimental investigation of the augmentation of forced convection heat transfer in a circular tube using spiral spring inserts, J. Heat Transfer 109 (1987) 300-307.

Cope WF. 1941. The friction and heat transmission coefficients of rough pipes, Proc. Inst. Mech. Engrs. 145 (1941) 99-105.

Coulson JM, Richardson JF. 1960. *Chemical Engineering*, Volume 1: Fluid flow, heat transfer and mass transfer, The English Language Book Society and Pergamon Press, Oxford.

Dipprey DF, Sabersky RH. 1963. Heat and momentum transfer in smooth and rough tubes at various Prandtl numbers. Int. J. Heat Mass Transfer 6 (1963) 329-353.

Eckert ERG, Drake RM. 1959. *Heat and Mass Transfer*, Second ed., McGraw-Hill, New York, U.S.A.

Ede AJ. 1967. *An Introduction to Heat Transfer — Principles and Calculations*, Pergamon Press, Oxford.

Hausen H. 1959. Neue Gleichungen für die Wärmeübertragung bei freier und erzwungener Strömung, Allg. Wärmetechn. 9 (1959) 75-79.

Hausen H. 1976. *Wärmeübertragung im Gegenstrom, Gleichstrom, und Kreuzstrom.* Zweite, neuarbeitete Auflage. Springer-Verlag, Berlin.

Herwig H. 1985. The effect of variable properties on momentum and heat transfer in a tube with constant heat flux across the wall. Int. J. Heat Mass Transfer 28 (1985) 423-431.

Holman JP. 1968. *Heat Transfer*, Second ed., McGraw-Hill, New York, U.S.A.

Hornbeck RW. 1965. An all-numerical method for heat transfer in the inlet of a tube, Am. Soc. Mech. Eng. Rep. 65-WA/HT-36.

Joshi SD, Bergles AE. 1980. Analytical study of heat transfer to laminar in-tube flow of non-newtonian fluids, AIChE Symp. Ser., 76 (1980) 199:270-281.

Joshi SD, Bergles AE. 1981. Analytical study of laminar flow heat transfer to pseudoplastic fluids with uniform wall temperature, AIChE Symp. Ser., 77 (1981) 208:114-122.

Judd RL, Wade JHT. 1963. Forced convection heat transfer in eccentric annular passages, Heat Transfer and Fluid Mechanics Institute, pp. 272-288, Stanford University Press, Stanford, California, U.S.A.

Kay JM, Nedderman RM. 1974. *An Introduction to Fluid Mechanics and Heat Transfer*, Cambridge University Press, Cambridge.

Kays WM, Crawford ME. 1980. *Convective Heat and Mass Transfer*, Second edition, McGraw-Hill, New York.

Kays WM, Leung EY. 1963. Heat transfer in annular passages: Hydrodynamically developed turbulent flow with arbitrarily prescribed heat flux, Int. J. Heat Mass Transfer 6 (1963) 537-557.

Knudsen JG, Katz DL. 1958. *Fluid Dynamics and Heat Transfer*, McGraw-Hill, New York, U.S.A.

Kreith F. 1965. *Principles of Heat Transfer*, Second ed., International Textbook Company, Pennsylvania, U.S.A.

Kreith F, Bohn MS. 1986. *Principles of Heat Transfer*, Fourth ed., Harper & Row, New York, U.S.A.

Leung EY, Kays WM, Reynolds WC. 1962. Heat transfer with turbulent flow in concentric and eccentric annuli with constant and variable heat flux, Rep. AHT-4, Mechanical Engineering Department, Stanford University, Stanford, California, U.S.A.

Lundberg RE, McCuen PA, Reynolds WC. 1963. Heat transfer in annular passages: Hydrodynamically developed laminar flow with arbitrarily prescribed wall temperatures or heat fluxes, Int. J. Heat Mass Transfer 6 (1963) 495-529.

Martinelli RC, Boelter LMK. 1942. The analytical prediction of superposed free and forced viscous convection in a vertical pipe, Univ. California Publ. Eng., Vol. 5, p. 23.

McAdams WH. 1954. *Heat Transmission*, McGraw-Hill, New York, U.S.A.

Merker GP. 1987. *Konvektive Wärmeübertragung*, Springer Verlag, Berlin Heidelberg.

Metais B, Eckert ERG. 1964. Forced, mixed and free convection regimes, J. Heat Transfer 86 (1964) 295-296.

Mullin TE, Gerhard ER. 1977. Heat transfer to water in downward flow in a uniform wall temperature vertical tube at low Graetz number, J. Heat Transfer 99 (1977) 586-589.

Norris RH. 1971. Augmentation of Convection Heat and Mass Transfer, American Society of Mechanical Engineers.

Notter RH, Sleicher CA. 1972. A solution to the turbulent Graetz problem — III. Fully developed and entry region heat transfer rates. Chem. Eng. Sci. 27 (1972) 2073-2093.

Perry RH, Chilton CH. 1973. *Chemical Engineer's Handbook*, fifth ed., McGraw-Hill, New York, U.S.A.

Petuhkov BS, Roizen LI. 1965. Heat exchange during gas flow in pipes with an annular cross section, Heat and Mass Transfer, Volume I, Minsk, U.S.S.R.

Petuhkov BS. 1970. Heat transfer and friction in turbulent pipe flow with variable physical properties. Adv. Heat Transfer 6 (1970) 503-565.

Pigford RL. 1955. Non-isothermal flow and heat transfer inside a vertical tube, Chem. Eng. Prog. Symp. Ser., 51 (1955) 79-92.

Pitts DR, Sissom LE. 1977. *Heat Transfer*, Schaum's Outline Series in Engineering, McGraw-Hill, New York, U.S.A.

Rohsenow WM, Choi HY. 1961. *Heat, Mass, and Momentum Transfer*, Prentice-Hall, New Jersey, U.S.A.

Rohsenow WM, Hartnett JP, Ganic EN. 1985. *Handbook of Heat Transfer Fundamentals*, Second ed., McGraw-Hill, New York.

Rohsenow WM, Hartnett JP, Ganic EN. 1985b. *Handbook of Heat Transfer Applications*, Second ed., McGraw-Hill, New York.

Shah RK, London AL. 1978. Laminar flow forced convection in ducts, Supplement 1 in Advances in Heat Transfer, ed. Irvine and Hartnett, Academic, New York, U.S.A.

Sieder EN, Tate GE. 1936. Heat Transfer and Pressure Drop of Liquids in Tubes, Ind. Eng. Chem. 28, pp. 1429-1435.

Stephan K. 1959. Wärmeübergang und Druckabfall bei nicht ausgebildeter Laminarströmung in Rohren und ebenen Spalten, Chem. Ing. Tek. 31 (1959) 773-778.

Uttarwar SB, Raja Rao M. 1985. Augmentation of laminar flow heat tansfer in tubes by means of wire coil inserts, J. Heat Transfer 107 (1985) 930-935.

VDI-Wärmeatlas, Berechnungsblätter für den Wärmeübergang, 5., erweiterte Auflage. 1988. VDI Verlag GMbh, Düsseldorf.

Watzinger A, Johnson DG. 1938. Wärmeübertragung von Wasser an Rohrwand bei senkrechter Strömung im Übergangsgebiet zwischen laminarer und turbulenter Strömung, Forschg. Ing.-Wes. 9 (1938) 182-196; 10 (1939) 182-196.

Welty JR. 1974. *Engineering Heat Transfer*, John Wiley & Sons, New York, U.S.A.

Welty JR, Wicks CE, Wilson RE. 1976. *Fundamentals of Momentum, Heat, and Mass Transfer*, Second ed., John Wiley & Sons, New York, U.S.A.

Yang KT. 1962. Laminar forced convection of liquids in tubes with variable viscosity, J. Heat Transfer 84 (1962) 353-362.

Chapter 8

Bennet J, Claesson J, Hellström G. 1987. Multipole method to compute the conductive heat flows to and between pipes in a composite cylinder, Notes on Heat Transfer 3-1987, Depts. of Building Physics and Mathematical Physics, Lund Institute of Technology, Box 118, S-221 00 Lund, Sweden.

Claesson J, Bennet J. 1987. Multipole method to compute the conductive heat flows between pipes in a cylinder, Notes on Heat Transfer 2-1987, Depts. of Building Physics and Mathematical Physics, Lund Institute of Technology, Box 118, S-221 00 Lund, Sweden.

Eskilson P, Claesson J. 1988. Simulation Model for Thermally Interacting Heat Extraction Boreholes, Numerical Heat Transfer, vol. 13, pp. 149-165.

Chapter 9

Carslaw HS, Jaeger JC. 1959. *Conduction of Heat in Solids*, Second ed., Oxford University Press, Great Britain.

Gradshteyn IS, Ryzhik IM. 1980. *Table of Integrals, Series, and Products*, Academic Press, New York, U.S.A.

Morse P, Feshbach H. 1953. *Methods of Theoretical Physics*, McGraw Hill, New York.

Chapter 10

Abramowitz M, Stegun IA. 1964. *Handbook of Mathematical Functions*, National Bureau of Standards, Applied Mathematics Series 55, U.S. Department of Commerce.

Baudoin A. 1988. Stockage intersaisonnier de chaleur dans le sol par batterie d'échangeurs baionnette verticaux; modèle de prédimensionnement, thesis, L'Université de Reims Champagne-Ardenne, France.

Carslaw HS, Jaeger JC. 1959. *Conduction of Heat in Solids*, Second ed., Oxford University Press, Great Britain.

Claesson J, Eskilson P. 1988. Conductive Heat Extraction by a Deep Borehole. Thermal Analyses and Dimensioning Rules, Energy, Vol. 13, No. 6, pp.509-527.

Eskilson P. 1987. Thermal Analyses of Heat Extraction Boreholes, thesis, Dept. of Mathematical Physics, Lund Institute of Technology, Box 118, S-221 00 Lund, Sweden.

Chapter 11

Abramowitz M, Stegun IA. 1964. *Handbook of Mathematical Functions*, National Bureau of Standards, Applied Mathematics Series 55, U.S. Department of Commerce.

Carslaw HS, Jaeger JC. 1959. *Conduction of Heat in Solids*, Second ed., Oxford University Press, Great Britain.

Veillon F. 1972. Quelques nouvelles méthodes pour le calcul numérique de la transformée inverse de Laplace, Thèse de Doctorat de 3° Cycle, Université de Grenoble, France.

Chapter 12

Areskoug M, Claesson J. 1981. Periodic Model of Duct System for Ground Heat Storage. Dept. of Mathematical Physics, Lund Institute of Technology,
Box 118, S-221 00 Lund, Sweden.

Carslaw HS, Jaeger JC. 1959. *Conduction of Heat in Solids*, Second ed., Oxford University Press, Great Britain.

Claesson J, Eftring B, Eskilson P, Hellström G. 1985. "Markvärme — en handbok om termiska analyser", BFR-rapport T16-18:1985.

Eftring B, Claesson J. 1978. Stationary Heat Losses from a Cylindrical Storage Volume in the Ground. Dept. of Mathematical Physics, Lund Institute of Technology, Box 118, S-221 00 Lund, Sweden.

Hagentoft CE. 1988. Temperature under a house with variable insulation, Building and Environment, Vol. 23, No. 3, pp. 225-231.

Appendix A

Sundberg J. 1988. Thermal Properties of Soils and Rocks, thesis, Publ. A57, Department of Geology, Chalmers University of Technology and University of Gothenburg, S-412 96 Gothenburg, Sweden.

Appendix C

Bennet J, Claesson J, Hellström G. 1987. Multipole method to compute the conductive heat flows to and between pipes in a composite cylinder, Notes on Heat Transfer 3-1987, Depts. of Building Physics and Mathematical Physics, Lund Institute of Technology, Box 118, S-221 00 Lund, Sweden.

Claesson J, Bennet J. 1987. Multipole method to compute the conductive heat flows between pipes in a cylinder, Notes on Heat Transfer 2-1987, Depts. of Building Physics and Mathematical Physics, Lund Institute of Technology, Box 118, S-221 00 Lund, Sweden.